

School of Biosciences
Division of Crop and Plant Science

Understanding the Role of Photoprotection in Disease Resistance to Septoria Tritici Blotch in Wheat

Dimitra Angelopoulou (BSc, MSc)

Thesis submitted to the University of Nottingham for the degree of Doctor of Philosophy

March 2022

Abstract

Zymoseptoria tritici, a fungal pathogen of wheat and the causal agent of Septoria Tritici Blotch (STB), is a particular challenge to wheat production on a global level, causing severe crop losses. As the site of photosynthesis, the chloroplast plays a crucial role in energy balance and trade-off between growth demands and response to environmental stresses and it is gaining an ever-growing attention due to its multi-layered involvement in disease response and downstream signalling. However, very little is known regarding wheat resistance responses to *Z. tritici* and the involvement of chloroplastic photoprotection. In the following thesis, I present data indicating the importance of photoprotection, through non-photochemical quenching (NPQ), in disease resistance of wheat plants against virulent and avirulent *Z. tritici* isolates.

This study presents novel data on wheat plants with increased, "primed" photoprotection resulting in enhanced tolerance towards virulent and avirulent isolates. Plants were over-expressing the photoprotective chloroplastic protein PsbS and maintained a greener phenotype and reduced pycnidia upon inoculation with virulent strains of *Z. tritici*. *Stb6*, which encodes a wall-associated kinase protein that confers resistance to *Z. tritici* isolates expressing the corresponding AvrStb6 effector, has recently been cloned. In this study, I also used *Stb6* near-isogenic lines and present findings on the association between the photoinhibitory component of NPQ, qI, and the avirulent isolate IPO323, at 24 hours after inoculation. Transcriptomic analysis also revealed the importance of the oxygen-evolving complex and photosystem II antenna proteins in resistance responses. In contrast, avirulent *Z. tritici* had no effect on photoprotection; however results indicated a potential virulent strategy that exploits the photosynthetic repair machinery. Also, this study presents early findings on interactions and potential mechanisms of effector-triggered susceptibility from *Z. tritici*, utilising necrotrophic effectors from another foliar wheat pathogen, *Parastagonospora nodorum*.

This study represents an important contribution to our understanding of chloroplastic responses to the important pathogen *Z. tritici* and suggests putative mechanisms of photoprotective, chloroplastic defence. Understanding and incorporating chloroplastic mechanisms into breeding programs could help develop more productive crop plants with a novel durable genetic resistance to plant pathogens.

Acknowledgments

First and foremost I would like to thank the Perry Foundation for their generous funding and financial support for this project, as well as the great opportunity for networking in their Forums. Similarly, I would like to express my gratitude to my supervisors, Professor Rumiana Ray, Professor Erik Murchie and Dr Kostya Kanyuka, for trusting in me this project and for their guidance along the way.

I wish to also thank all technical staff for always being there to help and support when needed, especially Sue Flint and Mark Meacham. A special thank you and big gratitude to Kamal Swarup for always going above and beyond to help, guide and support me.

To all my friends for supporting me and always being there to offer a cup of coffee and a chocolate bar when science was not behaving. Thank you to Jon, Keely, Adam, Elodie, Lena, Elina and Niki for being my second family. A special mention to my best friend, lab mate, colleague and mentor, Dr Lorna McAusland for just being who she is.

Thank you to my future husband, Mark, for the encouragement, support, advice, help but mainly, love throughout the years.

Finally, I would like to thank my family who have supported me beyond all expectations, through their own personal sacrifices, along this journey. Thank you for everything.

To my Mum and Dad

Στους γονείς μου

Table of Contents

Chapter 1 General Introduction 21

1.1 Septoria Tritici Blotch (STB) of wheat 21

1.1.1 Wheat 21
1.1.2 Epidemiology of STB and life cycle 21
1.1.3 Symptoms of STB and infection process 23
1.1.4 Disease management 26
1.1.5 *Stb* resistance genes 28
1.1.6 The resistance gene *Stb6* 32

1.2 Plant Immunity 33

1.2.1 PAMP Triggered Immunity (PTI) and Effector Triggered Immunity (ETI) 33
1.2.2 The Wheat – *Z. tritici* pathosystem 37
1.2.3 Necrotrophic effectors 39
1.2.4 Reactive Oxygen Species (ROS) 41
1.2.5 Chloroplastic Defence 45

1.3 Photosynthesis, Photoprotection and Signalling 47

1.3.1 Structure and function of the photosynthetic apparatus 47
1.3.2 Energy imbalance inside the chloroplast 50
1.3.3 Photoinhibition & Photoprotection 51
1.3.4 Non-Photochemical Quenching (NPQ) 52
1.3.5 The xanthophyll cycle 54
1.3.6 The photoprotective protein PsbS 55

1.4 Photoprotection and Biotic Stress 56

1.5 Aim of the present study 58

Chapter 2 Wheat plants overexpressing the photoprotective protein PsbS possess enhanced tolerance against isolates of the fungal pathogen Zymoseptoria tritici 60

2.1 Introduction 60

2.2 Materials & Methods 64

2.2.1 Plant material and growth conditions 64
2.2.2 Molecular analysis of transgenic wheat lines 65
2.2.3 *Zymoseptoria tritici* isolates and inoculation of plant material 70
2.2.4 Chlorophyll fluorescence (CF) and gas exchange (GE) measurements 71
2.2.5 Disease assessment and pycnidia development 74
2.2.6 ROS staining 74
2.2.7 Statistical analysis 75

2.3 Results 77

2.4 Discussion 111

2.5 Supplementary data 117

Chapter 3 Role of photoprotection in Stb6-mediated responses to Zymoseptoria tritici 118

3.1 Introduction 118

3.2 Materials & Methods 121

3.2.1 Plant material and growth conditions 121

3.2.2 *Zymoseptoria tritici* isolates and inoculations 121
3.2.3 Chlorophyll fluorescence (CF) and gas exchange (GE) measurements 122
3.2.4 Absorbance measurements 123
3.2.5 Carotenoid extraction and quantification 124
3.2.6 ROS staining 124
3.2.7 RNA sequencing and differential expression gene (DEG) analysis 125
3.2.8 RNA extraction 126
3.2.9 Gene expression 127
3.2.10 Thylakoid extractions 129
3.2.11 Western blots 130
3.2.12 Disease assessment and pycnidia development 130
3.2.13 Statistical analysis 131

3.3 Results 133
3.3.1 Disease assessment and pycnidia counts 133
3.3.2 Physiological phenotype 133
3.3.3 Carotenoid expression and quantification 143
3.3.4 ROS 147
3.3.5 Transcriptome analysis 149

3.4 Discussion 174

3.5 Supplementary data 181

Chapter 4 Effect of virulence of Zymoseptoria tritici on wheat sensitivity to necrotrophic effectors by Parastagonospora nodorum 197

4.1 Introduction 197

4.2 Materials & Methods 201
4.2.1 Plant material and growth conditions 201
4.2.2 Inoculations and infiltrations 201
4.2.3 Sampling, RNA extractions and qPCRs 203
4.2.4 Symptoms monitoring 204
4.2.5 Statistical analysis 204

4.3 Results 205
4.3.1 Presence and expression of wheat sensitivity genes 205
4.3.2 Sensitivity assessment of the parental lines 208
4.3.3 Sensitivity assessment of *Z. tritici*-inoculated and Toxin-infiltrated plants 211
4.3.4 Gene expression 219

4.4 Discussion 222

Chapter 5 General Discussion 227

5.1 Main Findings 227

5.2 Recommendations for future studies 230

5.3 Final conclusions 232

Chapter 6 References 234

Table of Figures

Figure 1-1. A schematic representation of the life cycle of the pathogen. Modified from Ponomarenko et al. (2011)..... 23
Figure 1-2. Flag leaves of wheat showing typical STB symptoms (field trial, Sutton Bonington 2017). 24
Figure 1-3. A schematic representation of PAMP-triggered immunity (PTI) and effector-triggered immunity (ETI) in plants. PTI events are indicated by black arrows and ETI events are indicated by blue arrows. Image taken from Nguyen et al. (2021). 35
Figure 1-4. Model of the PSII repair cycle. 'P's in purple circles represent phosphate groups, red labelled D1 is photodamaged D1, light-green labelled D1 a new copy of the protein. Proteins labelled in blue represent factors exclusively involved in PSII repair while proteins labelled in gold are factors that are likely involved in PSII repair. Picture taken from Theis and Schroda (2016)..... 50
Figure 1-5. Schematic diagram of different NPQ states/components in the PSII-LHCII complexes, along with their associates enzymes and genes involved. Picture taken from Malnoë (2018). 56
Figure 2-1. Final plasmid construct of PsbS-overexpressing (PsbS-OX) wheat lines (NIAB, 2014). Rice (*Oryza sativa*) *PsbS* was used, Actin promoter and *nptII* as the selectable marker. 65
Figure 2-2. A snapshot of the Clustal Omega alignment between the coding sequences of rice PsbS (OsPsbS) used for the generation of the transgenic and wheat PsbS (TaPsbS) on all three genomes (3A, 3B and 3D). Nucleotides highlighted in red depict mismatches between the sequences, whereas sequences highlighted in yellow depict the Forward (5'-3') and Reverse (3'-5') OsPsbS primer sequences. 67
Figure 2-3. Example of chlorophyll fluorescence imaging and sample layout. The image pixels get translated into numeric values using the designated software (Fluorcam 7). 74
Figure 2-4. (a) Detection of transgene with PCR and OsPsbS primers. Lane 1: 1kb+ ladder, Lanes 2-9: Biological replicates of Null plants (0 copies), Lanes 10-21: Biological replicates of PsbS-OX plants (4 copies), Lane 22: -ve (H_2O)

control, Lane 23: +ve (plasmid) control, Lane 24: 1kb+ ladder. Expected product size was 184bp, (b) qRT-PCR for gene expression of OsPsbS and native TaPsbS on all genotypes used in this experiment. Horizontal bars above graph represent significant differences ($P < 0.05$). 78
Figure 2-5. Characterisation of NPQ kinetics of the transgenic plants compared to the WT Fielder. (a) NPQ Induction and Relaxation curve. Vertical bars indicate LSD of the significant interactions, (b) and (c) qE and qI components of NPQ, (d) and (e) NPQ Induction and Relaxation curve modelling, respectively, (f) and (g) ED_{50} values derived from the models, indicating the number of minutes required for NPQ to reach its 50% maximum (Induction) and 50% minimum (Relaxation) value, respectively. Bars and lines represent means ± SEM (n = 12). Horizontal bars represent significant differences between the means ($P < 0.05$)..... 80
Figure 2-6. Stomatal conductance dynamics in light and dark conditions between the genotypes. Vertical lines represent LSD of the significant interactions (n=12). 81
Figure 2-7. (a) and (b) Disease phenotype of IPO323 and Zt22 on Fielder, Null and PsbS-OX at 14 and 21dai, respectively. Blue boxes indicate the presence of pycnidia on the necrotic tissue, (c) AUDPC from visual disease assessment. Vertical bar represents LSD on the significant interaction, (d) pycnidia counts from necrotic leaf sections past 21dai. Horizontal line indicates significant difference of the means ($P < 0.05$) (n=4), (e) correlation plot between AUDPC and pycnidia counts. No regression line is shown as there was no significant relationship observed..... 84
Figure 2-8. Induction ED_{50} (minutes required for NPQ to reach 50% of its maximum) over time between the Null and PsbS-OX upon inoculation. ANOVA only showed genotypic significant differences, as presented here (no treatment or interaction effect). Vertical bars represent LSD for the significant interactions..... 85
Figure 2-9. Detection of transgene with genomic DNA PCR and OsPsbS primers. Lane 1: 1kb+ ladder, Lanes 2-13: Biological replicates of Null plants, Lanes 14-23: Biological replicates of PsbS-OX plants, Lane 24: -ve (H_2O)

control, Lane 25: +ve (plasmid) control, Lane 26: 1kb+ ladder. Expected product size was 184bp. 87
Figure 2-10. Characterisation of NPQ kinetics of the transgenic plants compared to the WT Fielder. (a) NPQ Induction and Relaxation curve. Vertical bars indicate LSD of the significant interactions, (b) and (c) qE and qI components of NPQ, (d) and (e) NPQ Induction and Relaxation curve modelling, respectively, (f) and (g) ED_{50} values derived from the models, indicating the number of minutes required for NPQ to reach its 50% maximum (Induction) and 50% minimum (Relaxation) value, respectively. Bars and lines represent means ± SEM (n = 12). Horizontal bars represent significant differences between the means ($P < 0.05$). 89
Figure 2-11. Stomatal conductance dynamics in light and dark conditions between the genotypes. Vertical lines represent LSD of the significant interactions (n=12). 90
Figure 2-12. (a) and (b) Disease phenotype of Zt22 and Zt508 on Fielder, Null and PsbS-OX at 14 and 21dai, respectively. Blue boxes indicate the presence of pycnidia on the necrotic tissue, (c) AUDPC from visual disease assessment. Vertical bar represents LSD on the significant interaction (n=4)..... 92
Figure 2-13. Genotypic differences over time for NPQ-related parameters upon inoculation, (a) Induction ED_{50} (minutes required for NPQ to reach 50% of its maximum), (b) qE, (c) NPQ_{max} and (d) total NPQ. Solid black line represents the Null and broken black line represents the OX line. ANOVA only showed genotypic significant differences, as presented here (no treatment or interaction effect). Vertical bars represent LSD of the significant interactions (n=4). 94
Figure 2-14. (a) Carbon assimilation (A_{max}) and (b) maximum efficiency of PSII (F_v/F_m) over time for the different treatments. Solid lines represent the Null and broken lines represent the OX line. Vertical bars represent LSD of the significant interactions (n=4). 95
Figure 2-15. Molecular characterisation of the transgenic plants before inoculation. (a) Genomic DNA PCR to show the presence and absence of transgene in the Null and PsbS-OX, respectively. Lane 1: 1kb+ ladder, Lanes 2-5: Fielder, Lanes 6-9: Null, Lanes 10-13: PsbS-OX, Lane 14: -ve (H_2O)

control, Lane 15: +ve (plasmid) control, Lane 16: 1kb+ ladder, (b) Immunoblot of PsbS and Ubiquitin, showing Fielder, Null and PsbS-OX in two technical replicates. Total protein was extracted from prepared thylakoids, (c) Band signal/intensity translated into numeric values for comparison. Bars represent means of each genotype ± SEM. Significant differences between the means are shown with horizontal bars (t-tests $P < 0.05$)..... 99
Figure 2-16. Characterisation of NPQ kinetics of the transgenic plants compared to the WT Fielder. (a) NPQ Induction and Relaxation curve. Vertical bars indicate LSD of the significant interactions, (b) and (f) qE and qI components of NPQ, (d) and (e) NPQ Induction and Relaxation curve modelling, respectively, (c) and (g) ED_{50} values derived from the models for Induction and Relaxation, respectively, (h) and (i) maximum efficiency of PSII (F_v/F_m) and photochemical quenching (qP), respectively. Bars and lines represent means ± SEM (n = 4). Horizontal bars represent significant differences between the means ($P < 0.05$). 101
Figure 2-17. Disease phenotyping of all the isolates used in this experiment, at 14 and 21dai. The middle sections of the leaves are shown in these pictures. Blue boxes indicate presence of pycnidia on the necrotic tissue..... 103
Figure 2-18. (a) AUDPC and (b) pycnidia counts for all genotypes and isolates. For (a) ANOVA showed significant interactions between the genotypes and the treatments, as seen on the graph. However, for (b) ANOVA only showed a significant effect of either the genotypes (top panel) or treatments (bottom panel) and no significant interactions. Dark grey solid bars represent the Null and grey shaded bars represent the PsbS-OX. Vertical bars represent LSD for the significant interactions or main effects of the analysis (n=4). 104
Figure 2-19. (a) NPQ_{max} and (b) qE at 24hai for the interaction between the genotypes and the treatments. ANOVA showed significant interactions between the genotypes and the treatments, as shown on the graphs. Vertical bars represent LSD for the significant interaction. Dark grey solid bars represent mean values of the Null and grey shaded bars represent mean values of PsbS-OX (n=4). 107

Figure 2-20. ROS staining for superoxide O_2^- (blue stain - left) and hydrogen peroxide H_2O_2 (brown stain - right) at 24hai for both genotypes (Null and PsbS-OX) and all isolates used in this experiment. 109
Figure 2-21. Protein expression of PsbS on Fielder, Null and PsbS-OX that had been previously infected with the *Z. tritici* isolates IPO323, Zt22 and Zt508. (a) and (b) Blots, (c) signal intensity upon normalisation to Ubiquitin. Data represent means ± SEM. Significant differences between the means are shown with black horizontal bars (t-tests $P < 0.05$). 110
Figure 3-1. (a) Disease phenotype of the Near Isogenic Lines Courtot and Ct (+Stb6) at different stages of the infection process. Isolate IPO323 results in an incompatible reaction with *Stb6* and therefore no symptoms or pycnidia develop on the leaf, whereas it is extremely virulent on Courtot and results in full leaf necrosis and production of a lot of pycnidia. Zt22 is virulent on both genotypes and results in leaf necrosis and production of pycnidia. (b) Area under the disease progress curve (AUDPC) of assessed leaves based on % leaf coverage with disease symptoms and (c) Pycnidia counts at 21dai from leaf sections. Data represent means ± SEM (n=4). Horizontal bars represent significant differences between the means ($P < 0.05$). 134
Figure 3-2. NPQ kinetics before any inoculation occurred. (a) NPQ Induction and Relaxation curve during light and dark conditions, respectively, and (b) normalised Relaxation in the dark, (c) qE and (d) qI components of NPQ before inoculation. Solid black line represents Courtot and dashed black lines represents the near-isogenic Ct (+Stb6). Data represent means ± SEM (n=16). Horizontal line indicates significant difference between the means. 135
Figure 3-3. NPQ Induction and Relaxation kinetics along with Normalised NPQ in the dark for each Treatment across the different time points. (a-c) Curves for IPO323-inoculated plants at 6, 24 and 48hai, respectively, (d-f) Curves for Zt22-inoculated plants at 6, 24 and 48hai, respectively. Solid and dashed black lines indicate Courtot and Ct (+Stb6), respectively. Data represent means ± SEM (n=8). Vertical bars represent LSD for the significant interaction and stars (*) denote significant difference ($P < 0.05$) of the equivalent point in the kinetics. 137

Figure 3-4. NPQ-derived parameters for each isolate across the measurement timings. (a-d) IPO323-inoculated plants exhibiting differences in qE, Induction ED_{50}, qI and Relaxation ED_{50}, respectively, (e-h) Zt22-inoculated plants exhibiting no changes in qE, Induction ED_{50}, qI and Relaxation ED_{50}, respectively. Solid and dashed black lines indicate Courtot and Ct (+Stb6), respectively. Data represent means ± SEM (n=8). Stars (*) denote significant differences ($P < 0.05$) of the genotypes at the equivalent time point. 138
Figure 3-5. Chlorophyll absorbance, CO_2 assimilation (A_{max}) and stomatal conductance (g_s) for IPO323-inoculated plants (a-c) and Zt22-inoculated plants (d-f). Solid and dashed black lines indicate Courtot and Ct (+Stb6), respectively. Data represent means ± SEM (n=8). Stars (*) denote significant differences ($P < 0.05$) of the genotypes at the equivalent time point. 141
Figure 3-6. (a) Electron transport rate (ETR) and (b) operating efficiency of PSII for Ct (+Stb6) inoculated with IPO323 or Zt22 across the time measurements. Teal and black lines represent IPO323 and Zt22, respectively. Data represent means ± SEM (n=8). Stars (*) denote significant differences ($P < 0.05$) of the genotypes at the equivalent time point. 142
Figure 3-7. HPLC on carotenoids and relative gene expression ($2^{-\Delta Ct}$) of important catalytic enzymes and compounds of the xanthophyll cycle. (a) lutein, (b) a schematic representation of the biosynthetic pathway of β-Carotene-derived xanthophylls, (c) β-carotene, (d) zeaxanthin epoxidase ZEP, (e) zeaxanthin, (f) violaxanthin, (g) violaxanthin de-epoxidase VDE, (h) neoxanthin and (i) 9-*cis*-epoxycarotenoid dioxygenase NCED. Grey and teal bars indicate Courtot and Ct (+Stb6), respectively. Data represent means ± SEM (n=3). Significant differences of the means through t-tests are shown as horizontal black bars or as letters above bars ($P < 0.05$). 145
Figure 3-8. (a) NBT blue staining for the detection of superoxide, (b) DAB brown staining for the detection of hydrogen peroxide and (c) gene expression ($2^{-\Delta\Delta Ct}$) of iron superoxide dismutase (FeSOD), a chloroplastic enzyme that scavenges superoxide. Gene expression data represent means ± SEM (n=3). Letters above bars indicate statistical difference of the means using t-tests ($P < 0.05$). Grey and teal bars indicate Courtot and Ct (+Stb6), respectively. 148

Figure 3-9. (a) Pearson's correlation plot of all samples exhibiting high consistency among biological replicates. Blue coloured scale indicates R^2 correlation values. (b) 2D PCA plot indicating the clustering of different samples. Due to different annotations between the time of the bioinformatics analysis and writing of this thesis, there is a discrepancy in the labelling of the different samples between figures (a) and (b). C = Courtot; C(+) or N = Ct (+Stb6); IPO = isolate IPO323; Zt or HT22 = isolate Zt22; 0h, 6h, 24h = hours after inoculation..... 151
Figure 3-10. (a) Number of up- and downregulated differentially expressed genes (DEGs) for each pairwise comparison. Red bars represent upregulated genes and green bars represent downregulated genes. Numbers above bars indicate the exact number of DEGs for each comparison. (b) Venn intersection diagrams of the pairwise comparisons listed in Table 3-4. 153
Figure 3-11. Photosynthesis pathway KEGG map (osa00195) for the comparison between the resistant Ct (+Stb6) and the susceptible Courtot inoculated with IPO323 at 6hai. Genes involved in this pathway are highlighted in shades of green, grey or red, based on the Fold Change scale bar at the top right. Green represents downregulation, grey small change and red upregulation. In this instance, all grey filled boxes are downregulated genes. 161
Figure 3-12. Photosynthesis-antenna proteins KEGG map (osa00196) for the comparison between *Stb6* in susceptibility (Zt22 inoculation) and resistance (IPO323 inoculation) at 6hai. Genes involved in this pathway are highlighted in shades of green, grey or red, based on the Fold Change scale bar at the top right. Green represents downregulation, grey small change and red upregulation. In this instance, all grey filled boxes are downregulated genes. 162
Figure 3-13. Plant pathogen interaction KEGG maps (osa04626) for comparison S (+) Zt22 vs R (+) IPO323 6h. Genes involved in this pathway are highlighted in shades of green, grey or red, based on the Fold Change scale bar at the top right. Green represents downregulation, grey small change and red upregulation. 163

Figure 3-14. Plant pathogen interaction KEGG maps (osa04626) for comparison R (+) IPO323 vs S (-) IPO323 24h. Genes involved in this pathway are highlighted in shades of green, grey or red, based on the Fold Change scale bar at the top right. Green represents downregulation, grey small change and red upregulation. 164
Figure 3-15. Relative gene expression on selected genes from RNA sequencing. PsbP (a), Lhca1 (b), PsbS (c) and CERK1 (d) were selected to confirm their expression. Data represent means ± SEM (n=3). Relative gene expression was calculated using the $2^{-\Delta Ct}$ method. Different letters above bars indicate significant differences between the means (t-tests $P < 0.05$). Grey and teal bars indicate Courtot and Ct (+Stb6), respectively. 168
Figure 3-16. Western blot on PsbP protein and signal analysis. No statistical analysis could be performed as repetitions of these westerns are still ongoing. 169
Figure 3-17. Relative gene expression ($2^{-\Delta\Delta Ct}$) of defence-related compounds. AOS and ICS originate from the chloroplast and are precursor molecules of the defence hormones jasmonic acid and salicylic acid, respectively. PR1 is a pathogenesis-related protein that gets induced upon infections. Data represent means ± SEM (n=3). Significant differences between the means were derived through t-tests ($P < 0.05$) and are shown with letters above the bars. Grey and teal bars indicate Courtot and Ct (+Stb6), respectively. 170
Figure 3-18. Number of DEGs from the transcriptome of *Z. tritici*. Red bars represent upregulated genes and green bars represent downregulated genes. Numbers above bars indicate the exact number of DEGs for each comparison. 172
Figure 4-1. Gene expression validation of (a) *Tsn1*, (b) *Thf1* and (c) *Snn1* from RNAseq experiment (Chapter 3). Bars represent means ± SEM (n=3). Grey and teal bars represent Courtot and Ct (+Stb6), respectively. Letters above bars indicate statistical differences between the means (t-tests $P < 0.05$). 207
Figure 4-2. Tox1 infiltration assay for Courtot (Ct) and Chinese Spring (CS), along with the near-isogenic Ct (+Stb6), at 3 and 7 days after infiltration (dai). H_2O infiltration was used as a control. 209

Figure 4-3. ToxA infiltration assay for Courtot (Ct) and Chinese Spring (CS), along with the near-isogenic Ct (+Stb6), at 3 and 7 days after infiltration (dai). H_2O infiltration was used as a control. 210
Figure 4-4. Symptoms of *Z. tritici* inoculations followed by Toxin infiltrations at 2 days after inoculations (dai). 213
Figure 4-5. Symptoms of *Z. tritici* inoculations followed by Toxin infiltrations at 3 days after inoculations (dai). 214
Figure 4-6. Symptoms of *Z. tritici* inoculations followed by Toxin infiltrations at 5 days after inoculations (dai). 215
Figure 4-7. Symptoms of *Z. tritici* inoculations followed by Toxin infiltrations at 7 days after inoculations (dai). 216
Figure 4-8. Symptoms of *Z. tritici* inoculations followed by Toxin infiltrations at 9 days after inoculations (dai). 217
Figure 4-9. Symptoms of *Z. tritici* inoculations followed by Toxin infiltrations at 15 days after inoculations (dai). Red boxes indicate necrotic areas where pycnidia appeared..... 218
Figure 4-10. Gene expression analysis of (a) *Tsn1*, (b) *Thf1* and (c) *Snn1* across all treatments, 24h after infiltration. Grey and teal bars represent Courtot and Ct (+Sbt6), respectively. Bars represent means ± SEM (n=3). ANOVA of the interaction between the genotypes and treatments, along with the LSD, are shown on the top left of each graph. Abbreviation IPO stands for IPO323. 220
Figure 4-11. Gene expression analysis of (a) zeaxanthin epoxidase ZEP and (b) violaxanthin de-epoxidase VDE across all treatments. Grey and teal bars represent Courtot and Ct (+Sbt6), respectively. Bars represent means ± SEM (n=3). ANOVA of the interaction between the genotypes and treatments, along with the LSD, are shown on the top left of each graph. Abbreviation IPO stands for IPO323..... 221

Table of tables

Table 1-1. The major genes for resistance of *Triticum aestivum* to STB that have been discovered so far, with their chromosomal locations, corresponding avirulent *Z. tritici* isolates and resistant source line/variety. Modified from Brown et al., 2015. 31

Table 2-1. List of primers used to confirm expression of rice PsbS in the transgenic plants (OsPsbS), in relation to the native (WT) wheat PsbS (TaPsbS). TaPsbS primers were designed based on the coding sequence of the 3B chromosome. 67

Table 2-2. List of *Zymoseptoria tritici* isolates used in this study. Interaction compatibility is based on the wheat variety Fielder that was used for the transformation and contains *Stb6*. Isolates and further information were kindly provided by Henry Tidd, Dr Kostya Kanyuka and Dr Ruth Bryant (personal communication)..... 71

Table 2-3. Chlorophyll fluorescence parameters and photosynthesis (Amax) for the different genotypes. Shown below are individual means ± SEM (n=12). 81

Table 2-4. Chlorophyll fluorescence and gas exchange parameters for each treatment and genotype, over time. Data shown indicate means for each parameter, per genotype and treatment and per time point (n=4). Final three rows indicate significant values after repeated measurements ANOVA, followed by the respective LSD. TxG refers to Time x Genotype, TxT refers to Time x Treatment and TxGxT refers to the interaction of Time x Genotype X Treatment..... 86

Table 2-5. Chlorophyll fluorescence parameters and photosynthesis (A_{max}) for the different genotypes. Shown below are individual means ± SEM (n=12), letters in brackets indicate differences between the means. 90

Table 2-6. Chlorophyll fluorescence and gas exchange parameters for each treatment and genotype, over time. Data shown indicate means for each parameter, per genotype and treatment and per time point (n=4). Final three columns indicate significant values after repeated measurements ANOVA, followed by the respective LSD. TxG refers to Time x Genotype, TxT refers to

Time x Treatment and TxGxT refers to the interaction of Time x Genotype X Treatment..... 96
Table 2-7. Genotyping results from T_2 generation plants. Cells highlighted in light pink were the plants selected to be selfed to T_3 and used their seeds for this experiment..... 98
Table 2-8. Chlorophyll fluorescence parameters derived from the FluorCam at 24hai. Significant values along with LSDs (in brackets) are shown at the bottom of the table for the main effects (genotype or treatment) and the significant interaction (n=4)..... 108
Table 3-1. List of samples used in transcriptomics experiment. Interaction response of each genotype (Courtot or Ct (+Stb6)) to each isolate (IPO323 or Zt22) is given in brackets – R for resistance and S for susceptibility..... 126
Table 3-2. List of primers used in this study. Primers were designed based on the transcript ID in RNA sequencing DEG results and their respective coding DNA sequence. Ubiquitin was used as the housekeeping gene. 128
Table 3-3. Remaining carotenoids analysed by HPLC. Data represent means of each parameter under each treatment. Chl, chlorophylls; Car:Chl, ratio of total carotenoids to chlorophylls; Anth, carotenoid antheraxanthin; % XC pool/Car, ratio of xanthophyll cycle pool against total carotenoids; DEP, de-epoxidation state of the xanthophyll cycle. Significant differences between genotypes and treatments for each parameter (i.e. per row) are indicated by equal asterisks (*) next to the values (t-tests, $P < 0.05$). 146
Table 3-4. List of pairwise comparisons selected for Differential Expression analysis. (+) and (-) refer to the presence or absence of *Stb6* in Ct (+Stb6) and Courtot, respectively. R and S refer to Resistant (incompatible) or Susceptible (compatible) response based on the isolate. 150
Table 3-5. Top 10 significantly enriched “Biological Process” GO terms associated with each comparison. Gene ratio indicates the ratio of DEGs to all genes for this GO term, Cp indicates the pairwise comparison. (+) and (-) refer to the presence or absence of *Stb6* in Ct (+Stb6) and Courtot, respectively. R and S refer to Resistant (incompatible) or Susceptible (compatible) response based on the isolate. Table spans across two pages. 156

Table 3-6. All significantly enriched KEGG pathways associated with each comparison. Ratio indicates the ratio of DEGs to all genes for this KEGG ID. Cp indicates each pairwise comparison. Pathways and KEGG IDs are coming from rice (*Oryza sativa*). (+) and (-) refer to the presence or absence of *Stb6* in Ct (+Stb6) and Courtot, respectively. R and S refer to Resistant (incompatible) or Susceptible (compatible) response based on the isolate.159
Table 3-7. A list of putative *Z. tritici* effectors. Gene ID describes the significant DEG from the bioinformatic analysis on the fungal transcriptome, Log FC denotes the magnitude of the expression along with significance *P* value. Localizer and EffectorP are the online machine learning tools used for the prediction of effectors. Residues describe the length of amino acids in each predicted protein along with the percentage of their cysteine content. Transcripts highlighted in red indicate commonalities across comparisons. 173
Table 4-1. A list of all experimental treatments used in this study. 202
Table 4-2. A list of all the primers used in this study..... 203
Table 4-3. Presence and expression of the wheat toxin sensitivity genes, *Tsn1*, *Thf1* and *Snn1*, in RNAseq experiment (Chapter 3). Log FC refers to the level of transcript change (up- or downregulation) and *P* refers to the adjusted *P*-value of each transcript. Significantly differentially expressed transcripts are highlighted in bold. 206

Table of Supplementary Figures

SF 2-1. qPCR melt curve analysis showing a peak appearing with OsPsbS primers only on the transgenic PsbS-OX plants. 117
SF 3-1. NPQ Induction and Relaxation kinetics along with Normalised NPQ in the dark for Ct (+Stb6) between IPO323 and Zt22 at (a) 6hai, (b) 24hai and (c) 48hai. Teal and black lines represent IPO323 and Zt22, respectively. Data represent means ± SEM (n=8). 181
SF 3-2. NPQ-derived parameters for Ct (+Stb6) between the two isolates and across the measurement timings. (a) qE, (b) Induction ED_{50}, (c) qI and (d) Relaxation ED_{50}. Teal and black lines indicate IPO323 and Zt22, respectively. Data represent means ± SEM (n=8). Stars (*) denote significant differences ($P < 0.05$) of the genotypes at the equivalent time point. 182
SF 3-3. CF parameters for both isolates across the time measurements. (a-d) Maximum PSII efficiency (F_v/F_m), photochemical quenching (qP), operating PSII efficiency (φPSII) and electron transport rate (ETR) for IPO323-inoculated plants, (e-h) Maximum PSII efficiency (F_v/F_m), photochemical quenching (qP), operating PSII efficiency (φPSII) and electron transport rate (ETR) for Zt22-inoculated plants. Solid black line indicates Courtot and dashed black line indicates Ct (+Stb6). Data represent means ± SEM (n=8). 183
SF 3-4. (a) Chlorophyll absorbance, (b) CO_2 assimilation (A_{max}) and (c) stomatal conductance (g_s) for Ct (+Stb6) inoculated with IPO323 or Zt22, across the time measurements. Teal and black lines represent IPO323 and Zt22, respectively. Data represent means ± SEM (n=8). 184
SF 3-5. Maximum PSII efficiency (F_v/F_m) (top graph) and photochemical quenching (qP) (bottom graph) for Ct (+Stb6) inoculated with IPO323 or Zt22 across the time measurements. Teal and black lines represent IPO323 and Zt22, respectively. Data represent means ± SEM (n=8). 185
SF 3-6. Network of the top downregulated interacting proteins in the comparison between ± *Stb6* with IPO323 at 6hai. Green-coloured lines represent downregulation and their intensity denote the probability (=score) of the interaction to be true and accurate, according to String database. 191
SF 3-7. Network of the top upregulated interacting proteins in the comparison between ± *Stb6* with IPO323 at 6hai. Red-coloured lines represent

upregulation and their intensity denote the probability (=score) of the interaction to be true and accurate, according to String database. 192
SF 3-8. Network of the top downregulated interacting proteins in the comparison between ±Stb6 with IPO323 at 24hai. Green-coloured lines represent downregulation and their intensity denote the probability (=score) of the interaction to be true and accurate, according to String database. 193
SF 3-9. Network of the top upregulated interacting proteins in the comparison between ± *Stb6* with IPO323 at 24hai. Red-coloured lines represent upregulation and their intensity denote the probability (=score) of the interaction to be true and accurate, according to String database. 194
SF 3-10. Network of the top downregulated interacting proteins in the comparison of *Stb6* inoculated with IPO323 or Zt22 at 6hai. Green-coloured lines represent downregulation and their intensity denote the probability (=score) of the interaction to be true and accurate, according to String database. 195
SF 3-11. Due to the complexity and high number of PPIs, a snapshot of the top upregulated interacting proteins in the comparison of *Stb6* inoculated with IPO323 or Zt22 at 6hai is shown. Red-coloured lines represent upregulation and their intensity denote the probability (=score) of the interaction to be true and accurate, according to String database. 196

Table of Supplementary Tables

Supplementary Table 3-1. Table indicating the depth of coverage of the RNA sequencing experiment as well as the overall quality control, per sample (genotype, treatment, time and biological replicate). 186

Supplementary Table 3-2. A list of the top 10 up- and downregulated DEGs for each comparison. CP denotes the comparison number, as listed in Table 3-4. T_R denotes the direction of gene regulation (red arrow for upregulation, green arrow for downregulation). Transcript and Description refer to Transcript ID and molecular function or biological process, respectively. Average FPKM (Fragments Per Kilobase of transcript sequence per Millions base pairs sequenced) values denote the normalised read counts (considering sequencing depth and gene length) of all three biological replicates per comparison, reflecting gene expression levels. Log2 FC indicates the fold change of that transcript in the pairwise comparison. *P* value indicates the adjusted significant *P* value of that transcript. Table spans across four pages (1/4)..... 187

Chapter 1 General Introduction

1.1 Septoria Tritici Blotch (STB) of wheat

1.1.1 Wheat

Wheat (*Triticum aestivum*) is, globally, an economically important cereal grain crop, cultivated in over 200 million hectares and providing humans with most of their dietary energy and protein (Shewry, 2009). Within the EU it is considered the most important cereal (Fones & Gurr, 2015). By 2050, the current global wheat production must increase by 60-70% to adequately suffice projected rise in food demands (Ray et al., 2013; Pal, Saini & Kumar, 2022). However, a major challenge in increasing wheat production are the losses incurring by several abiotic and biotic stresses, such as drought, nutrient deficiency, bacterial and fungal infections, which are likely to increase in the future as a consequence of climate change (Fisher et al., 2012; Bebber et al., 2013; Fones et al., 2020). Globally, the most damaging fungal diseases of wheat are Fusarium head blight (caused by *Fusarium* spp.), powdery mildew (caused by *Blumeria graminis*), stem rust (caused by *Puccinia graminis*) and Septoria tritici blotch STB (caused by *Zymoseptoria tritici*) (Oerke, 2006; Dean et al., 2012; Torriani et al., 2015). STB is the most important foliar disease of winter wheat in Europe as it accounts for 5-10% of annual yield losses, while a further €1 billion is spent by farmers across Europe on fungicides to control STB (Orton et al., 2011; Fones & Gurr, 2015; Torriani et al., 2015). The emergence and dispersal of fungicide resistance in fungal populations severely threatens wheat production and compromises food security (Torriani et al., 2009; Cools & Fraaije, 2013; Estep et al., 2015).

1.1.2 Epidemiology of STB and life cycle

STB is a polycyclic disease with up to 30 cycles of asexual reproduction completed during each growing season (Kema et al., 1996; McDonald & Mundt, 2016). Ascospores released from the overwintered pseudothecia (small, dark brown, flask-shaped fruiting bodies) can be dispersed by wind currents over large geographical areas (Suffert et al., 2011) and are the primary inoculum for disease initiation. Pseudothecia formation depends on

the cross of strains of opposite mating types, MAT1-1 and MAT1-2 (Kema et al., 2018) and therefore, their appearance depends on the intensity of the epidemics. The fungus survives as mycelium on the residues of the previous crop left in the soil or on the infected seeds. Increased relative humidity during periods of moisture causes the perithecia to swell (mature), burst open and the ascospores disperse to infect seedling leaves of close proximity. The first symptoms are produced from mid-autumn onwards and spores are then spread by rain splash and physical contact to the upper and adjacent leaves. Ascospores will germinate on the leaf tissue to form thin hyphae, mycelium or pycnidiophores that will bear at their end long, threadlike, colourless, one- to several-celled pycnidia. Pycnidia form readily in high humidity, particularly if there is free water present on the leaves and disperse through rain wash and splashing, spreading the disease upwards through the canopy to uninfected leaves. Eventually, the asexual (imperfect) form of the fungus, pycnidia containing pycnidiospores, are produced roughly 14 to 40 days after infection, depending on the host and seasonal conditions (Figure 1-1). Many cycles of sexual and asexual reproduction during the growing season allow epidemics to develop rapidly. The optimum temperatures for STB are 15 - 20ºC (Filipe & Maule, 2004; Lovell et al., 2004b; Morais et al., 2016).

The asexual reproductive cycle allows *Z. tritici* to rapidly evolve new fitness traits such as fungicide resistant genotypes, while the sexual reproduction allows for rapid gene flow to facilitate the spread of such traits over large geographical areas (Orton et al., 2011; Fisher et al., 2012). This heterothallic nature makes *Z. tritici* a highly challenging pathogen in terms of durable disease control (Fisher et al., 2012; Talbot, 2015).

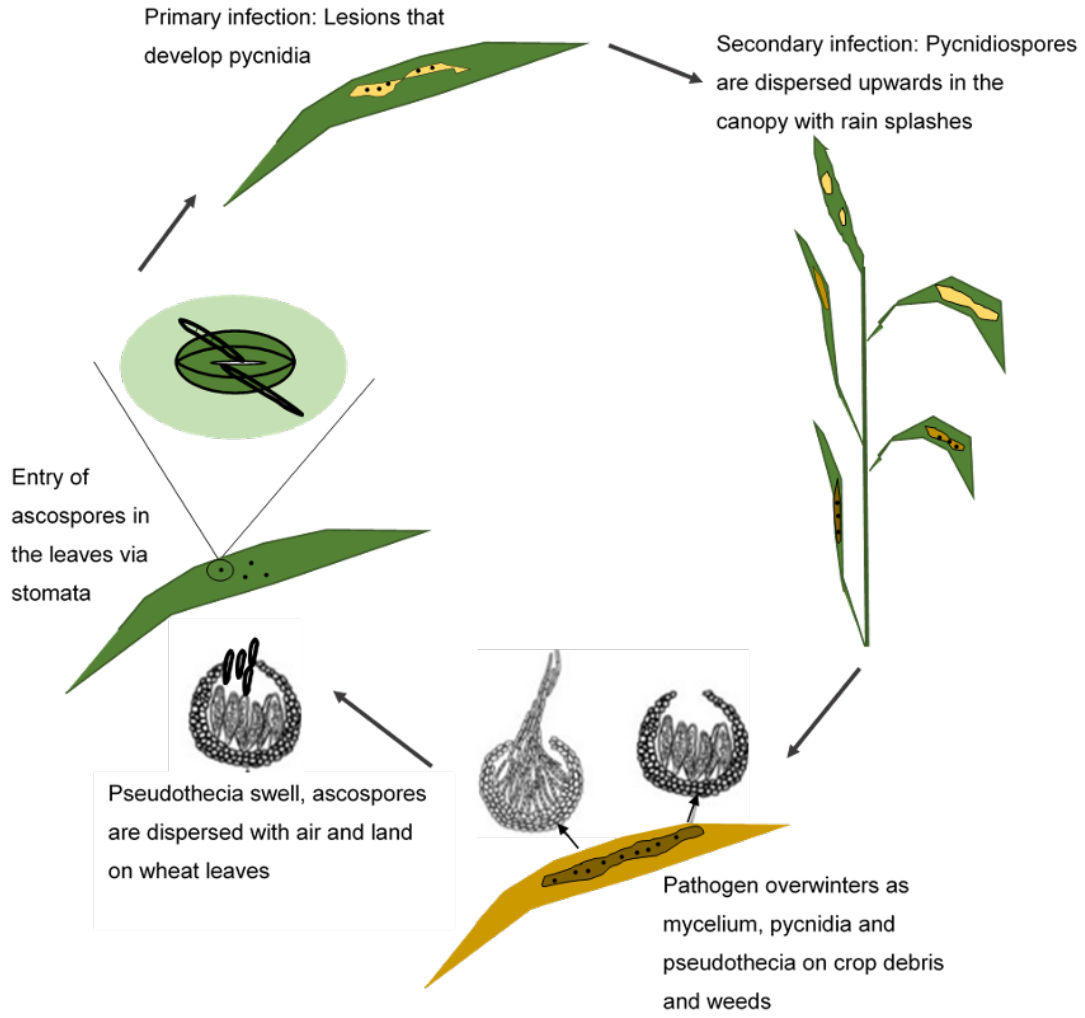


Figure 1-1. A schematic representation of the life cycle of the pathogen. Modified from Ponomarenko et al. (2011).

1.1.3 Symptoms of STB and infection process

Symptoms of STB can be seen very early in the growing season in most years. They first appear on the lower leaves as green to yellow or brown spots along the leaf blade and they soon become darker and spread rapidly forming irregular lesions/blotches (Figure 1-2). The lesions may be restricted or may coalesce and cover the entire leaf blade and sheath, depending on the variety and humidity (Kema et al., 1996). As the symptoms develop, numerous small but visible black pycnidia, asexual fruiting bodies of *Z. tritici*, will develop within the lesions. The pycnidia develop in the substomatal cavities of the host so are spaced regularly within the lesions (Ponomarenko et al., 2011). Consequently,

reduction in the photosynthetically active radiation intercepting green leaf area lowers the net photosynthetic capability of the infected plants. As a result, alteration to photosynthetic energy assimilation processes adversely affects normal growth, especially the development of grain bearing heads, which in turn reduces the wheat yield (Robert et al., 2006).

Z. tritici is considered a latent necrotrophic pathogen; early in the infection process, the pathogen grows in the apoplastic space, and then switches to a necrotrophic phase where symptoms begin. The infection pathway therefore can be divided in two phases (Kema et al., 1996; Steinberg, 2015), the asymptomatic (latent) phase and the symptomatic (necrotrophic) phase.

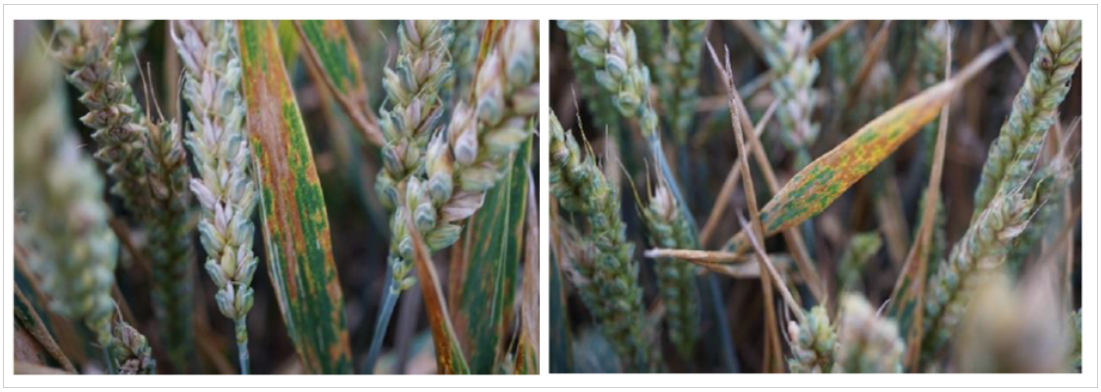


Figure 1-2. Flag leaves of wheat showing typical STB symptoms (field trial, Sutton Bonington 2017).

a) Asymptomatic phase

Z. tritici hyphae invade the host exclusively through the stomata (Rudd, 2015; Rudd et al., 2015; Steinberg, 2015). This contrasts with other pathogenic fungi that directly penetrate the host through specialised structures, such as the appressoria formed by *Magnaporthe oryzae* (Dagdas et al., 2012). More evidence of this invasive morphology comes from the fact that the genome of *Z. tritici* contains only 28 genes that encode plant cell wall degrading enzymes (PCWDE), which is a much smaller number as compared to other non-biotrophic plant pathogens (Goodwin et al., 2011). Furthermore, the majority of the PCWDE coding genes are expressed when switching from the asymptomatic to symptomatic phase (Brunner et al., 2013). The digestion of host cell wall by those enzymes releases polysaccharides, which act as

pathogen associated molecular patterns (PAMPs) and trigger PAMP-triggered immunity (PTI) (Boyd et al., 2013). Thus, it appears that *Z. tritici* has adapted to exclusive stomatal penetration and fine-tuned expression of the PCWDE coding genes to evade immunodetection and minimize PTI response.

The infection begins with the germination of either pycnidiospores or ascospores, both of which are pathogenic, upon contact with the leaf and the initiation of hyphal growth. These infectious propagules must adhere to the hydrophobic surface of wheat leaves in order to initiate the STB disease cycle. Fungal pathogens secrete hydrophobin proteins that play a role in adherence to the plant tissue (Perez-Nadales et al., 2014). Transcriptional data from *Z. tritici* (Yang et al., 2013; Rudd et al., 2015) show that four class II hydrophobin transcripts namely Mycgr3G48129, Mycgr3G40724, Mycgr3G96543 and Mycgr3G95491 were highly up regulated at early stages of infection. Spore germination occurs within 12-24 hours and hyphae enter the host's tissue via the stomatal openings (Shetty et al., 2003; Suffert et al., 2011). This rapid detection and adaptation to the host environment is evident from the high expression of around 200 *Z. tritici* genes within 24 hours after infection (hai) (Rudd, 2015; Rudd et al., 2015).

This phase of infection typically ranges from 8 to 14 days, and in some cases even 42 days, depending on climatic conditions and wheat cultivars (Lovell et al., 2004). During this latent period, no symptoms of disease are visible and the leaves appear healthy. Duration of this phase depends on the wheat genotype-fungal isolate combination and on the environmental conditions. As the fungus does not engage in biotrophic feeding and remains restricted to nutrient deficient apoplastic cavities within the mesophyll layer (Kema et al., 1996), *Z. tritici* can be better described as a latent necrotroph rather than a hemi-biotroph (Sánchez-Vallet et al., 2015). *Z. tritici* spores are rich in lipids and fatty acids, which are thought to provide the nutrition and energy for growth during disease initiation and asymptomatic phase of infection (Rudd, 2015; Rudd et al., 2015). This notion is strengthened by the early stage (between 24 and 96 hai) upregulation of genes encoding proteins that function in lipid and fatty acid transport and catabolism through β-oxidation and the glyoxylate cycle (Rudd, 2015; Rudd et al., 2015). Stored lipids and

fatty acid reserves are key source of energy in several necrotrophic fungal pathogens such as *Parastagonospora nodorum* and *Leptosphaeria maculans*, which cause Septoria nodorum blotch in wheat and blackleg disease in Brassica species, respectively (Idnurm & Howlett, 2002; Solomon et al., 2004). Therefore, the early stage upregulation of lipid metabolism in *Z. tritici* implies that, similarly to necrotrophic pathogens, this fungus is likely utilising stored lipid reserves to produce energy for sustaining minimal growth during the early stages of infection.

b) Symptomatic phase

The first signs of disease are chlorotic lesions followed by the development of necrotic areas known as “blotches” that appear at approximately 10-12 days post infection (dpi), and pycnidia formation in these lesions is initiated (Rudd et al., 2015; Steinberg, 2015). The disintegration of the host’s tissues due to plant cell death characterises the “necrotrophic” phase of infection. During this phase, the nutrients required for fungal growth are released from the plant cells, leading to rapid increase in the fungal biomass and ultimately the formation of mature pycnidia, which produce the pycnidiospores. Pycnidia develop underneath the stomata of infected wheat leaves and remain embedded in the plant epidermis (Kema et al., 1996; Steinberg, 2015). They vary in size, usually ranging from 60 to 200μm, depending on the fungal strain and on the intensity of the infection, but also with stomata density variations of wheat cultivars.

1.1.4 Disease management

There are different approaches that can be followed when a disease needs to be controlled depending on environment and/or pathogen involved and the available resources. Manipulating husbandry can play a key role in management, however, in modern agriculture fungicides are mostly employed. Epidemiological principles then become important in helping to time fungicide applications with greater precision in order to optimise dose, minimise applications and maximise effectiveness. For winter wheat, the priority is to

control foliar diseases on the upper two and, less essentially, third leaves. The lower leaves contribute relatively little to final dry matter but can act as potent sources of inoculum for the more important upper foliage (Cook and Yarham, 2006). Integrated disease control strategies comprising of fungicides applications, deployment of resistant wheat cultivars and agronomic practices are thought to be the best potential long-term solution for sustainable STB disease control (Torriani et al., 2015). Agronomic practices, such as modification of the crop canopy, significantly reduce STB disease incidence by minimising inoculum dispersal (Arraiano et al., 2006). Such strategies can be implemented by growing tall wheat cultivars (Arraiano et al., 2006; Brown et al., 2015). However, consideration must be taken as tall wheat cultivars are prone to lodging, especially during heavy rainfall and winds, which causes yield losses. Therefore, yield penalties may remain unchanged although the cause of wheat yield loss may shift from STB disease to lodging (O'Driscoll et al., 2014). Mixtures of susceptible and resistant wheat cultivars also reduce losses to STB disease by up to 45% as compared to single cultivar cropping systems (Gigot et al., 2013). However, mixing the cultivars could affect consistency of quality traits such as gluten or protein content, which can be precisely maintained in single cultivar cropping systems. Therefore, the practical difficulties in implementing such agronomic interventions present a major bottleneck in their wider uptake as a part of integrated STB control strategies (O'Driscoll et al., 2014).

Fungicides are the dominant strategy for combating STB outbreaks (O'Driscoll et al., 2014, Torriani et al., 2015). The three major fungicide classes that have been used for the control of STB over the past ~ 20 years are demethylation inhibitors (DMIs), quinone-outside inhibitors (QoIs) and succinate dehydrogenase inhibitors (SDHIs), all belonging to the "Respiration Inhibitors" category (Walter, 2011). DMIs target sterol biosynthesis, the dominant component of fungal cell membrane, by inhibiting the enzyme 14-a-sterol demethylase (a cytochrome P450) encoded by the *cyp51* gene. QoIs inhibit energy metabolism by blocking electron transfer in the respiration chain. SDHIs bind to the ubiquinone reduction site of complex II and inhibit succinate dehydrogenase, an enzyme in complex II within the fungal mitochondrial

respiration chain, causing an interruption of the respiration by affecting both the generation of energy and the formation of precursors needed for the synthesis of essential cellular compounds, such as amino acids (Walter, 2011).

Importantly, there has been loss of sensitivity to QoI and triazole fungicides since the early 2000s (Fraaije et al., 2005; 2007). Fungicide resistance may result from single or multiple gene mutations, starting from a very low natural rate of mutations, while it is inherited and will eventually become dominant in pathogen populations under selection pressure of fungicide use over time, resulting in failure of disease control (Ma & Michailides, 2005). Applying appropriate products at the right time and at the right dose is critical for effective disease control. Poor field performance can often be attributed to cutting recommended rates of use, or to poor or mistimed application, rather than resistance. Good resistance management is vital to maintain effective control by limiting the level of exposure of the target pathogen to the fungicide, thus using fungicides in integration with other crop management techniques such as disposal of crop debris, control volunteer plants, crop rotations etc., and in mixtures with other fungicides with different modes of action. It is therefore increasingly important for farmers to select disease resistant wheat varieties with optimal quality and high yield.

1.1.5 *Stb* resistance genes

There are different sources of resistance that breeders use. For example, land races or related species of the plant of interest may hold resistance genes for pathogens, or resistance can be achieved by mutation breeding and genetic modification (Breseghello & Siqueira Guedes Coelho, 2013). Unfortunately, introduction of resistance genes in varieties may have a drawback in yield and quality of the final product. This could appear with pleiotropic effects, where a resistance gene influences seemingly unrelated phenotypic traits, or with linkage drag, where the resistance genes are located on segments of chromosomes that reduce yield (Breseghello & Siqueira Guedes Coelho, 2013). Another instance would be competition drag, where there is a delay in the deployment of a useful gene because of the additional

time needed to raise yield and quality to the standard of the current market-leading cultivars (Brown & Rant, 2013).

Resistance to STB may be qualitative (isolate-specific) or quantitative (Chartrain et al., 2004). Isolate-specific resistance is near-complete, oligogenic, effective against particular isolates and follows a gene-for-gene relationship (Brading et al. 2002); whereas quantitative or partial resistance is incomplete, polygenic and isolate non-specific. Resistance to the pathogen may not always be durable, since the pathogen *Zymoseptoria tritici* is genetically diverse and may reproduce sexually several times during wheat's growing season, resulting in breakdown of the resistance genes. To date, 22 major genes (*Stb*) for resistance to STB have been identified and mapped on the wheat genome so far worldwide (Goodwin 2007; Brown et al. 2015), although without knowing the underlying mechanism in the majority of them, and over 100 resistance quantitative trait loci (QTLs), all spread across the wheat genome. However, varieties carrying *Stb* genes differ in their interaction with different strains of the pathogen (Brading et al., 2002; Chartrain et al., 2005) (Table 1-1). In the field, some *Stb* genes have been quite durable, while others have failed due to rapid evolution and genomic plasticity of *Z. tritici* (Adhikari et al. 2004a; 2004b). Also, resistance conferred by major resistance genes is narrow and often it only applies to specific isolates (gene-for-gene relationship). For example, *Stb15*, which confers resistance to the Ethiopian *Z. tritici* isolate IPO88004 (Arraiano & Brown, 2006) is widely present in European wheat cultivars, but is not associated with STB resistance there (Arraiano et al., 2009). This narrow resistance can lead to rapid breakdown, as *Z. tritici* evolves to overcome the individual disease resistance genes. A recently discovered Stb16q resistance locus was reported to confer broad spectrum resistance (Ghaffary et al., 2012) but recent reports suggest that this resistance has also been overcome (Kildea et al., 2020; Orellana-Torrejon et al., 2022). One of those genes, *Stb6*, is widely distributed in elite varieties and has demonstrated good levels of increased field resistance (Chartrain et al., 2005). Both gene-for-gene specific interactions and QTL quantitative resistance between wheat cultivars and *Z. tritici* isolates are an important

aspect in order to confer full resistance in the field and is actively investigated in modern breeding strategies.

Table 1-1. The major genes for resistance of *Triticum aestivum* to STB that have been discovered so far, with their chromosomal locations, corresponding avirulent *Z. tritici* isolates and resistant source line/variety. Modified from Brown et al., 2015.

Gene	Chromosome	Avirulent inoculum	Resistance source
Stb1	5BL	IN95-Lafayette-1196-WW 1-4 & Purdue local (USA)	Bulgaria 88
Stb2	1BS	Paskeville local (Australia) (and IPO92034)	Veranopolis
Stb3	7AS	Paskeville local isolate (Australia)	Israel 493
Stb4	7DS	IN95-Lafayette-1196-WW 1-4, I-89, IPBr1	Tadinia
Stb5	7DS	IPO94269	Synthetic 6x
Stb6	3AS	IPO323	Flame, Hereward
Stb7	4AL	MG2 (Canada) (and IPO87019)	ST6
Stb8	7BL	IN95-Lafayette-1196-WW 1-4	Synthetic W7984
Stb9	2BL	IPO89011	Courtot, Tonic
Stb10	1Dc	IPO94269 and ISR8036	Kavkaz-K4500
Stb11	1BS	IPO90012	TE9111
Stb12	4AL	ISR398 and ISR8036	Kavkaz-K4500
Stb13	7BL	MG96-36, MG2 (Canada)	Salamouni
Stb14	3BS	MG2 (Canada)	Salamouni
Stb15	6AS	IPO88004	Arina, Riband
StbSm3	3AS	MG96-36, MG2 (Canada)	Salamouni
Stb16q	3DL	IPO88018 and IPO94218	SH M3
Stb17	5AL	IPO88018	SH M3
Stb18	6DS	IPO323, IPO98022, IPO89011, IPO98046	Balance
StbWW	1BS	79, 2, 1A	WW1842, WW2449, WW2451
TmStb1	$7A^{m}S$	IPO323	MDR043 (*T. monococcum*)

1.1.6 The resistance gene *Stb6*

Stb6 is the most well characterized gene for resistance to STB, which, based on phenotypic evaluation, was reported to be present in wheat used in breeding programs worldwide (Brading et al., 2002; Chartrain et al., 2005). It is inherited as a semi-dominant trait and controls a gene-for-gene type resistance effective against *Z. tritici* isolates, such as IPO323, carrying a matching *AvrStb6* gene encoding small cysteine-rich effector protein. *Stb6* is particularly interesting because, whilst other disease resistance genes involved in gene-for-gene interactions induce hypersensitive response (HR) upon recognition of their respective effectors, *Stb6*-mediated resistance response lacks HR. *Stb6* resides in the subtelomeric portion on 3AS in wheat varieties such as Flame, Chinese Spring (CS) and Cadenza (Cad) (Saintenac et al., 2018). Using a map-based cloning approach, it was shown that *Stb6* encodes a conserved wall-associated receptor kinase (WAK)-like protein, which detects the presence of a matching apoplastic effector and confers pathogen resistance without HR (Saintenac et al., 2018). Receptor-like protein kinases (RLKs) are a large transmembrane protein family with a N-terminal region extending into the apoplast and a C-terminal kinase domain that resides inside the cytoplasm and transfers the signals into the intracellular environment. Specifically, wall-associated kinases (WAKs) are a class of cell surface immune receptors that are gaining interest, as they have been shown to recognise diverse invasion molecules by pathogens and orchestrate either broad-spectrum immunity or gene-for-gene interactions. Incompatible interactions involving *Stb6* usually result in very few disease symptoms, with none or very little chlorosis/necrosis and no pycnidia (Rudd et al., 2008). In-depth phenotyping of *Stb6* cv. Flame inoculated with IPO323 also reported inhibition of hyphal growth following stomatal penetration, accompanied by the accumulation of H_2O_2 in the substomatal cavity (Shetty et al., 2003). Upon inoculation with *Z. tritici*, the expression levels of *Stb6* were upregulated approx. 2-fold compared to mock-inoculated plants, up until 17dai (Saintenac et al., 2018).

1.2 Plant Immunity

1.2.1 PAMP Triggered Immunity (PTI) and Effector Triggered Immunity (ETI)

Plants, due to their sessile nature, are constantly exposed to a wide variety of biotic and abiotic environmental stresses for which they need to be able to adapt and respond accordingly if they are to successfully grow and reproduce. Biotic stresses include attacks by pathogenic microorganisms such as fungi, bacteria and viruses and plants have developed an intricate, multi-layered innate immune system that allows them to perceive the pathogen and coordinate their defence response (Freeman & Beattie, 2008). They have developed phenotypic traits that provide them with a physical barrier against their pathogens and pests (passive resistance), e.g., waxy or hairy leaves, increased deposition of lignin in tissues, as well as inner molecular mechanisms that are activated once a microorganism has entered the plant tissue or has broken the physical barrier (Freeman & Beattie, 2008). In addition, a plant can be either tolerant or resistant to a microorganism. Tolerance is characterised by the least impaired functionality of the plant in the presence of the pathogen, whereas resistance is expressed when the pathogen is counter attacked by the host and its pathogenicity factors cannot function or are neutralised by the plant (Pagán & García-Arenal, 2018).

Two branches of the plant immune system are recognised, initially proposed in the early 2000's by Jones & Dangl (2006) and it was termed as "the zig-zag model": PTI (PAMP-Triggered Immunity) and ETI (Effector-Triggered Immunity). PTI is triggered by the recognition of pathogen- or microbe-associated molecular patterns (PAMPs or MAMPs), which are conserved, pathogen-derived molecules such as the bacterial flagellin and fungal cell wall chitin and other polysaccharides (Jones & Dangl, 2006; Latgé, 2010). This recognition is based upon conserved plasma membrane-associated Pattern Recognition Receptors (PRRs), such as Receptor-Like Kinases (RLKs) (Jones & Dangl, 2006; Zipfel, 2009; Dodds & Rathjen, 2010; Thomma et al., 2011; Tang et al., 2017). PTI comprises of accumulation of reactive oxygen species (ROS), increase of cytoplasmic calcium (Ca^{2+}), cation

and anion effluxes, production of hydrolytic enzymes and low molecular weight antimicrobial compounds known as phytoalexins as well as biosynthesis of salicylate (SA), a key defence hormone (Tang et al., 2017). Pattern-triggered ROS production is required for stomatal closure and deposition of callose, a plant cell wall strengthening material (Mersmann et al., 2010; Macho et al., 2012). Pathogens overcome PTI by secreting effector molecules in the apoplast or directly inside the host cells in order to reprogram host cell metabolism and physiology to aid their colonisation (Lo Presti et al., 2015). Typically, the secreted effector proteins are characterised by cysteine rich content, small size and extracellular secretion sequence and are termed as small-secreted proteins (SSPs) (do Amaral et al., 2012; Vleeshouwers & Oliver, 2014; Mirzadi Gohari et al., 2015). In parallel to PTI suppression and subsequent effector triggered susceptibility, the effectors get recognised through direct or indirect interactions with the host intracellular receptors known as disease resistance (R) proteins, resulting in the activation of ETI (Jones & Dangl, 2006; Dodds & Rathjen, 2010). Most R proteins belong to the NB-LRR (Nucleotide Binding Site-Leucine Rich Repeat domain) class. ETI-derived defence is often but not always associated with accumulation of ROS that leads to host cell death of the affected cells, also known as the Hypersensitive Response (HR) (Jones & Dangl, 2006; Dodds & Rathjen, 2010). Pathogens have evolved to overcome ETI either by negatively selecting to lose the genotypes containing ETI-triggering effectors and/or positively selecting to gain multiple, additional ETI-suppressing effectors, which effectively reinstate susceptibility (Paulus & van der Hoorn, 2018). In turn, evolution of the R protein has enabled recognition of ETI-suppressing effectors and reinforcement of ETI response. Therefore, in incompatible reactions no disease will occur as the R protein will recognise the avirulence gene (*avr*) from the invading pathogen. If either the *R* or *avr* gene is lacking in either the host or the pathogen, disease will occur and the reaction will be compatible. PTI is considered to confer resistance to a broad spectrum of pathogens and it is thought of as a weak defence response, whereas, in contrast, ETI is thought to confer a narrower, isolate-specific, gene-for-gene resistance and is a much stronger and faster defence response (Dodds & Rathjen, 2010;

Thomma et al., 2011). A schematic representation of plant immunity cascade events among the different organelles is shown in Figure 1-3 (Nguyen et al., 2021).

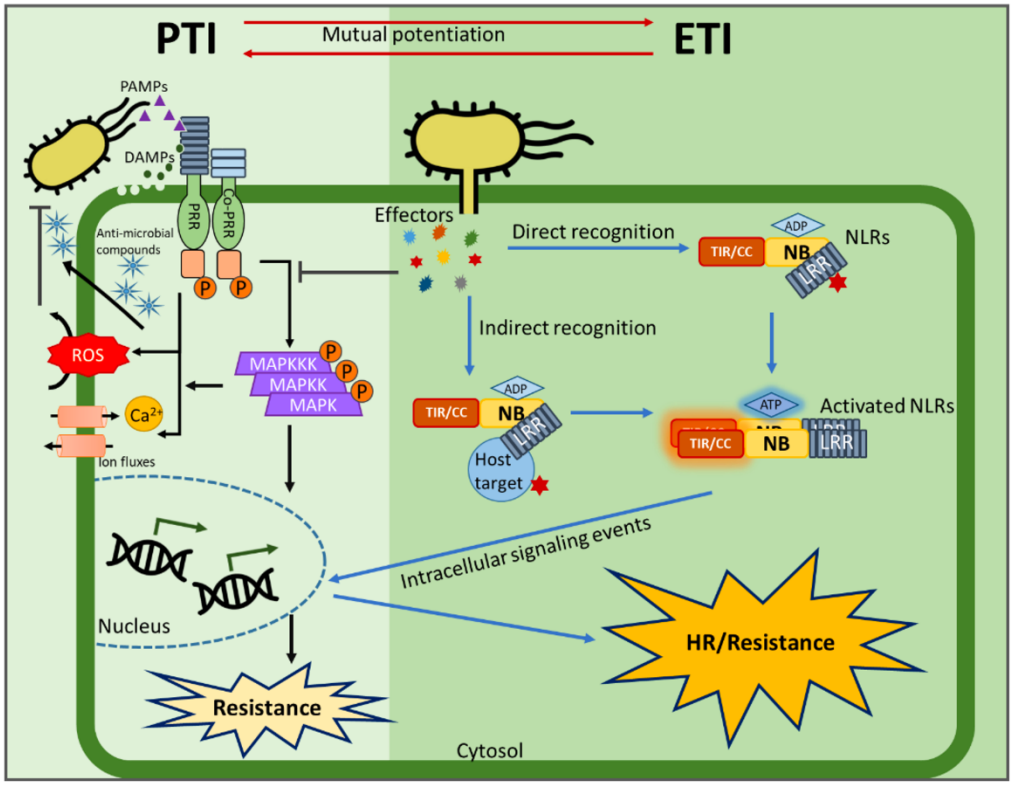


Figure 1-3. A schematic representation of PAMP-triggered immunity (PTI) and effector-triggered immunity (ETI) in plants. PTI events are indicated by black arrows and ETI events are indicated by blue arrows. Image taken from Nguyen et al. (2021).

The zig-zag model has a few limitations, as with new findings from more diverse pathosystems, it is becoming difficult to fit those into the model (Thomma et al., 2011). Kanyuka & Rudd (2019) recently proposed a new model, termed “Invasion model”, which incorporates a spatial dimension to it, reflecting the fact that the immune receptor recognition could take place either in the apoplast (cell surface immune receptors) or inside the cell (intracellular immune receptors). This Spatial Invasion Model highlights the importance of Cell Surface-localised Immune Receptors (CSIRs). These are membrane-bound proteins with extracellular domains involved in the recognition of apoplastic invasion molecules, specifically for those pathogens that colonize the apoplastic spaces and grow in close contact with the leaf mesophyll cells

but never penetrate them, such as the fungi *Zymoseptoria tritici*, *Leptosphaeria maculans*, *Mycosphaerella fijiensis* and *Passalora fulva* that infect wheat, oilseed rape, banana and tomato, respectively (Kanyuka & Rudd, 2019). There are several CSIRs, or receptor-like kinases (RLKs), in plants that have been identified in the model plant *Arabidopsis thaliana*, such as FLAGELLIN-SENSITIVE 2 (FLS2; Gómez-Gómez and Boller, 2000), ELONGATION FACTOR TU RECEPTOR (EFR; Zipfel et al., 2006), CHITIN ELICITOR RECEPTOR KINASE 1 (CERK1; Miya et al., 2007) and CHITIN ELICITOR-BINDING PROTEIN (CEBiP; Kaku et al., 2006). RLKs and RLPs (receptor-like proteins, similar to RLKs but with no intracellular kinase domain) recognise a wide range of invasion molecules and can be grouped into several classes based on the presence of specific motifs in their extracellular domains. For instance, leucine-rich repeat (LRR) containing receptors (e.g. FLS2) detect proteinaceous invasion molecules, whereas lysin motif (LysM) containing receptors (e.g. CERK1) bind to carbohydrates (Bouwmeester & Govers, 2009).

Detection of invasion molecules by CSIRs initiate signalling through a series of plasma membrane-localised phosphorylation/dephosphorylation events, that in turn activate corresponding immune response mechanisms. The signal is internalised through the activation of coreceptors, such as mitogen-activated protein kinases (MAPKs), Ca^{2+} -dependent protein kinases (CDPKs) and brassinosteroid insensitive 1-associated receptor kinase 1 (BAK1) (Kobayashi et al., 2012; Dubiella et al., 2013; Kadota et al., 2015). The downstream chain of events includes the activation of NADPH oxidases, in plants known as respiratory burst oxidase homologues (RBOHs), induction of ROS, induction of WRKY transcription factors and upregulation of immune-related genes (Kadota et al., 2014). RBOHs are responsible for the apoplastic oxidative burst (production of ROS), stomata closure and activation of signalling molecules such as salicylic acid (SA), jasmonic acid (JA), ethylene (ET) and abscisic acid (ABA). Calcium signals can also get transmitted to the chloroplast and rely on the presence of the thylakoid-associated calcium-sensing receptor (CAS) (Nomura et al., 2012). CAS regulates the PAMP-induced expression of defence genes and inhibits chloroplast-mediated transcriptional reprogramming, likely through an $^1O_2$-mediated pathway

(Nomura et al. 2012). Therefore, another ROS burst can take place inside the chloroplast to support cell death and the production of more signalling hormones (Göhre, 2015). The importance of CAS and Ca^{2+} signalling in defence response was demonstrated in a study using *cas-1* mutants which showed impaired resistance to strains of *P. syringae*, severely compromised PTI responses (such as stomata closure, callose deposition and accumulation of defence-related compounds) and suppressed/delayed ETI responses (such as localised cell death) (Nomura et al., 2012). Eventually, transcription regulators such as WRKYs activate defence genes and pathogenesis-related proteins (PR) in the nucleus (Stael et al., 2015).

1.2.2 The Wheat – *Z. tritici* pathosystem

During the asymptomatic phase, fungal presence triggers host immune response within 48 hai, as evident from chloroplast accumulation near the host cell walls and in contact with the *Z. tritici* hyphae (Kema et al., 1996). Between 72 and 120 hai, H_2O_2 accumulates in the vicinity of *Z. tritici* hyphae within the host cell walls and within the sub-stomatal cavities (Shetty et al., 2003). In addition, the detection of the pathogen from wheat leads to elevated expression of genes encoding for pathogen resistance (PR) proteins (Ray et al., 2003) and fungal cell wall degrading enzymes (Shetty et al., 2003, 2007, 2009). It is speculated that fungal cell wall polysaccharides, especially glucan and chitin, which are also key PAMPs that elicit PTI (Latgé, 2010), play a key role in detection of *Z. tritici* by wheat. Indeed, the β-(1,3)- glucan isolated from the *Z. tritici* cell wall has been shown to mediate PTI response during early stages of STB infection (Shetty et al., 2007; 2009).

Suppression of PTI by *Z. tritici* is evident from the reduced expression of wheat genes encoding defence related proteins, WRKY transcription factors, MAPKs and receptor kinases, and proteins involved in biosynthesis of defence signalling molecules, such as jasmonic acid and oxylipin, and lignin biosynthesis (Rudd et al., 2015). Thereafter, *Z. tritici* has evolved a variety of small secreted proteins (SSPs) which function as effectors (do Amaral et al., 2012) and are expressed in successive waves to correspond with typical stages of the bi-phasic infection cycle (Mirzadi Gohari et al., 2015). Such

waves of effector expression are common in fungal pathogens which engage in transition from asymptomatic to symptomatic phases, such as *Colletotrichum higginsianum* and *Colletotrichum graminicola* which infect *Arabidopsis thaliana* and maize (*Zea mays*), respectively (Mirzadi Gohari et al., 2015). Around 38% of the *Z. tritici* SSP coding genes were differentially expressed at various stages of the infection cycle and 16% showed peak expression within 24 hai (Rudd et al., 2015). This expression of the *Z. tritici* SSPs is similar to *M. oryzae*, which supresses PTI by secreting effectors (Mentlak et al., 2012) and showed early stage upregulation of more than two hundred SSP coding genes (Kawahara et al., 2013). Although a large number of SSPs have been suggested as putative effectors, however, only one *Z. tritici* effector, denoted as Mg3LysM, has been cloned to date (Marshall et al., 2011). Mg3LysM suppresses PTI by interfering with the wheat CERK1 receptor kinase and the CEBiP receptor-like proteins, which serve to detect this pathogen by recognising chitin, an important fungal cell wall component (Lee et al., 2014). The *Z. tritici* Mg3LysM is an ortholog of the *M. oryzae* effector Slp1, which is highly expressed during infection (Kawahara et al., 2013) to supress the PTI response in rice and to enable spread of the rice blast disease (Mentlak et al., 2012).

The symptomatic/necrotrophic phase leads to the emergence of typical STB disease symptoms, which include macroscopic chlorotic and necrotic lesions and the formation of pycnidia. The molecular mechanisms that signal for this phase transition are unknown, however, it is evident that host cell death plays a major role in the switch from asymptomatic to symptomatic phase. The host cell death is mediated through a programmed cell death (PCD)-like response leading to leakage of the host cytosolic components into the apoplastic cavities (Keon et al., 2007). In addition, ROS accumulation and activation of wheat defences by homeodomain protein TaR1 are also essential for normal switch to symptomatic phase of infection (Keon et al., 2007; O'Driscoll et al., 2014; Lee et al., 2015). Downregulation of *TaR1* gene, through gene silencing, impaired the transcriptional activation of the wheat genes with open chromatin and lead to early appearance of STB disease symptoms and reduced fungal sporulation (Lee et al., 2015). In addition to the host cell death

and the TaR1 protein, the switch to the symptomatic phase also overlapped with up- and downregulation of several wheat genes which encode proteins involved in biotic stress resistance, transport, metabolism, signal transduction and photosynthesis (Yang et al., 2013; Rudd et al., 2015). Overall, it appears that major molecular reprogramming of host defence plays a key role in modulating the switch from the asymptomatic to symptomatic phase of STB infection. In *Z. tritici*, switch to the symptomatic phase coincided with the biggest wave of gene expression involving peak expression of more than 24% SSP coding genes (Rudd et al., 2015).

Plants are well known to engage in PCD response upon ROS production in order to control the spread of a pathogen, however, in the wheat - *Z. tritici* pathosystem, the fungal biomass exponentially increases following host cell death (Keon et al., 2007, Shetty et al., 2007, Rudd, 2015). Thus, *Z. tritici* undermines the PCD mediated host defences to fuel the increase in fungal biomass possibly by utilising leaked host cytosolic contents including several polysaccharides (Shetty et al., 2009, Rudd, 2015). The increase in fungal biomass further escalates the host tissue collapse, which coincides with maturation of the pycnidia and formation of secondary inoculum, the asexual pycnidiospores.

1.2.3 Necrotrophic effectors

Biotrophic and hemi-biotrophic fungal and oomycete pathogens have evolved sophisticated methods for acquiring nutrition, whilst also suppressing the defence reactions that might have been otherwise triggered in these cells (Hammond-Kosack & Rudd, 2008). Their effectors, normally avirulence (*Avr*) genes, promote virulence in the absence of resistance (R) genes by suppressing innate immune responses, such as PAMP-triggered immunity (Vleeshouwers & Oliver, 2014). This effector-triggered susceptibility (ETS) allows the establishment of the biotrophic interaction and is essential during the early infection phases, in line with the peak expression of *Avr* genes at these early time points (Vleeshouwers & Oliver, 2014). However, necrotrophic pathogens overcome plant defences by secreting effector molecules in the apoplast or directly inside the host cells in order to reprogram host cell

metabolism and physiology to aid their colonisation, through the combined action of cell wall degrading enzymes, effector molecules and toxins, that ultimately result in host cell death, tissue necrosis and nutrient acquisition for the pathogen (Hammond-Kosack & Rudd, 2008; Lo Presti et al., 2015). Effectors of necrotrophic pathogens were originally designated as host-selective toxins (HST) and they encompass a range of molecular forms, from polyketides and non-ribosomal peptides to proper proteins (Vleeshouwers & Oliver, 2014). Effector proteins are narrowly defined as small, cysteine rich, secreted proteins (Shao et al., 2021). Effectors have a highly specific role during infection and their expression is tightly regulated throughout the infection cycle (Sánchez-Vallet et al., 2018). In addition, as effector molecules get recognised by specialised resistance plant proteins, successful pathogens need to continuously maintain the ability to escape host recognition and maintain virulence (Sánchez-Vallet et al., 2018). Evolution toward evasion of recognition and functional optimization is achieved by sequence modification, gene deletion, alteration of expression of existing effector genes, and the gain of new effectors (Sánchez-Vallet et al., 2018).

Recent advances in genome and transcriptome sequencing, along with computational prediction tools, suggest there are hundreds of putative effectors present in necrotrophic pathogens genomes (Sperschneider et al., 2016; le Marquer et al., 2019). In cereals, and specifically wheat, there has been extensive research on necrotrophic effectors (NEs) from economically important, adapted wheat pathogens, such as *Zymoseptoria tritici*, *Parastagonospora nodorum* and *Pyrenophora tritici-repentis*. Their effectors produce highly specific molecules to initiate necrosis of the leaf tissue. For *Z. tritici*, several fungal genes have been identified with suspected roles in pathogenicity (Kellner et al., 2014; Rudd et al., 2015; Palma-Guerrero et al., 2016), such as the LysM effectors Mg1LysM and Mg3LysM that are expressed early in the disease progression and are able to sequester chitin, and the necrosis-induced protein MgNLP that is expressed just before the emergence of disease symptoms (Marshall et al., 2011; Lee et al., 2014; Rudd et al., 2015). Additionally, there are two recently discovered avirulence factors of *Z. tritici*, that are recognised by resistance genes and result in incompatible

interactions, *AvrStb6* (Zhong et al., 2017) and *Avr3D1* (Meile et al., 2018). AvrStb6 is recognised by the resistance protein Stb6 in a gene-for-gene interaction that leads to a strong qualitative resistance response, completely blocking the progression of the infection (Brading et al., 2002; Kema et al., 2018; Saintenac et al., 2018). Avr3D1 is an avirulence factor, whose recognition is postulated to be by either *Stb7* or *Stb12*, and triggers an incomplete, quantitative resistance (Meile et al., 2018). *P. nodorum* and *P. tritici-repentis* produce host-specific toxins, such as Tox1 and ToxA respectively, that are recognised by specific sensitivity genes (*Snn1* and *Tsn1*, respectively) (Liu et al., 2004; Manning et al., 2007; Faris et al., 2010). Tox1 was the first HST identified in *P. nodorum* that requires a single host susceptibility locus, Snn1, to confer susceptibility (Liu et al., 2004). *Snn1* gene allows recognition of Tox1 in a light-dependent manner, triggering PCD through oxidative burst and a strong upregulation of pathogenesis-related (PR) genes (Liu et al., 2012). Recently, Tox1 was shown to have a chitin-binding domain, which presumably acts in protecting fungal cell walls from degradation by plant chitinases (Liu et al., 2016). *Tsn1* is required for plant susceptibility to ToxA, although *Tsn1* does not directly interact with ToxA (Faris et al., 2010). ToxA translocates into plant cells possibly through the recognition of arginine-glycine-aspartic acid (RGD) motif in the protein by a plant surface receptor (Manning & Ciuffetti, 2005) and eventually localises in the chloroplasts leading to light-dependent ROS accumulation and cell death (Ciuffetti et al., 2010). ToxA originated from *P. nodorum* but has been found almost identical in *P. tritici-repentis* and is therefore believed that *P. tritici-repentis* acquired ToxA from *P. nodorum* by horizontal gene transfer (Friesen et al., 2006).

1.2.4 Reactive Oxygen Species (ROS)

Rapid production of ROS, called the oxidative burst, is one of the hallmarks in the early stages of incompatible interactions between plants and pathogens. ROS are associated with cell defence, including direct and indirect signal transduction, antimicrobial effects, membrane lipid peroxidation, cell wall modification, induced transcription-dependent defence, and HR cell death in plants (Afzal et al., 2014; Kimura et al., 2017).

ROS are chemically active molecules including superoxide anion (O_2^-), singlet oxygen ($^1O_2$), hydrogen peroxide (H_2O_2) and hydroxyl radical ($^{\bullet}OH$), each with distinct chemical properties and roles in metabolic regulation, development, pathogen defence and abiotic stresses (Mittler et al., 2004; Camejo et al., 2016; Sierla et al., 2016). Sources of ROS include the chloroplasts, peroxisomes, mitochondria and the apoplast. Intracellular production is associated with photorespiration and metabolic processes characterised by high redox potentials, such as photosynthetic electron transport chains (Triantaphylidès & Havaux, 2009; Kimura et al., 2017; Foyer, 2018). In contrast, apoplastic ROS production results from the activation of plasma membrane-localised NADPH oxidases and cell wall peroxidases (Afzal et al., 2014; Choi et al., 2016). Superoxide (O_2^-) produced by NADPH oxidases is rapidly converted to H_2O_2 either spontaneously or by the enzyme superoxide dismutase (SOD) (Shapiguzov et al., 2012). The resulting H_2O_2, along with H_2O_2 produced by cell wall peroxidases, crosses the plasma membrane and enters the cell via free diffusion or aquaporin-facilitated diffusion. Among all ROS, H_2O_2 has been shown to have the most stable chemical properties, to be the most abundant and to play many diversified roles in plant defence (Smirnoff & Arnaud, 2019). H_2O_2 is the trigger for the induction of changes in gene expression, i.e. Systemic Acquired Resistance (SAR). Early in the infection process, transcripts include those involved in the production of secondary metabolism enzymes (phytoalexins). Later in the infection period, induction of transcripts encoding cell wall proteins and peroxidases as well as pathogenesis-related (PR) proteins (chitinases and β-1,3-glucanases) takes place (Camejo et al., 2016). The production of ROS is governed by a large network of genes. Just in *Arabidopsis*, this network consists of a total of 150 genes (Mittler et al., 2004).

During exogenous stress, ROS concentration in plant cells dramatically rises in order to eradicate the stress. High ROS concentrations, however, can at the same time be damaging to the plant cells themselves, leading to lipid peroxidation, protein oxidation, nucleic acid damage, and programmed cell death activation (Sharma et al., 2012). Therefore, plants have evolved various complex mechanisms to keep the concentrations of ROS under balance by

strict surveillance. Chloroplasts, mitochondria and peroxisomes are the key players in providing defence to plants against ROS by the production of several enzymatic and non-enzymatic antioxidants to scavenge ROS (Gill & Tuteja, 2010). A balance between ROS and antioxidants is typically maintained, as the complete eradication of ROS means the loss of an important second messenger in intracellular signalling cascades. Whenever this balance is disturbed, it leads to oxidative stress (Gill & Tuteja, 2010). Major ROS scavengers are enzymes such as glutathione peroxidase (GPX), catalase (CAT), ascorbate peroxidase (APX), and superoxide dismutase (SOD) (Afzal et al., 2014). For instance, as mentioned above, O_2^- produced in the different organelles is rapidly converted to H_2O_2 by the action of superoxide dismutase (SOD) (Alscher et al., 2002). As H_2O_2 is also a destructive oxidant, it is converted by catalases (CATs) and ascorbate peroxidases (APXs) to water and molecular oxygen (Davletova et al., 2005; Miller et al., 2007). Ascorbate is the most important reducing substrate for H_2O_2 detoxification throughout the plant cells with the participation of APXs via the ascorbate-glutathione cycle (Foyer & Noctor, 2011). Antioxidants expression is controlled according to the need for removal of ROS from the cells, with both environmental and developmental stimuli being involved in the regulation. In addition to antioxidant enzymes, ROS can also be neutralized by antioxidant non-enzymatic, phenolic-based chemical scavengers such as flavonoids, ascorbic acid, glutathione, carotenoids, and α-tocopherols (Gill & Tuteja, 2010; Foyer & Noctor, 2011; Afzal et al., 2014). Carotenoids and α-tocopherol are the prominent removers of singlet oxygen in photosystems inside the chloroplast (Apel & Hirt, 2004; Krieger-Liszkay et al., 2008; Havaux, 2014).

ROS can be produced either in the apoplast or inside the chloroplast. As described previously, RLKs on the plasma membrane initially recognise MAMPs in the apoplast which leads to a cascade of defence signalling involving activation of RBOHs and ROS burst (Kadota et al., 2015). One of the events linked with receptor signalling and ROS in the apoplast is stomatal closure. Stomatal movements are in response to environmental stimuli to balance photosynthetic CO_2 uptake and water loss and are regulated by guard cell turgor pressure, generated by anion and water fluxes across the plasma

membranes (Murata et al., 2015). The endogenous factors that regulate these movements are Ca^{2+} fluxes, abscisic acid (ABA) and ROS (Kim et al., 2010). RBOHs are the most studied ROS-producing enzymes in plants and they are involved in stomatal regulation (Sierla et al., 2016). The importance of these enzymes was highlighted in a study by Kwak et al. (2003) in which loss of AtRBOHF in *Arabidopsis* mutants led to partial impairment of ABA-induced stomatal closure, while other *atrbohD atrbohF* double mutants had further reduced stomatal closure and abolished ROS production. The role of ROS in CO_2-induced stomatal regulation was also recently demonstrated as CO_2-induced stomatal closure was absent in the same *atrbohD atrbohF* double mutants (Chater et al., 2014). Further research has also highlighted the function of RBOH-derived ROS in stomatal immunity against plant pathogens, for instance stomata of the *atrbohD* mutant were unresponsive to flg22 and elf18 (bacterial flagellin and elongation factor Tu, respectively) (Mersmann et al., 2010; Macho et al., 2012). While RBOHF plays an important role in ABA-induced stomatal closure, RBOHD is the major isoform involved in stomatal immunity (Macho et al., 2012; Kadota et al., 2014), and multiple studies describe differential RBOHD phosphorylation in response to MAMPs (Kadota et al., 2014; Kimura et al., 2017). RBOHs are activated and regulated by protein kinases, such as OPEN STOMATA 1 (OST1/SnRK2.6) which is a crucial signalling component in ABA-induced stomatal closure (Melotto et al., 2006; Sierla et al., 2016; Qi et al., 2018). The central role of OST1 in stomatal immunity is demonstrated by the phenotypes of *ost1* mutants that fail to respond to flg22 (Melotto et al., 2006). In response to ABA, OST1 phosphorylates and activates AtRBOHF which in turn triggers the accumulation of apoplastic ROS. Apart from OST1, there are other important proteins involved in ABA- and pathogen-mediated stomatal closure and interact with OST1 through phosphorylation events, such as GUARD CELL HYDROGEN PEROXIDE-RESISTANT 1 (GHR1) and SLOW ANION CHANNEL-ASSOCIATED 1 (SLAC1) (Melotto et al., 2008; Vahisalu et al., 2010; Hua et al., 2012; Sierla et al., 2018). GHR1 acts in stomatal closure via SLAC1 activation. The *ghr1* mutation impaired H_2O_2 activation of the calcium channel and ABA and H_2O_2 induction of stomatal closure (Hua et al., 2012).

The oxidative burst and its regulation by antioxidants have been studied for several plant-pathogen interactions, one of which is the wheat-*Z. tritici* pathosystem (Shetty et al., 2003, 2007; Yang et al., 2013). When Yang et al. (2013) inoculated one resistant and one susceptible variety with *Z. tritici*, they observed no symptoms appearing in the resistant variety and a low concentration of fungal DNA. In addition, the resistant variety accumulated high levels of H_2O_2 and other signalling molecules whereas ROS-scavenging enzymes such as SOD were upregulated in the susceptible variety. For *Z. tritici*, H_2O_2 is inhibitory during the early latent phase but can be tolerated during the necrotrophic stage of the fungus (Shetty et al., 2003, 2007). Early accumulation of H_2O_2 during the incompatible interaction is strictly regulated by the host to prevent cell death (Stotz et al., 2014). Also, Ajigboye et al. (2021) showed presence of superoxide only in susceptible genotypes and none in the resistant, accompanied by increases in antioxidant enzymes.

1.2.5 Chloroplastic Defence

More and more recent research is suggesting the chloroplast as a key organelle in defence, as they can integrate multiple environmental stimuli and accommodate biosynthetic pathways of amino acids, hormones, vitamins, secondary metabolites and lipids (Kangasjärvi et al., 2012). Chloroplastic ROS are vital for the onset of immune reactions and the induction of HR and several studies have revealed the contribution of photosynthetic electron transport and light-induced ROS production to the onset of cell death in response to bacterial pathogens (Liu et al., 2007; Bechtold et al., 2008). A first example is the *lesion simulating disease 1* (*lsd1*) mutant which fails to limit the spread of HR when infected with avirulent pathogens or is exposed to excess irradiance levels (Mateo et al., 2004). Double mutants of *lsd1* and *chlorophyll a/b binding harvesting organelle specific* (*cao*) display reduced PSII antenna size due to deficient folding of the light-harvesting antenna proteins (Mateo et al., 2004). These mutants are incapable of up-regulating genes encoding Cu/Zn SOD and CAT and indicate the significance of PSII electron transport in HR and cell death. Further analysis provided evidence that the light-dependent defence and death signals most probably originate from reduction of the plastoquinone

pool and are relayed to the nuclear genome through the cytosolic components LSD1, ENHANCED DISEASE RESISTANCE 1 (EDS1), and PHYTOALEXIN DEFICIENT4 (PAD4), which form central regulatory nodes in plant immunity (Mühlenbock et al., 2008). In another example, infiltration of wild-type tobacco leaves with a non-host pathogen *Xanthomonas campestris* pv. *vesicatoria* (Xcv) resulted in increased ROS accumulation, preceding the appearance of localised cell death, however, in Xcv-inoculated tobacco plants with compromised chloroplastic ROS production, localised cell death was significantly reduced (Zurbriggen et al., 2009). Overexpression of thylakoid-bound APX resulted in delayed HR and reduced symptoms (Yao & Greenberg, 2006) whereas in another study, by silencing a H_2O_2-scavenging enzyme, they showed enhanced spreading of *P. syringae*-induced PCD and enhanced bacterial growth and disease susceptibility (Ishiga et al., 2012). Chloroplastic ROS also upregulate the expression of defence-related genes in the nucleus. Silencing thylakoid-bound APX, resulted in increased levels of chloroplastic H_2O_2, accumulation of the stress hormone salicylic acid and activation of defence-related nuclear genes (Maruta et al., 2012).

Plant defence hormones are also tightly regulated by the chloroplasts. All major defence related hormones, namely jasmonic acid (JA), salicylic acid (SA), abscisic acid (ABA) and ethylene (ET), are either synthesized in the chloroplast or are induced through chloroplastic signalling (Robert-Seilaniantz et al., 2011; Denancé et al., 2013; Lu & Yao, 2018). ROS originating from the chloroplast readily oxidise the polyunsaturated fatty acids located in the thylakoid membranes, leading to lipid peroxidation. However, this initiates the biosynthesis of oxylipins, which, through the lipoxygenase (LOX) enzymatic pathway, lead to the formation of the messenger molecules 12-oxo-phytodienoic acid (OPDA), jasmonic acid (JA) and methyl jasmonate (MeJA) (Demmig-Adams et al., 2013). SA is synthesized via two routes, one of which, the isochorismate synthase (ICS) pathway, takes place inside the chloroplast and has been proposed as a retrograde signal generated by impaired PSII proteostasis (Duan et al., 2019). ABA is derived from xanthophylls as described above (Ton et al., 2009). Finally, ET is another important hormone involved in biotic stress and one of its precursor molecules, methionine, is

produced in the chloroplast (Ravanel et al., 2004). ET has been found to influence photosynthesis by regulating stomatal aperture, chlorophyll content, the expression of the chlorophyll a/b binding protein (CAB) and PSII and PSI efficiency (Ceusters & van de Poel, 2018).

Finally, it has been shown that pathogens can produce their own hormones as a virulence strategy or secrete effectors that directly target the chloroplasts (Denancé et al., 2013; Littlejohn et al., 2021). For instance, *Botrytis cinerea* and *Rhizoctonia solani* produce ABA, although through a different metabolic pathway than the one in plants. The role of ABA as a virulence factor has not been fully demonstrated but one hypothesis is that it contributes to the plant's susceptibility by suppressing the defence responses (Sánchez-Vallet et al., 2012). Moreover, chloroplast-targeting effectors have been found in bacteria (for example Jelenska et al., 2007; Zabala et al., 2015) and fungi (for example Manning et al., 2007; Xu et al., 2019; Tang et al., 2020; Wang et al., 2021).

Therefore, it is evident that the chloroplast is not a stand-alone cell organelle, only responsible for photosynthesis and energy supply, but it is intrinsically connected and involved with stress responses in all other compartments of a plant. However, a deep understanding of chloroplastic processes is required in order to understand and explore its possibilities in plant defence.

1.3 Photosynthesis, Photoprotection and Signalling

1.3.1 Structure and function of the photosynthetic apparatus

Photosynthesis is one of the most important biological processes on earth. It uses physicochemical processes to transform light energy into chemical energy through the fixing of carbon dioxide (CO_2) into starch or sugars (Murchie et al., 2015). Photosynthesis begins with the absorption of light by pigments and molecules located in the thylakoid membrane, whereby light energy excites chlorophyll molecules before it gets converted into chemical energy in the form of nicotinamide adenine dinucleotide phosphate (NADPH) and adenosine triphosphate (ATP) (Johnson, 2016). There are four

major protein complexes inside the thylakoid membranes, namely Photosystem I (540 kDa), Photosystem II (250 kDa), ATP synthase (520 kDa), and Cytochrome *b6f* complex (260 kDa) (Yamori & Shikanai, 2016).

Of the four major complexes, Photosystem II (PSII) plays a large role in overall photosynthesis as it has the ability to absorb photons from photolysis and transfer the excess electrons produced from the water molecules to plastoquinone (linear electron transport), which in turn results in the proton-motive force that drives photosynthesis (Nelson & Yocum, 2006). PSII is a multi-component pigment-protein complex, whereby the components can be classified into core proteins, low molecular mass proteins, extrinsic oxygen-evolving complex (OEC) proteins and light-harvesting complex II (LHCII) proteins. Namely, these proteins are D1 and D2 (i.e., PsbA and PsbD; Psb stands for PSII), core antenna proteins CP43 and CP47 (i.e., PsbC and PsbB), cytochrome b_{559} subunits α and β (i.e., PsbE and PsbF) and the low molecular mass proteins PsbH, PsbI, PsbJ, PsbK, PsbL, PsbM, PsbR, PsbTc (chloroplast-encoded), PsbTn (nuclear-encoded), PsbW, PsbX, PsbY and PsbZ (Nickelsen & Rengstl, 2013). The OEC contains the proteins PsbO, PsbP and PsbQ subunits (Theis & Schroda, 2016). Finally, LHCII contains three major trimeric PSII light-harvesting chlorophyll *a/b*-binding (LHCB) proteins LHCB1, LHCB2 and LHCB3 and three minor monomeric LHCB proteins LHCB4, LHCB5 and LHCB6 (Lu, 2016). All light-harvesting outer antenna proteins are encoded by the nuclear genome, whereas the majority of the core proteins (reaction centres, RCs) are encoded by the chloroplast genome (Belgio et al., 2012). A carefully orchestrated interaction between the two genomes is required for the response to changes in light quality and quantity because the amounts of RCs and LHCs must be carefully balanced to achieve optimal photosynthesis.

Photosynthesis and all related processes are dynamic and highly responsive to environmental conditions. In a natural environment, light fluctuations occur throughout the day. Theoretically, high light conditions would allow plants to photosynthesize at their maximal capacity. However, at high or excessive light levels, net photosynthesis is reduced as a result of the impairment of the photosynthetic mechanism. The deactivation of PSII under

this excess energy is termed photoinhibition (Horton, 2000; Matloobi, 2012; Takahashi & Badger, 2011). Photoinhibition results in an imbalance of absorption and utilisation of energy in the photosystems, which in turn can damage and destroy the PSII complex causing bleaching, chlorosis or necrosis of the leaves (photodamage) (Karpinski et al., 2003; Mateo et al., 2006). Photoinhibition occurs constantly followed by the repair of PSII, regardless of the light intensity intercepted on the plants, by removal and replacement of the protein D1 (Belgio et al., 2012). The PSII repair cycle is a sequential process that involves major events of phosphorylation and dephosphorylation, damage, disassembly of the complex, *de novo* synthesis of D1 and reassembly the complex (Lu, 2016; Theis and Schroda, 2016). A model of the PSII repair cycle can be seen in Figure 1-4 (Theis and Schroda, 2016).

Photosystem I (PSI), also known as P_{700}, is the other membrane-bound photosystem of plants. The PSI complex consists of at least 19 protein subunits, more than 170 chlorophyll molecules, 2 phylloquinones and 3 Fe_4S_4 clusters (Jensen et al., 2007; Caffarri et al., 2014). Similar to PSII, this complex is also comprised by core subunits and LHC antenna proteins (for PSI, annotation converts to “a” from “b”).

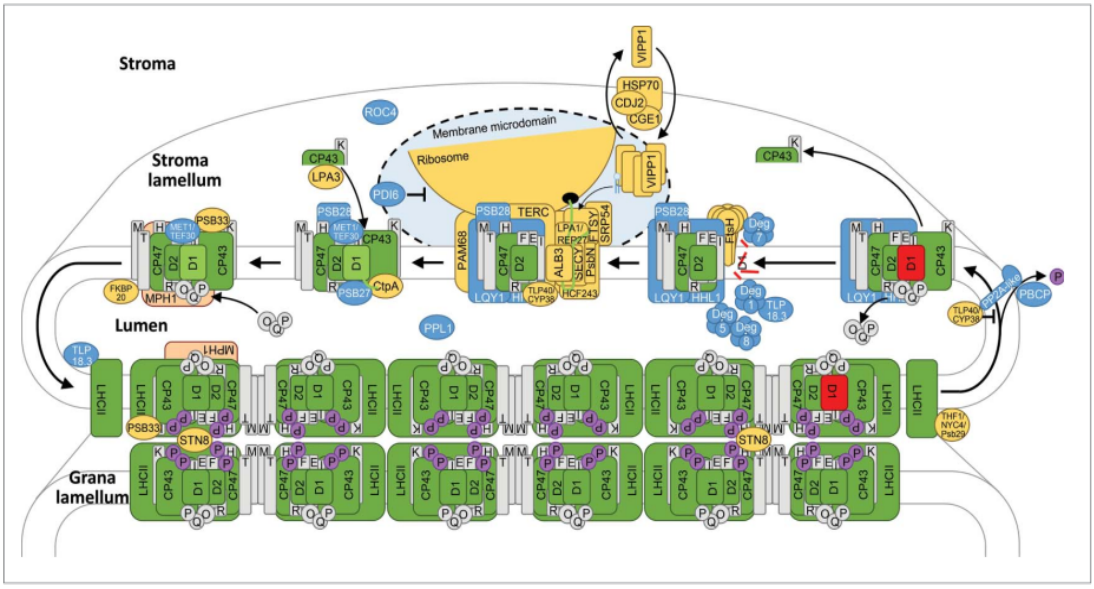


Figure 1-4. Model of the PSII repair cycle. 'P's in purple circles represent phosphate groups, red labelled D1 is photodamaged D1, light-green labelled D1 a new copy of the protein. Proteins labelled in blue represent factors exclusively involved in PSII repair while proteins labelled in gold are factors that are likely involved in PSII repair. Picture taken from Theis and Schroda (2016).

1.3.2 Energy imbalance inside the chloroplast

ROS are not solely produced as signalling molecules in response to biotic stresses but are also involved in stresses that promote an increase in excess excitation energy (EEE) in the photosynthetic apparatus of plants (Bechtold et al., 2005). Such stresses that limit the photosynthetic metabolism, either through effects on gas exchange or upon primary metabolism, include high light intensities, drought stress and pathogen invasion (Mittler et al., 2004; Shapiguzov et al., 2012; Singh et al., 2015). They can potentially be highly damaging to the plant leading to the destruction of photosynthetic reaction centres and oxidative damage is often manifested as bleaching, chlorosis or necrosis of leaves (Karpinski et al., 2003; Mateo et al., 2006). In the chloroplast, Photosystem I (PSI) and Photosystem II (PSII) are two main sources of ROS production (Apel & Hirt, 2004; Asada, 2006). PSI is a primary generator of O_2^- . During photosynthesis, O_2 is continuously reduced to O_2^- by PSI and O_2^- is quickly converted to H_2O_2 and O_2 by the Cu-Zn-SOD complex

attached to PSI (Apel & Hirt, 2004; Asada, 2006). PSII is a major generator of $^1O_2$. During photosynthesis, ground-state oxygen ($^3O_2$) is continuously excited to $^1O_2$ by triplet-excited-state chlorophyll (^{3}P680*) in the PSII reaction centre (Equation 1).

ROS production has both positive and negative effects on photosynthesis. On one hand, ROS production by the two photosystems acts as alternative electron sinks, alleviating the negative impacts of over-reduction and photo-inactivation of the photosynthetic apparatus (Asada, 1999). In this regard, chloroplastic ROS production protects the photosynthetic apparatus, especially when the absorbed excitation energy exceeds the energy consumed by the photosynthetic electron transport chain. On the other hand, non-physiological concentrations of chloroplastic ROS may cause irreversible damage to thylakoid membranes and photosynthetic components, by lipid peroxidation, protein damage, membrane destruction, and ion leakage (Triantaphylidès & Havaux, 2009; Shapiguzov et al., 2012; Dietz et al., 2016).

Chl (in the presence of light) → ^{3}Chl + $^3O_2$ →Chl + $^1O_2$ (highly destructive ROS)

Equation 1. The triplet chlorophyll molecule (^{3}Chl) reacts with $^3O_2$ and the $^1O_2$ ROS is liberated. The reaction thus occurs in the following way (Sharma et al., 2012).

1.3.3 Photoinhibition & Photoprotection

As described above, under excessive energy, net photosynthesis is reduced as a result of the impairment of the photosynthetic mechanism. The deactivation of PSII under this excess energy is termed photoinhibition (Horton, 2000; Matloobi, 2012; Takahashi & Badger, 2011). Other than high light, other environmental conditions such as high temperature or biotic stress also contribute to photoinhibition by lowering photosynthetic capacity and increasing the proportion of excess excitation energy. Some processes, such as stomatal closure or inactivation of Rubisco at high temperatures, can also result in photoinhibition (Murchie & Niyogi, 2011).

Plants have evolved a wide range of protective mechanisms to prevent damage and sustained photoinhibition. For instance, some plants are able to adjust their leaf orientations or even their chloroplasts to minimise the

absorption of high light radiation (Demmig-Adams & Adams, 1992; Murchie & Niyogi, 2011; Takahashi & Badger, 2011). At the cell level, excess excited electrons are removed through a range of molecular processes defined as photoprotection which take place within different timeframes. Removal of excitation energy occurs via three main pathways: photosynthesis, chlorophyll fluorescence and thermal dissipation. These processes are complementary, meaning an increase in one's efficiency will decrease the yield of the other two (Baker, 2008). In more detail, when light is intercepted on a leaf and absorbed by the chlorophyll molecules in the LHC, an electron is transferred to a higher energy state. This energy must either be used in photosynthesis (photochemical quenching), re-emitted as fluorescence radiation (chlorophyll fluorescence) or be dissipated as heat (Murchie & Lawson, 2013; Papageorgiou & Govindjee, 2014). Among these three, only thermal dissipation is considered photoprotection, as the excessive electrons are removed via a harmless non-photochemical pathway and is termed as non-photochemical quenching (NPQ) (Maxwell & Johnson, 2000; Müller et al., 2001; Murchie & Niyogi, 2011; Murchie & Lawson, 2013). Removal of any excessive excitation energy as part of the photoprotection mechanism is taking place at PSII (Murchie & Niyogi, 2011; Takahashi & Badger, 2011; Yamori & Shikanai, 2016), although certain processes can take place around PSI to protect the chloroplast but also to protect PSI itself from photoinhibition. Cyclic electron flow around PSI, in contrast to linear electron flow from PSII to PSI under "normal" conditions, plays an important role in preventing PSI photoinhibition. It operates either involving a complex termed NDH or mediated via a pathway involving a protein called PROTON GRADIENT REGULATION 5 (PGR5) (Johnson, 2011). Cyclic electron flow of PSI contributes to the production of additional ATP and enhances NPQ in the PSII antenna system (Tikkanen et al., 2014; Kono & Terashima, 2016; Lima-Melo et al., 2021).

1.3.4 Non-Photochemical Quenching (NPQ)

NPQ is an inherent protective mechanism found in plants that protects them from any potential damage caused by over-excitation of electrons in PSII, which is more susceptible to photoinhibition (Hajiboland, 2014; Hubbart et al.,

2018). NPQ is regulated by at least three major components: energy-dependent quenching (qE), state-transition induced quenching (qT) and photoinhibitory quenching (qI) (Nilkens et al., 2010). These components confer photoprotection over various timeframes ranging from seconds to days, while qE is the dominant component of NPQ as it is the fast-forming and rapidly dark-reversible type of NPQ (Murchie & Ruban, 2020). NPQ is induced by the increase in the pH gradient (ΔpH) across the thylakoid membrane and is modulated by the xanthophyll cycle and the PSII subunit protein PsbS (Kiss et al., 2008; Murchie & Niyogi, 2011; Roach & Krieger-Liszkay, 2012; Ruban, 2016). Acidification of the thylakoid lumen leads to a switch in properties of the antenna proteins that results in increased probability of energy dissipation (Horton et al., 2005). A diagram of all NPQ states and processes, some of which are described here, are shown in Figure 1-5.

The importance of NPQ for the protection of the photosynthetic apparatus is supported by its ubiquity in the plant kingdom (Niyogi & Truong, 2013; Murchie & Ruban, 2020). Mutants lacking the capacity to induce NPQ are more sensitive to photoinhibition and exhibit lower resistance to environment stressors, such as heat (Tang et al., 2007) and salinity (Lima Neto et al., 2014).

There are three requirements that signal the activation of NPQ (measured as qE); lumen pH gradient, involvement of the xanthophyll cycle and activation of the thylakoid membrane protein PsbS. Firstly, the pH gradient occurs when the trans-thylakoid proton gradient is formed faster than it is dissipated by ATP synthase. Its importance has been shown in studies where either uncouplers were used that prevent the formation of the pH gradient and NPQ was abolished or where chemicals were used that increased the pH and therefore qE (Johnson & Ruban, 2010). The second requirement for NPQ is the xanthophyll cycle, in particular the conversion of the carotenoid violaxanthin (Vio) to antheraxanthin (Anth) and zeaxanthin (Zea) through the action of the enzyme violaxanthin de-epoxidase (VDE) (Jahns & Holzwarth, 2012). The actual mechanism by which Zea plays a role in qE formation remains controversial, with some scientists attributing Zea's action to energy/charge transfer (for example Ahn et al., 2008) and others supporting

the idea of an indirect role where Zea acts as an allosteric regulator controlling the sensitivity of qE to the pH gradient (for example Crouchman et al., 2006) (Jahns & Holzwarth, 2012; Brooks et al., 2013). Finally, the third requirement is the thylakoid membrane protein PSII subunit S (PsbS), which also holds a large amount of uncertainty regarding its location within the thylakoid membrane, its interaction with other proteins and its biochemical mechanism by which it is involved in NPQ (Brooks et al., 2013). Both Zea and PsbS allosterically modulate LHCII and synergistically control the p*K* (proton-antenna association constant) of trimeric LHCII, allowing qE to be activated and sustained at a higher pH (Johnson & Ruban, 2010). The magnitude of ΔpH is usually proportional to the excitation pressure, acting as a signal that activates NPQ, while PsbS and certain LHCs act as sensors of proton concentration (García-Plazaola et al., 2012). Through the above mechanisms, NPQ (measured as qE) acts as a feedback mechanism to signal the trimeric LHCII antennae complexes to change conformation into a better-suited state that will allow excess energy quenching (Ruban, 2016).

1.3.5 The xanthophyll cycle

Xanthophylls are carotenoids found in all plant species. Three types of xanthophylls are involved in NPQ: violaxanthin (Vio), antheraxanthin (Anth), and zeaxanthin (Zea). The xanthophyll cycle is catalysed by two enzymes in the thylakoid membrane. Violaxanthin de-epoxidase (VDE), which is located in the thylakoid lumen, catalyses de-epoxidation under low pH and in the presence of ascorbate. The other enzyme, zeaxanthin epoxidase (ZEP), which is located on the stromal side of the thylakoid membrane, catalyses the reverse reaction for generating Vio. This reaction is carried out in the dark or under low illumination and at pH 7.5 (Jahns et al., 2009). Binding of protons and Zea to the light-harvesting antenna proteins induces some conformational changes resulting in energy quenching and heat dissipation. NPQ is related to a peripheral antenna protein of PSII, PsbS, which is necessary for NPQ (Li et al., 2002a; 2002b). The involvement of the catalysing enzymes ZEP and VDE in NPQ can be seen in Figure 1-5.

Carotenoids of the xanthophyll cycle (XC) are also involved in the production of plant hormones associated with defence. Zeaxanthin, which also plays a part in the qI component of NPQ (Demmig-Adams & Adams, 2006), is derived from β-carotene and is the first precursor of abscisic acid (ABA). Upon its conversion to Vio, it is converted to neoxanthin and xanthoxin through a series of isomerization reactions, resulting in a deoxygenation step by 9-cis-epoxycarotenoid dioxygenase (NCED) that cleaves xanthoxin from the C40 carotenoid (Ton et al., 2009). Conversely, Zea production through VDE is antagonizing ABA synthesis (Pastori et al., 2003).

1.3.6 The photoprotective protein PsbS

PsbS is a 22kDa chloroplastic protein, inherent and conserved in all plant species (Ishida et al., 2011; Kasajima et al., 2011). PsbS protein plays a significant role in the regulation of NPQ (Kereïche et al., 2010; Ikeuchi et al., 2014). Roach & Krieger-Liszkay (2012) found that *Arabidopsis thaliana* plants overexpressing *PsbS* were better protected from ROS molecules in PSII. However, PsbS might not be the primary protein that regulates NPQ but it certainly contributed to a quicker photoprotection mechanism (Johnson & Ruban, 2010). PsbS is one of the two known molecules that regulate qE by swiftly inducing qE response to light fluctuations in the environment (Johnson & Ruban, 2010; Murchie & Niyogi, 2011) (Figure 1-5). Additionally, it was very recently found, that only trimeric LHCII and ΔpH are required to induce qE, but the process was far less effective without PsbS (Saccon et al., 2020).

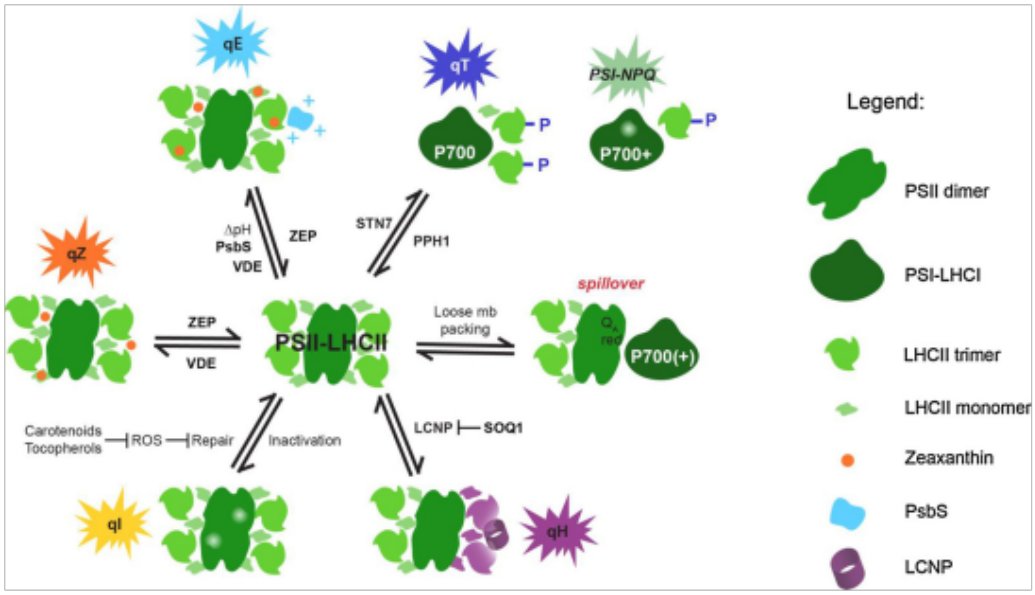


Figure 1-5. Schematic diagram of different NPQ states/components in the PSII-LHCII complexes, along with their associates enzymes and genes involved. Picture taken from Malnoë (2018).

1.4 Photoprotection and Biotic Stress

Although failure to quench excess excitation energy may be detrimental to light-exposed plants, imbalances in the photosynthetic electron transfer chain may also be beneficial, since they may initiate, mediate and even enhance the defence-associated processes in plant cells. Light-dependent formation of ROS in chloroplasts may induce an array of defence-related genes through chloroplast retrograde signalling pathways that share an intimate crosstalk with hormonal regulation and HR (Karpinski et al., 2003; Jelenska et al., 2007; Kangasjärvi et al., 2012; Nomura et al., 2012). The bacterial pathogen *Pseudomonas syringae* secrets an effector molecule HopN1, which annuls ROS production in chloroplasts, thereby inhibiting signals that otherwise would promote defensive measures in infected leaves. HopN1 is a cysteine protease that targets the PsbQ protein of the oxygen evolving complex (OEC) and is therefore likely to mediate its effects by deteriorating electron transport in PSII (Rodríguez-Herva et al., 2012). The OEC seems to be a strategic target also in plant-virus interactions, since viral proteins have been shown to interact with PsbO, another protein of the OEC, as well (Jang et al., 2013). Infection of

leaves with an aggressive flavum strain of *Tobacco mosaic virus* (TMV) showed that particles accumulate inside the chloroplast and the proteins of the OEC become degraded (Lehto et al., 2003). Another example of chloroplast redox homeostasis is the STN7 kinase, normally involved in PSII repair cycle, which impacts plant immunity regulation (Tikkanen & Aro, 2012). Analysis of gene expression profiles for *stn7* mutant leaves revealed reduced transcript levels for the NADPH-oxidase RBOHD, alternative oxidase 1a (AOX1a) and thioredoxin H5, all of which are key components in cellular redox signalling (Tikkanen & Aro, 2012). It has also been suggested that intentional downregulation of NPQ may be beneficial in plant-pathogen interactions. Göhre et al. (2012) demonstrated that abundance of the chloroplastic PsbS protein decreases after the treatment with flg22 and the recognition of PAMPs induced the downregulation of NPQ genes in the chloroplasts. In *Arabidopsis* mutants with impaired NPQ, the apoplastic ROS production increased while defence gene expression was affected displaying an increase in the induction of the early defence markers such as *WRKY22* and *WRKY29*, but the induction of the late markers such as *PR1* and *PR5* disappeared (Göhre et al., 2012). Zhou et al. (2015) and Zabala et al. (2015) both showed increases in NPQ as susceptibility responses to *Sclerotinia sclerotiorum* and *Pseudomonas syringae*, respectively. However, the first study also exhibited the manipulation of the xanthophyll cycle and ABA production by the pathogen (Zhou et al., 2015). Another study worked with PsbS-deficient rice mutants and indicated that these plants were more resistant to both bacterial and fungal infections (Zulfugarov et al., 2016).

Very little is known on the relationship between photoprotection in wheat and the pathogen *Zymoseptoria tritici*. Silencing two key chloroplast genes involved in the carotenoid and chlorophyll biosynthesis, phytoene desaturase and Mg-chelatase H subunit, respectively, rendered *Stb6*-mediated resistance in wheat to *Z. tritici* partially compromised and resulted in increased susceptibility and PCD associated with excessive superoxide and H_2O_2 accumulation (Lee et al., 2015). Finally, a recent study by Ajigboye et al. (2021) provided the first proof of NPQ involvement in wheat resistance against *Z. tritici* during the early stages of infection. The authors de-convoluted NPQ and

showed that resistance to *Z. tritici* was mediated through the qI component. Moreover, they investigated the role of xanthophylls, hormones and ROS and they found that *Z. tritici* resistance was associated with increased biosynthesis of neoxanthin, ABA and enhanced detoxification (Ajigboye et al., 2021).

1.5 Aim of the present study

The aim of this project was to investigate the physiology of resistance to *Zymoseptoria tritici* and elucidate the associated underlying mechanism of photoprotection and chloroplast involvement. Moreover, we wanted to capture this response during the early stages of disease progression, as Photosystem II is the most sensitive stress sensor in plants, which in turn results in dynamic detoxification, signalling and re-organisation events. Specifically, this study aimed to address the following objectives:

- Characterise lines over-expressing the photoprotective protein PsbS and investigate their response to virulent *Z. tritici* isolates. We hypothesized that wheat plants over-expressing PsbS would possess increased tolerance (delayed symptom development) and/or resistance (no symptoms and/or no pycnidia) to virulent strains of *Z. tritici*, through increased photoprotective capacity via faster induction of qE and increased NPQ.
- Characterise the photoprotective and transcriptional response between compatible and incompatible wheat-*Z. tritici* interactions and investigate the role of the xanthophyll cycle, by using near-isogenic wheat genotypes containing or missing the resistance gene *Stb6*. We hypothesised that changes in the stoichiometry and activity of core and light-harvesting PSII proteins of the resistant host, caused by photoinhibitory photoprotection and aided by the action of the xanthophyll cycle, allow the host to downregulate PSII function to allow changes in metabolism for defence. In contrast, we explored the possibility that virulent *Z. tritici* may target the chloroplast to cause changes in the photosynthetic machinery associated with collapse over time.
- Explore the possible effect of *Z. tritici* virulence strategies on wheat sensitivity to other necrotrophic effectors (NEs). We used toxins associated with the wheat fungal pathogens *Parastagonospora nodorum* and

Pyrenophora tritici-repentis and we hypothesised that in the interaction between *Z. tritici* and Tox1/ToxA, sensitivity to the NEs will be reduced possibly because *Z. tritici* effectors antagonise similar NE effectors targeting the function of the chloroplast.

Chapter 2 Wheat plants overexpressing the photoprotective protein PsbS possess enhanced tolerance against isolates of the fungal pathogen *Zymoseptoria tritici*

Acknowledgement of contributions

Initial Western Blot optimisation was performed by myself, however all protein quantification presented in this chapter was performed by Mrs. Charlene Dambire, to whom I am very grateful.

2.1 Introduction

Due to their sessile nature, plants continuously face environmentally challenging conditions including saturating high light, which can damage the photosynthetic apparatus. Under excessive light conditions, maximal photosynthetic capacity is exceeded, leading to the accumulation of unused excitation energy in the pigment protein complexes and the production of singlet oxygen ($^1O_2$) and other reactive oxygen species (ROS). Excessive ROS accumulation in the chloroplast is potentially harmful to the reaction centres (RCs) of Photosystem II (PSII) and prolonged damage of PSII often results in a condition called photoinhibition, i.e. inability of the photosynthetic machinery to repair itself with a subsequent decrease in photochemical efficiency (Takahashi & Badger, 2011; Matloobi, 2012). Plants have developed an array of photoprotective mechanisms that operate within different timeframes to remove excessive excitation energy (i.e. quenching) and avoid permanent damage to photosystems (Murchie & Niyogi, 2011; Takahashi & Badger, 2011; Murchie, 2017). A major photoprotective mechanism for the removal of excessive electrons via harmless thermal dissipation is non-photochemical quenching (NPQ) of chlorophyll fluorescence (Jahns & Holzwarth, 2012; Murchie & Lawson, 2013; Ruban, 2016). NPQ is thought to limit the production of ROS by decreasing the lifetime of singlet-excited chlorophyll *a* and reducing the excitation pressure on PSII to prevent photoinhibition (Murchie & Niyogi, 2011; Roach & Krieger-Liszkay, 2012).

There are at least three different components of NPQ according to their relaxation kinetics in darkness: the energy-dependent, fast quenching (qE),

the state transitions quenching (qT) and the photoinhibitory quenching (qI) (Müller et al., 2001). qT relaxes within minutes and refers to the uncoupling of the light-harvesting complexes (LHCs) from PSII, however it is more important in algae and rather negligible in most plants (Müller et al., 2001). qE contributes to photoprotection, whereas the slow-relaxing qI combines both photoprotection and photodamage (Nilkens et al., 2010; Murchie & Niyogi, 2011; Hubbart et al., 2012; Roach & Krieger-Liszkay, 2012; Malnoë, 2018). The activation of NPQ (measured as qE) is dependent on change of the lumen pH gradient (ΔpH), regulation of the xanthophyll cycle (XC) and the activation of the thylakoid membrane protein PsbS (Photosystem II subunit S) (Malnoë, 2018).

PsbS is a 22kDa chloroplastic protein, inherent and conserved in all plant species (Ishida et al., 2011; Kasajima et al., 2011). It belongs to the LHC protein superfamily, but it has four transmembrane helices instead of three and different pigment-binding characteristics. The involvement and functional role of PsbS in NPQ were first discovered in the early 2000s using the *Arabidopsis thaliana npq4* mutant that lacked the qE component of NPQ and the *psbS* gene, although maintaining normal zeaxanthin (carotenoid of the XC) synthesis (Li et al., 2000). Past studies using both heterozygous and homozygous *npq4* mutants as well as plants with an additional copy of the *psbS* gene, showed that the amount of PsbS protein modulated qE and the control of excitation pressure of PSII under high or fluctuating light conditions (Li et al., 2002a; Li et al., 2002b; Johnson & Ruban, 2010). However, other studies observed the opposite, where a comparison of *Arabidopsis* ecotypes that exhibited differences in qE revealed equal amounts of PsbS (Jung & Niyogi, 2009) or when *Arabidopsis* ecotypes acclimated to field conditions had qE similar to a PsbS-overexpressing line (Mishra et al., 2012). It was recently shown, that only trimeric LHCII and ΔpH are required to induce qE, but the process was far less effective without PsbS (Saccon et al., 2020). Moreover, it is still unclear whether PsbS binds to pigments and is directly responsible for energy dissipation based on its sequence similarity with light-harvesting complex (LHC) proteins (Li et al., 2000), or whether it is unable to bind pigments and it plays an indirect role in NPQ by modulating the PSII antenna

protein transition from light harvesting to an energy dissipative state (Crouchman et al., 2006; Johnson et al., 2011). Although the precise identity of PsbS interactors, the PsbS oligomerisation state and its localisation within PSII supercomplexes remain undefined, PsbS is considered to act synergistically with the carotenoid zeaxanthin as allosteric regulators to alter the structure of the membrane and antenna conformation to ultimately enhance its affinity for protons, thus facilitating qE formation and relaxation (Johnson & Ruban, 2010; Goral et al., 2012; Ruban, 2016; Sacharz et al., 2017).

Photoprotection has been shown to be involved in defence responses of plants against biotic stresses (Göhre et al., 2012; Jänkänpää et al., 2013; Zabala et al., 2015; Zhou et al., 2015; Zulfugarov et al., 2016; Ghosh et al., 2017; Zhang et al., 2017; Ajigboye et al., 2021). The majority of these studies have focused on *Arabidopsis* and PsbS-mutants (*npq4*) and have attributed enhanced defence response to increased ROS production in the mutants and initiation of defence through ROS signalling. Additionally, depending on the pathosystem, different authors have observed contrasting NPQ responses, for example susceptibility of Arabidopsis to the necrotroph *Sclerotinia sclerotiorum* increased NPQ upon inoculation (Zhou et al., 2015), whereas susceptibility of rice (*Oryza sativa*) to *Rhizoctonia solani* downregulated NPQ after infection (Ghosh et al., 2017). Recently, Ajigboye et al. (2021) investigated the role of photoprotection in wheat (*Triticum aestivum*) defence against the foliar fungal pathogen *Zymoseptoria tritici*. Both resistant and susceptible genotypes exhibited higher levels of the qE component of NPQ, although resistance to this pathogen was associated with the elevated qI component. They also found that the resistant NPQ response was also linked with reduced ROS formation and alterations in the plant's stomata morphology (Ajigboye et al., 2021).

Z. tritici, the causal agent of Septoria Tritici Blotch (STB), is a fungal foliar pathogen that poses a major threat to wheat production particularly in temperate regions (Fones & Gurr, 2015). Due to heavy fungicide applications, *Z. tritici* populations have evolved a widespread resistance to all major fungicides, forcing breeders to focus on plant genetic resistance to reduce the

impact of STB in wheat. *Z. tritici* is an apoplastic pathogen and invades the plant through the stomata (Kema et al., 1996). In compatible interactions, it is characterised by a symptomless phase of up to 14 days following infection where the pathogen colonises the apoplastic spaces of the mesophyll prior to switching to a necrotrophic phase, whereby plant cell death is accompanied by a release of metabolites and a rapid increase in fungal biomass (Rudd et al., 2015). The disease culminates in the production of pycnidia, the asexual fruiting bodies of the fungus, that are formed in the substomatal cavities. Resistance is conferred by major genes challenged by specific isolates (gene-for-gene relationship) and can lead to rapid breakdown, as *Z. tritici* evolves new effectors to overcome individual resistance genes. A newly discovered *Stb16q* resistance locus was reported to confer broad spectrum resistance (Ghaffary et al., 2012) but recent reports suggest that this resistance has also been overcome (Kildea et al., 2020; Orellana-Torrejon et al., 2022). The best characterised STB-resistance gene is *Stb6*, which confers resistance to *Z. tritici* isolates that contain *AvrStb6* (such as the reference isolate IPO323) and is present in most European wheat cultivars (Arraiano & Brown, 2006; Saintenac et al., 2018). Incompatible interactions of *Stb6* result in few disease symptoms with limited necrosis and no pycnidia (Rudd et al., 2008).

There are no published studies that have investigated the mechanistic effects of elevated NPQ responses in wheat, possibly due to difficulties in transforming hexaploid crops such as wheat. The role of PsbS as part of photoprotection on wheat disease resistance/susceptibility is not understood and to our knowledge, no research has been conducted on wheat plants with altered levels of PsbS challenged with *Z. tritici*. Therefore, here we investigated the role of increased levels of PsbS in the wheat-*Z. tritici* pathosystem. As aforementioned, *Z. tritici* solely colonises the plant through the stomata and reports have described the involvement of photoprotection in this pathosystem (Ajigboye et al., 2021). We hypothesized that wheat plants over-expressing PsbS, with a confirmed photoprotective phenotype, would possess increased tolerance (delayed symptom development) and/or resistance (no symptoms and/or no pycnidia) to virulent strains of *Z. tritici*, through increased photoprotective capacity via faster induction of qE and increased thermal

quenching. By combining protein quantification, disease monitoring and chlorophyll fluorescence measurements on the over-expressing lines (OX lines), we aimed to understand the effect of *Z. tritici* on the PsbS-OX plants and whether the response would be isolate-specific or PsbS-OX specific.

2.2 Materials & Methods

2.2.1 Plant material and growth conditions

Gene cloning of rice (*Oryza sativa*) *psbS* coding sequence (previously Os01g64960, currently Os01g0869800), using a Gateway destination vector pCR8 and a strong Actin promoter, was carried out by Dr Ranjan Swarup (University of Nottingham, UK, 2014). The construct was sent to NIAB (Cambridge, 2014) and upon further cloning, the final construct pEW269-PSBS (Figure 2-1) was electro-transformed into *Agrobacterium* strain EHA105-U1 (Chuan Ching Foo, personal communication). Embryos from the spring wheat cv. Fielder, which contains *Stb6*, were used for the *Agrobacterium* infection (NIAB, Cambridge, 2014). A total of 37 independent wheat lines were generated (NIAB, 2014) and for this project, T_1 generation seeds were available to us (Chuan Ching Foo and Erik Murchie, personal communication and supply of plant material). Upon an initial *Z. tritici* disease screen on a selection from those 37 lines (data not shown in this thesis), one line (CW10-17) with confirmed presence of the construct, potentially 3-4 copy numbers of the transgene and confirmed higher NPQ, as well as an empty construct/control line (CW10-Con1) (Chuan Ching Foo, personal communication), were selected to be taken forward for this project (hereafter termed PsbS-OX and Null, respectively). T_2 generation plants from that line (CW10-17 or here PsbS-OX) were used for Experiments 1 and 2, whereas homozygous T_3 plants were used for Experiment 3. However, as the T_1 generation could potentially keep segregating and plants were not homozygous, transgene presence and phenotype had to be confirmed before each experiment and in each generation. All experiments included Fielder as the WT control. The presence and expression of the transgene were confirmed in non-inoculated material prior to any treatment application. Furthermore, all

transformants were phenotyped for NPQ to confirm rapid induction prior to being selected for experiments.

Seeds were germinated in FS2 soil compost in modular trays and then transplanted in 1L pots with John Innes no.2 soil compost. Plants were grown at 18 °C day and night temperature, 16h photoperiod, 55 ± 5% RH and ~250 µmols m^{-2} s^{-1} Photosynthetic Photon Flux Density (PPFD) light intensity. All experiments were performed on ~4-week-old plants. 12 seeds were sown per genotype and all biological replicates were used for the characterisation before inoculation. Upon inoculation, the 12 plants were split into treatments in order for each treatment to consist of 4 biological replicates. Experiment was performed once.

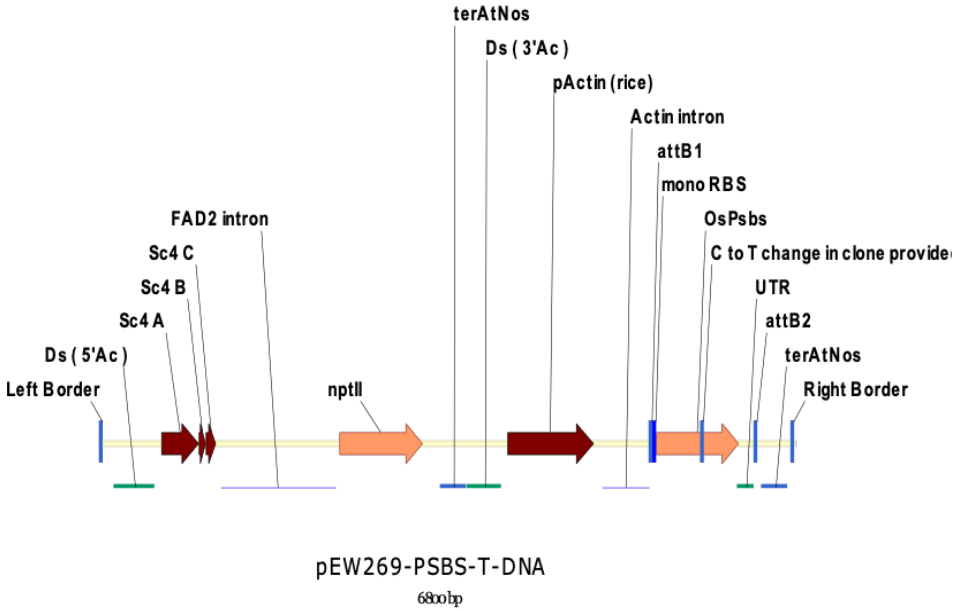


Figure 2-1. Final plasmid construct of PsbS-overexpressing (PsbS-OX) wheat lines (NIAB, 2014). Rice (*Oryza sativa*) *PsbS* was used, Actin promoter and *nptII* as the selectable marker.

2.2.2 Molecular analysis of transgenic wheat lines

a) DNA extraction

Plant genomic DNA was extracted using either a crude, in-house DNA extraction protocol, or a DNA extraction kit using the manufacturer's instructions (DNeasy Plant Pro kit, Qiagen). Briefly, ground leaf material with

2% CTAB was placed at 65 °C for 30 min and then cooled immediately on ice. 5M potassium acetate was added in each sample and centrifuged for 5 min at 10,000 RPM to collect the supernatant. Chloroform (100%) and isopropanol (100%) were then used to bind to and precipitate the DNA, respectively, and DNA was finally resuspended in TE buffer. In order to be used as a positive control, plasmid DNA was extracted using a Miniprep extraction kit according to the manufacturer's instructions (GeneJet Plasmid Miniprep kit, Thermo Fisher Scientific).

b) RNA extraction and cDNA synthesis

Leaf material was ground using liquid nitrogen and total RNA was extracted with Trizol and chloroform, following the guidelines of the RNeasy Mini Kit (Qiagen), with the addition of a RNase-free DNase step (Qiagen) to remove any traces of DNA in the RNA extracts. Samples were eluted in 35 µl RNA-free water and their concentration and purity were determined with a NanoDrop ND-1000 Spectrophotometer. 1 µg per sample were used for cDNA synthesis using the iScript cDNA synthesis kit (Biorad).

c) Genotyping

In order to confirm copy numbers and homozygosity of the transformed plants, gDNA was sent to iDNA Genetics (Norwich, UK) for a qualitative assay, using real time qPCR, to determine the copy numbers of the *nptII* selectable marker gene that was used in the transformation construct.

d) Primer design

As PsbS is a conserved protein across all plant species and rice and wheat share high homology in gene sequences, primers for OsPsbS were carefully designed to be as specific as possible to OsPsbS and not wheat (TaPsbS). The coding sequence of OsPsbS that was used in the transformation was aligned against the coding sequence of all three copies of TaPsbS (TraesCS3A02G381000, TraesCS3B02G413700 and TraesCS3D02G374200) using a Clustal Omega Alignment Algorithm (Figure 2-2). TaPsbS primers were designed based on the coding sequence of the 3B

chromosome (TraesCS3B02G413700). The primer sequences used to detect OsPsbS and TaPsbS are presented in Table 2-1 as well as on the alignment in Figure 2-2. OsPsbS specificity only for the overexpressing plants was confirmed by the melt curve peak during qPCR (Supplementary Figure 2-1).

Table 2-1. List of primers used to confirm expression of rice PsbS in the transgenic plants (OsPsbS), in relation to the native (WT) wheat PsbS (TaPsbS). TaPsbS primers were designed based on the coding sequence of the 3B chromosome.

Gene	Forward primer (5' – 3')	Reverse primer (5' – 3')
OsPsbS	CTGAGCCGAAGCCAAAGTTC	ATCCCCGTCTCCAGGTTCAG
TaPsbS (3B)	GCAGAGCAAAGTCCCCCAAG	ACTCGCTCACGCACGTACTC

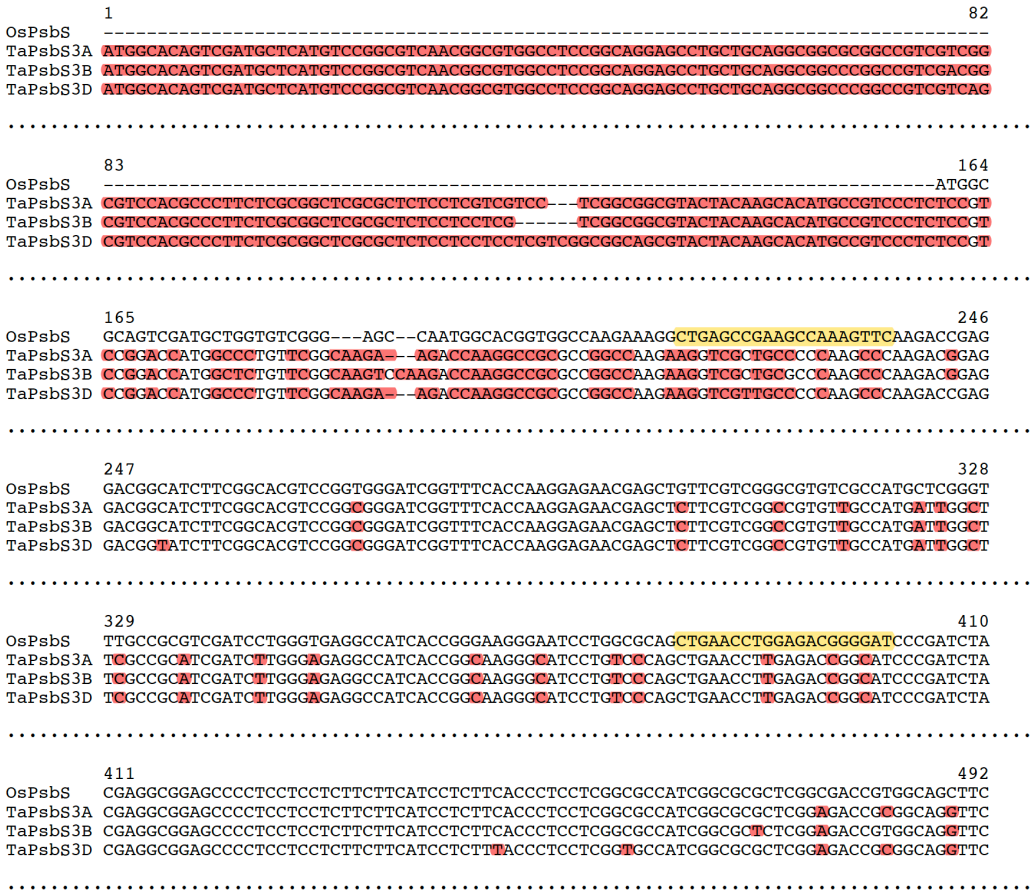


Figure 2-2. A snapshot of the Clustal Omega alignment between the coding sequences of rice PsbS (OsPsbS) used for the generation of the transgenic and wheat PsbS (TaPsbS) on all three genomes (3A, 3B and 3D). Nucleotides highlighted in red depict mismatches between the sequences, whereas sequences highlighted in yellow depict the Forward (5'-3') and Reverse (3'-5') OsPsbS primer sequences.

e) Transgene presence and expression

The presence of the transgene was detected using polymerase chain reaction (PCR) using the OsPsbS primers designed above (50μM concentration). RedTaq DNA polymerase (Sigma) and 20 ng/μl gDNA were used in the reaction, whereas water and plasmid DNA were used as negative and positive controls, respectively. The conditions were: Initial denaturation 94 °C for 2 min, 35 cycles of denaturation at 94 °C for 30 sec, annealing at 56 °C for 30 sec and extension at 72 °C for 2 min, and final extension at 72 °C for 5 min. The PCR product was visualised through 0.5x TBE 1.5% gel electrophoresis for 1h at 100V.

In order to check whether the transgene is not only present but also expressed together with the native gene, 12.5 ng of cDNA were used for qPCR reaction with SYBR reaction mix (Biorad) and 50μM OsPsbS or TaPsbS primers, respectively. Ubiquitin was used as the housekeeping gene, as it didn't show any significant change in expression across the experimental conditions. Samples had 12 biological replicates (before inoculation) and qPCR consisted of 2 technical replicates. The conditions were: 95 °C for 30 sec, 40 cycles of 95 °C for 15 sec and 56 °C (OsPsbS) or 60 °C (TaPsbS and Ubiquitin) for 30 sec, followed by a melt curve between 65 and 95 °C. Primers used for TaPsbS were Forward primer 5'-GCAGAGCAAAGTCCCCCAAG-3' and Reverse primer 5'-ACTCGCTCACGCACGTACTC-3'. Primers for Ubiquitin were 5'-GCACCTTGGCGGACTACAACATTC-3' for the Forward strand and 5'-GACACCGAAGACGAGACTTGTGAACC-3' for the Reverse. Gene expression analysis was carried out using the comparative Ct method.

f) Thylakoid extraction, protein extraction and Bradford assay

Fresh thylakoid membranes from intact chloroplasts were extracted from green, healthy leaves pulled from 4 separate plants. All buffers were made fresh and stored at 4 °C. Plants were kept in the dark for 1h prior to extraction in order to remove some of the starch. Leaves were ground and homogenised in a metal blender with pre-chilled Grinding media (0.33M sorbitol, 10mM sodium pyrophosphate decahydrate, 130mg D-Iso ascorbate pH 6.5). The solution was filtered twice through 4 layers of wet muslin and a strip of

absorbent cotton wool to remove debris and then the filtered solution was centrifuged at 5000rpm at 4 °C for 10 min. The supernatant was discarded and the pellet was gently re-suspended in Wash medium (0.33M sorbitol, 10mM MES, pH 6.5). After another step of centrifugation, the supernatant was carefully discarded once more and the pellet was gently re-suspended in Re-suspension medium (0.33M sorbitol, 1mM EDTA, 50mM Hepes, pH 7.6). Chloroplasts were burst open with the addition of Break medium (80mM Hepes, pH 7.6), followed by Osmoticum medium (0.66M sorbitol, 40mM MES, pH 6.5) and solution was centrifuged once more. The supernatant was discarded and the final pellet was re-suspended in Particle Wash medium (5mM EDTA, pH 6.3). Tubes were spun briefly to pellet any starch and debris and the extracted thylakoids were aliquoted in tubes for follow up analysis and kept in -80 °C. Extraction was repeated once more from another set of plants to have two technical replicates.

In order to quantify protein content in extracted thylakoids, absorbance measurements normally take place based on the absorption of chlorophyll at 646.6, 663.6 and 750nm, before the final concentration of chlorophyll and other proteins are calculated as per Porra et al. (1989). From our experience, this method didn't prove to be very reliable. When we used the Bradford assay to quantify the protein content, we found that the method by Porra et al. (1989) overestimated the actual protein content in the sample by nearly five times. Several repeats of the Bradford assay compared to the [Chl] method indicated that, with the latter, we were not accurately quantifying the actual protein content in the sample. Therefore, we decided to quantify chloroplastic proteins directly from the prepared thylakoid samples using the Bradford Biorad assay kit. We also extracted total protein from plant leaves and compared results against those of thylakoid protein samples and results were comparable. To extract proteins from leaves, the MP BIO homogeniser was used to grind samples, after which extraction buffer, containing 50mM Tris (pH 8), 0.1% SDS, 1x protease inhibitor cocktail and H_2O, was added in each thylakoid sample. Samples were vortexed and then centrifuged for 30 min at 14000 rpm at 4 °C. Supernatant was transferred into a new tube and protein concentration

was quantified by Bradford assay using the Biorad Bradford assay kit, according to the manufacturer's instructions.

g) Western blots

Western blots presented in this chapter were performed by Mrs. Charlene Dambire. Protein amounts of PsbS, relative to the WT Fielder and the Null, were confirmed through Western Blot analysis. After quantification of total protein concentration (Bradford assay on extracted proteins from thylakoid membranes), samples were denatured at 96 °C for 10 min and then immediately placed in ice for 10 min. 10 µg protein was separated by 12% SDS-PAGE electrophoresis and blotted to Biorad PVDF membrane using a wet transfer. Blots were incubated in 5% milk + PBST for 1h and then immuno-labelled in 5% milk + PBST with 1:4000 primary antibody raised against PsbS (AS09533, Agrisera) and against Ubiquitin (AS08307, Agrisera). Blots were washed in PBST (3 x 10 min), followed by secondary antibody incubation (goat anti-rabbit IgG HRP conjugate (1:20000)) for 2 h (AS09602, Agrisera). Blots were washed with PBST + 300mM salt 3 times for 10 min. Chemiluminescence was detected using a LiCor Odyssey FC Imager at 10 min exposure. A protein ladder SeeBlue™ Plus2 Pre-stained Protein Standard was used as a protein band size indicator on each gel. Band signal/intensity of PsbS was normalised against the expression of Ubiquitin.

2.2.3 *Zymoseptoria tritici* isolates and inoculation of plant material

A number of *Zymoseptoria tritici* isolates varying in virulence were kindly provided by Dr Kostya Kanyuka (previously at Rothamsted Research, currently at NIAB, Cambridge, UK) and Dr Ruth Bryant (RAGT, Cambridge, UK). The reference isolate IPO323 which contains the avirulent gene *AvrStb6*, results in an incompatible interaction with any wheat variety containing *Stb6* (Zhong et al., 2017). All other isolates were expected to result in compatible interactions with wheat varieties containing *Stb6* (Henry Tidd and Kostya Kanyuka, personal communication). A list of all isolates is given in the table below (Table 2-2).

Isolates were kept in 70% sterile glycerol stock solutions in -80 °C and were grown on yeast peptone dextrose (YPD) agar (Sigma Aldrich) for 5 days at room temperature. Spores were then suspended in sterile, deionised 0.01% (v/v) Tween20 H_2O and concentration was calculated and adjusted to 10^6 spores/ml using a haemocytometer. Four-week-old plants were placed in PVC transparent bags and spray-inoculated with the inoculum suspension (or deionised sterile H_2O in the case of mock-inoculated control plants) until runoff could be observed on the leaves. Bags were kept closed for 3 days to enhance high humidity for successful pathogen establishment and only opened temporarily for the physiological measurements.

Table 2-2. List of *Zymoseptoria tritici* isolates used in this study. Interaction compatibility is based on the wheat variety Fielder that was used for the transformation and contains *Stb6*. Isolates and further information were kindly provided by Henry Tidd, Dr Kostya Kanyuka and Dr Ruth Bryant (personal communication).

***Z. tritici* isolates**	**Cultivar collected from**	**Year of collection**	**Interaction**
IPO323	Arminda	1984	Incompatible
Zt508	unknown	unknown	Compatible
Zt-18	KWS Santiago	2015	Compatible
Zt-22	KWS Cashel	2015	Compatible
Zt-25	Consort	2016	Compatible
Zt-52	Dickens	2016	Compatible
Zt-74	Siskin	2017	Compatible
Zt-96	Dickens	2016	Compatible

2.2.4 Chlorophyll fluorescence (CF) and gas exchange (GE) measurements

NPQ kinetics were always measured prior to inoculations (hereafter referred to as “0h”), not only to confirm the activity of PsbS on the OX lines but also as a control measurement of the physiological status of the plants before inoculation. The youngest, fully expanded leaf on the primary tiller was selected for all measurements.

a) PsbS-OX plants challenged with IPO323, Zt22 or Zt508

CF and GE were simultaneously measured with an infrared gas analyser (IRGA), LI6400XT, equipped with leaf chamber pulse-amplitude modulated fluorometer (LI6400-40XT, LI-COR Biosciences, Nebraska, USA). For all measurements, the IRGA was kept at a gas flow rate of 500 mL min^{-1}, a cuvette temperature of 20 °C, CO_2 concentration of 400 ppm, and RH between 55-65%. Leaves were dark adapted in the growth chamber for 1h by wrapping sections of the leaf in low-weight aluminium foil, to allow for maximal plastoquinone A (Q_A) oxidation (removal of all e^-) and removal of zeaxanthin. For all measurements, dark-adapted leaves were left for 2 min in the cuvette in darkness until the light period started. The sample and reference IRGAs were equilibrated (matched) automatically to prevent drift prior to each measurement. Minimal fluorescence (F_o) was measured by applying a low measuring light insufficient to induce significant variable fluorescence, followed by a saturating pulse to determine maximum fluorescence (F_m). Actinic light sufficient to drive photosynthesis (1500 µmol m^{-2} s^{-1}) was turned on and after a period of 2 min, a saturating pulse of 7000 µmol m^{-2} s^{-1} (for 0.8 s) was applied to determine maximum fluorescence (F_m'). Actinic light was switched off for 2 s and far-red (FR) light was applied to determine F_o'. Application of a series of saturating pulses every 2 min over a period of 12 min under actinic light (Induction) and for another 12 min under darkness (actinic light turned off) (Relaxation), under an automated programme, allowed determination of a series of F_o' and F_m' readings from which time-dependent changes in fluorescence yield were determined. Fluorescence parameters, including nonphotochemical quenching (NPQ), maximum quantum efficiency of PSII photochemistry (F_v/F_m) and photochemical quenching (qP) were automatically calculated directly from LICOR 6400XT software. Quenching analysis was followed by analysis of relaxation of NPQ kinetics. The rapidly reversible component of NPQ, energy-dependent NPQ (qE), was calculated as (F_m/F_m') - (F_m/F_m''), while the slowly relaxing component (qI) was calculated as ($F_m - F_m''$)/F_m'', where F_m'' is the maximal yield of fluorescence after 12 min of dark relaxation following the actinic illumination. Total NPQ was calculated as the sum of qE and qI. The assumption was that after 12 min of dark treatment, the

remaining quenching consisted only of qI (Ruban, 2016). Measurements were taken at 0h prior to inoculation and then at 24, 48 and 72 hours after inoculation (hai).

b) PsbS-OX plants challenged with all isolates

In order to assess the physiological status of the PsbS-OX plants under inoculation with a range of 8 *Zymoseptoria tritici* isolates (Table 2-2), a closed FluorCam CF imager (FC800-222, Photon Systems Instruments, Drásov, Czech Republic) was used to record and image CF parameters. Approximately 2 cm leaf material was excised and placed on damp filter paper between two sheets of glass plates, in a randomised design. Leaf sections were dark-adapted inside the FluorCam for 1h before initiation of an equivalent protocol as described above. Actinic light was ~1000 µmol m^{-2} s^{-1} and the duration of actinic illumination and dark relaxation was 16min. Chlorophyll fluorescence imaging was performed using a customised FluorCam imaging fluorometer fitted with a white and red LED panel. Shutter time and sensitivity of the charge-coupled device (CCD) were adjusted at 10 µs and 11%, respectively. The FluorCam was located in a temperature controlled dark room maintained between 20 and 22 °C. Images were processed and data extracted using Fluorcam 7 software (Photon Systems Instruments) (example image can be seen in Figure 2-3). Further quenching analysis (qE and qI) was calculated as described above. Measurements were taken at 0h and then at 24hai.

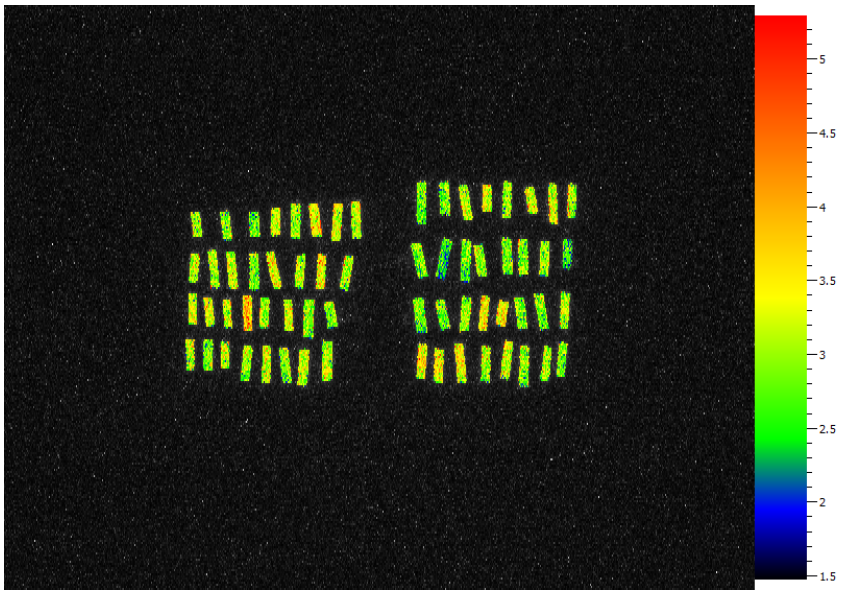


Figure 2-3. Example of chlorophyll fluorescence imaging and sample layout. The image pixels get translated into numeric values using the designated software (Fluorcam 7).

2.2.5 Disease assessment and pycnidia development

The same leaf used for the GE and CF measurements was also monitored for disease progression over time. Disease assessment was made by assessing the total percentage (%) of leaf area covered with symptoms (both chlorotic and necrotic symptoms). Assessments were made at 10, 14, 17 and 21 days after inoculation (dai). The Area Under the Disease Progress Curve (AUDPC) was calculated to determine disease development over time (Jeger & Viljanen, 2001). Spore wash counts were performed as described by Lee, Rudd & Kanyuka (2015). In brief, ~3 cm leaf segments were placed in tubes on sterile H_2O-saturated cotton wool and incubated in the dark for 48h. Leaf sections were then vortexed in sterile water and released spores were measured using a haemocytometer.

2.2.6 ROS staining

Histochemical staining of hydrogen peroxide (H_2O_2) was carried out using 3,3′-diaminobenzidine (DAB). Leaf sections were vacuum-infiltrated with 1 mg/ml DAB-HCl (pH 3.8) and incubated overnight with gentle shaking at room temperature in the dark. The DAB solution was removed, and the leaf sections were washed with distilled water. To stop the reaction and fix the tissue,

samples were boiled for 5 min in 95% ethanol and then were kept in 95% ethanol with gentle shaking until all chlorophyll was removed. Generation of superoxide anion ($O_2^{\bullet -}$) in leaves was detected with nitroblue tetrazolium (NBT). Leaf sections were vacuum-infiltrated with 50mM phosphate buffer (pH 7.8) containing 0.5% NBT and incubated at room temperature for 1h in darkness. Subsequent sample preparation was identical to DAB staining. Leaf sections were sampled simultaneously as NPQ screening. After staining, DAB and NBT stained samples were imaged using an Olympus OM-D e-M10 Mark II camera.

2.2.7 Statistical analysis

All experiments were designed as Completely Randomised Design. Statistical analysis was performed using Genstat 19th edition (VSN International). Data were tested for normal distribution using Shapiro-Wilk's test for normality. If the test discarded the null hypothesis, data were analysed with non-parametric tests. If data followed normal distribution, ANOVA was used in order to elucidate the significance of the main factors (Genotype and Treatment) and/or their interaction (if any) or for simple comparisons (residual degrees of freedom <16), t-tests were used to find any significant differences of means. In case of non-normally distributed data, Kruskal-Wallis one-way ANOVA or Wilcoxon/Mann-Whitney pairwise tests were used. Datasets of NPQ kinetics (Induction & Relaxation curves) and Time Series data were analysed by Repeated Measurements ANOVA.

Dynamic modelling of NPQ was performed using a dose-response curve fitting method in R. The 'drc' (v. 3.0) package was used due to its ability to analyse and extract several useful parameters for both curve induction and relaxation responses (Ritz et al., 2015). These include curve slope, lower limit, upper limit and the time taken to reach a defined percentage of the dependant variable, in this case we focused on 50% (ED_{50}). The LL.3 (log-logistic 3-parameter) model was used for Induction responses, whereas the LL.4 (log-logistic 4-parameter) model was chosen as the best model fit for Relaxation responses. The comparison of 8 different models, followed by Akaike's

information criterion analysis was used to select the best model fit. ED_{50} values were subsequently analysed in Genstat as described above.

2.3 Results

Each experiment consisted of the physiological and molecular characterisation of the OX plants before any treatment was applied (0h). These included the confirmation studies of the presence/absence and/or expression of the transgene as well as gas exchange and/or chlorophyll fluorescence measurement to characterise their NPQ capacity. T_2 generation seeds from the independent T_1 line CW10-17 (here named PsbS-OX) and from the independent T_1 empty construct line (Null) were used for this experiment, as well as WT Fielder. From all 37 T_1 independent transformations (details in Materials & Methods), CW10-17 (PsbS-OX) and the Null were chosen upon an initial *Z. tritici* inoculation (data not shown in this thesis) and their NPQ phenotype (Chuan Ching Foo, personal communication). Twelve (12) seeds were sown per genotype to serve as biological replicates and were used for the characterisation before inoculation (0h). Upon inoculation, the 12 plants were split into treatments in order for each treatment to consist of 4 biological replicates. Three separate experiments took place using Fielder, Null and the PsbS-overexpressing line and their results are separated and listed below.

a) PsbS-OX plants challenged with IPO323 and Zt22

Genomic PCR, qPCR and *nptII* genotyping were used to molecularly characterise the plants used in this experiment. No bands appeared in the null-construct genotype (Lanes 2-9) compared to the OXs and the positive control (Figure 2-4a), which was further confirmed from the genotyping assay (*nptII* = 0 copies). RT-PCR detected the expression of PsbS only in the OX-lines (OsPsbS primers, Supplementary Figure 2-1) whilst the native PsbS was upregulated in all genotypes (TaPsbS primers) (Figure 2-4b). The transgene was expressed, although it had significantly less expression compared to the native (Figure 2-4b).

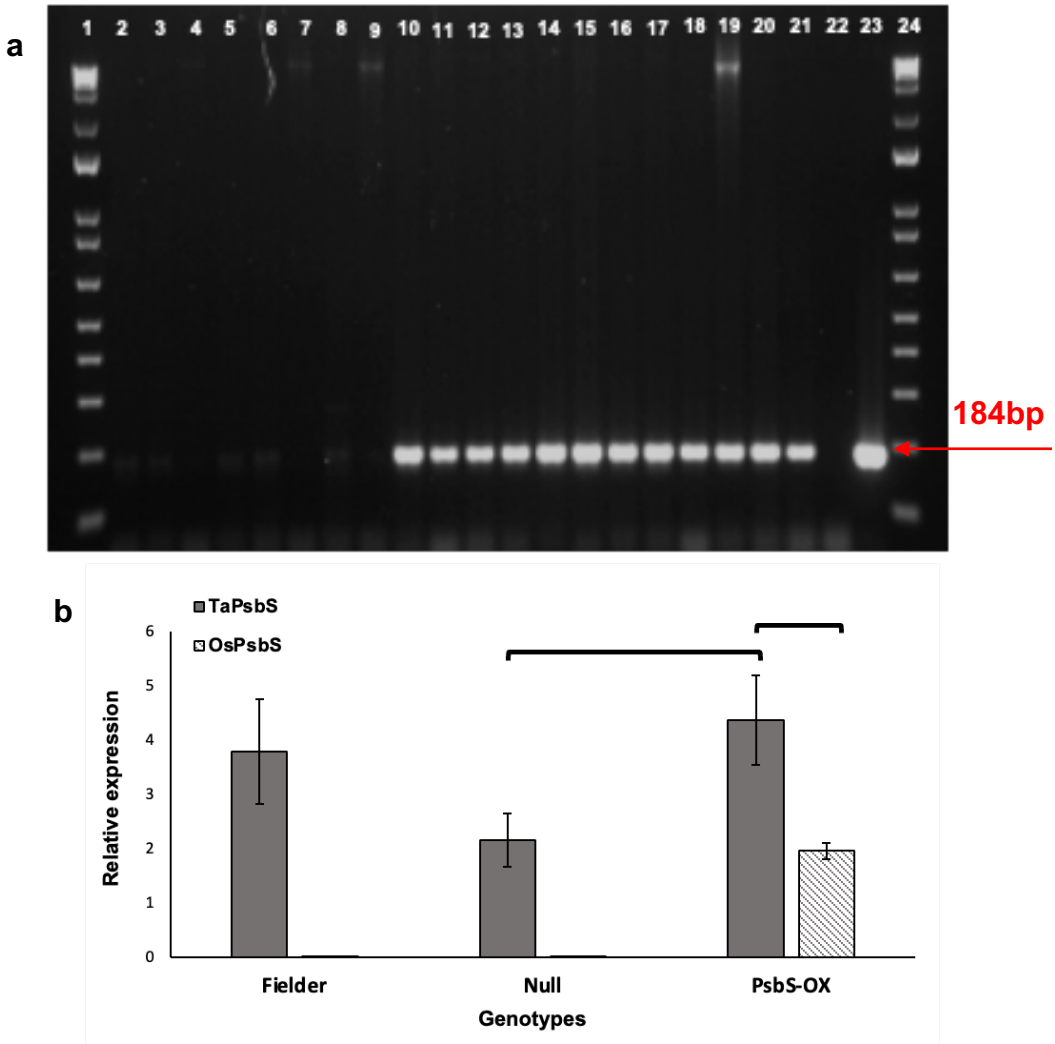


Figure 2-4. (a) Detection of transgene with PCR and OsPsbS primers. Lane 1: 1kb+ ladder, Lanes 2-9: Biological replicates of Null plants (0 copies), Lanes 10-21: Biological replicates of PsbS-OX plants (4 copies), Lane 22: -ve (H_2O) control, Lane 23: +ve (plasmid) control, Lane 24: 1kb+ ladder. Expected product size was 184bp, **(b)** qRT-PCR for gene expression of OsPsbS and native TaPsbS on all genotypes used in this experiment. Horizontal bars above graph represent significant differences ($P < 0.05$).

Characterisation of the physiological phenotype revealed significant differences of NPQ kinetics (Induction and Relaxation) between the genotypes (Figure 2-5a). Although the Null appeared to rise faster in the early stages of the induction (Figure 2-5a), there was significantly higher NPQ capacity in the OX line, measured as qE (Figure 2-5b). NPQ of the OX line took a significantly longer time to reach 50% of its maximum theoretical value (Induction ED_{50}) (Figure 2-5f), which could be attributed to the fact that the OX line has a greater NPQ capacity than the Null and WT Fielder. There were no differences observed on the relaxation of NPQ, measured as qI (Figure 2-5c), even though the Null appeared to relax significantly faster than the WT and the OX line (Relaxation ED_{50}) (Figure 2-5g). PsbS-OX had significantly lower stomatal conductance than Fielder and the Null (12.5% less than Fielder and almost 10% less than the Null), at the end of the light period (12min) when stomata should have opened at almost their maximum capacity (Figure 2-6). The remaining physiological parameters measured, namely F_v/F_m (maximum quantum efficiency of PSII), qP (photochemical quenching), φPSII (PSII operating efficiency) and A_{max} (total carbon assimilation in the light), did not show any significant differences among the genotypes (Table 2-3).

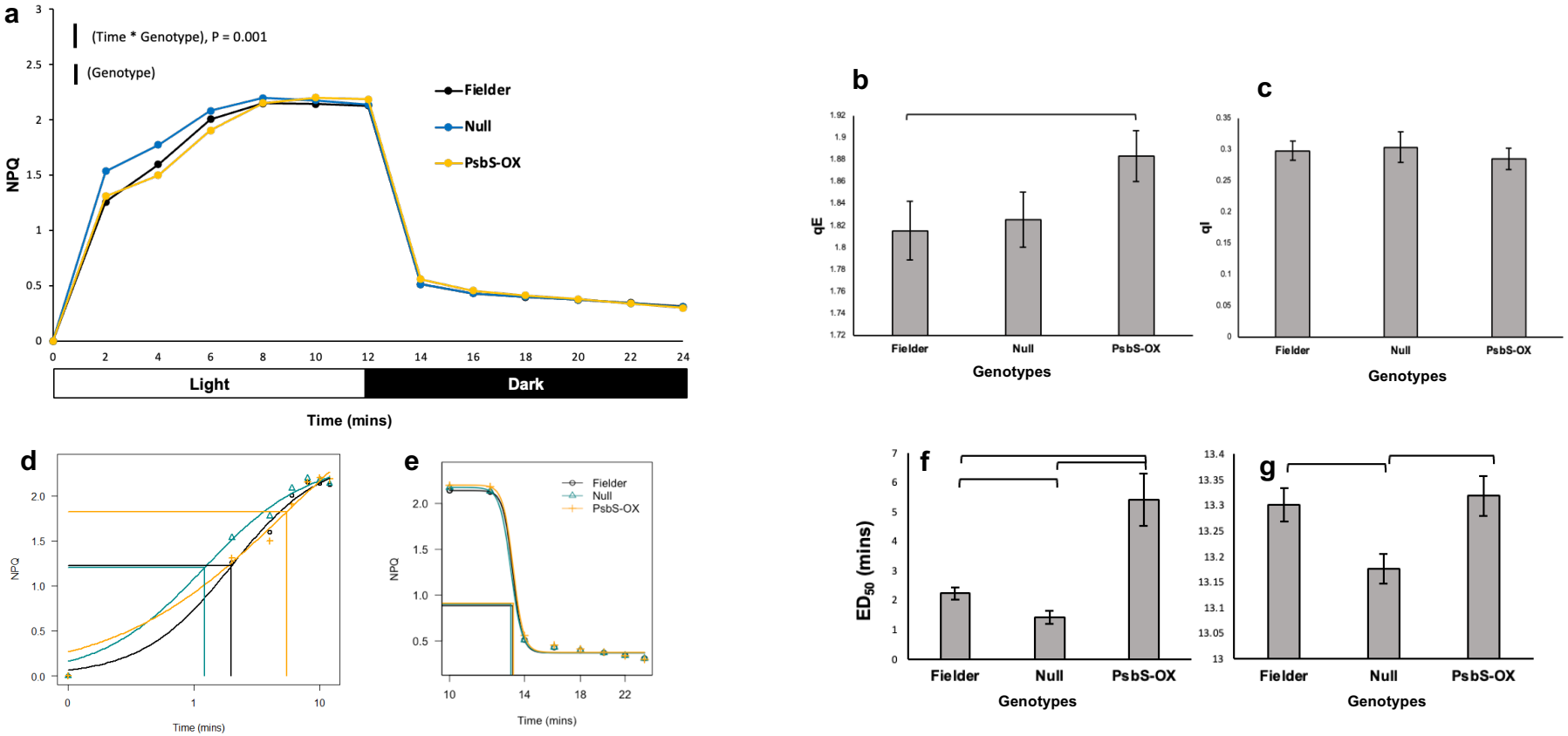


Figure 2-5. Characterisation of NPQ kinetics of the transgenic plants compared to the WT Fielder. **(a)** NPQ Induction and Relaxation curve. Vertical bars indicate LSD of the significant interactions, **(b)** and **(c)** qE and qI components of NPQ, **(d)** and **(e)** NPQ Induction and Relaxation curve modelling, respectively, **(f)** and **(g)** ED_{50} values derived from the models, indicating the number of minutes required for NPQ to reach its 50% maximum (Induction) and 50% minimum (Relaxation) value, respectively. Bars and lines represent means ± SEM (n = 12). Horizontal bars represent significant differences between the means ($P < 0.05$).

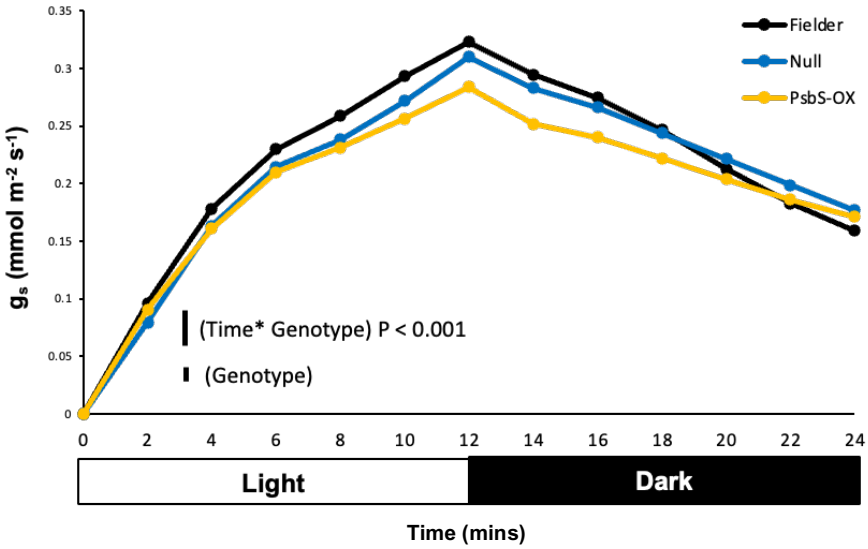


Figure 2-6. Stomatal conductance dynamics in light and dark conditions between the genotypes. Vertical lines represent LSD of the significant interactions (n=12).

Table 2-3. Chlorophyll fluorescence parameters and photosynthesis (Amax) for the different genotypes. Shown below are individual means ± SEM (n=12).

	F_v/F_m	qP	φPSII	A_{max}
Fielder WT	0.81 ± 0.001	0.49 ± 0.01	0.23 ± 0	25.57 ± 0.8
Null	0.81 ± 0.002	0.48 ± 0.01	0.22 ± 0.01	24.56 ± 0.84
PsbS-OX	0.81 ± 0.001	0.47 ± 0.01	0.22 ± 0	23.12 ± 0.8
***P* value**	0.778	0.06	0.06	0.115

The plants used for genomic analysis and NPQ characterisation before inoculation (0h) confirmed the presence and expression of the transgene. They were subjected to inoculations first with the isolates IPO323 and Zt22 as well as a mock-inoculation with sterile, deionised H_2O. The isolate IPO323 contains the avirulent gene *AvrStb6* and Fielder contains the equivalent resistance gene *Stb6*, therefore it was expected that the transformed lines will also exhibit the resistant phenotype for IPO323. Disease progression was monitored for the initiation of symptoms and then for the appearance of pycnidia. The disease phenotype of each genotype for each isolate is shown in Figures 2-7a (14dai) and 2-7b (21dai). As expected, no symptoms or pycnidia developed on any of the genotypes inoculated with IPO323 (Figure 2-7, top panel). In contrast, Zt22 is virulent to plants with functional *Stb6* and caused disease symptoms on the WT Fielder and the Null, while the PsbS-OX was able to maintain greater healthy, green area by 21dai (Figure 2-7, bottom panel). AUDPC revealed significant interaction between the isolates and genotypes; there were no significant differences between the genotypes for IPO323, however the PsbS-OX had significantly lower AUDPC with Zt22 compared to Fielder and the Null, and was not significantly different from IPO323 (Figure 2-7c). The Null inoculated with Zt22 developed pycnidia earlier than the OX line, at 14dai (Figure 2-7a, bottom panel), however pycnidia counts failed to show significant differences between the Null and PsbS-OX (Figure 2-7d). Pycnidia formation was only significantly different between Fielder and the Null (Figure 2-7d). Finally, no relationship was observed between AUDPC and pycnidia counts (Figure 2-7e).

Plants were assessed for their physiological phenotype upon inoculation with IPO323, Zt22 and mock-inoculation (Treatment). Physiological measurements took place at 24, 48 and 72 hours after inoculation (hai). As the Null was confirmed as sufficient control, Fielder was not included in the analysis. Upon all chlorophyll fluorescence (CF) and gas exchange (GE) parameters measured, the Induction ED_{50} (minutes for NPQ to reach 50% of its maximum) showed a significant decrease over time being different prior to inoculation between the Null and PsbS-OX, regardless of the applied treatment (Figure 2-8). As previously described, before inoculation (0h), the OX line was

significantly slower to reach half the maximum of NPQ compared to the Null (Figures 2-5f and 2-8). Thus, the effect of inoculation on the OX line was to reduce ED_{50} significantly in the first 24 hours whilst the Null remained the same over the time course of measurements (Figure 2-8). No significant differences were observed for the remaining CF and GE parameters (Table 2-4). NPQ_{max}, the maximum NPQ that the plants achieved at the end of the light period, qE and total NPQ, remained unchanged over time and there were no significant differences between the treatments and genotypes (NPQ_{max} P = 0.389, qE P = 0.525, total NPQ P = 0.278) (Table 2-4). Relaxation ED_{50} (minutes for NPQ to reach 50% of its minimum) increased over time, with the biggest increase in PsbS-OX inoculated with IPO323 at 24hai, however there was no statistical significance overall (P = 0.329) (Table 2-4). qI also seemed to drop across the treatments at 24hai before rising again, but similarly to Relaxation ED_{50}, there were no statistical differences (P = 0.714) (Table 2-4). Carbon assimilation (A_{max}) and stomatal conductance (g_s) decreased over time, while the isolate effect seemed to be separating at 72hai with Zt22 maintaining higher A_{max} and g_s than IPO323 and then the Mock. However, no significant differences were detected (A_{max} P = 0.987, g_s P = 0.839) (Table 2-4). Quantum efficiency (F_v/F_m) appeared to increase at 24hai before dropping again, for all treatment combinations, with no significant differences (P = 0.662) (Table 2-4). Finally, no obvious trends could be observed for photochemical quenching (qP) and PSII efficiency (φPSII) and there were no significant differences over time (P = 0.252 and P = 0.236, respectively) (Table 2-4).

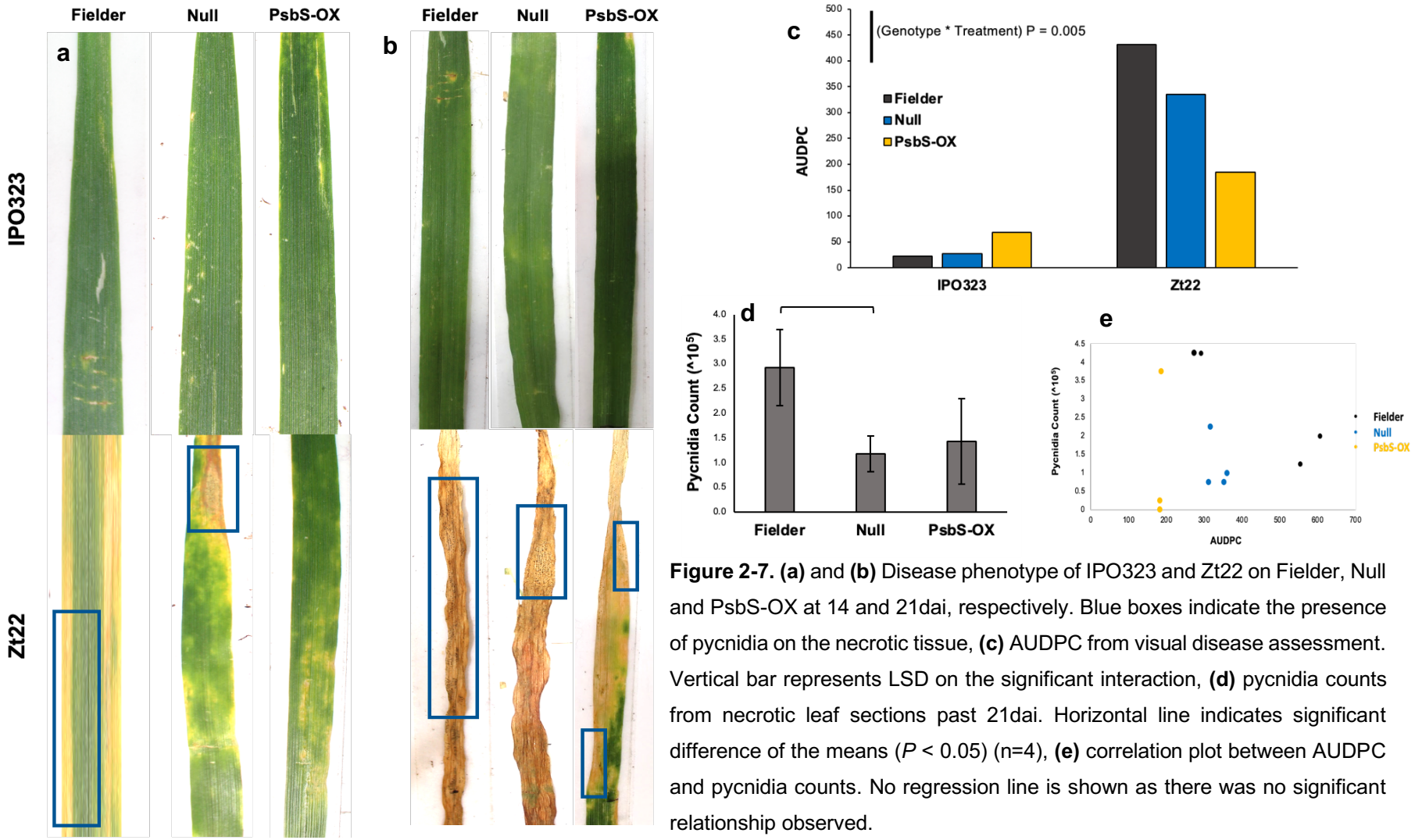


Figure 2-7. (a) and **(b)** Disease phenotype of IPO323 and Zt22 on Fielder, Null and PsbS-OX at 14 and 21dai, respectively. Blue boxes indicate the presence of pycnidia on the necrotic tissue, **(c)** AUDPC from visual disease assessment. Vertical bar represents LSD on the significant interaction, **(d)** pycnidia counts from necrotic leaf sections past 21dai. Horizontal line indicates significant difference of the means ($P < 0.05$) (n=4), **(e)** correlation plot between AUDPC and pycnidia counts. No regression line is shown as there was no significant relationship observed.

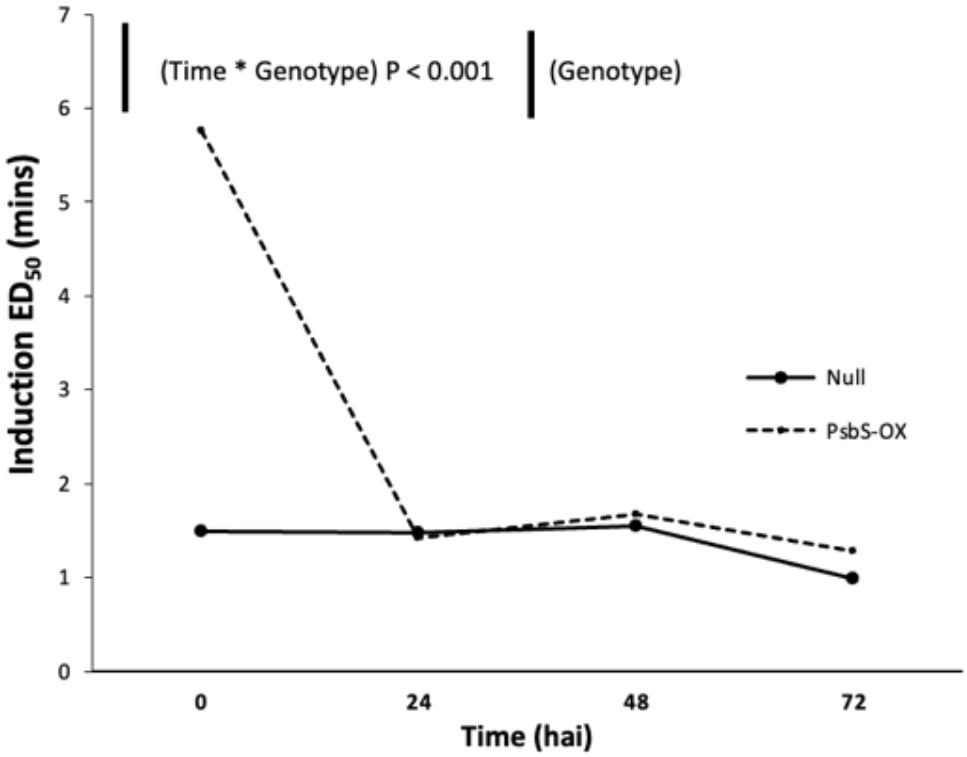


Figure 2-8. Induction ED_{50} (minutes required for NPQ to reach 50% of its maximum) over time between the Null and PsbS-OX upon inoculation. ANOVA only showed genotypic significant differences, as presented here (no treatment or interaction effect). Vertical bars represent LSD for the significant interactions.

Table 2-4. Chlorophyll fluorescence and gas exchange parameters for each treatment and genotype, over time. Data shown indicate means for each parameter, per genotype and treatment and per time point (n=4). Final three rows indicate significant values after repeated measurements ANOVA, followed by the respective LSD. TxG refers to Time x Genotype, TxT refers to Time x Treatment and TxGxT refers to the interaction of Time x Genotype X Treatment.

			NPQ_{max}	Relaxation ED_{50}	qE	qI	Total NPQ	F_v/F_m	qP	φPSII	A_{max}	g_s
0h	Mock	Null	2.22	13.17	1.89	0.33	2.22	0.81	0.45	0.21	23.66	0.29
		OX	2.14	13.36	1.86	0.25	2.11	0.81	0.46	0.22	19.98	0.28
	IPO323	Null	2.09	13.16	1.77	0.31	2.08	0.81	0.49	0.23	25.94	0.33
		OX	2.2	13.36	1.88	0.31	2.19	0.81	0.46	0.21	25.22	0.29
	Zt22	Null	2.12	13.2	1.83	0.28	2.11	0.81	0.49	0.23	23.85	0.3
		OX	2.2	13.23	1.92	0.29	2.21	0.81	0.48	0.22	24.16	0.28
24h	Mock	Null	2.3	13.36	2.09	0.18	2.27	0.82	0.44	0.2	17.14	0.21
		OX	2.39	13.37	2.16	0.17	2.33	0.82	0.43	0.2	15.86	0.21
	IPO323	Null	2.28	13.37	2.06	0.18	2.24	0.82	0.42	0.2	16.16	0.22
		OX	2.39	13.55	2.15	0.22	2.37	0.82	0.4	0.18	18.43	0.2
	Zt22	Null	2.34	13.41	2.1	0.21	2.31	0.82	0.39	0.18	15.02	0.19
		OX	2.33	13.36	2.09	0.2	2.29	0.82	0.43	0.2	16.92	0.22
48h	Mock	Null	2.24	13.34	1.99	0.2	2.2	0.81	0.41	0.19	17.7	0.21
		OX	2.35	13.46	2.1	0.2	2.3	0.82	0.42	0.19	16.91	0.21
	IPO323	Null	2.35	13.43	2.11	0.22	2.33	0.82	0.37	0.17	12	0.16
		OX	2.27	13.45	2.02	0.17	2.19	0.82	0.43	0.2	15.01	0.17
	Zt22	Null	2.3	13.44	2.04	0.24	2.28	0.82	0.4	0.19	17.36	0.22
		OX	2.3	13.5	2.03	0.24	2.27	0.82	0.41	0.19	20.01	0.24
72h	Mock	Null	2.33	13.45	2.09	0.3	2.39	0.81	0.35	0.15	11.33	0.14
		OX	2.3	13.43	2.06	0.22	2.27	0.82	0.4	0.18	11.83	0.16
	IPO323	Null	2.24	13.41	2	0.29	2.28	0.81	0.38	0.17	14.53	0.18
		OX	2.32	13.54	2.06	0.25	2.31	0.81	0.39	0.18	13.89	0.22
	Zt22	Null	2.2	13.5	1.96	0.27	2.23	0.81	0.39	0.18	17.67	0.25
		OX	2.22	13.47	1.96	0.24	2.2	0.81	0.41	0.19	17.7	0.22
T x G ***P*-value, LSD**			0.862, 0.1016	0.235, 0.0833	0.805, 0.1015	0.418, 0.0479	0.537, 0.1109	0.587, 0.0043	0.123, 0.0376	0.186, 0.0217	0.63, 4.414	0.632, 0.0573
T x T ***P*-value, LSD**			0.846, 0.1245	0.507, 0.1020	0.76, 0.1243	0.628, 0.0587	0.78, 0.1358	0.858, 0.0053	0.365, 0.0460	0.55, 0.0265	0.088, 5.406	0.087, 0.0702
T x G x T ***P*-value, LSD**			0.389, 0.1761	0.329, 0.1443	0.525, 0.1759	0.714, 0.0830	0.278, 0.1920	0.662, 0.0075	0.252, 0.0651	0.236, 0.0375	0.987, 7.645	0.839, 0.0992

b) PsbS-OX plants challenged with Zt22 and Zt508

Based on the results from Experiment 1, where the PsbS-OX plants showed tolerance to Zt22, we investigated another virulent isolate, Zt508, with Zt22 used as the control to which response was assessed in the previous experiment. Another set of T_2 generation seeds from the independent T_1 line CW10-17 (here named PsbS-OX) and from the independent T_1 empty construct line (Null) were used for this experiment, as well as WT Fielder. 12 seeds were sown per genotype to serve as biological replicates and were used for the characterisation before inoculation (0h). Upon inoculation, the 12 plants were split into treatments in order for each treatment to consist of 4 biological replicates.

Genomic PCR and *nptII* genotyping were used to molecularly characterise the plants used in this experiment. Faint bands for the presence of the transgene appeared in the null-construct genotype (Lanes 2-13), as compared to the OXs and the positive control (Figure 2-9). However, these were neglected as they came in contrast with the genotyping results that showed no presence of *nptII*, identical to Experiment 1 as described previously. Due to limited DNA quantity, DNA concentration was not adjusted to 20 ng/µl per sample.

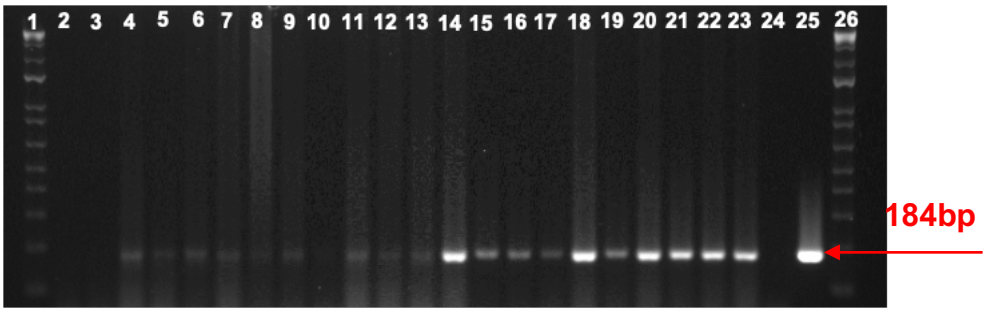


Figure 2-9. Detection of transgene with genomic DNA PCR and OsPsbS primers. Lane 1: 1kb+ ladder, Lanes 2-13: Biological replicates of Null plants, Lanes 14-23: Biological replicates of PsbS-OX plants, Lane 24: -ve (H_2O) control, Lane 25: +ve (plasmid) control, Lane 26: 1kb+ ladder. Expected product size was 184bp.

Similarly to Experiment 1, plants were subjected to physiological characterisation before inoculation (0h). The magnitude of NPQ and qE was much greater than detected in Experiment 1 and the PsbS-OX plants showed significantly higher NPQ and qE than the WT and Null (Figures 2-10a and 2-10b). The Null also had significantly higher NPQ and qE compared to Fielder (Figures 2-10a and 2-10b). NPQ of the OX line was slower to reach 50% of its maximum (Induction ED_{50}) compared to the Null, but it was not different than the WT Fielder (Figure 2-10f). There were no differences observed on the relaxation of NPQ (measured as qI) (Figure 2-10c) neither on the speed of the relaxation (Relaxation ED_{50}) (Figure 2-10g). PsbS-OX had significantly lower stomatal conductance than Fielder and the Null during the dark period and closed stomata rapidly (Figure 2-11). There were no significant differences between the genotypes for photochemical quenching (qP) (Table 2-5). However, F_v/F_m, φPSII and photosynthetic assimilation were significantly reduced in the OX line compared to the Null and Fielder (Table 2-5).

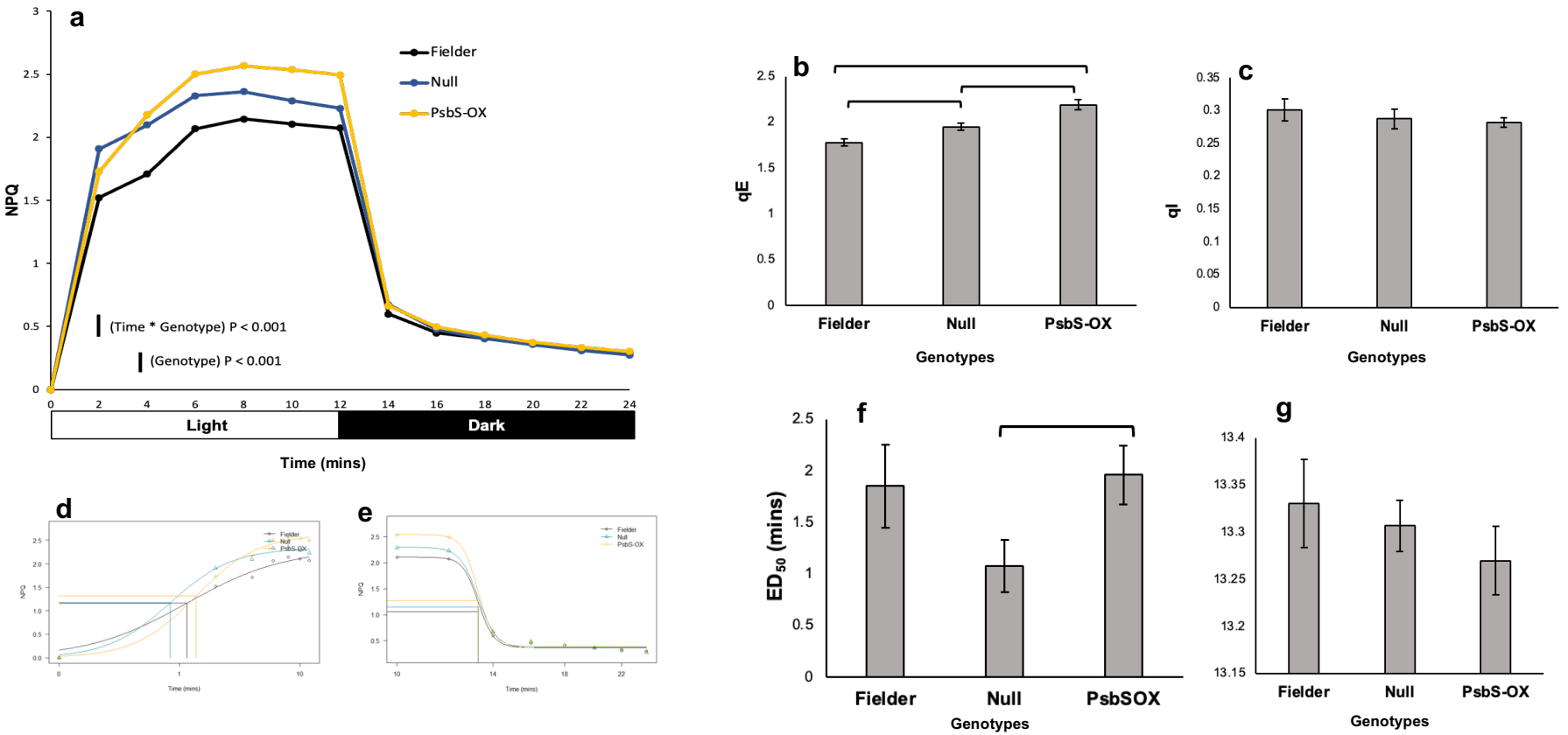


Figure 2-10. Characterisation of NPQ kinetics of the transgenic plants compared to the WT Fielder. **(a)** NPQ Induction and Relaxation curve. Vertical bars indicate LSD of the significant interactions, **(b)** and **(c)** qE and qI components of NPQ, **(d)** and **(e)** NPQ Induction and Relaxation curve modelling, respectively, (**f)** and **(g)** ED_{50} values derived from the models, indicating the number of minutes required for NPQ to reach its 50% maximum (Induction) and 50% minimum (Relaxation) value, respectively. Bars and lines represent means ± SEM (n = 12). Horizontal bars represent significant differences between the means ($P < 0.05$).

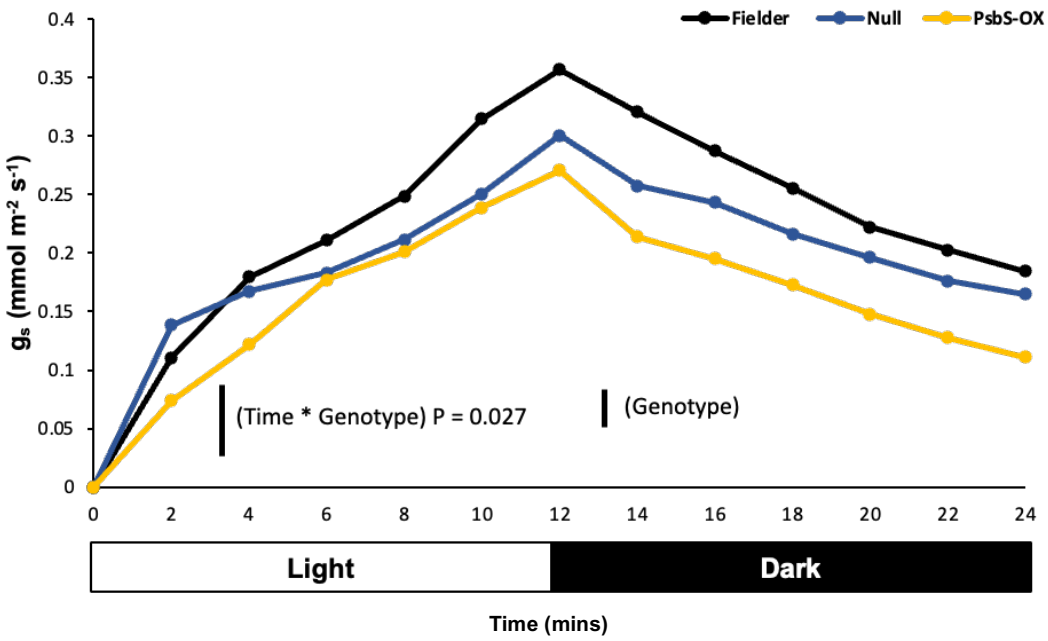


Figure 2-11. Stomatal conductance dynamics in light and dark conditions between the genotypes. Vertical lines represent LSD of the significant interactions (n=12).

Table 2-5. Chlorophyll fluorescence parameters and photosynthesis (A_{max}) for the different genotypes. Shown below are individual means ± SEM (n=12), letters in brackets indicate differences between the means.

	F_v/F_m	qP	φPSII	A_{max}
Fielder WT	0.813 ± 0.001 (a)	0.49 ± 0.01	0.232 ± 0.005 (a)	25.54 ± 0.56 (a)
Null	0.806 ± 0.002 (b)	0.48 ± 0.01	0.215 ± 0.005 (b)	21.46 ± 1.05 (b)
PsbS-OX	0.794 ± 0.003 (c)	0.41 ± 0.02	0.169 ± 0.01 (c)	18.30 ± 0.87 (c)
***P* value**	< 0.001	0.291	< 0.001	< 0.001

The plants used for genomic analysis and NPQ characterisation before inoculation (0h) confirmed the presence of the transgene and exhibited higher NPQ than the controls (Figures 2-9 and 2-10). They were then subjected to inoculations with the isolates Zt508 and Zt22 as well as a mock-inoculation with sterile, deionised H_2O. Zt22 was used in the previous experiment and OX plants showed less disease symptoms and pycnidia formation than the controls. Both Zt22 and Zt508 are virulent isolates on genotypes containing *Stb6* and were expected to cause the full spectrum of disease on the control genotypes. The disease phenotype of each genotype for each isolate is shown in Figures 2-12a (14dai) and 2-12b (21dai). Zt508 was more virulent than Zt22 on Fielder and PsbS-OX, as by 14dai, there were more symptoms on the leaves inoculated with Zt508 (Figure 2-12a). However, the Null was equally susceptible to both isolates at 14dai (Figure 2-12a). By 21dai, Zt508 had produced pycnidia on all genotypes, however PsbS-OX maintained green, healthy tissue in comparison to the severe necrosis on Fielder and the Null (Figure 2-12b). Zt22 also developed full symptoms and pycnidia on the controls, whereas PsbS-OX had the least amount of symptoms and less pycnidia (Figure 2-12b). AUDPC analysis showed significant interactions between the treatments and the genotypes (Figure 2-12c). PsbS-OX inoculated with Zt22 or Zt508 had significantly lower AUDPC and greater tolerance to the disease (Figure 2-12c). However, Fielder had increased AUDPC due to Zt508 compared to Zt22.

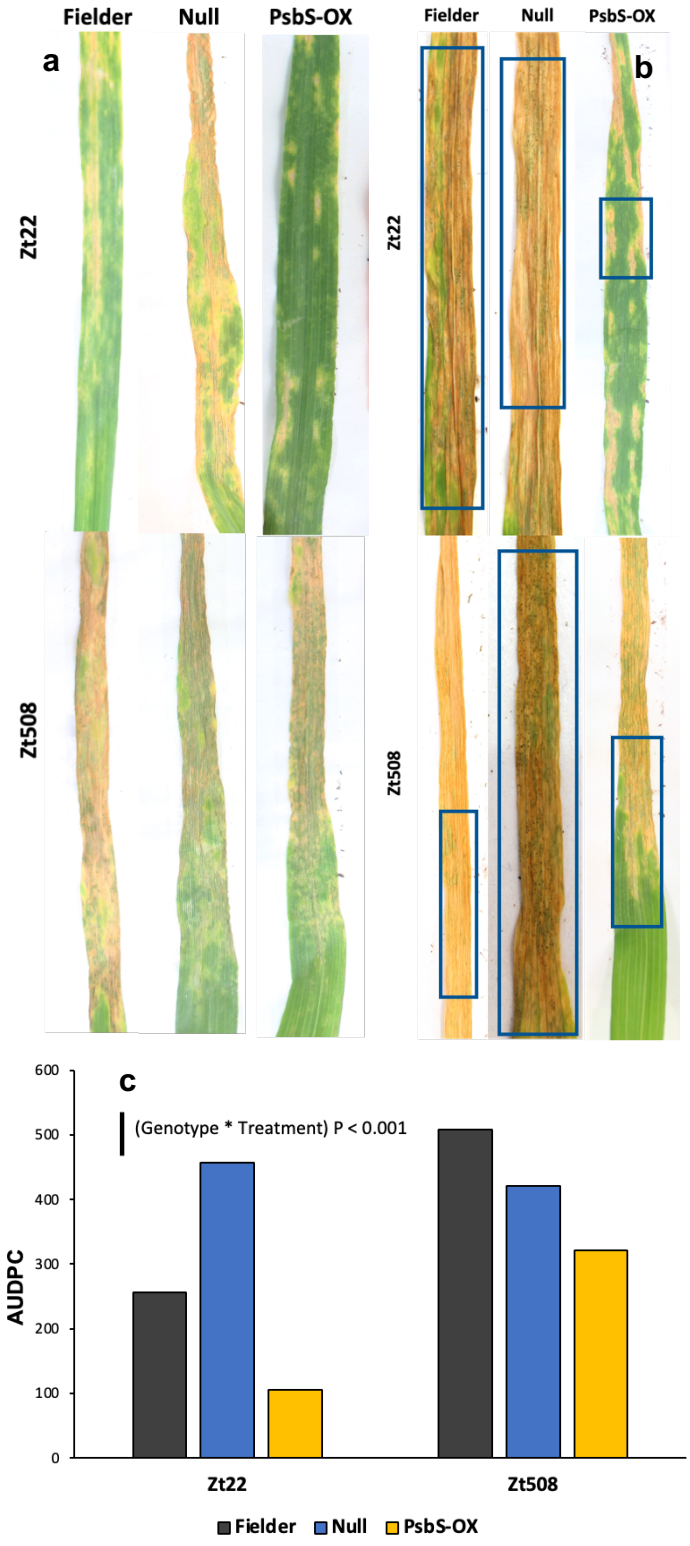


Figure 2-12. (a) and **(b)** Disease phenotype of Zt22 and Zt508 on Fielder, Null and PsbS-OX at 14 and 21dai, respectively. Blue boxes indicate the presence of pycnidia on the necrotic tissue, **(c)** AUDPC from visual disease assessment. Vertical bar represents LSD on the significant interaction (n=4).

The plants were also assessed based on their physiological phenotype upon inoculation with Zt22, Zt508 and mock-inoculation (Treatment). Physiological measurements took place at 24, 48 and 72 hours after inoculation (hai). As the Null was a sufficient control for this experiment, Fielder was excluded from the analysis. There were apparent differences between the Null and PsbS-OX in their NPQ response and NPQ-derived parameters irrespective of inoculation (Figures 2-13a-d). PsbS-OX under inoculation was able to reach maximum NPQ faster (i.e. reduction in ED_{50}) compared to its pre-inoculation state (0h) and the Null in the first 24 hours (Figure 2-13a). This is in coordination with NPQ_{max}, qE and total NPQ as the OX was primed for NPQ at 0h and remained upregulated until 24hai before dropping at 48 and 72hai (Figures 2-13b-d). Carbon assimilation (A_{max}) of the OX line reduced significantly at 24hai, before recovering at 48hai onwards (Figure 2-14a). A_{max} also significantly reduced for the Null until 48hai, before recovering at 72hai (Figure 2-14a). Significant interactions between the treatments and the genotypes only appeared in F_v/F_m ($P = 0.052$) (Figure 2-14b). The Null did not respond to any inoculations over time and it always remained at ~0.8 (Figure 2-14b). Significant differences were observed in PsbS-OX, as it increased in F_v/F_m at 24hai for all treatments, but it was only Zt508 that maintained higher F_v/F_m by 48hai (Figure 2-14b). No significant differences were observed for the remaining chlorophyll fluorescence and gas exchange parameters (Table 2-6). Relaxation ED_{50} and qI, both referring to dark conditions, didn't change significantly over time. Similarly, efficiency of PSII (φPSII) and photochemical quenching (qP) remained unchanged over time and there were no significant interactions, although there were some small reductions in both parameters on the OX line at 24hai regardless of inoculation (φPSII $P = 0.534$, qP $P = 0.647$). Finally, no significant differences were observed for stomatal conductance over time, but PsbS-OX inoculated with Zt22 seemed to maintain the highest g_s over time compared to rest of the of the treatments (g_s $P = 0.74$).

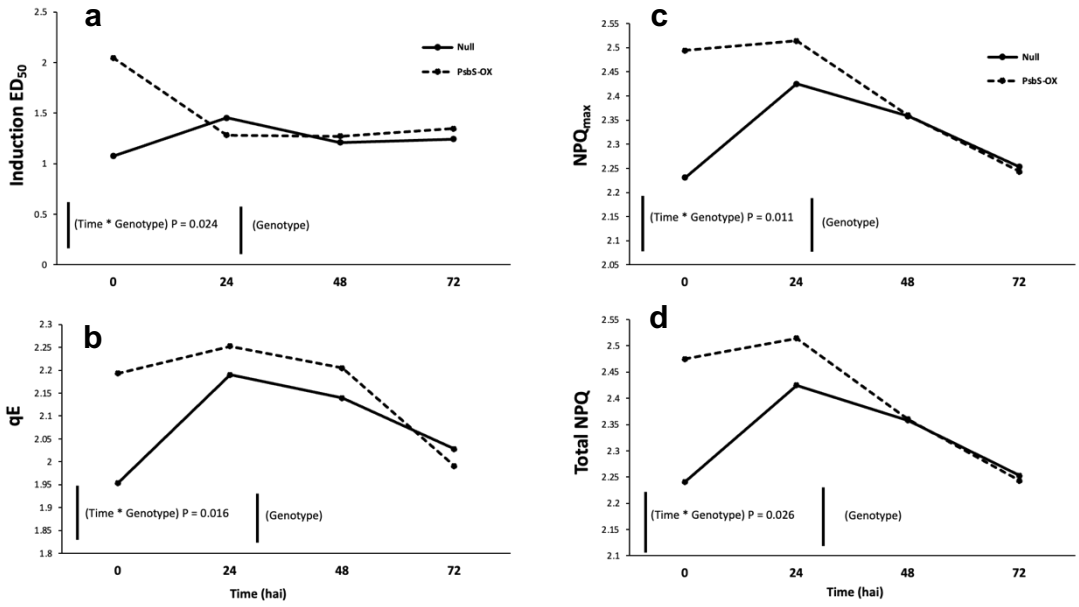


Figure 2-13. Genotypic differences over time for NPQ-related parameters upon inoculation, **(a)** Induction ED_{50} (minutes required for NPQ to reach 50% of its maximum), **(b)** qE, **(c)** NPQ_{max} and **(d)** total NPQ. Solid black line represents the Null and broken black line represents the OX line. ANOVA only showed genotypic significant differences, as presented here (no treatment or interaction effect). Vertical bars represent LSD of the significant interactions (n=4).

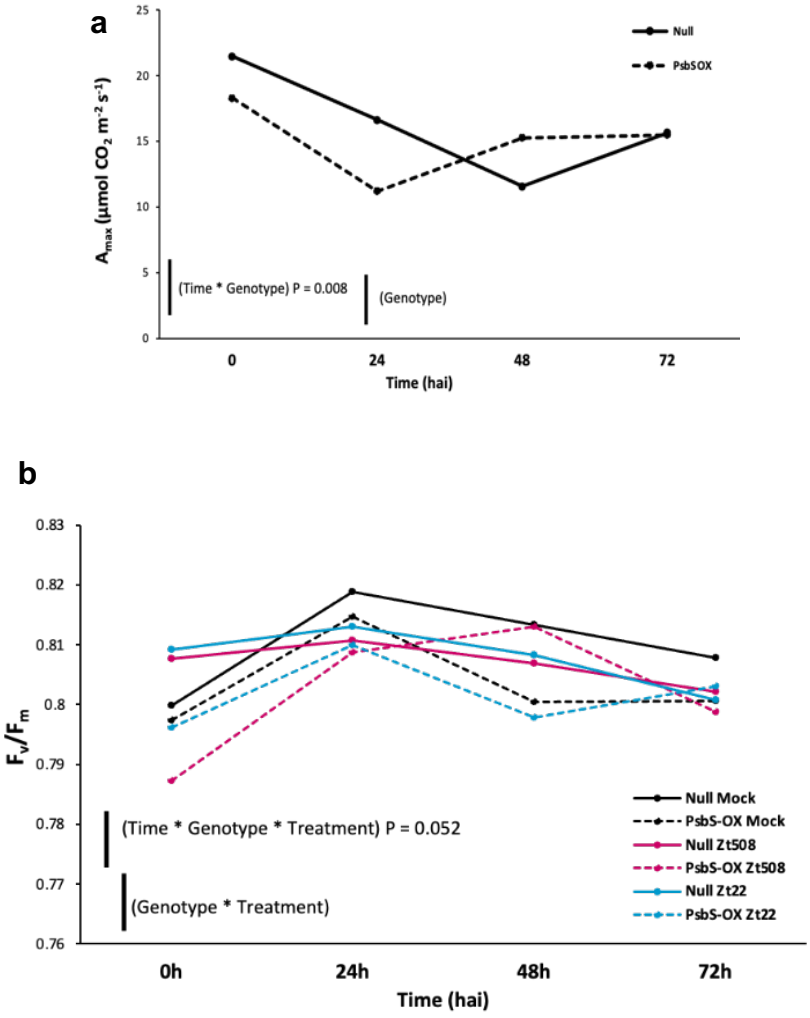


Figure 2-14. (a) Carbon assimilation (A_{max}) and **(b)** maximum efficiency of PSII (F_v/F_m) over time for the different treatments. Solid lines represent the Null and broken lines represent the OX line. Vertical bars represent LSD of the significant interactions (n=4).

Table 2-6. Chlorophyll fluorescence and gas exchange parameters for each treatment and genotype, over time. Data shown indicate means for each parameter, per genotype and treatment and per time point (n=4). Final three columns indicate significant values after repeated measurements ANOVA, followed by the respective LSD. TxG refers to Time x Genotype, TxT refers to Time x Treatment and TxGxT refers to the interaction of Time x Genotype X Treatment.

			Relaxation ED_{50}	qI	qP	φPSII	g_s
0h	Mock	Null	13.25	0.3	0.48	0.21	0.3
		OX	13.28	0.29	0.39	0.16	0.26
	IPO323	Null	13.3	0.29	0.49	0.22	0.34
		OX	13.31	0.27	0.41	0.16	0.26
	Zt22	Null	13.37	0.27	0.47	0.21	0.27
		OX	13.21	0.28	0.43	0.18	0.3
24h	Mock	Null	13.44	0.23	0.43	0.19	0.19
		OX	13.56	0.27	0.31	0.13	0.1
	IPO323	Null	13.39	0.22	0.41	0.18	0.19
		OX	13.48	0.25	0.34	0.14	0.13
	Zt22	Null	13.47	0.25	0.38	0.17	0.15
		OX	13.54	0.27	0.39	0.18	0.25
48h	Mock	Null	13.47	0.23	0.37	0.16	15
		OX	13.5	0.25	0.34	0.14	0.15
	IPO323	Null	13.48	0.23	0.42	0.18	0.15
		OX	13.47	0.24	0.37	0.16	0.15
	Zt22	Null	13.52	0.23	0.39	0.17	0.17
		OX	13.52	0.23	0.42	0.18	0.2
72h	Mock	Null	13.54	0.22	0.4	0.18	0.19
		OX	13.51	0.28	0.32	0.13	0.12
	IPO323	Null	13.48	0.23	0.42	0.18	0.23
		OX	13.47	0.23	0.43	0.19	0.17
	Zt22	Null	13.46	0.23	0.37	0.16	0.19
		OX	13.56	0.25	0.41	0.18	0.21
T x G *P*-value, LSD			0.061, 0.0674	0.278, 0.031	0.104, 0.0419	0.073, 0.0246	0.669, 0.0661
T x T *P*-value, LSD			0.526, 0.0826	0.751, 0.0379	0.533, 0.0513	0.584, 0.0301	0.801, 0.081
T x G x T *P*-value, LSD			0.543, 0.1168	0.787, 0.0537	0.647, 0.0725	0.534, 0.0425	0.74, 0.1145

c) *PsbS-OX plants challenged with an increased number of virulent isolates*

To investigate the durability of the tolerance response exhibited against *Z. tritici* by the over-expressing plants in another generation, a greater number of isolates with varying virulence against known *Stb* genes (Henry Tidd, personal communication) were included in inoculation assays (Table 2-2).

A new set of plants from T_2 generation (originating from that initial T_1 independently transformed line) were sown and were sent for genotyping (Table 2-7). From the genotyping results, we selected a homozygous plant with 2 copy numbers of the transgene and a Null plant with no copies. Those plants were selfed and seeds collected from those mother plants (T_3 generation) were used in this experiment. The presence of the construct and expression of the gene was confirmed with genomic DNA PCR and Western Blot analysis (Figures 2-15a-c). PsbS protein expression was significantly higher in the OX line compared to Fielder and the Null, confirming the successful over-expression of the inserted gene (Figure 2-15c).

Table 2-7. Genotyping results from T_2 generation plants. Cells highlighted in light pink were the plants selected to be selfed to T_3 and used their seeds for this experiment.

Sample	Copies *nptII*
PsbS-OX 1	3
PsbS-OX 2	3
PsbS-OX 3	3
PsbS-OX 4	3
PsbS-OX 5	3
PsbS-OX 6	3
PsbS-OX 7	3
PsbS-OX 8	3
PsbS-OX 9	2
PsbS-OX 10	3
Null 1	0
Null 2	0
Null 3	0
Null 4	0
Null 5	0
Null 6	0
Null 7	0
Null 8	0
Null 9	0
Null 10	0

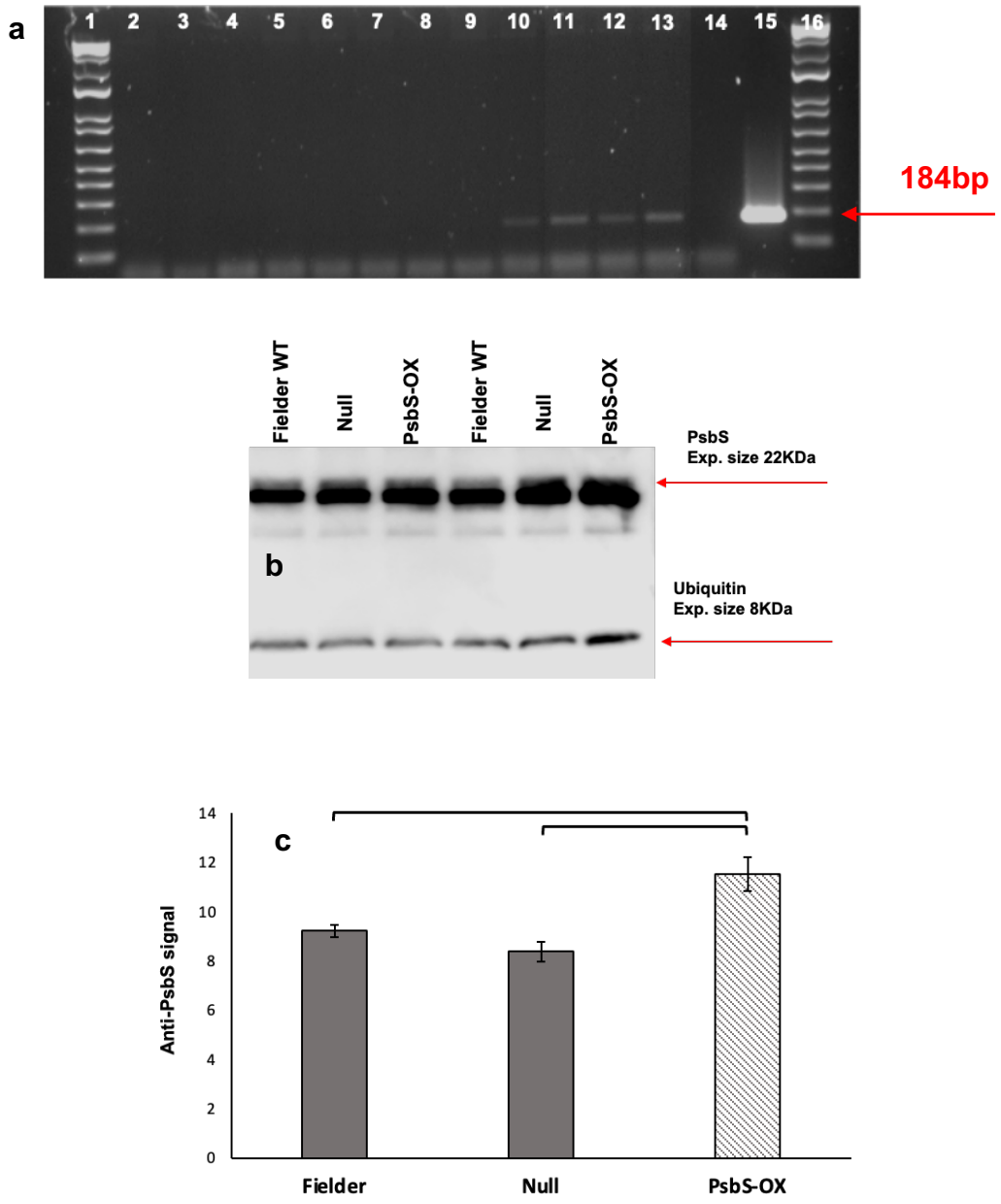


Figure 2-15. Molecular characterisation of the transgenic plants before inoculation. **(a)** Genomic DNA PCR to show the presence and absence of transgene in the Null and PsbS-OX, respectively. Lane 1: 1kb+ ladder, Lanes 2-5: Fielder, Lanes 6-9: Null, Lanes 10-13: PsbS-OX, Lane 14: -ve (H_2O) control, Lane 15: +ve (plasmid) control, Lane 16: 1kb+ ladder, **(b)** Immunoblot of PsbS and Ubiquitin, showing Fielder, Null and PsbS-OX in two technical replicates. Total protein was extracted from prepared thylakoids, **(c)** Band signal/intensity translated into numeric values for comparison. Bars represent means of each genotype ± SEM. Significant differences between the means are shown with horizontal bars (t-tests $P < 0.05$).

As described previously, the plants were also screened for their NPQ capacity. Due to the complexity of this experiment and the high number of experimental treatments, leaf sections of each plant were phenotyped using a chlorophyll fluorescence imaging method (FluorCam) at 0h and then at 24hai. The FluorCam allows the simultaneous measurement and imaging of chlorophyll fluorescence, however it cannot be used to measure gas exchange. Therefore, no stomatal conductance or assimilation data were obtained on this experiment. Additionally, as there were only two time points measured (0 and 24h), results were not analysed as Repeated Measurements, instead each time point is analysed separately.

The OX plants in this experiment exhibited significantly higher NPQ than the Null and Fielder but similar qE and ED_{50} compared to the Null (Figures 2-16a, b and c). Consistent with previous observations, plants showed no differences for qI (Figure 2-16f), however the Null seemed to have a significantly higher rate of relaxation (ED_{50}) than Fielder (Figure 2-16g). Finally, PsbS-OX plants had a reduced F_v/F_m and qP, compared to Fielder (Figures 2-16h and 2-16i).

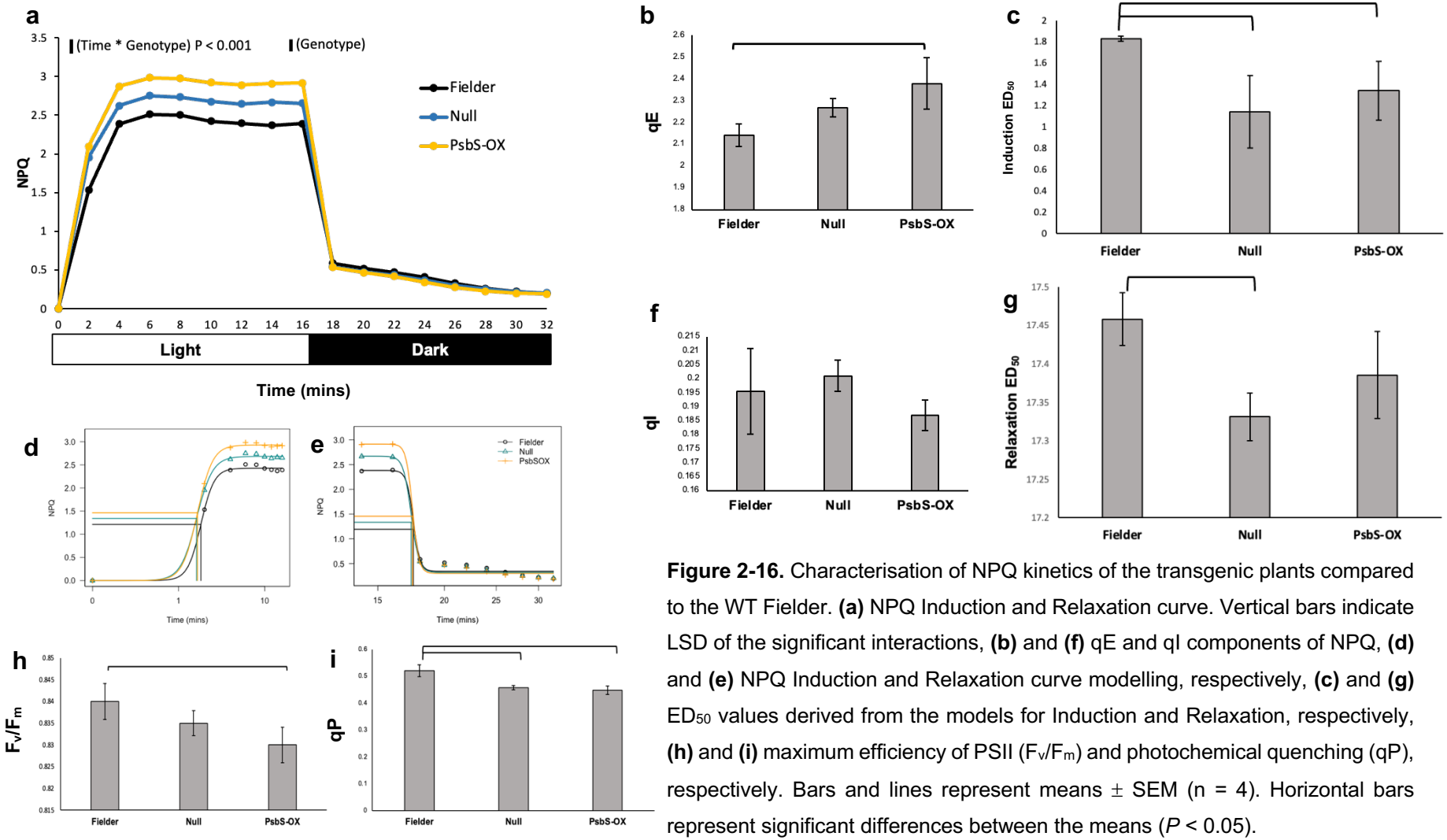


Figure 2-16. Characterisation of NPQ kinetics of the transgenic plants compared to the WT Fielder. **(a)** NPQ Induction and Relaxation curve. Vertical bars indicate LSD of the significant interactions, **(b)** and **(f)** qE and qI components of NPQ, **(d)** and **(e)** NPQ Induction and Relaxation curve modelling, respectively, **(c)** and **(g)** ED_{50} values derived from the models for Induction and Relaxation, respectively, **(h)** and **(i)** maximum efficiency of PSII (F_v/F_m) and photochemical quenching (qP), respectively. Bars and lines represent means ± SEM (n = 4). Horizontal bars represent significant differences between the means ($P < 0.05$).

Plants were inoculated with 8 isolates and phenotyped using the FluorCam at 24hai. The full list of isolates used is shown in Table 2-2. Disease was monitored for symptom initiation and pycnidia formation, visually assessed at different time points to produce the AUDPC and formed pycnidia were also counted at the end of the disease assessment (Figures 2-17 and 2-18). PsbS-OX always had significantly less pycnidia produced ($P = 0.031$) and exhibited lower AUDPC to all isolates apart from Zt96 which had significantly greater disease progression on the OX and Zt74 which behaved the same as the Null (Figure 2-18). Zt22, Zt25 and Zt52 caused significantly less disease on the OX line than in the Null (Figure 2-18a), whereas it was Zt508, Zt22 and Zt52 that did not yield much pycnidia overall ($P < 0.001$) (Figure 2-18b, bottom graph).

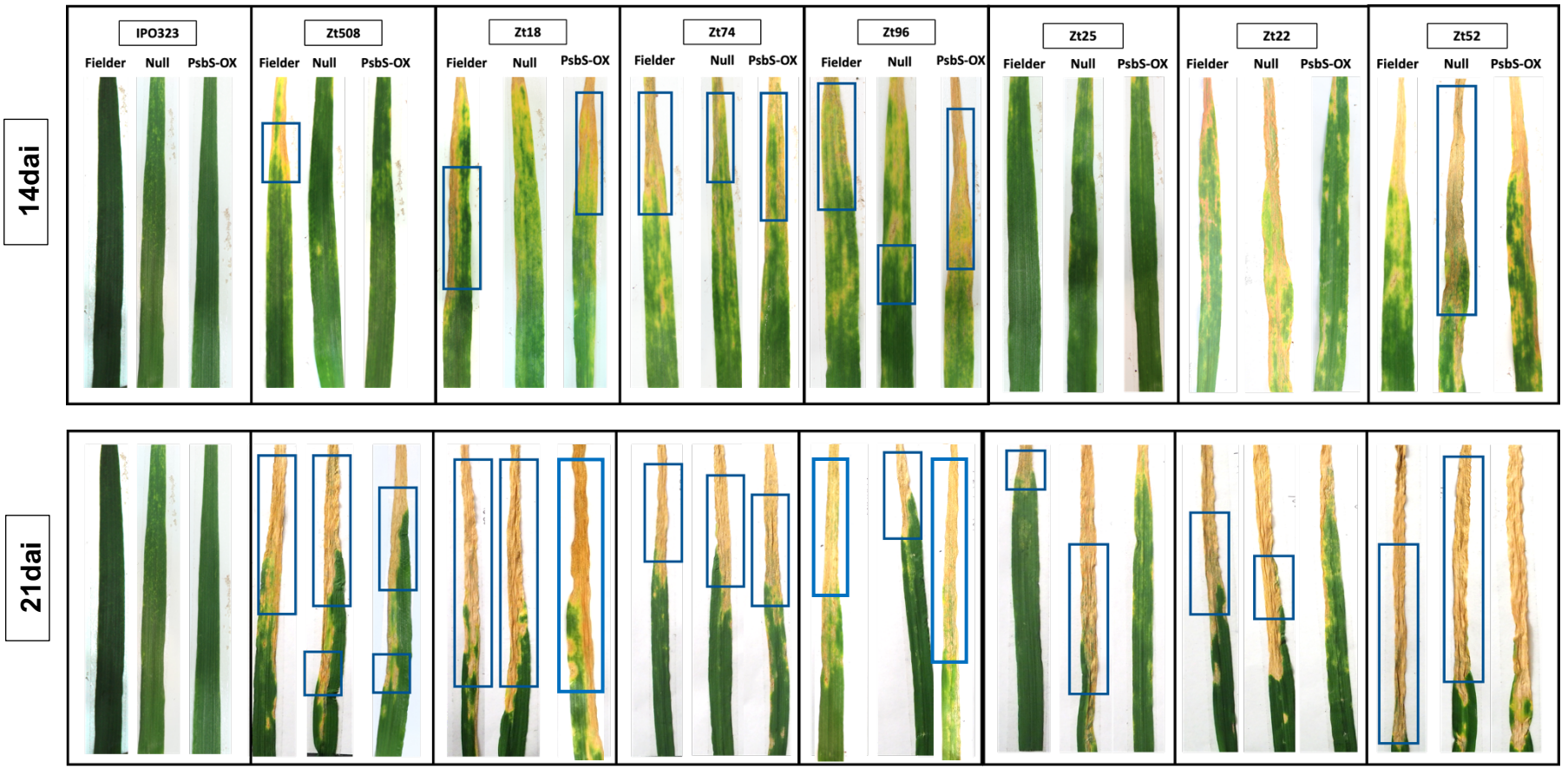


Figure 2-17. Disease phenotyping of all the isolates used in this experiment, at 14 and 21dai. The middle sections of the leaves are shown in these pictures. Blue boxes indicate presence of pycnidia on the necrotic tissue.

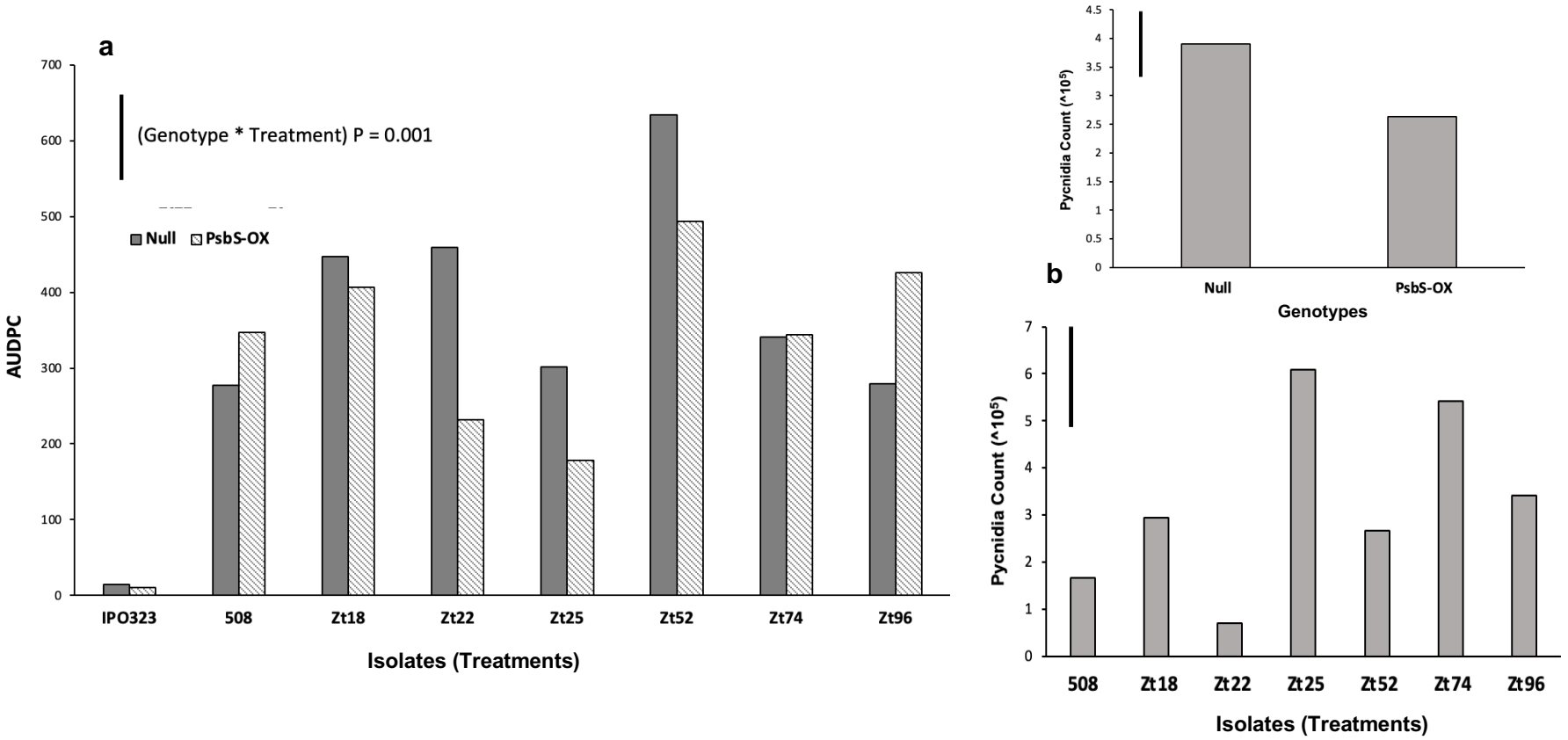


Figure 2-18. (a) AUDPC and **(b)** pycnidia counts for all genotypes and isolates. For **(a)** ANOVA showed significant interactions between the genotypes and the treatments, as seen on the graph. However, for **(b)** ANOVA only showed a significant effect of either the genotypes (top panel) or treatments (bottom panel) and no significant interactions. Dark grey solid bars represent the Null and grey shaded bars represent the PsbS-OX. Vertical bars represent LSD for the significant interactions or main effects of the analysis (n=4).

There was a significant interaction between the genotypes and the treatments at 24hai for maximum NPQ and qE (Figure 2-19a and 2-19b). There were no differences between the genotypes for isolates IPO323, Zt508, Zt18, Zt22, Zt74 and Zt96 for both NPQ_{max} and qE. However, PsbS-OX inoculated with Zt25 and Zt52 seemed to maintain higher NPQ and qE than the Null (Figure 2-19a and 2-19b). The Null had the lowest NPQ_{max} with Zt18, Zt25 and Zt74 that varied significantly from Zt96 that provided the highest NPQ for this genotype. However, it was only inoculation with Zt25 in the Null that also exhibited low qE and was significantly different to most of the isolates (Figure 2-19b). No significant differences for maximum NPQ or qE were observed for PsbS-OX inoculated with any of the isolates (Figures 2-19a and 2-19b). Additionally, no significant interactions between the genotypes and treatments were observed for the rest of the parameters, instead isolate (i.e. Treatment) was significant for all of them (Table 2-8). Zt18 and Zt74, two very virulent isolates, did not affect the relaxation of NPQ and maintained low qI compared to the other isolates. They also reduced F_v/F_m, associated with PSII efficiency, although not to photoinhibitory levels (< 0.78) (Table 2-8). Photochemical quenching was only significantly downregulated from the effect of isolate Zt22, irrespective of the genotype (Table 2-8).

ROS staining was performed simultaneously as NPQ screening, by sampling the same leaf for the FluorCam and the staining. No obvious differences came through the ROS staining, however in Zt22 and Zt25, the two isolates to which PsbS-OX provided enhanced tolerance, there was enhanced DAB staining for H_2O_2 and more superoxide in the PsbS-OX inoculated with Zt25 (Figure 2-20).

Finally, we checked PsbS quantity in newly emerged leaves of plants pre-infected with *Z. tritici*. We sampled asymptomatic flag leaves of plants inoculated with IPO323, Zt22 and Zt508 as they were used across all three experiments. Plants were approximately 4 weeks older from time of inoculation. Total proteins were extracted from the leaves and quantified with a Bradford assay (not through thylakoid extraction) and western blots were performed as previously described. Figures 2-21a and 2-21b show different trials of PsbS western blots and Figure 2-21c shows PsbS expression for each

genotype and treatment upon normalisation to ubiquitin. The amount of PsbS present in the Null had significantly dropped in plants pre-inoculated with Zt22 and Zt508, compared to IPO323 (Figure 2-21c). In contrast, it was OX plants pre-inoculated with Zt508 that maintained significantly high levels of PsbS protein compared to the other two treatments (Figure 2-21c). This work is still currently on progress by Mrs. Charlene Dambire, aiming to measure the amount of PsbS protein from inoculated leaves (sampled at 22 dai) with same isolates, in order to understand whether inoculation had an effect on PsbS protein levels or whether the over-expressers were able to maintain their high expression upon inoculation.

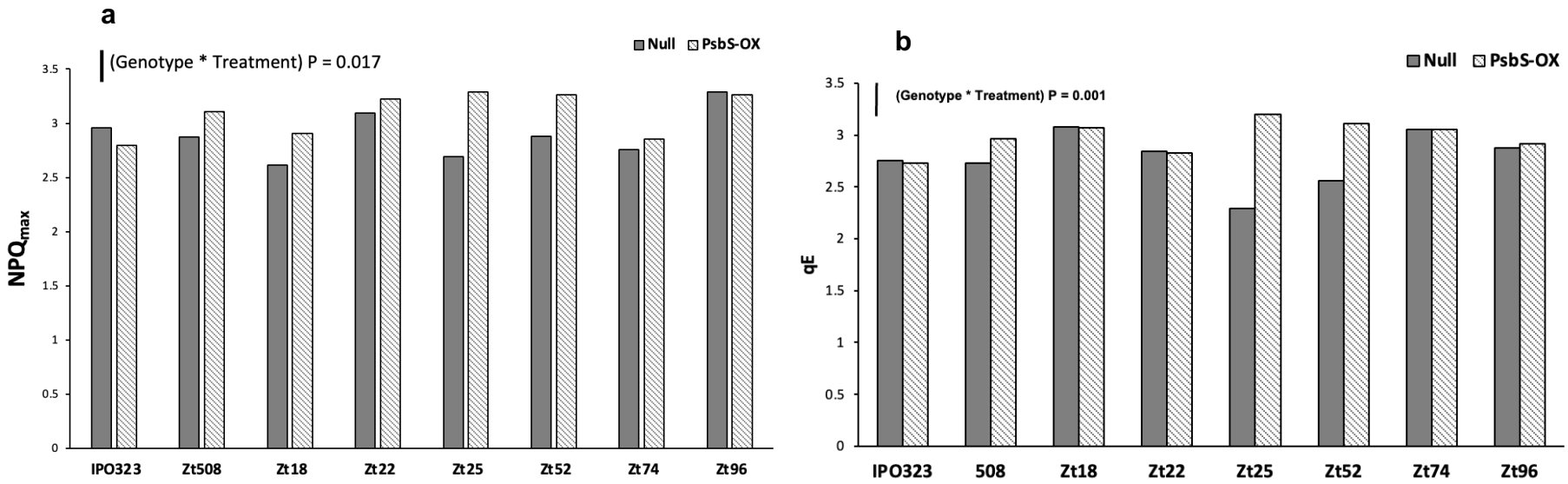


Figure 2-19. (a) NPQ_{max} and **(b)** qE at 24hai for the interaction between the genotypes and the treatments. ANOVA showed significant interactions between the genotypes and the treatments, as shown on the graphs. Vertical bars represent LSD for the significant interaction. Dark grey solid bars represent mean values of the Null and grey shaded bars represent mean values of PsbS-OX (n=4).

Table 2-8. Chlorophyll fluorescence parameters derived from the FluorCam at 24hai. Significant values along with LSDs (in brackets) are shown at the bottom of the table for the main effects (genotype or treatment) and the significant interaction (n=4).

	Induction ED_{50}		**qI**		**F_v/F_m**		**qP**	
	Null	**PsbS-OX**	**Null**	**PsbS-OX**	**Null**	**PsbS-OX**	**Null**	**PsbS-OX**
IPO323	1.73	1.60	0.18	0.19	0.82	0.82	0.38	0.38
Zt508	1.63	1.73	0.16	0.22	0.83	0.82	0.41	0.41
Zt18	1.38	1.06	0.14	0.14	0.82	0.81	0.39	0.38
Zt22	1.41	1.64	0.21	0.22	0.85	0.84	0.31	0.31
Zt25	0.95	0.98	0.18	0.17	0.84	0.84	0.36	0.37
Zt52	1.03	1.23	0.21	0.22	0.84	0.85	0.36	0.35
Zt74	1.36	1.58	0.14	0.16	0.82	0.83	0.39	0.42
Zt96	0.78	0.94	0.20	0.19	0.84	0.84	0.38	0.36
Genotype (*LSD*)	0.278 (0.113)		0.095 (0.015)		0.595 (0.002)		0.782 (0.018)	
Treatment (*LSD*)	**< 0.001** (0.226)		**< 0.001** (0.029)		**< 0.001** (0.005)		**< 0.001** (0.036)	
Genotype x Treatment (*LSD*)	0.19 (0.32)		0.465 (0.041)		0.161 (0.007)		0.956 (0.051)	

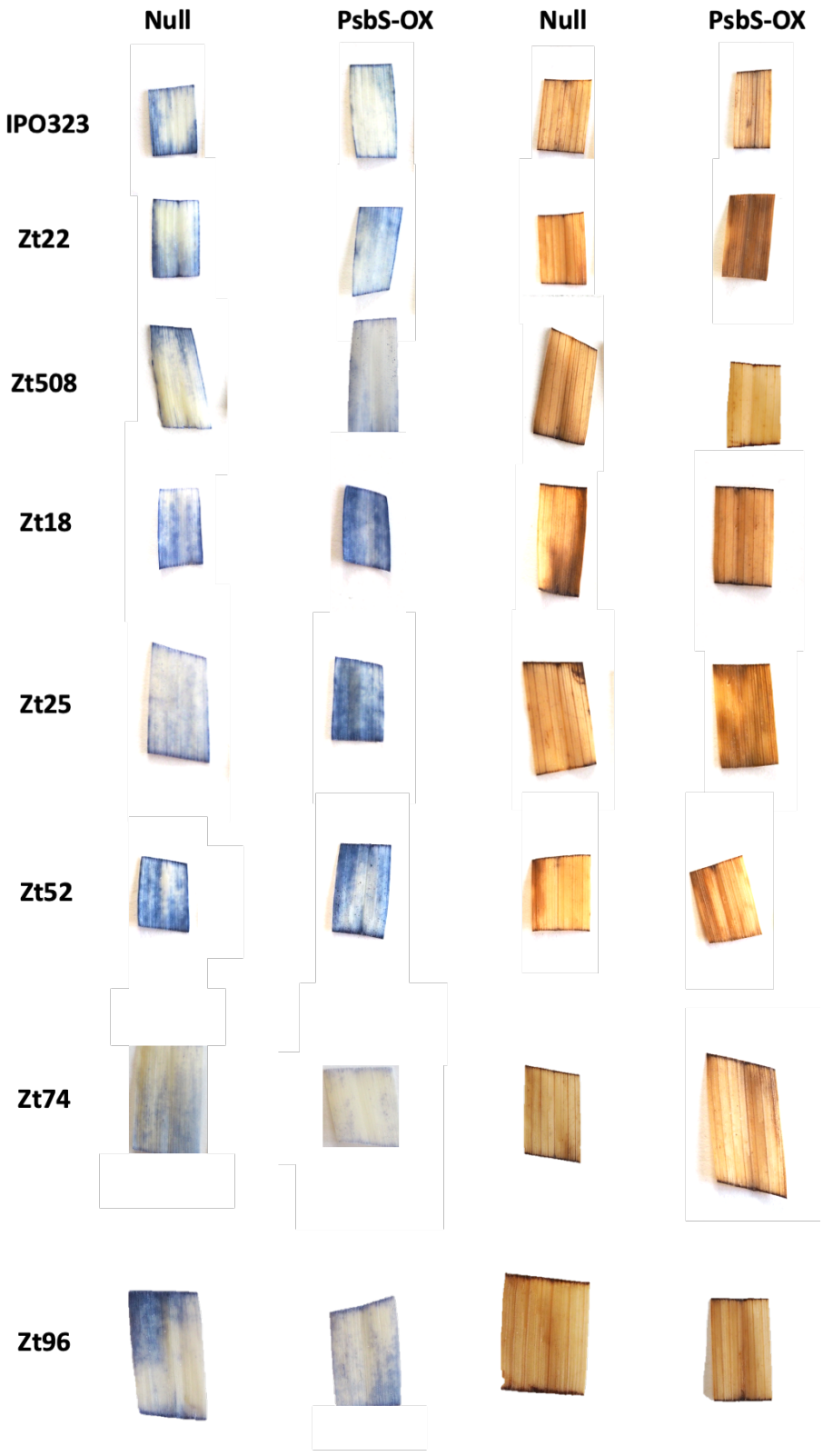


Figure 2-20. ROS staining for superoxide O_2^- (blue stain - left) and hydrogen peroxide H_2O_2 (brown stain - right) at 24hai for both genotypes (Null and PsbS-OX) and all isolates used in this experiment.

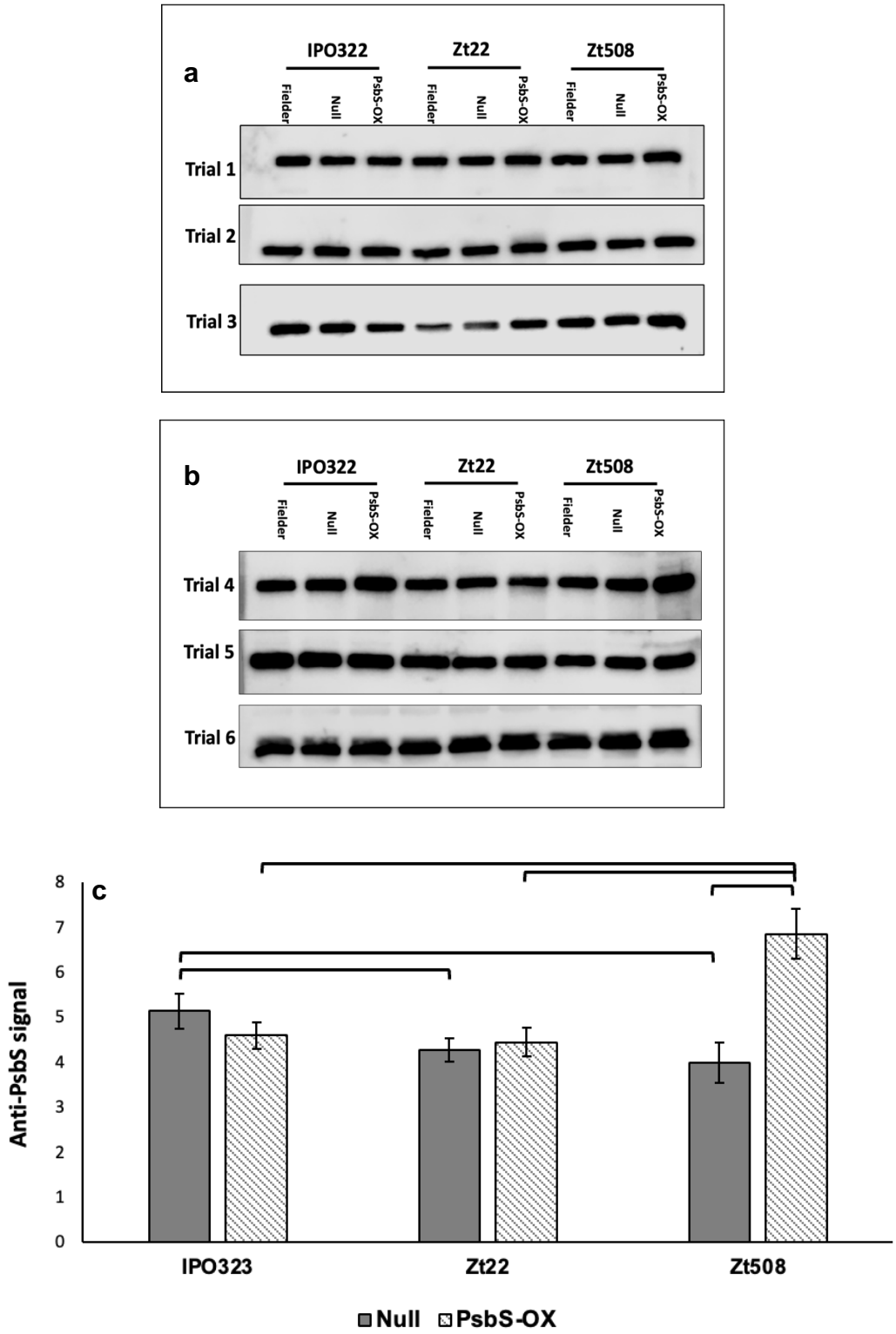


Figure 2-21. Protein expression of PsbS on Fielder, Null and PsbS-OX that had been previously infected with the *Z. tritici* isolates IPO323, Zt22 and Zt508. **(a)** and **(b)** Blots, **(c)** signal intensity upon normalisation to Ubiquitin. Data represent means ± SEM. Significant differences between the means are shown with black horizontal bars (t-tests $P < 0.05$).

2.4 Discussion

Here, we have shown for the first time a broad tolerance and a durable response to a range of *Z. tritici* isolates in wheat plants over-expressing the photoprotective protein PsbS. This was manifested as reduced pycnidia and AUDPC in the OX line. The mechanism appears to operate via NPQ-priming of wheat lines, as enhanced qE, providing evidence of photoprotection being involved in plant basal defence. There is limited research on the involvement of the photoprotective protein PsbS in plant defence responses against pathogens. Moreover, no studies have been published on the involvement of PsbS in the wheat – *Zymoseptoria tritici* pathosystem. The range of isolates used in this study have been tested against multiple *Stb* resistance genes, such as *Stb7* and *Stb16*, and they all resulted in necrosis and pycnidia production (Henry Tidd and Kostya Kanyuka, personal communication). However, over-expressing PsbS resulted in significantly less symptoms and/or pycnidia development for the majority of those isolates. The involvement of PsbS in defence, and consequently NPQ, has been previously shown to vary upon pathosystems. Specifically, reduction of NPQ and PsbS deficiency have been shown to be beneficial for defence against herbivory, biotrophic or hemi-biotrophic pathogens. For instance, PsbS and NPQ were downregulated in *Arabidopsis* in response to the bacterial flagellin flg22 (Göhre et al., 2012) or in susceptible rice in response to *Rhizoctonia solani* (Ghosh et al., 2017), but increased, through the enhanced production of zeaxanthin, in *Arabidopsis* susceptible response to *Sclerotinia sclerotiorum* (Zhou et al., 2015) and in resistant rice in response to *R. solani* (Zhang et al., 2017). However, only a few studies have shown the involvement of altered copies of PsbS in defence response. Research from the Jansson group (Frenkel et al., 2009; Jänkänpää et al., 2013) used both an *Arabidopsis* PsbS-deficient mutant (*npq4*) and an over-expressing PsbS to show enhanced levels of the stress hormone jasmonic acid in the former and enhanced preference of herbivory in the latter. Using PsbS knock-out (KO) rice plants, Zulfugarov et al. (2016) showed that the PsbS-deficient rice plants exhibited enhanced resistance to the rice-specific fungus *Magnaporthe oryzae* and bacteria *Xanthomonas oryzae* pv.*oryzae*. However, excessive ROS, typical for PsbS deficient plants (KO), is

likely be counterproductive in the wheat-*Z. tritici* pathosystem, where the pathogen benefits from hypersensitive response and cell death. Furthermore, the accumulation of ROS can be particularly damaging to photosystems under excessive light conditions, which benefits *Z. tritici* virulence (Ajigboye et al., 2021). Therefore, PsbS-mediated NPQ can effectively remove the potential damage by accelerating the process of thermal dissipation in the chloroplast. Indeed, elevated NPQ acting as a dissipative mechanism is associated with suppression of ROS (Göhre et al., 2012; Zulfugarov et al., 2016; Kress & Jahns, 2017). As shown in our staining here, ROS was difficult to quantify in response to *Z. tritici* isolates and we could not show consistent ROS response, which could also be related to the detoxification systems operating in the PsbS over-expressing lines or even in the background line, Fielder.

In this work, we found that reduced *Z. tritici* symptoms in PsbS over-expressing wheat plants was associated not just with their higher capacity for NPQ but also with other physiological traits, such as reduced stomatal conductance, reduced operating efficiency of PSII (φPSII) and reduced photochemical quenching (qP) before any inoculations occurred. The chloroplastic quinone A (Q_A) is the primary electron acceptor downstream of PSII and its oxidation state (i.e. how many electrons it carries) reflects the balance between excitation energy at PSII and the rate of the Calvin-Benson cycle in the electron transport chain (Głowacka et al., 2018). It has also been suggested that the redox state of Q_A acts as an early signal for stomatal opening in response to light, with a more reduced Q_A pool (i.e. more electrons) corresponding to increased stomatal opening (Busch, 2014). NPQ through PsbS, acts to relieve the excitation pressure on PSII and consequently directly affects the rate at which excitation energy absorbed by PSII is used to reduce Q_A. Over-expressing PsbS in *Nicotiana tabacum*, Głowacka et al. (2018) showed that those plants had a decreased stomatal opening in response to light while keeping the redox state of Q_A more oxidised (i.e. less electrons) and without affecting CO_2 assimilation. It is highly possible that this could also be contributing to the underlying mechanism behind the wheat plants over-expressing PsbS in our experiments.

No effects on photoinhibitory quenching (qI) were observed upon any *Z. tritici* inoculations on the OX plants, confirming the notion that qE is able to regulate the excess excitation pressure on PSII and lower its susceptibility to photoinhibition (Roach & Krieger-Liszkay, 2012). Photoinhibition has been associated with zeaxanthin, the xanthophyll cycle carotenoid that also takes part in activation of NPQ (Kress & Jahns, 2017). High NPQ capacity of the OX plants could also be an indication of higher levels of zeaxanthin, which also serves as a powerful antioxidant in the chloroplast (Kress & Jahns, 2017). Finally, the xanthophyll cycle carotenoids are precursor molecules of important plant hormones associated with defence (Zhou et al., 2015), but are also involved in the organisation of PSII within the thylakoid membrane (Johnson et al., 2011). Therefore, enhanced tolerance to *Z. tritici* through elevated levels of PsbS could also be a result of the intricate communication between PsbS and the carotenoids or even binding affinity to other LHCs. PsbS has been shown to bind to another PSII protein, Light-Harvesting Complex II subunit 5 (LHCB5) (Liu et al., 2019; Littlejohn et al., 2021). Liu et al. (2019) showed that rice infected with the foliar leaf pathogen *Magnaporthe oryzae* activated the promoter of LHCB5 in a light-dependent expression and through phosphorylation events, LHCB5 and superoxide accumulated in the chloroplast and enhanced basal immunity to that pathogen. They predicted that phosphorylated LHCB5 forms a trimeric complex that disrupts its binding to PsbS, which leads to reduced electron transfer, increase in chloroplastic ROS and ultimately enhancement of basal resistance (Liu et al., 2019). The opposite event maybe taking place with the OX plants here. In addition, a study on the *Arabidopsis* Thylakoid Formation 1 (Thf1), a critical protein in PSII dynamics, organisation and repair, observed similar properties of PsbS with Thf1, involving the stabilisation of PSII macrostructure and the fluidity of the thylakoid membrane (Huang et al., 2013). Therefore, PsbS could be indirectly involved in several more chloroplastic processes that influence our observed tolerance to *Z. tritici*.

Colonization of substomatal cavities and the intercellular space between mesophyll cells, formation of mature pycnidia in the substomatal cavities and subsequent extrusion of pycnidiospore-bearing cirrhi are the key steps in

completing a successful infection cycle (Kema et al., 1996). Also, there are several ways disease progression on *Zymoseptoria tritici*-inoculated leaves can be monitored. Assessment can either separate the percentage of chlorotic against necrotic area or consider the total percentage of leaf covered with disease symptoms. The presence and/or abundance of pycnidia contributes to increased severity, virulence and progression of disease. Previous work in *Z. tritici* clearly established that necrosis and pycnidia formation were controlled by separate genetic loci (Stewart et al., 2017). Also, it has been previously proposed that three major factors affect the pycnidia production of *Z. tritici* on infected wheat leaves: nutrients, the fitness of the pathogen and the host response (Stewart & McDonald, 2014), of which the latter two are interconnected. In this work, we assessed STB disease based on total percentage of the assessed leaf that had both chlorotic and necrotic lesions, as well as the abundance of pycnidia at the end of the assessment period (21dai). Certain *Z. tritici* isolates that would normally be virulent on genotypes carrying the *Stb6* resistance gene, appeared to have reduced virulence on plants over-expressing PsbS. Specifically Zt22, Zt25 and Zt508 not only exhibited reduced necrosis but were also impaired in forming pycnidia. On the other hand, Zt52 caused necrosis on the leaves, however it was impaired in pycnidia production. This could potentially indicate that PsbS-mediated resistance to pycnidia formation and tolerance operates through durable, quantitative effects. Various studies with mutated virulent strains of *Z. tritici* have shown quantitative effects on disease progression. For example, the avirulence gene *Avr3D1* interacts with *Stb7*-containing wheat cultivars in a gene-for-gene manner, however it is still able to cause infection even after its expression and recognition (Meile et al., 2018). Earlier studies by Poppe et al. (2015) showed that one deletion mutant strain of IPO323 showed reduced pycnidia formation on infected wheat leaves whereas another showed a hypervirulent phenotype with enhanced pycnidia formation during infection. Also, transcriptomic studies on *Z. tritici* suggest that the pathogen actively reprogrammes its gene expression when transitioning from the latent period to the necrotrophic stage of infection (Kellner et al., 2014; Rudd et al., 2015; Palma-Guerrero et al., 2016; Haueisen et al., 2019). Palma-Guerrero et al.

(2016) were able to show quantitative differences in virulence between isolates that infected the same wheat cultivar. However, by the end of this present study, it remains unknown how PsbS may alter the expression of virulence-related *Z. tritici* genes, delay the initiation of symptoms or the onset of pycnidia formation, or whether PsbS could even interact directly with the pathogen. These are key questions that require further investigation.

Finally, it is possible that the basal defence the PsbS over-expressing plants exhibited to *Z. tritici* isolates in this study, operated through elevated levels of chloroplast-associated salicylic acid (SA). Previous studies have shown that plants lacking PsbS were accompanied by increased levels of jasmonate metabolism, induced via increased ROS and lipid peroxidation (Frenkel et al., 2009; Demmig-Adams et al., 2013; Jänkänpää et al., 2013; Zulfugarov et al., 2014, 2016). Jasmonic acid (JA) is usually antagonistic to SA, while it has also been shown that SA is essential for regulating redox homeostasis (Mateo et al., 2006) and is induced upon PSII re-organisation conditions (Duan et al., 2019).

Further investigation is mandatory in order to characterise and understand how PsbS could interact with the pathogen or affect its growth on the plant. Future experiments could include:

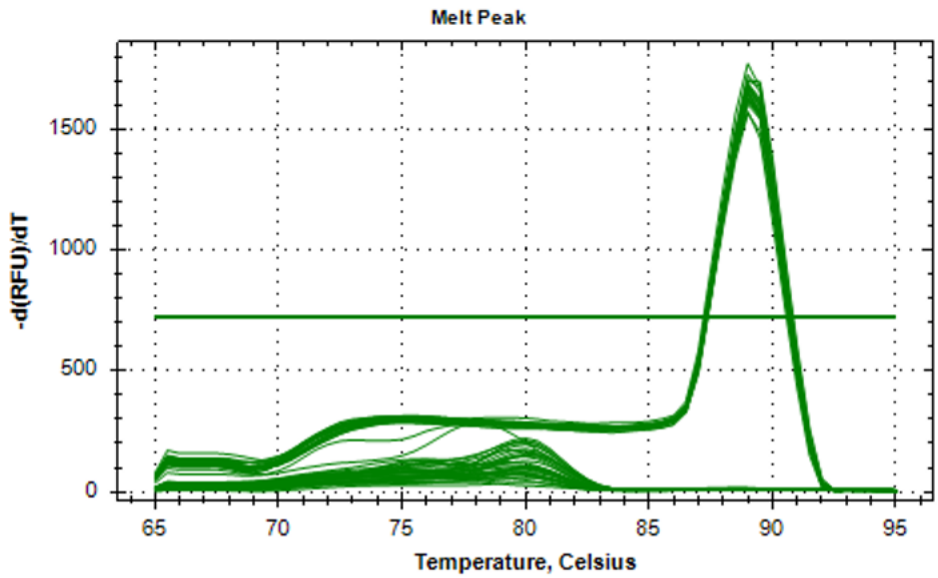
- NPQ is induced under a variety of environmental stressors, with a major one being high light intensities. The work of Liu et al. (2019) exhibited the importance of light intensity in defence response through the involvement of key PSII proteins. To our knowledge, this has never been done for the wheat – *Z. tritici* pathosystem and in combination with over-expressing PsbS, it could be an extremely informative experiment to be conducted. Perhaps, if PsbS is already primed by high light intensities, the response to infection would be even greater.
- Virus-Induced Gene Silencing (VIGS) could be used to transiently silence PsbS while similar NPQ and disease screening experiments could take place. This, in combination with plants over-expressing PsbS, would enable us to further understand this interaction.
- In this work we showed how over-expressing PsbS can impact either the extend of necrosis on the leaf caused by *Z. tritici* or the ability of the

pathogen to sporulate. From the plants with reduced pycnidia formation due to the over-expression of PsbS, pycnidia could be harvested and tested, *in vitro* or *in vivo*, for their virulence and viability. Isolates that were able to sporulate, even in such reduced levels, on the OX lines perhaps have lost their virulence and would be unable to cause disease on subsequent infections.

- If PsbS over-expression is indeed affecting stomatal aperture and in turn, *Z. tritici* proliferation, further investigation is needed involving microscopy studies and/or mutant strains of the pathogen. Also, it would be interesting to investigate whether droughted WT and OX plants, would exhibit the same disease phenotype as well-watered plants. Closed stomata to preserve water losses in combination with reduced stomatal conductance from PsbS over-expression, would perhaps make the plant a very unfavourable host.

As resistance keeps breaking down and Septoria isolates keep evolving, the chloroplast is still an underestimated, less studied source for modifications and investigation for disease resistance. Although PsbS is not the only mechanism plants possess to modify NPQ capacity, the rapid kinetics of PsbS-dependent qE make the latter an attractive component of plant defence, which could be harder for *Z. tritici* to exploit and manipulate. PsbS could be included in breeding programs, aiming to pyramid individual resistance genes with the durable tolerant phenotype that the PsbS provides.

2.5 Supplementary data



SF 2-1. qPCR melt curve analysis showing a peak appearing with OsPsbS primers only on the transgenic PsbS-OX plants.

Chapter 3 Role of photoprotection in *Stb6*-mediated responses to *Zymoseptoria tritici*

Acknowledgement of contributions

We would like to thank Dr. Cyrille Saintenac (INRAE, France) for providing the plant material used in this study. Also, Mrs. Charlene Dambire performed the western blot presented in this chapter, upon initial optimisation performed by myself. Finally, we would like to thank Dr Petra Ungerer and Dr Vasco Giovagnetti for assisting with the HPLC analysis of the carotenoids (Queen Mary University of London, UK).

3.1 Introduction

Zymoseptoria tritici is an adapted wheat (*Triticum aestivum*) pathogen causing Septoria Tritici Blotch (STB) and is one of the most important fungal pathogens of wheat production in Europe (Fones & Gurr, 2015) . *Z. tritici* is considered a latent necrotroph, as in the initial symptomless phase of host invasion (up to 14 days), the pathogen does not acquire any nutrients from the host and does not significantly increase in biomass (Rudd et al., 2015; Sánchez-Vallet et al., 2015). *Z. tritici* grows initially on the leaf surface without producing any penetrating structures, such as appressoria or haustoria (Kema et al., 1996) before entering the plant through the stomata. The pathogen invades the intercellular space to colonise the apoplast prior to switching to the necrotrophic phase to complete its reproduction with the development of pycnidia in the substomatal cavities (Kema et al., 1996). *Z. tritici* is fast-evolving to quickly gain resistance to many major fungicides but also to overcome plant resistance genes (R genes) (Petit-Houdenot et al., 2021). Great efforts have taken place to characterise and understand major plant R genes that provide durable resistance and can be incorporated in breeding strategies. *Stb6* is a major R gene that was recently cloned and characterised (Brading et al., 2002; Brown et al., 2015; Saintenac et al., 2018). It is a member of the Wall-Associated Kinase (WAK) gene family and confers immunity against isolates of *Z. tritici* expressing specific isoforms of the secreted effector protein AvrStb6 (Brading et al., 2002; Zhong et al., 2017). *Stb6* is only

expressed in wheat leaves and does not seem to play a role in plant growth and development, as wheat *stb6*-knockout lines do not show any phenotypic differences from the wild-type, other than susceptibility to *Z. tritici* carrying AvrStb6 (Saintenac et al., 2018). The same authors demonstrated that *Stb6* is involved in a gene-for-gene interaction with *AvrStb6* and that Stb6 kinase activity is required for *Stb6*-mediated immune response (Saintenac et al., 2018). However, it is still unknown whether *Stb6* and *AvrStb6* interact directly with each other or there is another component involved in the pathogen recognition.

Pathogen recognition generally triggers the accumulation of reactive oxygen species (ROS) which are necessary for the initiation of hypersensitive response (HR), a form of programmed cell death (PCD), and successful immunity (Serrano et al., 2016). A major source of ROS in plants is the chloroplast (Foyer, 2018). Pathogenesis-related continuous ROS formation from excessive excitation energy due to over-reductions of the photosynthetic electron transport chain increases the imbalance in the chloroplast redox state and induces oxidative stress leading to photodamage in leaves (Triantaphylidès & Havaux, 2009). Plants possess highly sophisticated mechanisms to detoxify and regulate ROS and protect the integrity of the photosynthetic apparatus, mainly on the side of Photosystem II (PSII). These photoprotective mechanisms, or else photoprotection, vary depending on the timeframes they operate and on the underlying molecular mechanisms, however photoprotection through thermal dissipation of excess excitation energy via non-photochemical quenching (NPQ) is considered as the major mechanism (Murchie & Lawson, 2013; Murchie & Ruban, 2020). NPQ is characterised by different components based on their formation timescales; qE is the dominant component of NPQ as it is the fast-forming, energy-dependent quenching form, qT is associated with state transitions processes (energy balancing between the two photosystems) and qI is the slow-relaxing component of NPQ normally associated with a combination of photoinhibition of PSII and photoprotection (Demmig-Adams & Adams, 2006; Nilkens et al., 2010; Murchie & Ruban, 2020). Activation of the qE component of NPQ is achieved through production of zeaxanthin (Zea) in the xanthophyll cycle (XC),

involving conversion of violaxanthin (Vio) to Zea via the enzyme violaxanthin de-epoxidase (VDE) and structural re-organisation of the light-harvesting complex (LHC) proteins of PSII, triggered by acidification of the lumen (ΔpH) and protonation of the protein PsbS (Ruban, 2016). Under low light, Zea is converted back to Vio via zeaxanthin epoxidase (ZEP), and can be further converted to Neoxanthin (Neo) and xanthoxin through a series of isomerisation reactions (Jahns et al., 2009). 9-*cis*-epoxycarotenoid dioxygenase (NCED) ultimately cleaves xanthoxin from the C_{40} carotenoid to form abscisic acid (ABA), which can positively regulate plant immunity at the early stages of defence response (Ton et al., 2009). Other hormones involved in plant defence also originate in the chloroplast, for example membrane lipid peroxidation triggers the formation of OPDA, a precursor molecule in the biosynthesis of jasmonic acid (JA), a defence-related plant hormone (Demmig-Adams et al., 2013; Wasternack & Feussner, 2017). Additionally, salicylic acid (SA) biosynthesis, another defence-related plant hormone, originates in the chloroplast through the catalytic activity of isochorismate synthase (Rekhter et al., 2019).

The chloroplast is not only the site of photosynthesis but has also been demonstrated to be increasingly involved in the regulation of defence and response to numerous plant pathogens, but also for *Z. tritici*. First Kema et al. (1996) showed major changes in the chloroplast morphology and movement in the first 48 hours following infection by *Z tritici*. Previously (Chapter 1), we had observed how photoprotection and specifically the photoprotection-regulating protein PsbS is involved in disease tolerance to *Z. tritici* and how NPQ kinetics are associated with defence responses. The US spring wheat variety Fielder, that contains *Stb6*, was used for the transformation to create PsbS-overexpressing plants. However, not much is known between photoprotective responses and *Stb6*. For instance, Lee et al. (2015) showed compromised *Z. tritici* resistance on *Stb6*-containing genotypes after silencing two key chloroplast genes involved in the carotenoid and chlorophyll biosynthesis (phytoene desaturase and Mg-chelatase subunit H, respectively). Recently, Ajigboye et al. (2021) associated resistance to *Z. tritici* in the wheat cultivar Cougar, that contains *Stb6*, with qI type of NPQ, increased xanthophyll

neoxanthin and ABA/JA modulated defence. Here, we characterised the photoprotective mechanism of *Stb6*-mediated resistance at the early time points of disease development, using detailed chlorophyll fluorescence measurements with RNA sequencing studies of Near Isogenic Lines of *Stb6* in compatible and incompatible interactions with two *Z. tritici* strains. We hypothesised that changes in the stoichiometry and activity of core and light-harvesting PSII proteins of the resistant host, caused by photoinhibitory photoprotection and aided by the action of the xanthophyll cycle, allow the host to downregulate PSII function to allow changes in metabolism for defence. In contrast, we explored the possibility that virulent *Z. tritici* may target the chloroplast to cause changes in the photosynthetic machinery associated with collapse over time.

3.2 Materials & Methods

3.2.1 Plant material and growth conditions

Two Near-Isogenic wheat lines (NILs) were used in this study, the spring wheat Courtot with susceptible phenotype (S) and its near-isogenic line Ct (+Stb6) (through backcrossing with the *Stb6*-containing variety Chinese Spring) with the resistant immune phenotype (R) for *Z. tritici* strains that contain the avirulent gene *AvrStb6* (Zhong et al., 2017). Seeds were germinated in FS2 soil compost in modular trays and then transplanted in 1 L pots with John Innes no.2 soil compost. Plants were grown at 18 °C day and night temperature, 16h photoperiod, 55 ± 5% RH and ~250 µmols m^{-2} s^{-1} Photosynthetic Photon Flux Density (PPFD) light intensity. All experiments were performed on ~4-week-old plants. Physiological measurements were repeated twice with 4 biological replicates per treatment/genotype, whereas all other experiments were conducted with 3 biological replicates.

3.2.2 *Zymoseptoria tritici* isolates and inoculations

Two *Z. tritici* (Zt) isolates with different level of virulence were used in this study, kindly provided by Dr Kostya Kanyuka (previously at Rothamsted Research, currently at NIAB, Cambridge, UK). The reference isolate IPO323 contains the avirulent gene *AvrStb6* and results in an incompatible interaction

with any wheat variety carrying *Stb6* (Zhong et al., 2017). The other isolate, hereafter termed as Zt22, has an isoform of *AvrStb6*, named I-17 (Stephens et al., 2021), resulting in compatible interactions with both genotypes, Courtot and Ct (+Stb6).

All isolates were kept in 70% sterile glycerol stock solutions in -80 °C and were grown on yeast peptone dextrose (YPD) agar (Sigma Aldrich) for 5 days at room temperature. Spores were then suspended in sterile, deionised 0.01% (v/v) Tween20 H_2O and concentration was calculated and adjusted to 10^6 spores/ml using a haemocytometer. Plants were placed in PVC transparent bags and spray-inoculated with the inoculum suspensions until runoff could be observed on the leaves. Bags were kept closed for 3 days to enhance high humidity for successful pathogen establishment and only opened temporarily for measurements and sampling. No mock inoculation (sterile H_2O) was included in this study.

3.2.3 Chlorophyll fluorescence (CF) and gas exchange (GE) measurements

NPQ kinetics were always measured prior to inoculations (hereafter referred to as “0h”) as a control measurement to establish that there were no physiological differences between the genotypes and therefore any differences observed would be due to inoculation. The youngest, fully expanded leaf on the primary tiller was selected for all measurements.

CF and GE were simultaneously measured with an infrared gas analyser (IRGA), LI6400XT, equipped with leaf chamber pulse-amplitude modulated fluorometer LI6400-40 (LI-COR Biosciences, Nebraska, USA). For all measurements, the IRGA was kept at a gas flow rate of 500 mL min^{-1}, a cuvette temperature of 20 °C, extracellular CO_2 concentration of 400 ppm, and RH between 55-65%. Leaves were dark adapted in the growth chamber for 1 h by wrapping sections of the leaf in low-weight aluminium foil, to allow for maximal plastoquinone A (Q_A) oxidation and removal of zeaxanthin. For all measurements, dark-adapted leaves were left for 2 min in the cuvette in darkness until the light period started. The sample and reference IRGAs were equilibrated (matched) automatically to prevent drift prior to each

measurement. Minimal fluorescence (F_o) was measured by applying a low measuring light insufficient to induce significant variable fluorescence, followed by a saturating pulse to determine maximum fluorescence (F_m). Actinic light sufficient to drive photosynthesis (1500 μmol m^{-2} s^{-1}) was turned on and after a period of 2 min, a saturating pulse of 7000μmol m^{-2} s^{-1} (for 0.8 s) was applied to determine maximum fluorescence (F_m'). Actinic light was switched off for 2 s and far-red (FR) light was applied to determine F_o'. Application of a series of saturating pulses every 2 min over a period of 16 min under actinic light (Induction) and for another 16 min under darkness (actinic light turned off) (Relaxation), under an automated programme, allowed determination of a series of F_o' and F_m' readings from which time-dependent changes in fluorescence yield were determined. Fluorescence parameters, including nonphotochemical quenching (NPQ), maximum quantum efficiency of PSII photochemistry (F_v/F_m) and photochemical quenching (qP) were automatically calculated directly from LICOR 6400XT software. Quenching analysis was followed by analysis of relaxation of NPQ kinetics. The rapidly reversible component of NPQ, energy-dependent NPQ (qE), was calculated as (F_m/F_m') - (F_m/F_m''), while the slowly relaxing component (qI) was calculated as ($F_m - F_m''$)/F_m'', where F_m'' is the maximal yield of fluorescence after 16 min of dark relaxation following the actinic illumination. Total NPQ was calculated as the sum of qE and qI. The assumption is that after 16 min of dark treatment, the remaining quenching consists only of qI (Ruban, 2016; Zhao et al., 2017). Measurements were taken at 0h and then at 6, 24 and 48 hours after inoculation (hai).

3.2.4 Absorbance measurements

An integrating sphere (LI-COR Biosciences, Nebraska, USA) was used for absorbance measurements for dual purpose. Firstly, to identify whether inoculation with *Zymoseptoria tritici* had any effect on light absorption, associated with reduced chlorophyll abundance in the leaf. Secondly, we wanted to accurately calculate the true electron transport rate (ETR) from PSII to PSI, as the equation assumes that absorption remains constant and is 0.84. φPSII is the operating efficiency of PSII, PAR is the light level in which the

measurements were made and 0.5 refers to the assumption that electron transport is equally divided between the two photosystems.

Equation (1) $ETR = \varphi PSII \times PAR \times 0.84 \times 0.5$

3.2.5 Carotenoid extraction and quantification

Carotenoids were extracted in 100% acetone (HPLC grade), placed in amber 1.5 ml Eppendorf tubes for light protection, centrifuged for 2 min at 10,000g at 4 °C, and filtered through a 13 mm diameter 0.2 µm polytetrafluoroethylene (PTFE) syringe filter (Whatman). Pigment separation was performed by reverse-phase HPLC as described in Färber et al. (1997). HPLC analysis was performed using a BioLC HPLC system (Dionex) with LiChrospher 100 RP-18 (5 µm) column (Merck). Three biological replicates per treatment/genotype were measured. For each sample, the amount of each carotenoid was calculated as a percentage of total carotenoids. In wheat, the total carotenoids (Car) comprise neoxanthin (Neo), violaxanthin (Vio), antheraxanthin (Anth), lutein (Lut), zeaxanthin (Zea), and β-carotene (β-Car). The size of the xanthophyll cycle (XC) pool of carotenoids, expressed as a percentage of total carotenoids, and de-epoxidation state (DEP) of the xanthophyll cycle pigments were calculated from Equations 2 and 3, respectively.

Equation (2) $$\frac{\text{XCpool}}{\text{Car}}(\%) = \frac{\text{Zea+Anth+Vio}}{\text{Neo+Vio+Anth+Lut+Zea+ }\beta\text{Car}} \text{ x } 100$$

Equation (3) $$\text{DEP }(\%) = \frac{\text{Zea+ 0.5 x Anth}}{\text{Zea+Anth+Vio}} \text{ x } 100$$

3.2.6 ROS staining

To get a basic visual quantification of ROS, we used histochemical staining for hydrogen peroxide (H_2O_2) and superoxide ($O_2^{\bullet -}$). Staining of H_2O_2 was carried out using 3,3′-diaminobenzidine (DAB). Leaf sections were vacuum-infiltrated with 1 mg/ml DAB-HCl (pH 3.8) and incubated overnight with gentle shaking at room temperature in the dark. The DAB solution was removed, and the leaf sections were washed with distilled water. To stop the reaction and fix the

tissue, samples were boiled for 5 min in 95% ethanol and then were kept in 95% ethanol with gentle shaking until all chlorophyll was removed. Generation of superoxide anion ($O_2^{\bullet -}$) in leaves was detected with nitroblue tetrazolium (NBT). Leaf sections were vacuum-infiltrated with 50 mM phosphate buffer (pH 7.8) containing 0.5% NBT and incubated at room temperature for 1h in darkness. Subsequent sample preparation was identical to DAB staining. Leaf sections were sampled simultaneously as NPQ screening. After staining, DAB and NBT stained samples were imaged using an Olympus OM-D e-M10 MK II camera.

3.2.7 RNA sequencing and differential expression gene (DEG) analysis

RNA sequencing was used to examine the early transcriptional changes of the *Z. tritici* – wheat interaction while exploring both compatible and incompatible interactions. Leaves from 3-week-old plants were collected right before inoculation (0h) and then at 6 and 24 hai. Three biological replicates were collected for each time point and for each treatment combination (Courtot with IPO323, Courtot with Zt22, Ct (+*Stb6*) with IPO323 and Ct (+*Stb6*) with Zt22), with each sample consisting of leaves from three individual plants as a sample pool. All samples were snap-frozen in liquid nitrogen and stored at -80 °C. RNA was extracted as described below. The list of samples used for sequencing is given in Table 3-1. No mock-inoculated samples were included in this study.

Library preparation and sequencing were performed by Novogene (Cambridge, UK) on an Illumina NovaSeq platform. Data were subjected to quality control (error rate and GC content distribution) and then filtered to remove adaptor sequences and low-quality reads (>10% uncertain nucleotides and >50% low quality nucleotides). Filtered sequence reads were mapped to the reference genome of wheat and *Zymoseptoria tritici* using HISAT2 algorithm and gene expression levels were estimated using the Fragments Per Kilobase of transcript sequence per Millions base pairs sequenced (FPKM) method. Pearson's correlation coefficient and Principal Component Analysis (PCA) were used in all samples to test for data variability. Differential gene expression (DEG) analysis of pairwise comparisons was performed using the

DESeq2 R package and the resulting *P* values were adjusted using the Benjamini and Hochberg approach for controlling the false discovery rate (Padj < 0.05). Hierarchical clustering analysis was carried out of log10(FPKM+1) of union DEGs, within all comparison groups. Enrichment analysis of the DEGs was performed using the clusterProfiler software, including GO Enrichment, GSEA, KEGG and Reactome database Enrichment. Protein-protein interactions (PPI) were constructed by searching STRING protein interaction database and visualised in Cytoscape. Finally, gene information and annotations were obtained using Knetminer (Hassani-Pak et al., 2021).

Table 3-1. List of samples used in transcriptomics experiment. Interaction response of each genotype (Courtot or Ct (+Stb6)) to each isolate (IPO323 or Zt22) is given in brackets – R for resistance and S for susceptibility.

RNAseq samples	
Courtot 0h	Ct (+Stb6) 0h
Courtot 6h IPO323 (S)	Ct (+Stb6) 6h IPO323 (R)
Courtot 24h IPO323 (S)	Ct (+Stb6) 24h IPO323 (R)
Courtot 6h Zt22 (S)	Ct (+Stb6) 6h Zt22 (S)
Courtot 24h Zt22 (S)	Ct (+Stb6) 24h Zt22 (S)

3.2.8 RNA extraction

Leaf material was ground using liquid nitrogen and total RNA was extracted with Trizol and chloroform, followed by the guidelines of the RNeasy Mini Kit (Qiagen), with the addition of a RNase-free DNase step (Qiagen) to remove any traces of DNA in the RNA extracts. Samples were eluted in 35 µl RNA-free water and their concentration and purity were determined with a NanoDrop ND-1000 Spectrophotometer. 1 µg per sample were used for cDNA synthesis using the iScript cDNA synthesis kit (Biorad).

3.2.9 Gene expression

Selected transcripts from the RNAseq as well as other defence- or photoprotection-related molecular markers were used for gene expression studies. 12.5 ng of cDNA were used for qPCR reaction with SYBR reaction mix (Biorad) and primers were at 50 μM concentration. Ubiquitin was used as the housekeeping gene, as it didn't show any significant change in expression across the experimental conditions. All samples had 3 biological replicates and qPCRs were performed twice. The conditions were as following; 95 °C for 30 sec, 40 cycles of 95 °C for 15 sec and 56-60 °C for 30 sec, followed by a melt curve between 65 and 95 °C. Primers for transcript validation were designed based on the coding sequence of each significant DE gene. Primers used are shown in Table 3-2. All primers were run at 60 °C, apart from ZEP, VDE and NCED4 (58 °C) and AOS (56 °C). Relative expression was calculated as $2^{-\Delta Ct}$, whereby ΔCt was calculated as (Ct target – Ct housekeeping gene). The 0h samples were only considered as the calibrator samples for the calculation of ΔΔCt (ΔCt target – ΔCt calibrator 0h) for FeSOD, AOS, ICS and PR1 genes (Livak & Schmittgen, 2001).

Table 3-2. List of primers used in this study. Primers were designed based on the transcript ID in RNA sequencing DEG results and their respective coding DNA sequence. Ubiquitin was used as the housekeeping gene.

Gene symbol	Gene name	Forward primer (5' – 3')	Reverse primer (5' – 3')
ZEP	Zeaxanthin epoxidase	GGACTTCAACGACCCCTTGT	TACCCTATTGTACACCCTCGGT
VDE	Violaxanthin de-epoxidase	CCCGAGCTAGAAAGGGCTAC	ACCACAGGTGTTGTCTGTCC
NCED	9-*cis*-epoxycarotenoid dioxygenase	TAAGTGCTACAAGAGTGACTACC	CCTGTAGCGAAGCAGTAGG
ICS	Isochorismate synthase	AGAAATGAGGACGACGAGTTTGAC	CCAAGTAGTGCTGATCTAATCCCAA
AOS	Allene oxide synthase	TCATCGGCGACAACGGATTA	TACGTACGTGCGTGCTGAC
PR1	Pathogenesis-related protein 1	CATGCACCTTCGTATGCCTAACT	TGGCTTATTACGGCATTCCTTT
FeSOD	Iron-superoxide dismutase	GCTTCAGAGCAAGGGGACTT	GGAAAACCAGGGGCTGTTCT
PsbP	Photosystem II subunit P	AATCGGAAACAAAAGTGTGAGGGGT	TGCCATTGAACCTCACGCC
PsbS	Photosystem II subunit S	AAAGTCCCCCAAGCTGTAGCA	TCGACTGTGCCATGGATGC
CERK1	Chitin elicitor receptor kinase 1	GCCCCTATCCGCTACGACG	TTGTTGGCCGGGTAGGTGTT
Lhca1	Photosystem I Light-harvesting complex protein 1	CGTCGTCAAGCGGGCTG	CCGGAGGTGGTGGCGTAG
Ubi	Ubiquitin	GCACCTTGGCGGACTACAACATTC	GACACCGAAGACGAGACTTGTGAACC

3.2.10 Thylakoid extractions

Fresh thylakoid membranes from intact chloroplasts were extracted from green, healthy leaves pulled from 4 separate plants. All buffers were made fresh and stored at 4 °C. Plants were kept in the dark for 1h prior to extraction in order to remove some of the starch. Leaves were ground and homogenised in a metal blender with pre-chilled Grinding media (0.33M sorbitol, 10mM sodium pyrophosphate decahydrate, 130mg D-Iso ascorbate pH 6.5). The solution was filtered twice through 4 layers of wet muslin and a strip of absorbent cotton wool to remove debris and then the filtered solution was centrifuged at 5000rpm at 4 °C for 10 min. The supernatant was discarded and the pellet was gently re-suspended in Wash medium (0.33M sorbitol, 10mM MES, pH 6.5). After another step of centrifugation, the supernatant was carefully discarded once more and the pellet was gently re-suspended in Re-suspension medium (0.33M sorbitol, 1mM EDTA, 50mM Hepes, pH 7.6). Chloroplasts were burst open with the addition of Break medium (80mM Hepes, pH 7.6), followed by Osmoticum medium (0.66M sorbitol, 40mM MES, pH 6.5) and the solution was centrifuged once more. The supernatant was discarded and the final pellet was re-suspended in Particle Wash medium (5mM EDTA, pH 6.3). Tubes were spun briefly to pellet any starch and debris and the extracted thylakoids were aliquoted in tubes for follow up analysis and kept in -80 °C. Extraction was repeated once more from another set of plants (same treatments/conditions/genotypes) to have two technical replicates.

In order to quantify protein content in extracted thylakoids, absorbance measurements normally take place based on the absorption of chlorophyll at 646.6, 663.6 and 750nm, before the final concentration of chlorophyll and other proteins are calculated as per Porra et al. (1989). From our experience, this method didn't prove to be very reliable. When we used the Bradford assay to quantify the protein content, we found that the method by Porra et al. (1989) overestimated the actual protein content in the sample by nearly five times. Several repeats of the Bradford assay compared to the [Chl] method indicated that, with the latter, we were not accurately quantifying the actual protein content in the sample. Therefore, we decided to quantify chloroplastic proteins

directly from the prepared thylakoid samples using the Bradford Biorad assay kit. We also extracted total protein from plant leaves and compared results against those of thylakoid protein samples and results were comparable. To extract proteins from leaves, the MP BIO was used to grind samples, after which extraction buffer, containing 50mM Tris (pH 8), 0.1% SDS, 1x protease inhibitor cocktail and H_2O, was added in each thylakoid sample. Samples were vortexed and then centrifuged for 30 min at 14000 rpm at 4 °C. Supernatant was transferred into a new tube and protein concentration was quantified by Bradford assay using the Biorad Bradford assay kit, according to the manufacturer's instructions.

3.2.11 Western blots

Western blots presented in this chapter were performed by Mrs. Charlene Dambire. Protein levels of PsbP, relative to the WT Fielder and the Null, were confirmed through Western Blot analysis. After quantification of total protein concentration (Bradford assay on extracted proteins from thylakoid membranes), samples were denatured at 96 °C for 10 min and then immediately placed in ice for 10 min. 10 µg protein was separated by 12% SDS-PAGE electrophoresis and blotted to Biorad PVDF membrane using a wet transfer. Blots were incubated in 5% milk + PBST for 1h and then immuno-labelled in 5% PBST with 1:4000 primary antibody raised against PsbP (AS06142-23, Agrisera) and against Ubiquitin (AS08307, Agrisera). Blots were washed in PBST (3 x 10 min), followed by secondary antibody incubation (goat anti-rabbit IgG HRP conjugate (1:20000)) for 2 h (AS09602, Agrisera). Blots were washed with PBST + 300mM salt 3 times for 10 min. Chemiluminescence was detected using a LiCor Odyssey FC Imager at 10 min exposure. A protein ladder SeeBlue™ Plus2 Pre-stained Protein Standard was used as a protein band size indicator on each gel. Band signal/intensity of PsbS was normalised against the expression of Ubiquitin.

3.2.12 Disease assessment and pycnidia development

The same leaf used for the GE and CF measurements was also monitored for disease progression over time. Disease assessment was made by assessing the total percentage (%) of leaf area covered with symptoms (both chlorotic

and necrotic symptoms). Assessments were made at 10, 14, 17 and 21 days after inoculation (dai), consisting of four biological replicates. The Area Under the Disease Progress Curve (AUDPC) was calculated to provide information on the disease development over time (Jeger & Viljanen, 2001). Spore wash counts were performed as described by Lee, Rudd & Kanyuka (2015). In brief, ~ 3 cm leaf segments were placed in tubes on sterile H_2O-saturated cotton wool and incubated in the dark for 48h. Leaf sections were then vortexed in sterile water and released spores were measured using a haemocytometer.

3.2.13 Statistical analysis

All experiments were designed as Completely Randomised Design. Statistical analysis was performed using Genstat 19th edition (VSN International). In the absence of significant interactions between individual experiments and the main treatments, individual experiments were used as replicates in the analysis. Data were tested for normal distribution using Shapiro-Wilk's test for normality. If the test discarded the null hypothesis, data were analysed with non-parametric tests. If data followed normal distribution, ANOVA was used in order to elucidate the significance of the main factors (Genotype and Treatment) and/or their interaction (if any) or for simple comparisons, t-tests were used to find any significant differences of means. In case of non-normally distributed data, Kruskal-Wallis one-way ANOVA or Wilcoxon/Mann-Whitney pairwise tests were used. Datasets of NPQ kinetics (Induction & Relaxation curves) and Time Series data were analysed by Repeated Measurements ANOVA.

Dynamic modelling of NPQ was performed using a dose-response curve fitting method in R. The 'drc' (v. 3.0) package was used due to its ability to analyse and extract several useful parameters for both curve induction and relaxation responses (Ritz *et al*., 2015). These include curve slope, lower limit, upper limit and the time taken to reach a defined percentage of the dependant variable, in this case we focused on 50% (ED_{50}). The LL.3 (log-logistic 3-parameter) model was used for Induction responses, whereas the LL.4 (log-logistic 4-parameter) model was chosen as the best model fit for Relaxation responses. The comparison of 8 different models, followed by Akaike's

information criterion analysis was used to select the best model fit. ED_{50} values were subsequently analysed in Genstat as described above.

3.3 Results

3.3.1 Disease assessment and pycnidia counts

Disease was assessed as percentage (%) of assessed leaf covered with disease symptoms. *Z. tritici* isolate IPO323 resulted in an incompatible reaction with Ct (+Stb6) and therefore very few symptoms and no pycnidia developed on the leaf, whereas it was virulent on Courtot and resulted in leaf necrosis and the production of abundant pycnidia (Figures 3-1a-c). Zt22 was virulent on both genotypes and resulted in leaf necrosis and production of pycnidia, however it was less virulent on Courtot than IPO323 (P = 0.029) (Figures 3-1a-c). IPO323 also developed significantly faster on Courtot than Zt22 as seen in differences in AUDPC (P = 0.002) (Figure 3-1b).

3.3.2 Physiological phenotype

Gas exchange and chlorophyll fluorescence measurements were taken prior to inoculation (0h) to establish that the genotypes did not vary significantly and that any difference observed upon inoculation would only be attributed to the effect of the pathogen.

There were no significant differences between the genotypes before inoculation (Figures 3-2a-d). Repeated measurements ANOVA on the NPQ curves (Figures 3-2a and 3-2b) demonstrated that the plants did not vary in their NPQ capacity before inoculation (P = 0.714). Similarly, no differences were observed in the qE component of NPQ (P = 0.345), however qI in the near-isogenic Ct (+Stb6) was reduced compared to Courtot (P = 0.034) (Figures 3-2c and 3-2d). The genotypes did not vary in any other CF or GE parameter (ED_{50}, F_v/F_m, φPSII, ETR, qP, A_{max} and g_s).

Plants were subsequently inoculated with the reference isolate IPO323 and the virulent isolate Zt22. Measurements took place at 6, 24 and 48 hours after inoculation (hai).

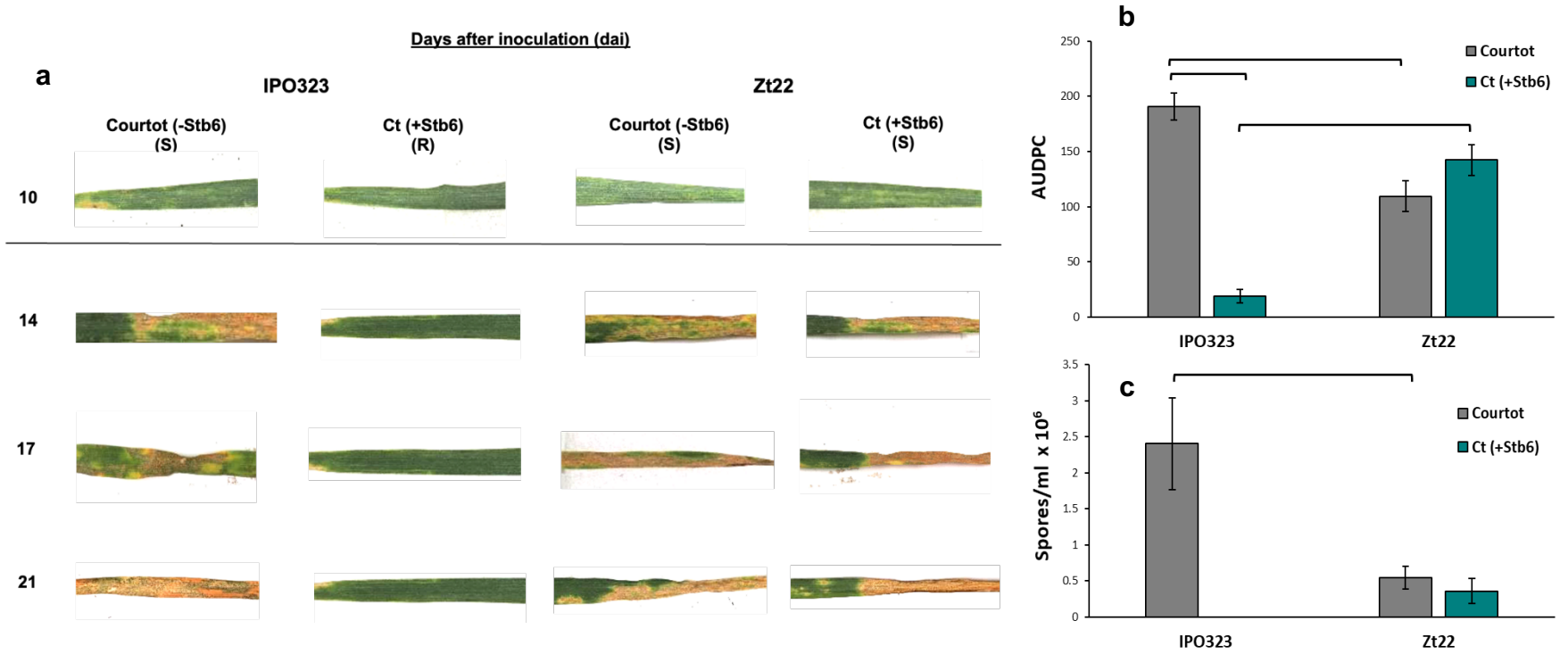


Figure 3-1. (a) Disease phenotype of the Near Isogenic Lines Courtot and Ct (+Stb6) at different stages of the infection process. Isolate IPO323 results in an incompatible reaction with *Stb6* and therefore no symptoms or pycnidia develop on the leaf, whereas it is extremely virulent on Courtot and results in full leaf necrosis and production of a lot of pycnidia. Zt22 is virulent on both genotypes and results in leaf necrosis and production of pycnidia. **(b)** Area under the disease progress curve (AUDPC) of assessed leaves based on % leaf coverage with disease symptoms and **(c)** Pycnidia counts at 21dai from leaf sections. Data represent means ± SEM (n=4). Horizontal bars represent significant differences between the means ($P < 0.05$).

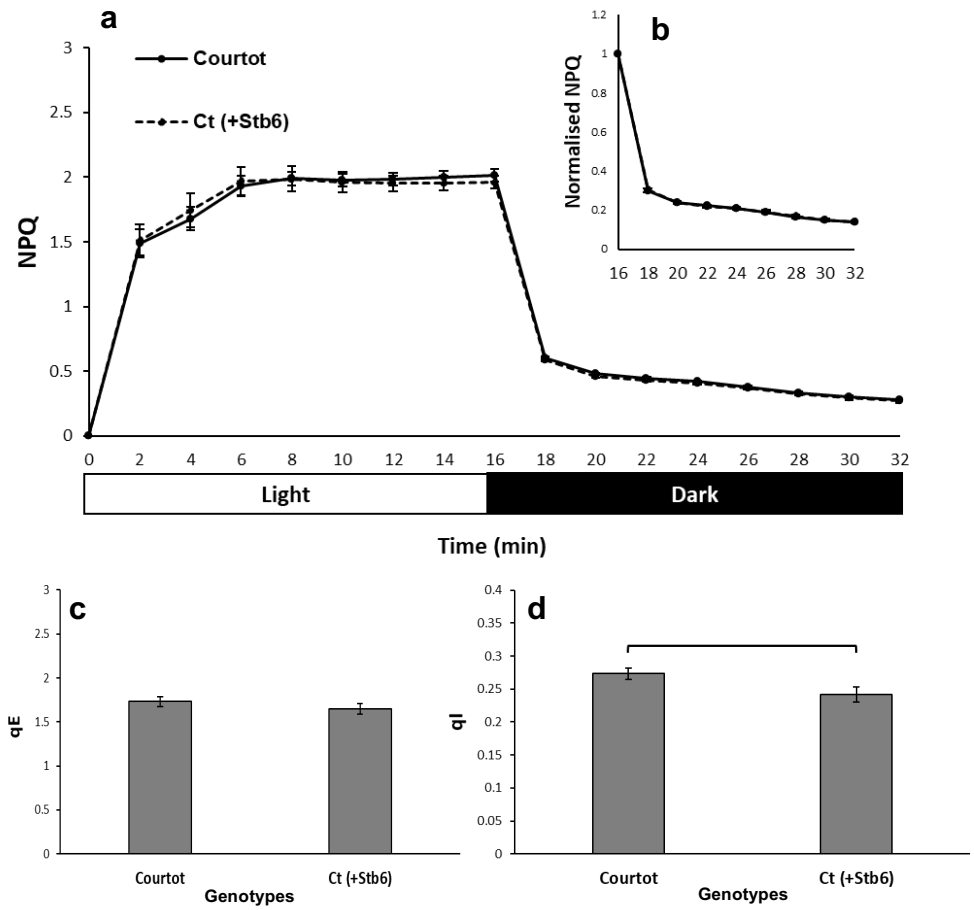


Figure 3-2. NPQ kinetics before any inoculation occurred. **(a)** NPQ Induction and Relaxation curve during light and dark conditions, respectively, and **(b)** normalised Relaxation in the dark, **(c)** qE and **(d)** qI components of NPQ before inoculation. Solid black line represents Courtot and dashed black lines represents the near-isogenic Ct (+Stb6). Data represent means ± SEM (n=16). Horizontal line indicates significant difference between the means.

Inoculation with IPO323 was the only treatment that resulted in significant NPQ differences between the genotypes across the different time points (Figures 3-3a-c). The near-isogenic Ct (+Stb6) downregulated NPQ in the light in response to inoculation at 6 and 24hai, before restoring it at 48hai. NPQ relaxation in the dark was significantly higher in Ct (+Stb6) compared to Courtot for IPO323 (Figure 3-3b). In contrast, inoculation with Zt22 caused no alterations in NPQ of the two genotypes (Figures 3-3d-f). NPQ-derived parameters, qE and qI, referring to components of Induction and Relaxation respectively, showed significant differences only for IPO323-inoculated plants (Figures 3-4a-d). Ct (+Stb6) downregulated qE in response to infection with IPO323 and was significantly different to Courtot at 6hai (Figure 3-4a). In contrast, the qI component of NPQ significantly increased at 24hai (Figure 3-4c). Speed of Induction of NPQ (ED_{50}) was overall slower in Ct (+Stb6) throughout the measurements (i.e. higher ED_{50}), exhibiting a zig-zag pattern and significant differences at 0 and 24hai (Figure 3-4c). Similar to NPQ kinetics (Figure 3-3), Zt22 infection caused no alterations in NPQ components and Induction rates (Figures 3-4e-g). Relaxation ED_{50} exhibited the same pattern between the genotypes and treatments across time, whereby NPQ was able to relax much faster (i.e. lower ED_{50}) in 6hai compared to the initial slow 0h before gradually becoming slower again by 48hai (Figures 3-4d and 3-4h).

No differences in NPQ kinetics were observed when Ct (+Stb6) was compared between the treatment of the two isolates, IPO323 and Zt22 (Supplementary Figure 3-1). Similarly, no differences were observed for qE, qI and Relaxation ED_{50} (Supplementary Figure 3-2). However, inoculation of Ct (+Stb6) with IPO323 significantly slowed NPQ Induction (Supplementary Figure 3-2b).

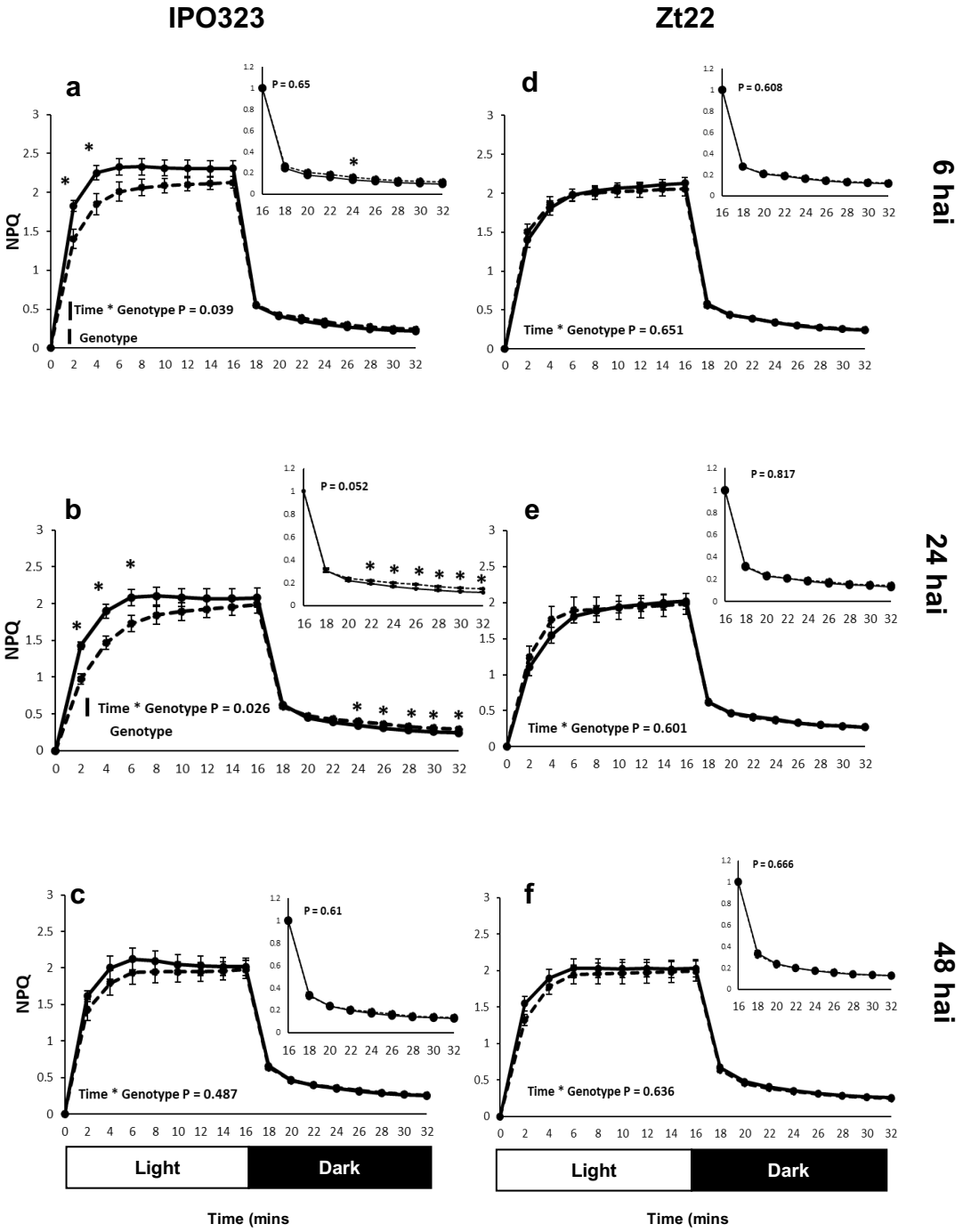


Figure 3-3. NPQ Induction and Relaxation kinetics along with Normalised NPQ in the dark for each Treatment across the different time points. **(a-c)** Curves for IPO323-inoculated plants at 6, 24 and 48hai, respectively, **(d-f)** Curves for Zt22-inoculated plants at 6, 24 and 48hai, respectively. Solid and dashed black lines indicate Courtot and Ct (+Stb6), respectively. Data represent means ± SEM (n=8). Vertical bars represent LSD for the significant interaction and stars (*) denote significant difference ($P < 0.05$) of the equivalent point in the kinetics.

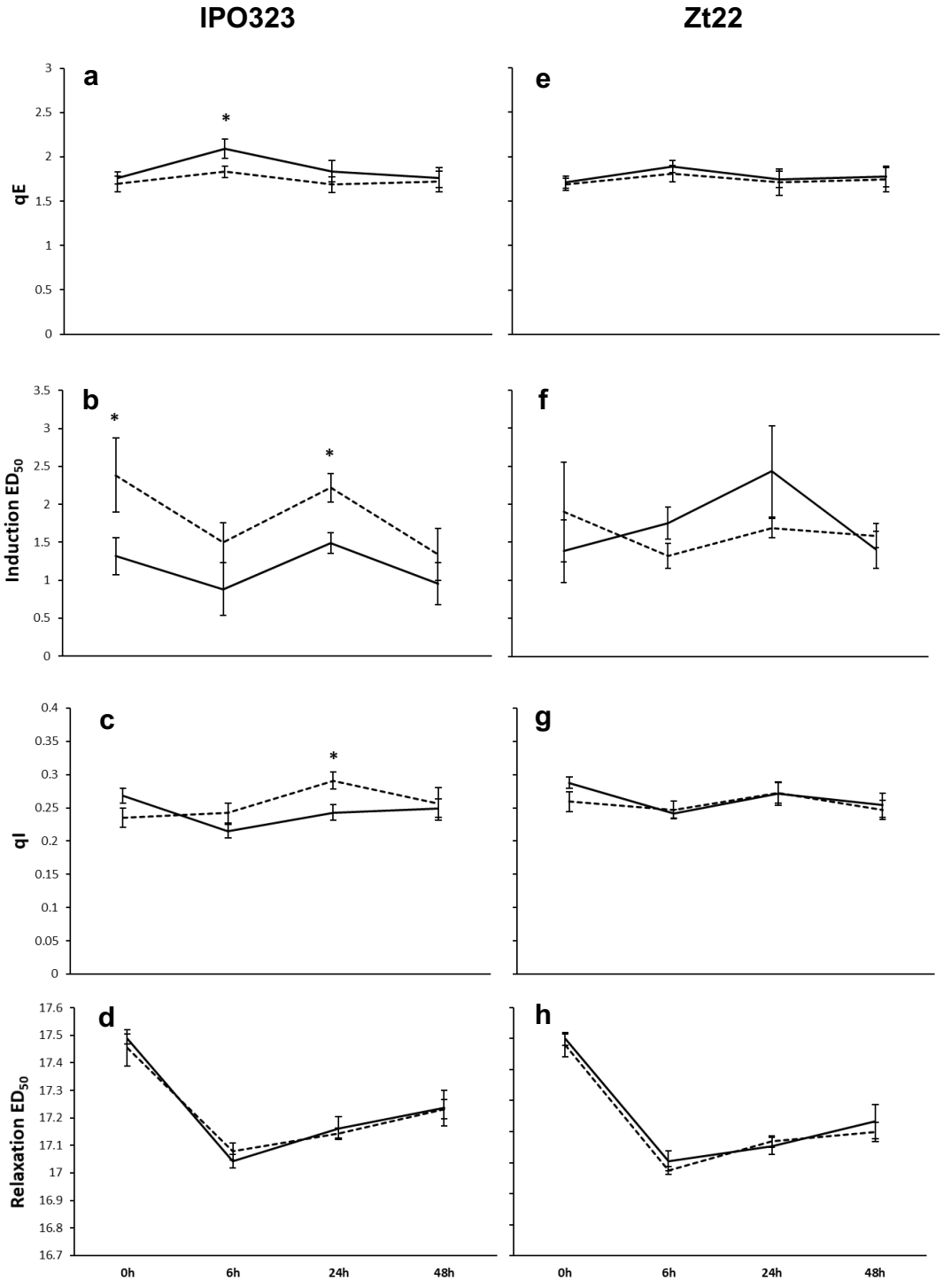


Figure 3-4. NPQ-derived parameters for each isolate across the measurement timings. **(a-d)** IPO323-inoculated plants exhibiting differences in qE, Induction ED_{50}, qI and Relaxation ED_{50}, respectively, **(e-h)** Zt22-inoculated plants exhibiting no changes in qE, Induction ED_{50}, qI and Relaxation ED_{50}, respectively. Solid and dashed black lines indicate Courtot and Ct (+Stb6), respectively. Data represent means ± SEM (n=8). Stars (*) denote significant differences ($P < 0.05$) of the genotypes at the equivalent time point.

Chlorophyll absorbance was reduced significantly by 9% in Ct (+Stb6) upon inoculation with IPO323 and Zt22 at 6hai, before increasing again, although to lower levels than before inoculation (0h) (Figures 3-5a and 3-5d). Inoculation also affected absorbance capacity in Courtot, however it remained low until 48hai for IPO323 whereas it rose again at 24hai for Zt22 and was significantly higher than Ct (+Stb6) by 48hai (Figures 3-5a and 3-5d). Ct (+Stb6) maintained higher CO_2 assimilation (A_{max}) and stomatal conductance (g_s) in the incompatible interaction with IPO323 (Figures 3-5b and 3-5c). In contrast, A_{max} and g_s were significantly compromised in Courtot upon infection with IPO323 as early as 6hai, and remained low until the end of the measurement period. Zt22 also reduced CO_2 assimilation and stomatal conductance for both genotypes with no significant differences (Figures 3-5e and 3-5f).

No differences were observed for the remaining CF parameters (F_v/F_m, qP, φPSII and ETR (Supplementary Figure 3-3). There was a decreasing trend for maximum PSII efficiency (F_v/F_m) and photochemical quenching (qP) over time with inoculations (approx. 1 and 13%, respectively), although the reduction was not significant between lines (Supplementary Figure 3-3a, b, e and f), whereas PSII operating efficiency (φPSII) and electron transport rate (ETR) remained unchanged over time and upon inoculations with either isolate (Supplementary Figure 3-3c, d, g and h).

Inoculation with either IPO323 or Zt22 caused a decrease in chlorophyll absorbance, A_{max} and g_s for Ct (+Stb6) at 6hai, however no difference was observed between the treatments (Supplementary Figure 4). Both isolates had the same effect on the *Stb6* line and there were no differences over time (Supplementary Figure 3-4). Although it was not statistically significant, the resistant phenotype (Ct (+Stb6) and IPO323) appeared to recover photosynthetic capacity and stomata responsiveness by 48hai, whereas in the incompatible interaction with Zt22, A_{max} and g_s continued to exhibit a downward trend (Supplementary Figure 3-4b and c). Moreover, the effect of both isolates was the same for F_v/F_m and qP, resulting in reductions over time (Supplementary Figure 3-5). However, there were significant reductions in ETR and φPSII for Ct (+Stb6) inoculated with IPO323 at 6hai, compared to

inoculation with Zt22 (Figures 3-6a and 3-6b). Both parameters continued to drop over time, however it was not statistically significant (Figures 3-6a and 3-6b).

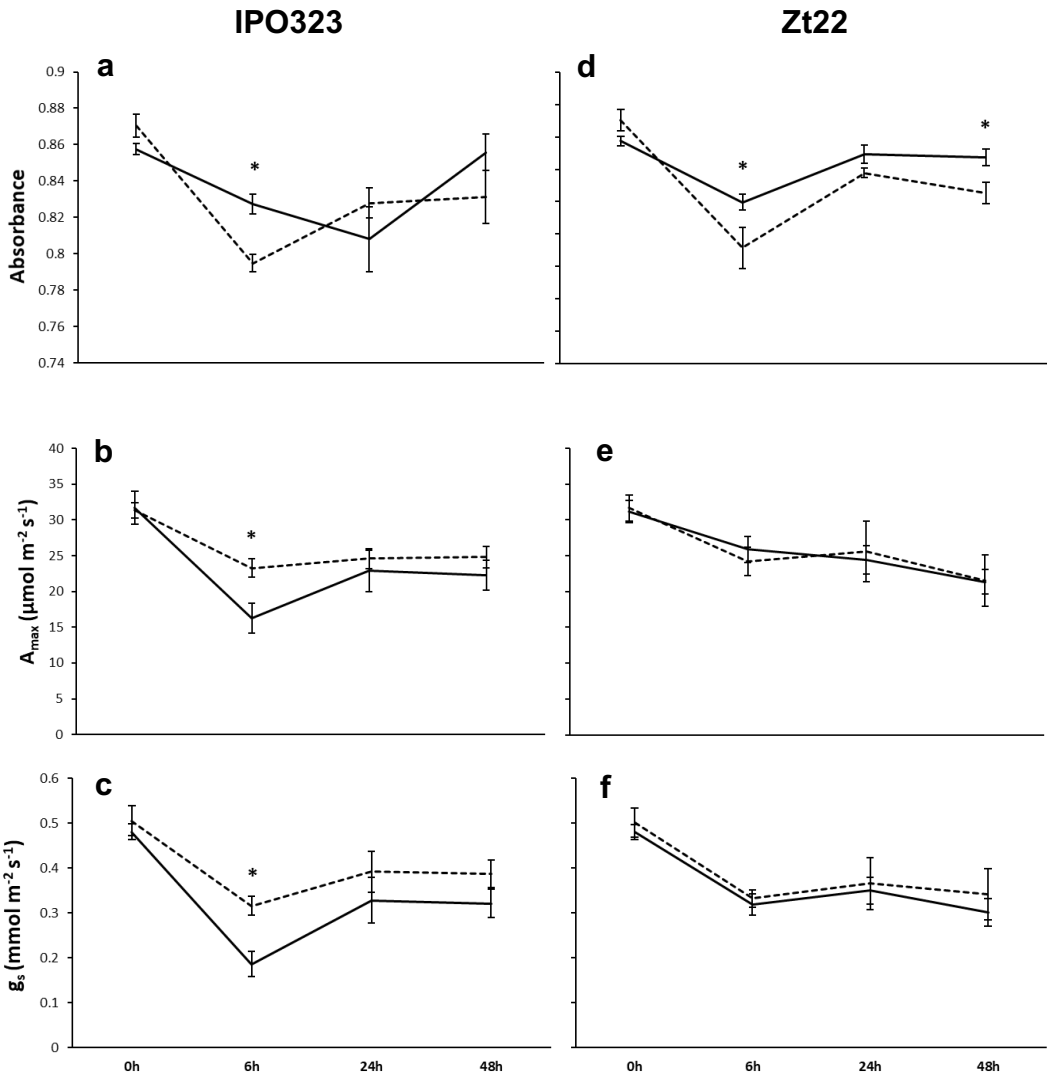


Figure 3-5. Chlorophyll absorbance, CO_2 assimilation (A_{max}) and stomatal conductance (g_s) for IPO323-inoculated plants **(a-c)** and Zt22-inoculated plants **(d-f)**. Solid and dashed black lines indicate Courtot and Ct (+Stb6), respectively. Data represent means ± SEM (n=8). Stars (*) denote significant differences ($P < 0.05$) of the genotypes at the equivalent time point.

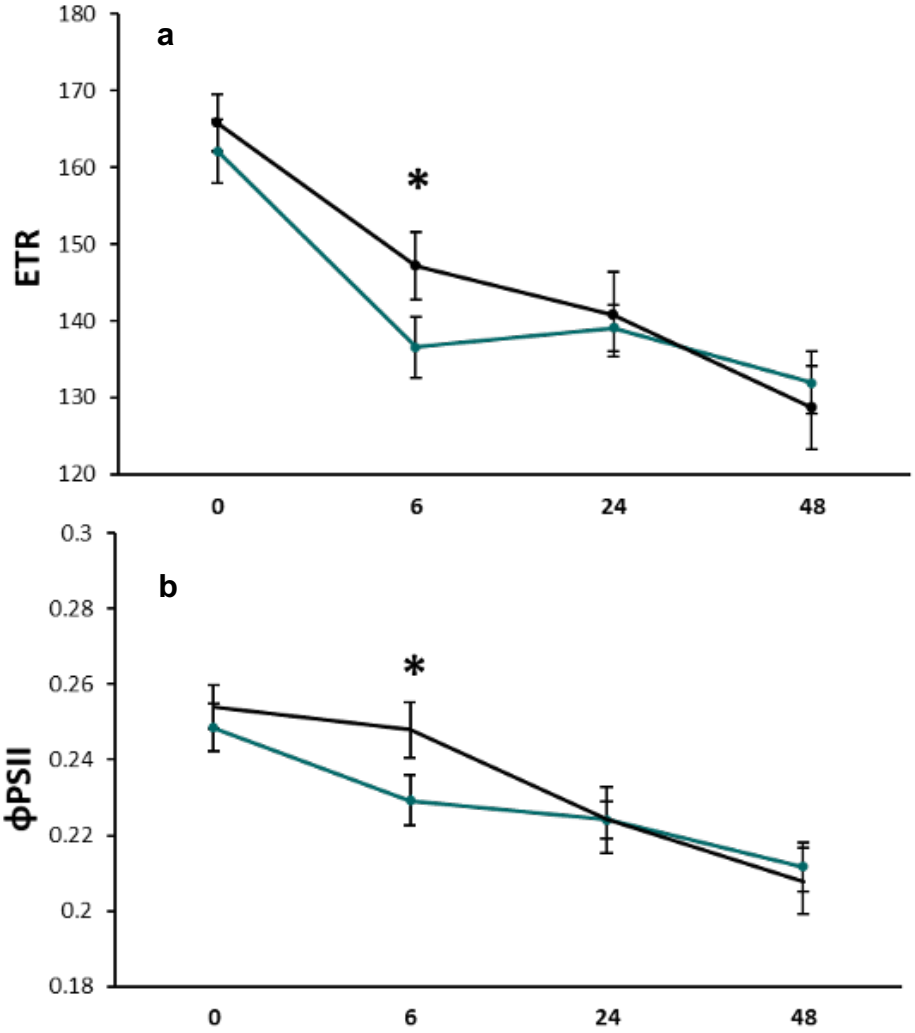


Figure 3-6. (a) Electron transport rate (ETR) and **(b)** operating efficiency of PSII for Ct (+Stb6) inoculated with IPO323 or Zt22 across the time measurements. Teal and black lines represent IPO323 and Zt22, respectively. Data represent means ± SEM (n=8). Stars (*) denote significant differences ($P < 0.05$) of the genotypes at the equivalent time point.

3.3.3 Carotenoid expression and quantification

HPLC and gene expression analysis were used on the Near-Isogenic Lines infected with IPO323 and Zt22 to determine the activity of the xanthophyll cycle in resistant or susceptible responses before inoculation and at 6 and 24hai. HPLC data are presented as percentage (%) of each carotenoid in relation to total carotenoids. Data are shown in Figure 3-7 and Table 3-3.

Lutein levels in Ct (+Stb6) at 6hai with IPO323 were significantly lower than Courtot (Figure 3-7a) and at the same timing β-carotene increased (Figure 3-7c). In contrast, lutein increased and β-carotene was reduced in the interaction of Ct (+Stb6) and Zt22 (Figures 3-7a and 3-7c). There was no difference between the treatments and the genotypes over time for Chl *a:b* and Car:Chl (Table 3-3). However, inoculation with Zt22 at 6hai reduced Car:Chl for Ct (+Stb6), whereas Courtot inoculated with the same isolate showed a significant increase at 24hai for that ratio (Table 3-3). There was a downregulation of the XC pool by 24hai, however the decrease was not statistically significant (Table 3-3). Interestingly, there was no zeaxanthin present at 0h and none in Courtot infected with Zt22 at 24hai (Figure 3-7e). There were opposite trends for Ct (+Stb6), whereby zeaxanthin decreased by 24hai when inoculated with IPO323 in contrast to zeaxanthin increasing over time upon infection with Zt22 (Figure 3-7e). In accordance, de-epoxidation state (DEP) increased with infection compared to 0h, but decreased over time for the *Stb6* line with IPO323 and increased with Zt22 (Table 3-3). VDE was also significantly upregulated upon infection, compared to 0h, and significantly higher as a response to IPO323 at 6hai for both genotypes (Figure 3-7g). However, its expression reduced over time and it was significantly less in Ct (+Stb6) inoculated with Zt22 (Figure 3-7g). Antheraxanthin levels, the intermediate carotenoid between violaxanthin and zeaxanthin, were not significantly altered upon inoculation, although the trend appeared to follow that of zeaxanthin and DEP, whereby IPO323 caused a decrease and Zt22 caused an increase for Ct (+Stb6) (Table 3-3). ZEP, the enzyme that catalyses the conversion of zeaxanthin to antheraxanthin and violaxanthin, increased over time and peaked in its expression significantly at 24hai for Ct (+Stb6) and Zt22 (Figure 3-7d). Expression of ZEP was not different between the

genotypes, except at 6hai for IPO323 inoculation (Figure 3-7d). Violaxanthin reduced over time for both genotypes and treatments, as expression of neoxanthin increased (Figures 3-7f and 3-7h). Neoxanthin peaked at 6hai for Ct (+Stb6) and Zt22 inoculation and was significantly different to IPO323 infection at 6hai as well as before inoculation at 0h (Figure 3-7h). However, this high expression did not result in similar levels of NCED expression (Figure 3-7i). Instead, Zt22 infection at 6 and 24hai for both genotypes resulted in significantly reduced levels of NCED in both genotypes, compared to before inoculation. However, it was Courtot with IPO323 that maintained high levels of NCED by 6hai, followed by the near-isogenic with the same isolate and time point (Figure 3-7i).

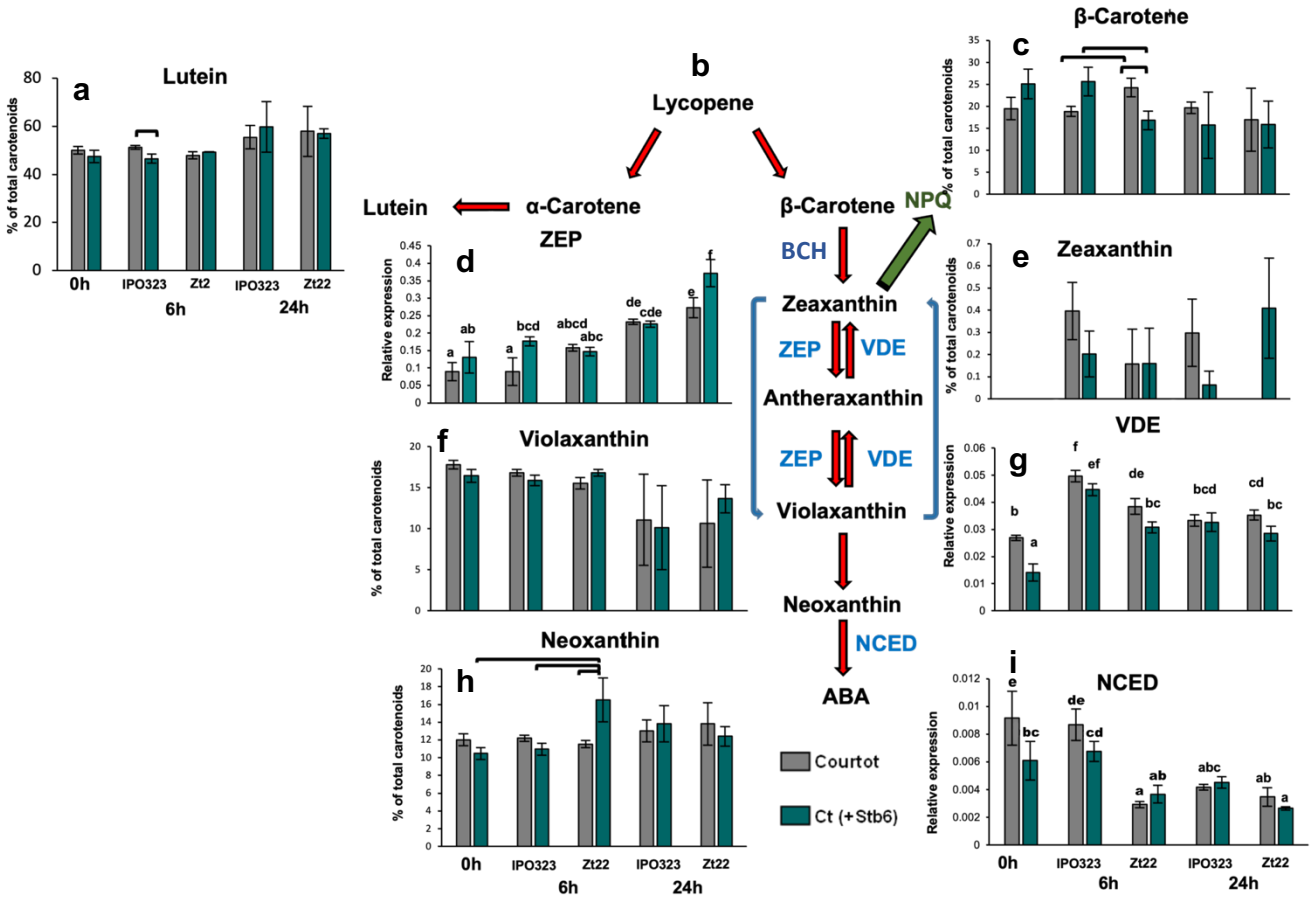


Figure 3-7. HPLC on carotenoids and relative gene expression ($2^{-\Delta Ct}$) of important catalytic enzymes and compounds of the xanthophyll cycle. **(a)** lutein, **(b)** a schematic representation of the biosynthetic pathway of β-Carotene-derived xanthophylls, **(c)** β-carotene, **(d)** zeaxanthin epoxidase ZEP, **(e)** zeaxanthin, **(f)** violaxanthin, **(g)** violaxanthin de-epoxidase VDE, **(h)** neoxanthin and **(i)** 9-*cis*-epoxycarotenoid dioxygenase NCED. Grey and teal bars indicate Courtot and Ct (+Stb6), respectively. Data represent means ± SEM (n=3). Significant differences of the means through t-tests are shown as horizontal black bars or as letters above bars ($P < 0.05$).

Table 3-3. Remaining carotenoids analysed by HPLC. Data represent means of each parameter under each treatment. Chl, chlorophylls; Car:Chl, ratio of total carotenoids to chlorophylls; Anth, carotenoid antheraxanthin; % XC pool/Car, ratio of xanthophyll cycle pool against total carotenoids; DEP, de-epoxidation state of the xanthophyll cycle. Significant differences between genotypes and treatments for each parameter (i.e. per row) are indicated by equal asterisks (*) next to the values (t-tests, $P < 0.05$).

	0h		6hai				24hai			
			IPO323		Zt22		IPO323		Zt22	
	Courtot	Ct (+Stb6)	Courtot	Ct (+Stb6)	Courtot	Ct (+Stb6)	Courtot	Ct (+Stb6)	Courtot	Ct (+Stb6)
Chl *a*:*b*	2.83	2.87	2.74	2.71	2.84	2.62	2.75	3.08	2.16	2.49
Car:Chl	0.49	0.52	0.48	0.49*	0.42**	0.44*	0.58	0.51	0.68**	0.50
Anth	0.63*	0.44*	0.48	0.68	0.54	0.31	0.47	0.40	0.62	0.63
%XC pool/Car	18.41	16.90	17.69	16.76	16.23	17.29	11.85	10.60	11.26	14.70
DEP	***1.71**	1.29*	3.54	3.23*	2.49	1.72	4.45**	2.60	***2.76	4.30

3.3.4 ROS

Histochemical staining and gene expression analysis were used to investigate the presence of ROS between the genotypes and treatments at the early time points of disease development. No obvious superoxide visual differences were observed between the genotypes inoculated with either isolate over time, except a slight increase in NBT staining for the susceptible Ct (+Stb6) with Zt22 at 6hai and the susceptible Courtot at 48hai for Zt22 (Figure 3-8a). Gene expression analysis of iron superoxide dismutase (FeSOD), a chloroplastic enzyme that scavenges superoxide, was found to be highly upregulated in Ct (+Stb6), due to inoculation, irrespective of isolate, peaking at 6hai and then dropping at 24hai (Figure 3-8c). FeSOD expression in Courtot was also significantly different to before inoculation for Zt22 infection, however it was overall significantly less that Ct (+Stb6) (Figure 3-8c).

DAB staining for hydrogen peroxide (H_2O_2) revealed an increase in this compound in the susceptible interactions at 6hai, but not in the incompatible IPO323-*Stb6* interaction (Figure 3-8b). Ct (+Stb6) had a small burst of H_2O_2 at 24hai in response to both isolates before being cleared off at 48hai. In contrast, it wasn't until 48hai that darker staining developed for the susceptible Courtot (Figure 3-8b).

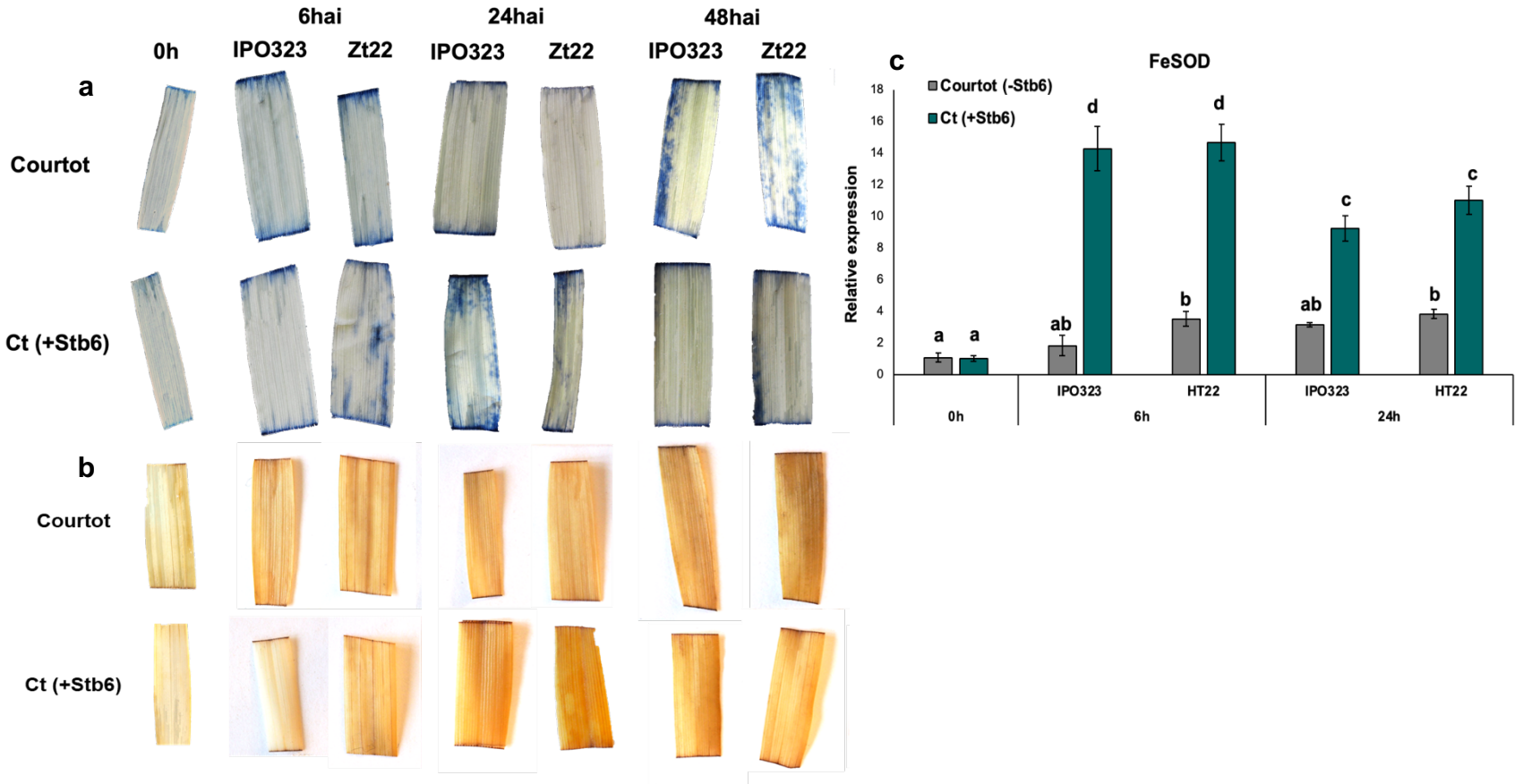


Figure 3-8. (a) NBT blue staining for the detection of superoxide, **(b)** DAB brown staining for the detection of hydrogen peroxide and **(c)** gene expression ($2^{-\Delta\Delta Ct}$) of iron superoxide dismutase (FeSOD), a chloroplastic enzyme that scavenges superoxide. Gene expression data represent means ± SEM (n=3). Letters above bars indicate statistical difference of the means using t-tests ($P < 0.05$). Grey and teal bars indicate Courtot and Ct (+Stb6), respectively.

3.3.5 Transcriptome analysis

The library was sequenced and almost 26.6million 150bp paired-end clean reads were obtained. All samples passed quality control, with the average Q30 percentage exceeding 94%, the error rate being below 0.03% and GC content being ~56% for all samples. All information regarding quality control along with total number of reads, per sample, is given in Supplementary Table 1. Mapping efficiency was ~94% across all samples for wheat's genome, however the total mapping rate for the pathogen's genome was extremely low (~0.1%). PCA showed a good correlation among samples and Pearson's correlation coefficient showed that all correlation coefficients between replicate samples exceeded 0.89, demonstrating high consistency of biological replicates (Figure 3-9). A pairwise, cross-conditional differential expression analysis, from normalised read counts of all 3 biological replicates per condition, was performed, not only to elucidate the difference between Resistant or Susceptible temporal responses based on the presence or absence of *Stb6*, respectively, but also to ascertain how *Stb6* responds to stimuli coming from either an avirulent (IPO323) or virulent (Zt22) strain of *Zymoseptoria tritici*. Control samples were considered either the susceptible genotype Courtot (-*Stb6*) or the reference isolate IPO323. A list of all comparisons is given in Table 3-4. DEG significance threshold was set to Padj < 0.05, however no log2 fold change cut-off point was set during the downstream analysis.

Table 3-4. List of pairwise comparisons selected for Differential Expression analysis. (+) and (-) refer to the presence or absence of *Stb6* in Ct (+Stb6) and Courtot, respectively. R and S refer to Resistant (incompatible) or Susceptible (compatible) response based on the isolate.

DEGs comparisons
1. Ct (+*Stb6*) vs Courtot (-Stb6) 0h
2. R (+) vs S (-) IPO323 6h
3. R (+) vs S (-) IPO323 24h
4. S (+) Zt22 vs R (+) IPO323 6h
5. S (+) Zt22 vs R (+) IPO323 24h

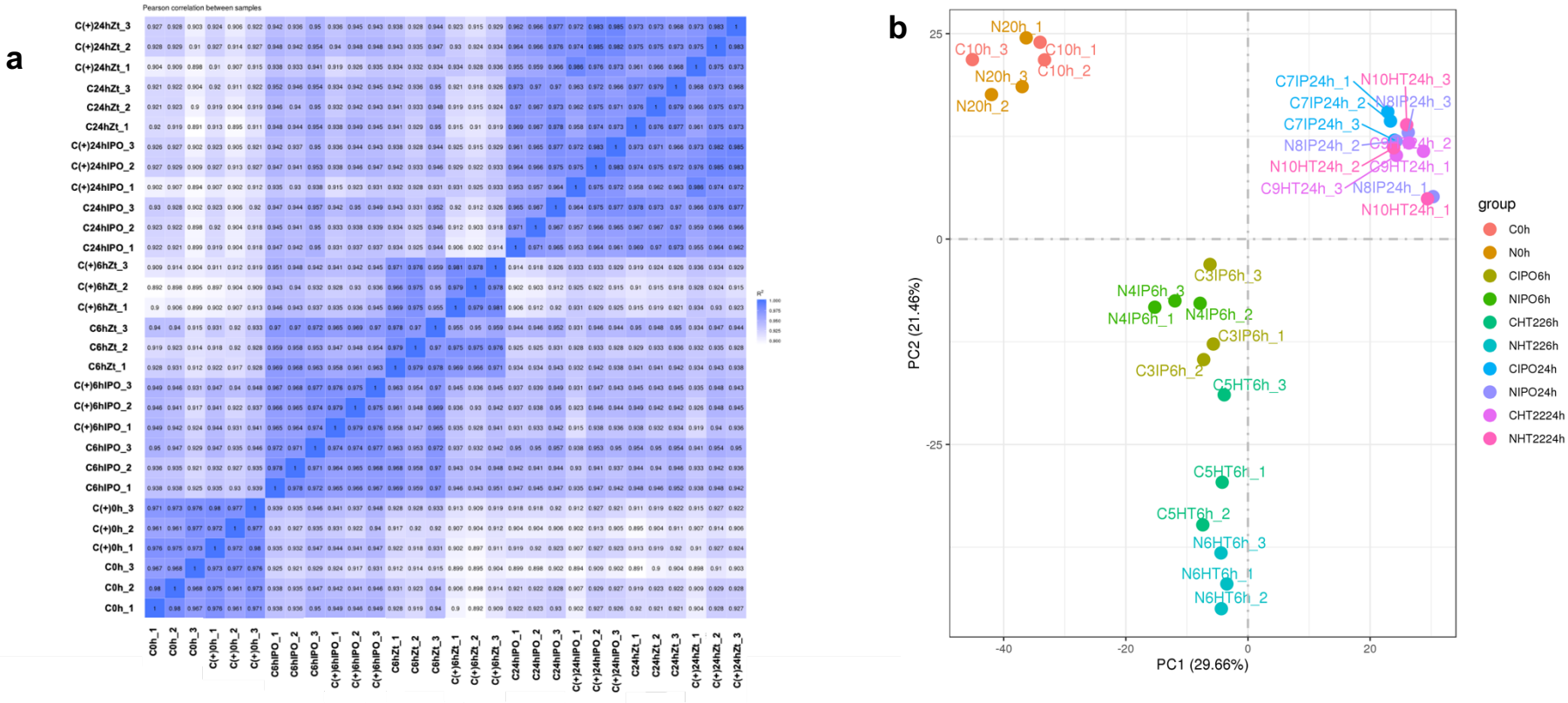


Figure 3-9. (a) Pearson's correlation plot of all samples exhibiting high consistency among biological replicates. Blue coloured scale indicates R^2 correlation values. **(b)** 2D PCA plot indicating the clustering of different samples. Due to different annotations between the time of the bioinformatics analysis and writing of this thesis, there is a discrepancy in the labelling of the different samples between figures (a) and (b). C = Courtot; C(+) or N = Ct (+Stb6); IPO = isolate IPO323; Zt or HT22 = isolate Zt22; 0h, 6h, 24h = hours after inoculation.

a) Temporal patterns of host gene expression in response to Z. tritici

Pathogen infection, almost immediately after inoculation (6hai), had a dramatic effect in transcriptional changes for all genotypes (Figure 3-10a). The highest number of DEGs was observed in comparison no. 4, whereby the virulent isolate Zt22 seemed to cause the most dramatic transcriptional changes in the Ct(+Stb6) genotype at 6hai, although interestingly, this same comparison but at 24hai (comparison no. 5), yielded no significant DEGs and will not be discussed further (Figure 3-10a).

The majority of DEGs were expressed solely in Ct (+Stb6) in response to the two isolates (81%) (Figure 3-10b). There were several genes involved between comparisons in response to inoculation (397 and 500 common DEGs) and 33 genes were involved across all three comparisons in response to inoculation (Figure 3-10b). A negligible percentage of DEGs were transcriptionally different between the 0h and the comparisons under inoculation (Figure 3-10b).

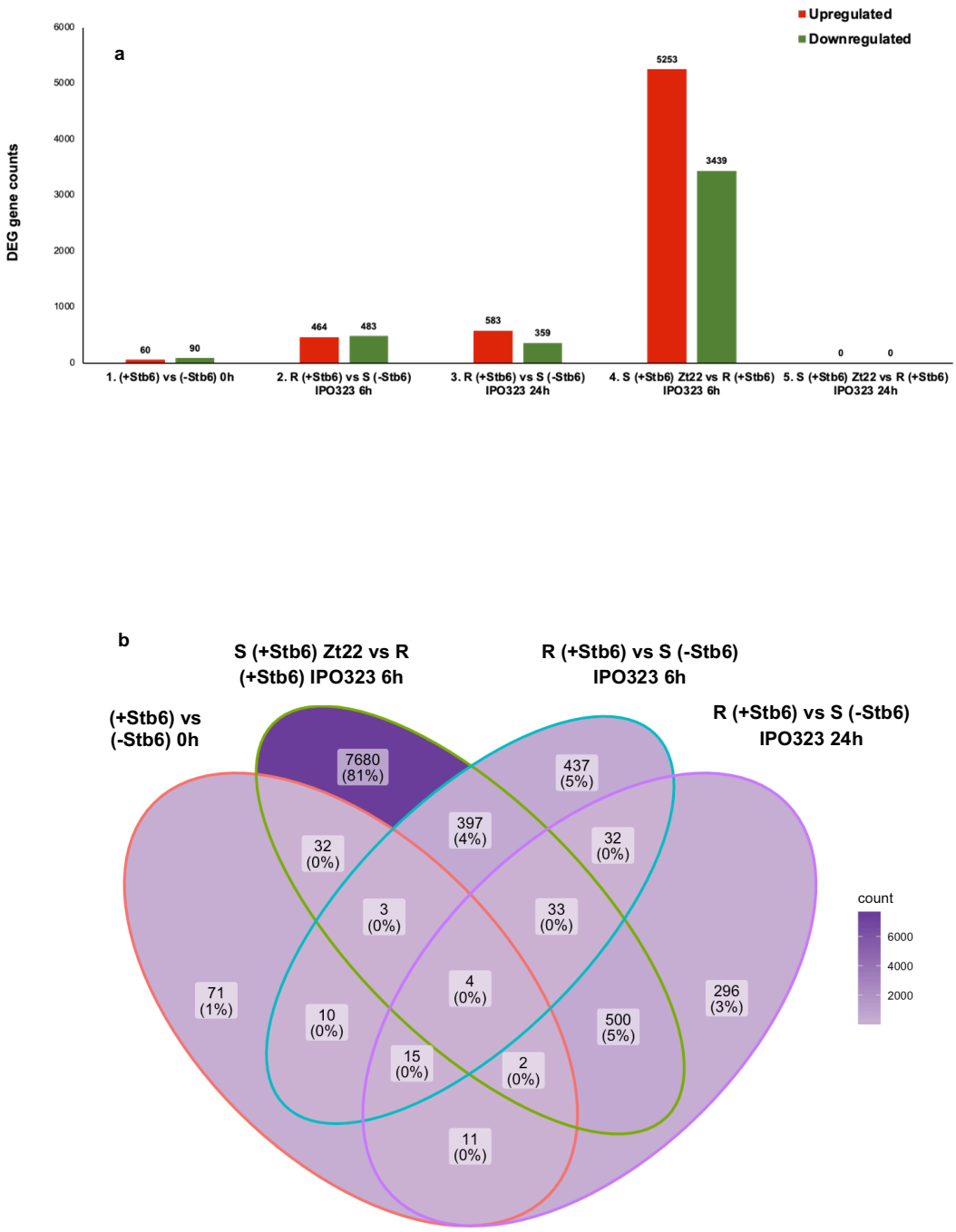


Figure 3-10. (a) Number of up- and downregulated differentially expressed genes (DEGs) for each pairwise comparison. Red bars represent upregulated genes and green bars represent downregulated genes. Numbers above bars indicate the exact number of DEGs for each comparison. **(b)** Venn intersection diagrams of the pairwise comparisons listed in Table 3-4.

For each pairwise comparison, a list of the top 10 significantly DEGs is shown in Supplementary Table 3-2. For Ct (+Stb6), the majority of the top 10 DEGs appeared to exist on the 3A chromosome, as seen also by the low FPKM counts in Courtot, in close physical proximity to *Stb6* (TraesCS3A02G049500), suggesting the possibility that these genes are tightly linked to *Stb6* and were transferred together during the backcrossing event. Additionally, the majority of the genes were either uncharacterised or not annotated. *Stb6* was not found in the top 10 DEGs (Supplementary Table 3-2).

The transcripts were investigated using the Knetminer platform for their involvement in certain biological processes or their molecular functions. The majority of the top downregulated genes in the incompatible *Stb6*-IPO323 interaction at both 6 and 24hai (comparisons 2 and 3) were associated with cellular homeostasis and photosynthesis. In contrast, the majority of the upregulated genes were located on the 3A chromosome, as described above, and according to Knetminer, they were associated with defence responses, signal transduction and lipid metabolic processes. Among them, there were genes associated with stomata and brassinosteroid-mediated signalling (Supplementary Table 3-2). When Ct (+Stb6) was challenged with the virulent Zt22 (comparison 4), Knetminer search showed that the top upregulated genes were also involved in defence responses and secondary metabolic processes, however there were also genes involved with ABA response. In contrast, the majority of the top downregulated genes are involved in carbohydrate metabolic processes and cell growth (Supplementary Table 3-2).

GO and KEGG enrichment analysis were conducted to examine the main biological pathways involved in the set of up- and downregulated DEGs. The top 10 GO terms and metabolic pathways of the pairwise comparisons are shown in Tables 3-5 and 3-6, respectively. “Photosynthesis” or “Photosynthesis, light harvesting” (GO:0015979, GO:0009765) were the two GO terms that appeared at the top of the enrichment analysis in response to inoculations for all comparisons (Table 3-5). Interestingly, it was only the resistance response of *Stb6* against the avirulent isolate IPO323 at 6h (comparison 2) that was associated with electron transport, photorespiration,

Photosystem I (PSI) and H_2O_2 catabolic processes in the chloroplast (GO:0022900, GO:0009853, GO:0009773, GO:0042744) (Table 3-5). The comparison associated with virulence of Zt22 on *Stb6* included defence-related GO terms, such as secondary metabolite biosynthetic process (GO:0044550) and chitin metabolic process (GO:0006030) (Table 3-5).

Table 3-5. Top 10 significantly enriched "Biological Process" GO terms associated with each comparison. Gene ratio indicates the ratio of DEGs to all genes for this GO term, Cp indicates the pairwise comparison. (+) and (-) refer to the presence or absence of *Stb6* in Ct (+Stb6) and Courtot, respectively. R and S refer to Resistant (incompatible) or Susceptible (compatible) response based on the isolate. Table spans across two pages.

Cp	Annotation	GO ID	Gene Ratio	Up	Down
1. (+Stb6) vs (-Stb6) 0h	Negative regulation of peptidase activity	GO:0010466	3|63	n/a	n/a
	Negative regulation of proteolysis	GO:0045861	3|63	n/a	n/a
	Inositol metabolic process	GO:0006020	2|63	n/a	n/a
	Negative regulation of hydrolase activity	GO:0051346	3|63	n/a	n/a
	Alcohol catabolic process	GO:0046164	2|63	n/a	n/a
	Negative regulation of catalytic activity	GO:0043086	3|63	n/a	n/a
	Organic hydroxy compound metabolic process	GO:1901615	4|63	n/a	n/a
	Regulation of hydrolase activity	GO:0051336	3|63	n/a	n/a
	Regulation of transcription by RNA polymerase II	GO:0006357	4|63	n/a	n/a
	Negative regulation of cellular protein metabolic process	GO:0032269	3|63	n/a	n/a
2. R (+) vs S (-) IPO323 6h	Photosynthesis	GO:0015979	64|536	0	64
	Photorespiration	GO:0009853	17|536	0	17
	Carbon fixation	GO:0015977	18|536	0	18
	Photosynthesis, light reaction	GO:0019684	24|536	0	24
	Cellular metabolic compound salvage	GO:0043094	17|536	0	17
	Photosynthetic electron transport in photosystem I	GO:0009773	10|536	0	10
	Hydrogen peroxide catabolic process	GO:0042744	26|536	23	3
	Electron transport chain	GO:0022900	18|536	0	18
	Phosphatidylcholine biosynthetic process	GO:0006656	5|536	0	5

	Cell wall organization	GO:0071555	22|536	22	0
3. R (+) vs S (-) IPO323 24h	Photosynthesis, light harvesting	GO:0009765	34|469	0	34
	Photosynthesis	GO:0015979	41|469	0	41
	Protein-chromophore linkage	GO:0018298	15|469	0	15
	Regulation of response to osmotic stress	GO:0047484	10|469	7	3
	Sulphur compound metabolic process	GO:0006790	23|469	6	17
	Regulation of response to stress	GO:0080134	17|469	11	6
	Negative regulation of response to stimulus	GO:0048585	13|469	10	3
	Regulation of response to stimulus	GO:0048583	23|469	17	6
	Negative regulation of gibberellic acid mediated signalling	GO:0009938	5|469	5	0
	Protein folding	GO:0006457	19|469	1	18
4. S (+) Zt22 vs R (+) IPO323 6h	Photosynthesis, light harvesting	GO:0009765	57|4557	0	57
	Organic acid catabolic process	GO:0016054	69|4557	48	21
	Protein-chromophore linkage	GO:0018298	40|4557	0	40
	Benzene-containing compound metabolic process	GO:0042537	37|4557	35	2
	Cellular amino acid catabolic process	GO:0009063	54|4557	40	14
	Secondary metabolite biosynthetic process	GO:0044550	38|4557	31	7
	Aromatic amino acid family catabolic process	GO:0009074	35|4557	32	3
	Small molecule catabolic process	GO:0044282	73|4557	50	23
	L-phenylalanine catabolic process	GO:0006559	27|4557	26	1
	Chitin metabolic process	GO:0006030	27|4557	26	1

No KEGG pathways were enriched before any inoculation occurred. “Photosynthesis” (osa00195) and “Carbon fixation” (osa00710) were the two enriched, downregulated pathways associated with the resistance response at 6hai, whereas “Porphyrin and chlorophyll metabolism” (osa00860) was also downregulated for the same comparison at 24hai (Table 3-6). “Plant-pathogen interaction” (osa04626) were enriched in comparisons 3 and 4, however many more genes were involved in this pathway when *Stb6* was challenged with Zt22 (Table 3-6). Several more pathways were enriched for the response of *Stb6* to two isolates, including “Protein export” (osa03060) and “Protein processing in endoplasmic reticulum” (osa04141) which refer to protein processing and translocation into the different organelles of the cells, such as the chloroplast, but they also represent a common mechanism by which pathogenic microorganisms secrete their proteins, including virulence factors, into their hosts’ cells. Moreover, “Photosynthesis – antenna proteins” (osa00196) was involved and downregulated in this comparison (Table 3-6). Finally, “Galactose metabolism” (osa00052) was enriched. This pathway is required for the production of sugars necessary for plant metabolism but it is also involved in the biosynthesis of ascorbate, the necessary substrate in the VDE production in the XC.

Table 3-6. All significantly enriched KEGG pathways associated with each comparison. Ratio indicates the ratio of DEGs to all genes for this KEGG ID. Cp indicates each pairwise comparison. Pathways and KEGG IDs are coming from rice (*Oryza sativa*). (+) and (-) refer to the presence or absence of *Stb6* in Ct (+Stb6) and Courtot, respectively. R and S refer to Resistant (incompatible) or Susceptible (compatible) response based on the isolate.

Cp	Annotation	GO ID	Ratio	Up	Down
1. (+Stb6) vs (-Stb6) 0h	n/a	n/a	n/a	n/a	n/a
2. R (+) vs S (-) IPO323 6h	Photosynthesis	osa00195	7|68	0	7
	Carbon fixation in photosynthetic organisms	osa00710	7|68	0	7
3. R (+) vs S (-) IPO323 24h	Porphyrin and chlorophyll metabolism	osa00860	4|46	0	4
	Plant-pathogen interaction	osa04626	7|46	6	1
4. S (+) Zt22 vs R (+) IPO323 6h	Plant-pathogen interaction	osa04626	48|471	39	9
	Protein processing in endoplasmic reticulum	osa04141	46|471	41	5
	Amino sugar and nucleotide sugar metabolism	osa00520	31|471	17	14
	Photosynthesis - antenna proteins	osa00196	9|471	0	9
	Protein export	osa03060	14|471	10	4
	Galactose metabolism	osa00052	13|471	5	8
	Sphingolipid metabolism	osa00600	9|471	6	3
	Phenylpropanoid biosynthesis	osa00940	27|471	12	15
	Various types of N-glycan biosynthesis	osa00513	10|471	9	1

We focused on three significantly enriched KEGG pathways related to the chloroplast and plant-pathogen interactions; photosynthesis (osa00195), photosynthesis-antenna proteins (osa00196) and plant-pathogen interactions (osa04626) (Figures 3-11 to 3-14). The oxygen-evolving complex (OEC) protein PsbP, plastocyanin (PC or PetE), ferredoxin (Fd or PetF), ferredoxin NADP+ oxidoreductase (FNR or PetH) and the delta- and b-ATPase proteins were significantly downregulated in the resistance response of *Stb6* to IPO323 (Figure 3-11). The light-harvesting complex (LHC) antenna proteins of both photosystems also responded to *Z. tritici* infection. PSII LHC protein B1 (Lhcb1) was the most downregulated protein in Ct (+Stb6) in response to Zt22, whereas the remaining LHC antenna proteins were slightly downregulated (Figure 3-12). Finally, we investigated transcript differences among comparisons for genes involved in plant-pathogen interactions (Figure 3-13 and 3-14). Calmodulin/calmodulin-like proteins (CaMCML), mitogen-activated protein kinases 3 and 6 (MPKs) and WRKY transcription factors were highly induced in Ct (+Stb6), regardless of isolate. However, it was only when Ct (+Stb6) was challenged with Zt22 that we observed transcriptional change in chitin elicitor-binding protein (CEBiP), chitin elicitor receptor kinase 1 (CERK1), calcium-dependent protein kinase (CDPK), Pto interaction protein (Pti1), RPM1-interacting protein 4 (RIN4) and heat-shock protein 90 (HSP90) (Figure 3-13). These proteins are directly involved in plant disease perception and signalling and work synergistically to promote Ca^{2+} molecules across the different cell compartments. Several other proteins were involved in this pathway, such as cyclic nucleotide gated channel proteins (CNGCs) and nitric oxide synthase (NOS), however their downregulation was to a smaller extend (Figure 3-14).

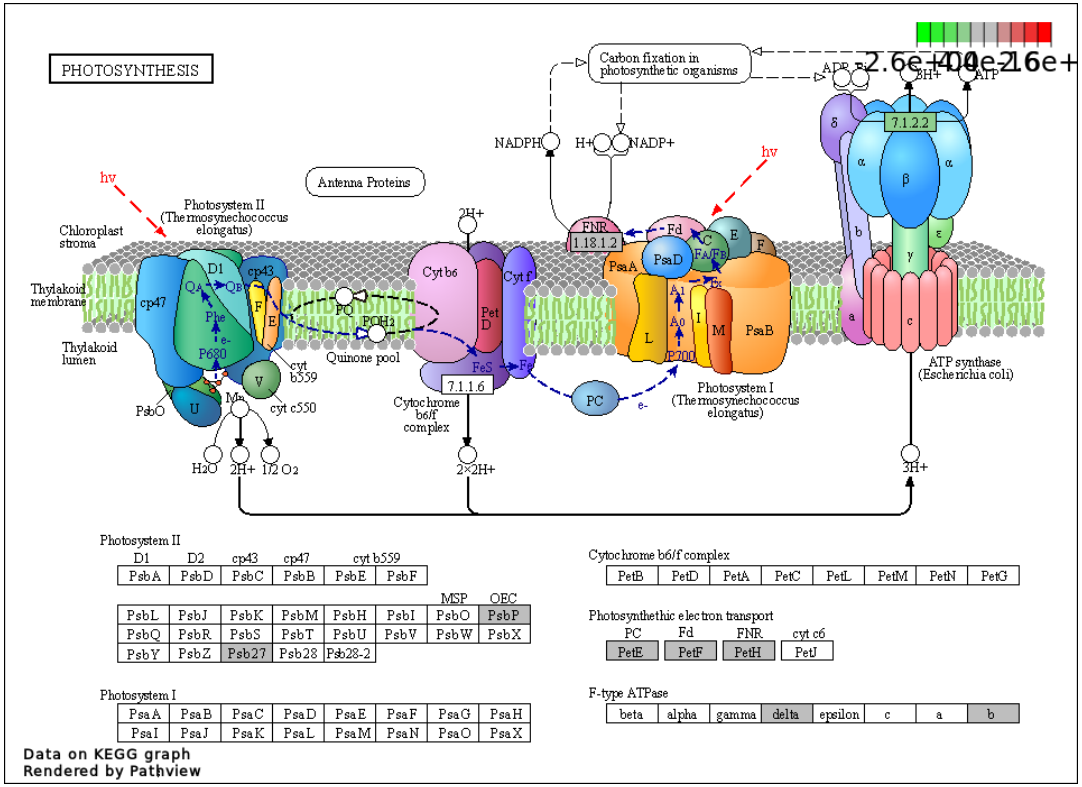


Figure 3-11. Photosynthesis pathway KEGG map (osa00195) for the comparison between the resistant Ct (+Stb6) and the susceptible Courtot inoculated with IPO323 at 6hai. Genes involved in this pathway are highlighted in shades of green, grey or red, based on the Fold Change scale bar at the top right. Green represents downregulation, grey small change and red upregulation. In this instance, all grey filled boxes are downregulated genes.

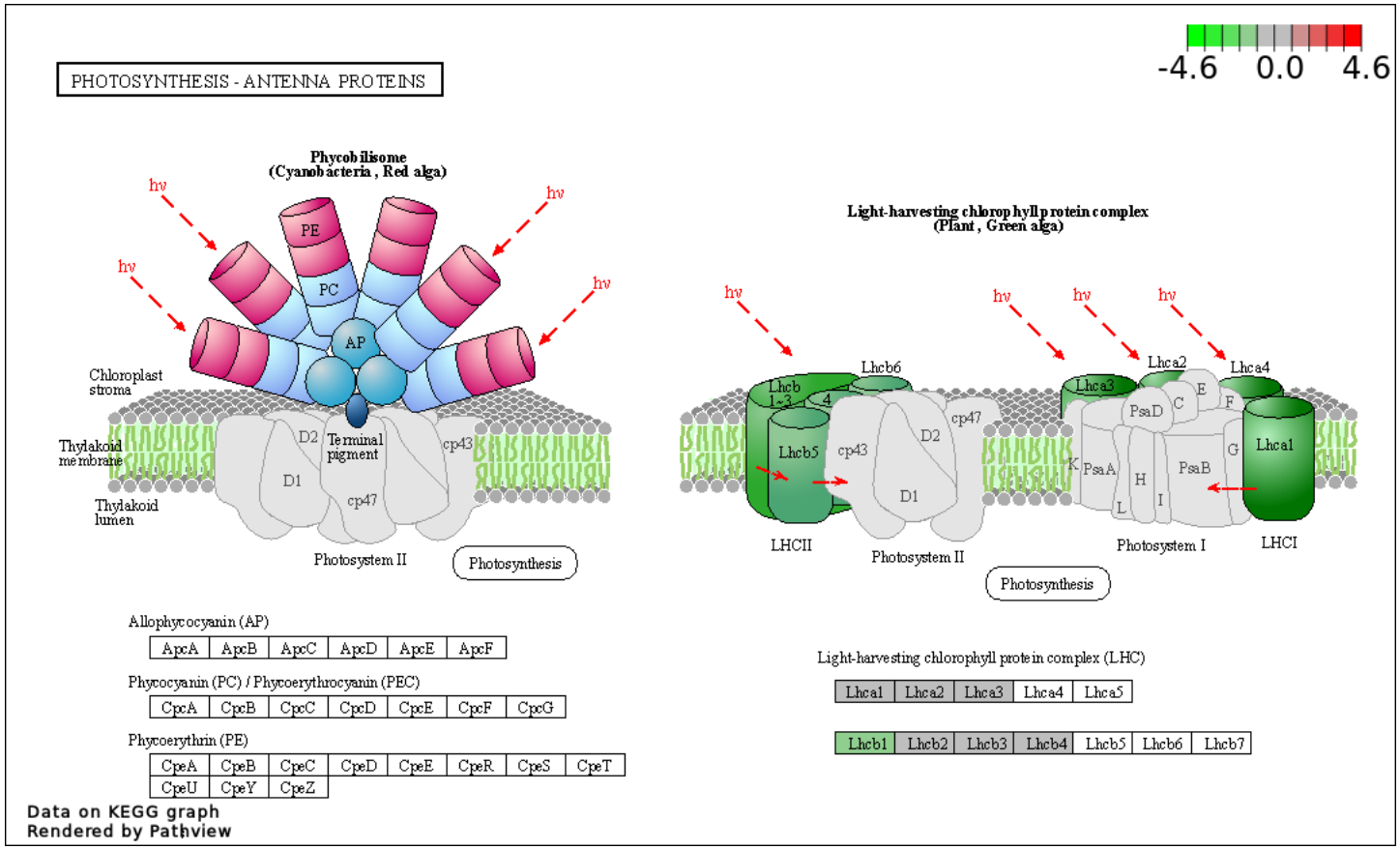


Figure 3-12. Photosynthesis-antenna proteins KEGG map (osa00196) for the comparison between *Stb6* in susceptibility (Zt22 inoculation) and resistance (IPO323 inoculation) at 6hai. Genes involved in this pathway are highlighted in shades of green, grey or red, based on the Fold Change scale bar at the top right. Green represents downregulation, grey small change and red upregulation. In this instance, all grey filled boxes are downregulated genes.

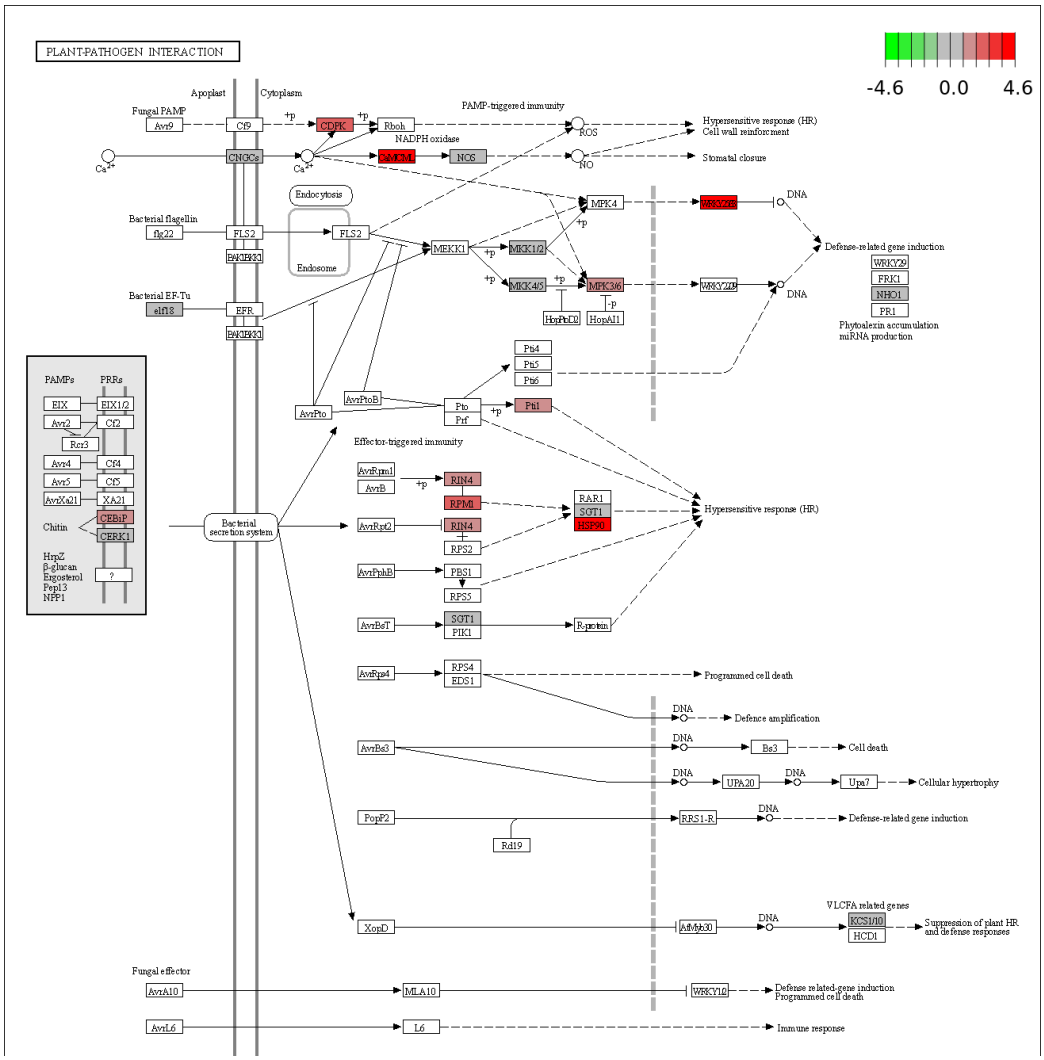


Figure 3-13. Plant pathogen interaction KEGG maps (osa04626) for comparison S (+) Zt22 vs R (+) IPO323 6h. Genes involved in this pathway are highlighted in shades of green, grey or red, based on the Fold Change scale bar at the top right. Green represents downregulation, grey small change and red upregulation.

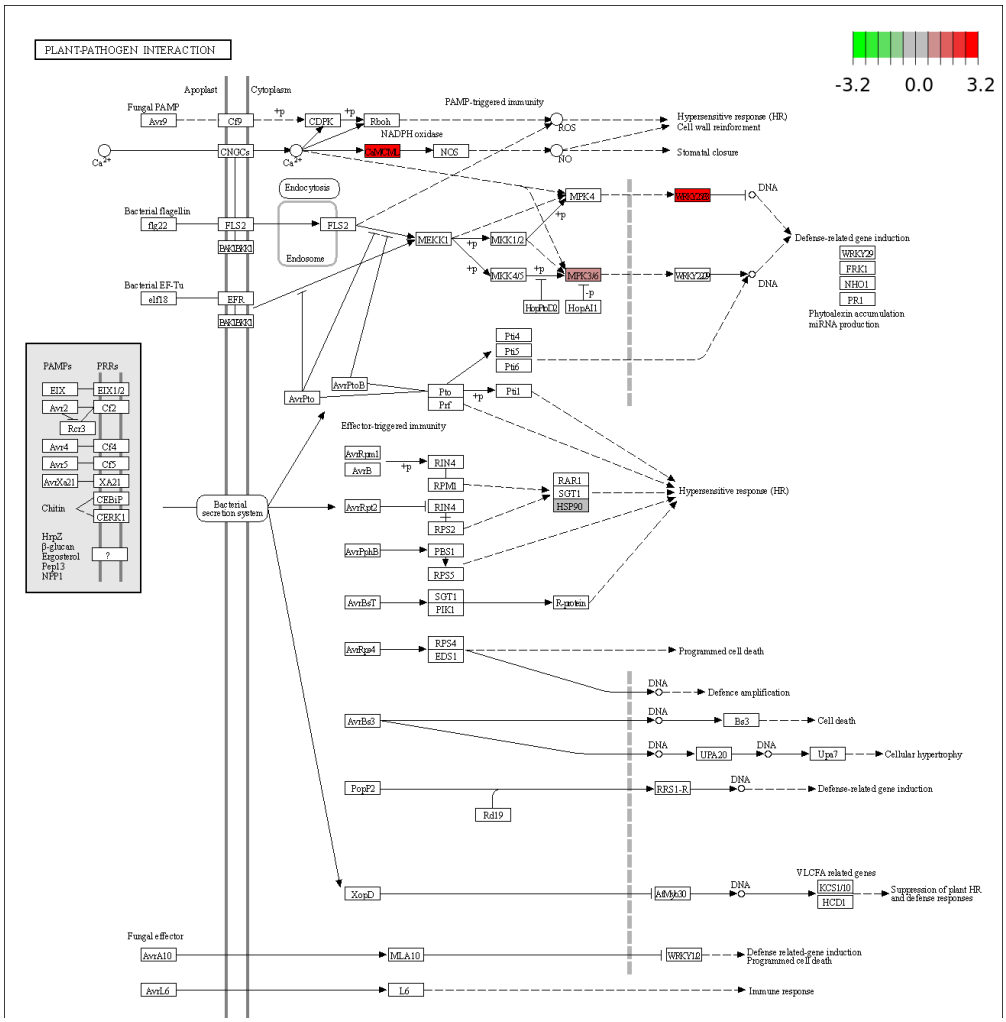


Figure 3-14. Plant pathogen interaction KEGG maps (osa04626) for comparison R (+) IPO323 vs S (-) IPO323 24h. Genes involved in this pathway are highlighted in shades of green, grey or red, based on the Fold Change scale bar at the top right. Green represents downregulation, grey small change and red upregulation.

The last step of this analysis investigated Protein-Protein interactions (PPIs) for our most interesting comparisons, i.e. either presence or absence of *Stb6* with IPO323 and Zt22 inoculations. Transcript IDs from PPI data were first subjected through a Knetminer search in order to be annotated for easier visualisation. ± *Stb6* PPI at 6hai revealed top interacting downregulated proteins related to photosynthesis, such as Lhcb1, PsaD, PPL1 (or PsbP), Psb27 and Psb28, plastocyanin (PetE), ferredoxin and FNR, CHLH, ATPD, VDE and the tocopherol-related VTE (Supplementary Figure 3-6). In contrast, the top interacting upregulated proteins involved defence-related proteins, such as lipoxygenase (LOX), ROS scavenging proteins, such as catalase (CAT2) and a plethora of transcription factors (TFs) (Supplementary Figure 3-7). By 24hai, more photosynthesis-related proteins were at the top downregulated, now including, among others, lutein (LUT2), photochlorophyllide reductase (PORA), degradation protease (DEGP2), heat shock protein 90 (HSP90) and ascorbate peroxidase (APX) (Supplementary Figure 3-8). At the top upregulated interacting proteins at 24hai, we observed Calmodulin-like proteins (CMLs), protein phosphatases 2C (PP2C), WRKY TFs and a ferric chelate oxidoreductase (FRO6) (Supplementary Figure 3-9).

Differences in Ct (+Stb6) transcriptome depending on avirulent or virulent isolate can be interpreted in two ways, as we selected our control to be the IPO323 inoculation. Therefore, the proteins described below can either be interpreted as being downregulated as a response to Zt22, or upregulated as a response to IPO323. Photosynthesis-related proteins were also involved, however several other significant ones appeared in this comparison. Among them they were FtsH proteases, STN7, HY5, chlorophyll biosynthesis proteins (CABs), FRO6, proteins on the side of PSI (Lhca), NDPK2 and SERK2 (Supplementary Figure 3-10). Also, defence-related proteins were observed, such as mitogen-activated protein kinases (MKKs), HSPs, SERK 1 and 4, the brassinosteroid-related BIR2 and BAK1, CERK1, LOX, FtsH4, CMLs and PP2Cs (Supplementary Figure 3-11).

Selected genes were used to confirm the expression patterns that were observed through the RNA sequencing, but also to further investigate some interesting genes associated with defence and signalling. These included *PsbP*, *Lhca1*, *PsbS*, *CERK1*, *AOS*, *ICS* and *PR1*. *PsbP* and *Lhca1* were chosen due to their significant appearance and downregulation in resistance. *Lhca1* was also selected as Le et al. (2014) showed that this protein, along with Lhcb3, interacted with CERK1 in *Arabidopsis* through a Y2H assay. *PsbS* was selected due to its involvement in NPQ and *CERK1* was selected as it appeared to be in Ct (+Stb6)-Zt22. AOS and ICS are precursor molecules on two diverse disease signalling pathways: jasmonic acid (JA) and salicylic acid (SA), respectively. Both allene oxide synthase (AOS) and isochorismate (ICS) are chloroplastic compounds involved in the early formation of jasmonic and salicylic acid, respectively. The pathogenesis-related protein 1 (PR1) is induced as a defence response, normally associated with SA-mediated signalling.

PsbP gene expression analysis did not show downregulation in Ct (+Stb6) inoculated with IPO323 at 6hai, however the difference in gene expression was not statistically significant (Figure 3-15a). However, *PsbP* expression significantly increased at 24hai in relation to susceptibility (Courtot with IPO323 and Zt22, Ct (+Stb6) with Zt22) (Figure 3-15a). *Lhca1* expression for Ct (+Stb6) was downregulated in Zt22 compared to IPO323 at 6hai, however expression increased in Ct (+Stb6) significantly at 24hai with Zt22 (Figure 3-15b). Courtot downregulated *Lhca1* (Figure 3-15b). *PsbS* was downregulated in Ct (+Stb6) compared to Courtot for both inoculations and significantly reduced upon Zt22 inoculation at 24hai (Figure 3-15c). Finally, *CERK1* confirmed the observed transcriptomic result, as there was a significant upregulation of this gene at 6hai for Ct (+Stb6) and infection with Zt22. However, it dropped significantly at 24hai, whereas expression for *Stb6* and IPO323 inoculated plants increased by 24hai (Figure 3-15d).

PsbP activity was also confirmed with western blot analysis, kindly completed by Mrs. Charlene Dambire (Figure 3-16). No statistical analysis could be performed, as western blot repetitions are still ongoing. However, even at this stage of two experimental replications, PsbP expression confirmed

the sequencing results, whereby PsbP in Ct (+Stb6) gets downregulated in response to IPO323 (Figures 3-11 and 3-16).

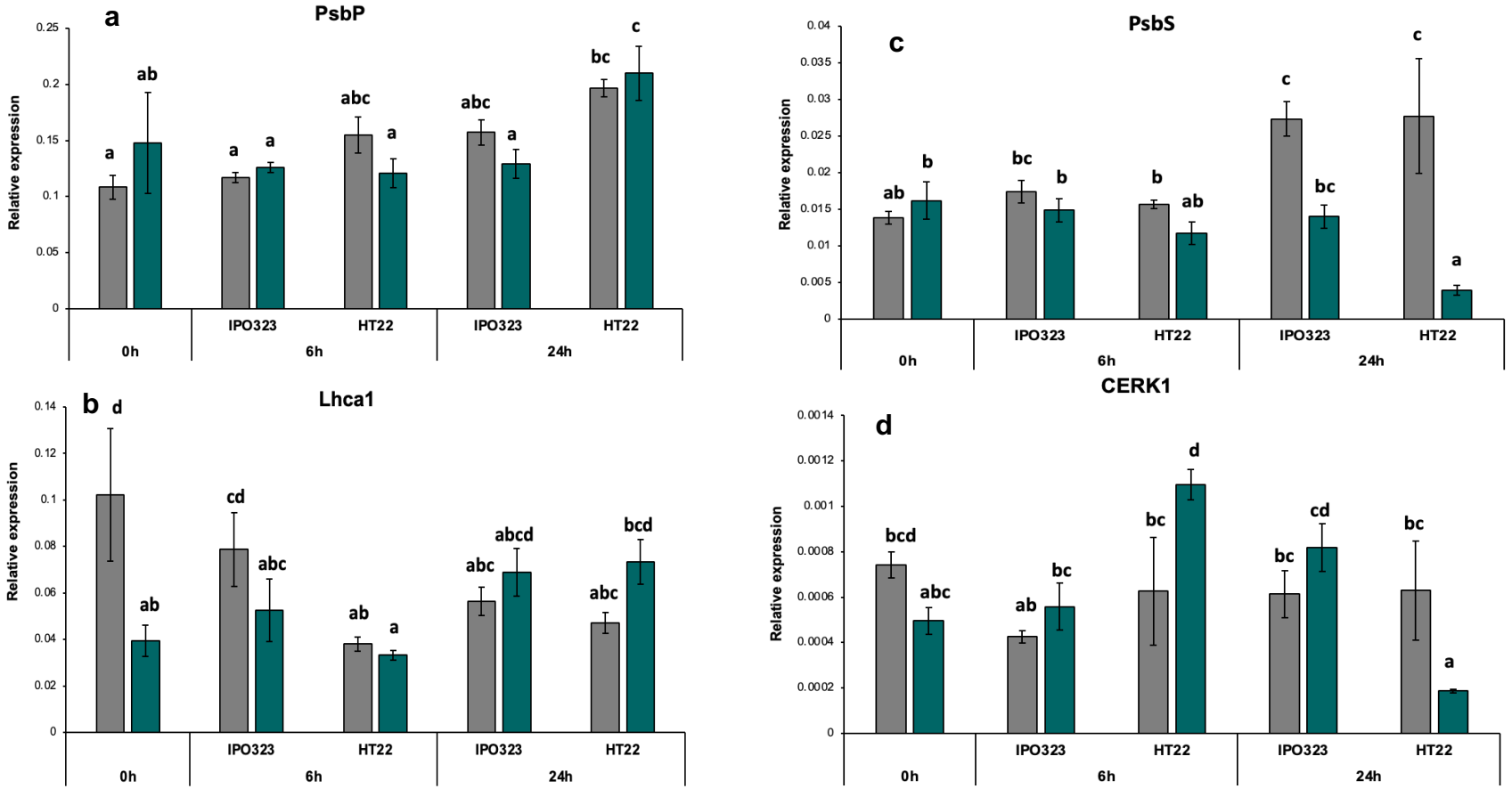


Figure 3-15. Relative gene expression on selected genes from RNA sequencing. PsbP **(a)**, Lhca1 **(b)**, PsbS **(c)** and CERK1 **(d)** were selected to confirm their expression. Data represent means ± SEM (n=3). Relative gene expression was calculated using the $2^{-\Delta Ct}$ method. Different letters above bars indicate significant differences between the means (t-tests $P < 0.05$). Grey and teal bars indicate Courtot and Ct (+Stb6), respectively.

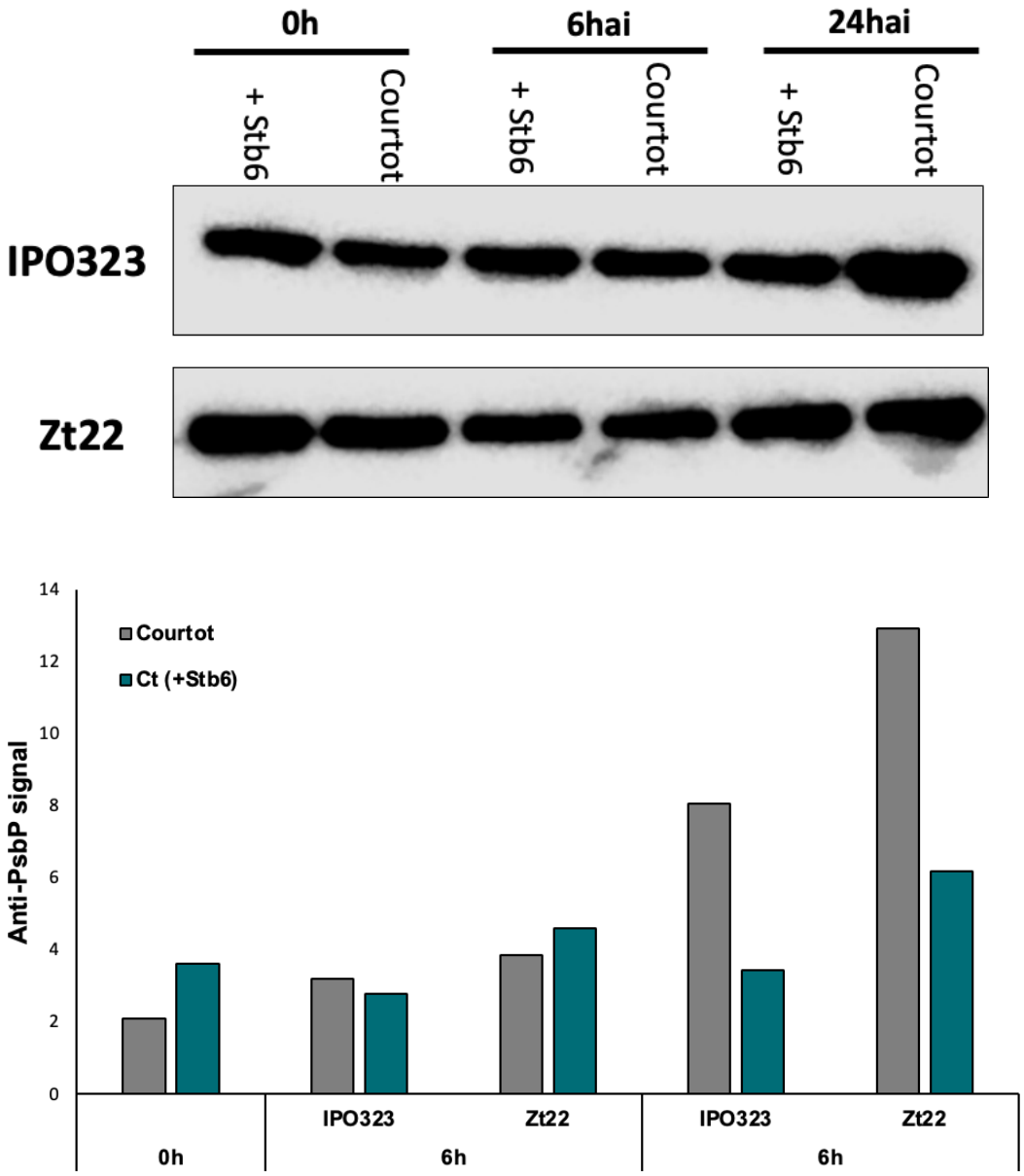


Figure 3-16. Western blot on PsbP protein and signal analysis. No statistical analysis could be performed as repetitions of these westerns are still ongoing.

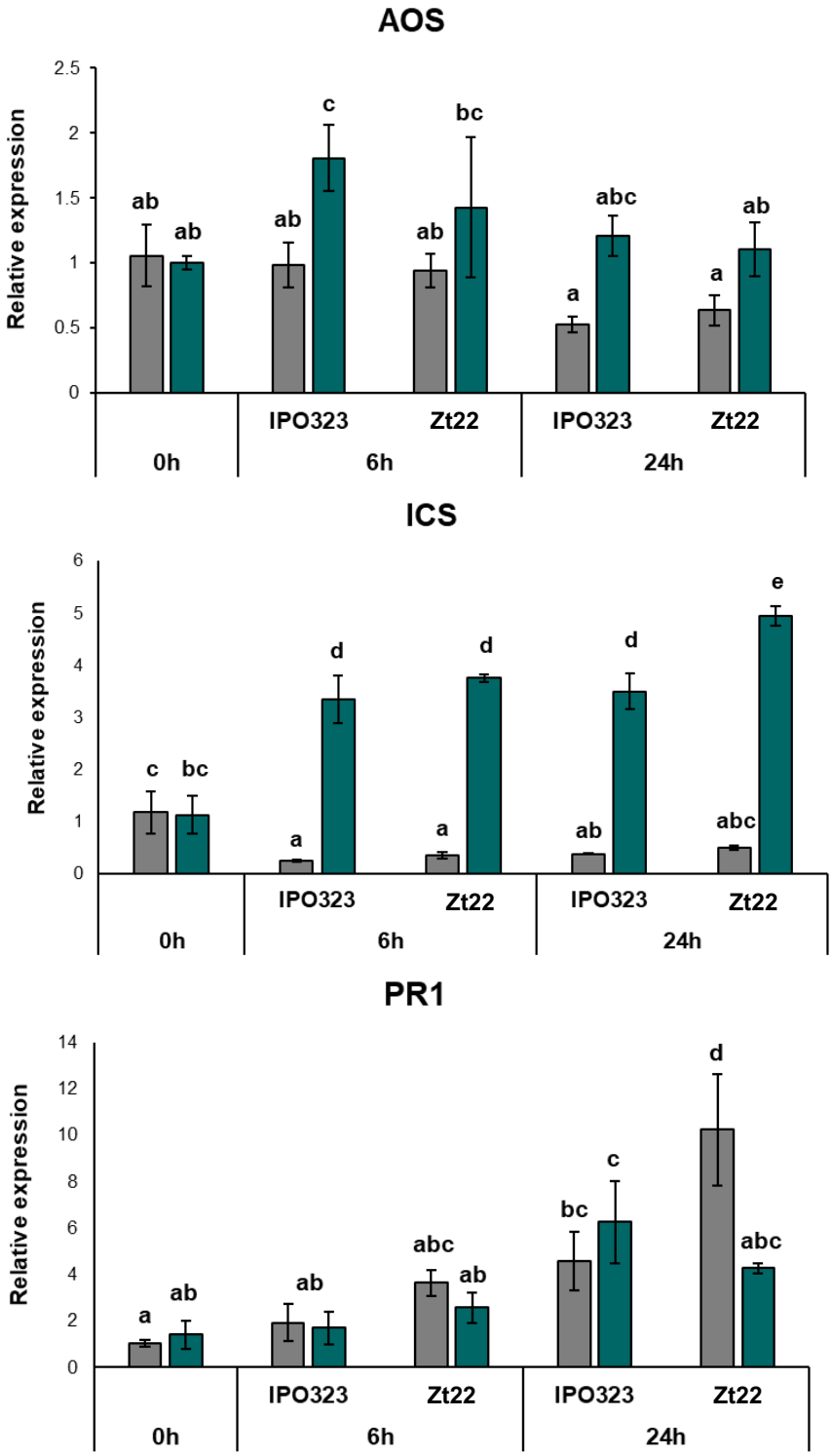


Figure 3-17. Relative gene expression ($2^{-\Delta\Delta Ct}$) of defence-related compounds. AOS and ICS originate from the chloroplast and are precursor molecules of the defence hormones jasmonic acid and salicylic acid, respectively. PR1 is a pathogenesis-related protein that gets induced upon infections. Data represent means ± SEM (n=3). Significant differences between the means were derived through t-tests ($P < 0.05$) and are shown with letters above the bars. Grey and teal bars indicate Courtot and Ct (+Stb6), respectively.

To elucidate whether resistance responses were driven by JA or SA, we measured the expression of two precursor molecules of these hormones, namely allene oxide synthase (AOS) and isochorismate (ICS), along with the pathogenesis-related protein 1 (PR1) which is typically associated with SA-mediated defence. *Z. tritici* infection induced the expression of all three genes, however the response of *AOS* and *ICS* was associated with the presence of *Stb6* (Figure 3-17). However, *AOS* expression was significantly different only for Ct (+Stb6) inoculated with IPO323 at 6hai, compared to Courtot. In contrast, *ICS* had the same high expression in that genotype regardless the inoculation at 6hai and only increased significantly at 24hai upon Zt22 infection. The susceptible Courtot downregulated *AOS* and mainly *ICS*, over the course of infection (Figure 3-17). Finally, *PR1* gradually increased over time and appeared significantly different to 0h for *Stb6* inoculated with IPO323 at 24 hai but was downregulated to Zt22 at the same time point (Figure 3-17).

b) Transcriptional changes of the pathogen Z. tritici

Bioinformatic analysis also took place on the transcriptome of the pathogen *Z. tritici*. Here, we also investigated time effects (6 to 24hai) as well as more comparisons between the genotypes, as seen in Figure 3-18. There were very few genes differentially expressed, whereas in some cases there were zero (Figure 3-18). The highest number of DEGs was observed in the incompatible interaction with *Stb6* at 24hai, followed by compatible interactions resulting from the virulent isolates Zt22 (Figure 3-18).

We were interested to investigate potential effector molecules by *Z. tritici* that not only contribute to susceptibility but could also potentially target the chloroplast as a virulence strategy. We used the online software EffectorP and Localizer, which are able to predict potential fungal effectors based on a given sequence as well as predict their potential subcellular localisation (Sperschneider et al., 2016, 2017). Not many transcripts resulted in predictions, however a list of them is given in the table below (Table 3-7).

All predicted effector proteins appeared to be secreted in the apoplast or the cytoplasm and, with one exception, they all had <300 amino acid residues. Only one transcript out of all them was predicted to locate in the

chloroplast, Mycgr3G77055. Unfortunately, not much information was publicly available (Ensembl or Knetminer), except that it is a cell wall mannoprotein or a hydrophobic surface binding protein involved in lipid degradation. This protein was found both in IPO323 and Zt22 genomes, being expressed at 24hai (Table 3-7).

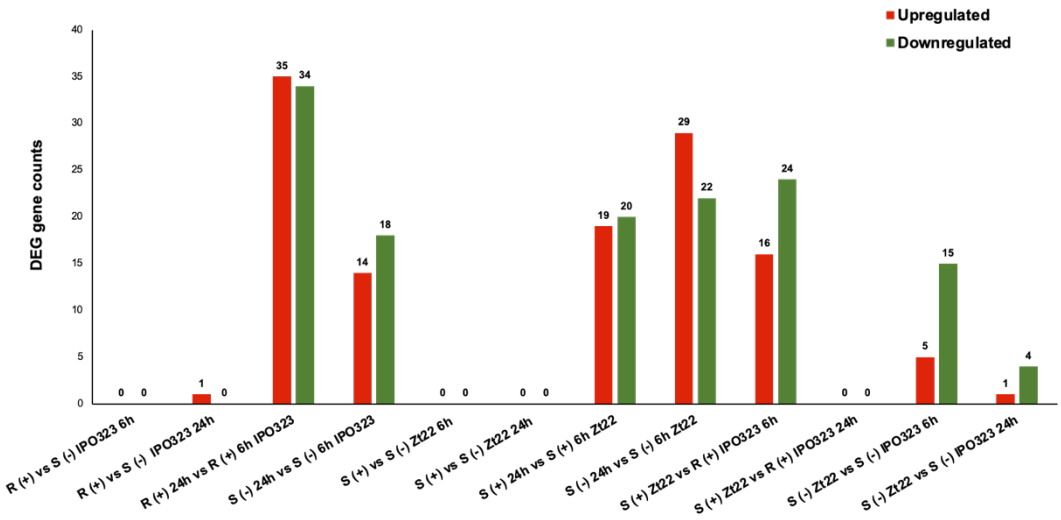


Figure 3-18. Number of DEGs from the transcriptome of *Z. tritici*. Red bars represent upregulated genes and green bars represent downregulated genes. Numbers above bars indicate the exact number of DEGs for each comparison.

Table 3-7. A list of putative *Z. tritici* effectors. Gene ID describes the significant DEG from the bioinformatic analysis on the fungal transcriptome, Log FC denotes the magnitude of the expression along with significance *P* value. Localizer and EffectorP are the online machine learning tools used for the prediction of effectors. Residues describe the length of amino acids in each predicted protein along with the percentage of their cysteine content. Transcripts highlighted in red indicate commonalities across comparisons.

R (+) 24h vs R (+) 6h IPO323						
Gene ID	**Log FC**	***p***	**Localizer**	**Residues**	**% Cysteine**	**EffectorP**
Mycgr3G96543	8.90	0.0000	---|---|---	143	5.59	Apoplastic
Mycgr3G104000	7.77	0.0000	---|---|---	180	3.33	Cytoplasmic/apoplastic
Mycgr3G90017	6.68	0.0001	---|---|---	159	0.00	Apoplastic
Mycgr3G77055	1.61	0.0044	**Chl**|---|---	193	0.00	Cytoplasmic
Mycgr3G102849	-1.29	0.0163	---|---|---	285	2.11	Apoplastic
Mycgr3G104697	-1.56	0.0030	---|---|---	149	2.69	Apoplastic
Mycgr3G104404	-2.90	0.0044	---|---|---	179	2.24	Apoplastic
Mycgr3G106106	-4.59	0.0351	---|---|---	156	3.85	Apoplastic/cytoplasmic
S (+) 24h vs S (+) 6h Zt22						
Gene ID	**Log FC**	***p***	**Localizer**	**Residues**	**% Cysteine**	**Effector P3**
Mycgr3G96543	8.22	0.0000	---|---|---	143	5.59	Apoplastic
Mycgr3G104000	6.20	0.0001	---|---|---	180	3.33	Cytoplasmic/apoplastic
Mycgr3G77055	2.44	0.0002	**Chl**|---|---	193	0	Cytoplasmic
Mycgr3G102849	-1.17	0.0343	---|---|---	285	2.11	Apoplastic
Mycgr3G83835	-1.45	0.0437	---|---|**Nuc**	659	0.30	Cytoplasmic
Mycgr3G104697	-2.37	0.0000	---|---|---	149	2.69	Apoplastic
S (+) Zt22 vs R (+) IPO323 6h						
Gene ID	**Log FC**	***p***	**Localizer**	**Residues**	**% Cysteine**	**Effector P3**
Mycgr3G104794	-2.20	0.0024	---|---|---	157	2.55	Cytoplasmic/apoplastic
Mycgr3G105182	-3.12	0.0000	---|---|---	143	4.20	Apoplastic
Mycgr3G104404	-7.17	0.0000	---|---|---	179	2.24	Apoplastic
S (-) 24h vs S (-) 6h IPO323						
Gene ID	**Log FC**	***p***	**Localizer**	**Residues**	**% Cysteine**	**Effector P3**
Mycgr3G96543	6.63	0.0004	---|---|---	143	5.59	Apoplastic
Mycgr3G102792	4.02	0.0105	---|---|**Nuc**	114	7.02	Cytoplasmic
Mycgr3G105182	-2.50	0.0226	---|---|---	143	4.20	Apoplastic
S (-) 24h vs S (-) 6h Zt22						
Gene ID	**Log FC**	***p***	**Localizer**	**Residues**	**% Cysteine**	**Effector P3**
Mycgr3G96543	8.02	0.0000	---|---|---	143	5.59	Apoplastic
Mycgr3G104000	6.76	0.0109	---|---|---	180	3.33	Cytoplasmic/apoplastic
Mycgr3G102792	3.99	0.0028	---|---|**Nuc**	114	7.02	Cytoplasmic
Mycgr3G77055	3.36	0.0001	**Chl**|---|---	193	0.00	Cytoplasmic
Mycgr3G102849	-1.58	0.0063	---|---|---	285	2.11	Apoplastic
Mycgr3G106329	-2.26	0.0394	---|---|---	135	0.74	Cytoplasmic
Mycgr3G104697	-2.57	0.0001	---|---|---	149	2.69	Apoplastic
S (-) Zt22 vs S (-) IPO323 6h						
Gene ID	**Log FC**	***p***	**Localizer**	**Residues**	**% Cysteine**	**Effector P3**
Mycgr3G105182	-1.98	0.0304	---|---|---	143	4.20	Apoplastic
Mycgr3G106106	-5.08	0.0434	---|---|---	156	3.85	Apoplastic/cytoplasmic
Mycgr3G104404	-7.01	0.0000	---|---|---	179	2.24	Apoplastic

3.4 Discussion

We have shown here that *Stb6* resistance against the avirulent IPO323 was characterised by an effective energy regulation achieved through qE and qI types of NPQ and the XC in the chloroplast. The importance of the chloroplast in the host-pathogen interaction between wheat and *Z. tritici* was first pointed out by Kema et al. (1996) who showed chloroplast migration towards the cell wall and the apoplastic growing hyphae at 48hai. More recent work reported NPQ-mediated responses to *Z. tritici* as early as 8hai (Ajigboye et al., 2021). Here, we also focused on the early infection by *Z. tritici* at 6, 24 and 48hai to effectively capture the initial reprogramming of PSII function, as PSII is the most sensitive environmental stress sensor in plants.

We identified 6 to 24hai as key time points in *Stb6*-mediated defence to *Z. tritici*. At these time points we observed slower Induction and faster Relaxation kinetics of NPQ, showing downregulation of qE and upregulation of qI up to 24hai, significant but temporary reduction in chlorophyll absorbance and overall reduction in qP and F_v/F_m, but not below the 0.8 threshold, suggesting photoinhibition. Photoinhibition, often associated with the qI form of NPQ, is a term that is often used to refer to light-induced decrease in φPSII and/or A_{max}, although dynamic photoprotective processes would also reduce F_v/F_m (Murchie & Niyogi, 2011). Because F_v/F_m, ETR, φPSII and A_{max} remained unaffected in the resistant response, the observed photoinhibition was rather transient, confirmed by the recovery of NPQ components by 48hai. We observed significant reductions in electron transport rate and φPSII at 6hai when *Stb6* was challenged with IPO323 compared to Zt22. This photoinhibition (qI) as part of the early defence response of *Stb6* was associated with enrichment of transcripts related to the re-organisation of LHCs and downregulation of the proteins of the oxygen-evolving complex (OEC). In evergreens this mechanism is considered photoprotective as it leads to long-term Chl and LHC maintenance (Demmig-Adams et al., 2012). Temporary inactivation of OEC also allows for long term oxidative shielding of PSI and redirection of metabolism from photosynthesis to defence. The OEC resides on the lumenal side of PSII, it oxidizes water into molecular oxygen and is comprised by several extrinsic proteins, namely PsbO, PsbP, PsbQ and PsbR

(Sasi et al., 2018; Che et al., 2020). PsbP is essential for plant growth, as it regulates and stabilises PSII and is required for PSII repair and assembly (Ifuku et al., 2005; Theis & Schroda, 2016). Moreover, PsbP is required for the recovery from photoinhibition as well for the stability of PSI, as *Arabidopsis* mutants lacking this protein showed delayed recovery from photoinhibition under high light and decrease in the PSI antenna protein Lhca1 (Ishihara et al., 2007). Similarly, the protein Psb27 is essential for PSII repair as it binds to PSII complexes and facilitates the formation of the manganese cluster of the OEC, thus enabling the plants to adapt to excess energy conditions (Hou et al., 2015; Lu, 2016; Theis & Schroda, 2016). Here, we provide evidence that in the resistant response between Ct (+Stb6) and IPO323, lower accumulation of zeaxanthin associated with the downregulation of qE while increasing qI, caused by OEC downregulation, allowed for PSII core protein phosphorylation, transient disassembly, assembly and reorganisation of the LHCs, as a photoprotective function (Demmig-Adams et al., 2012). If dissipation occurs in a ΔpH-independent manner, this is associated with a rearrangement of phosphorylated PSII core proteins, or with degradation of D1 and OEC proteins and an accumulation of several stress-induced PsbS-related proteins and the carotenoid lutein (Demmig-Adams et al., 2012). In this scenario, zeaxanthin is retained and F_v/F_m reductions are sustained (Demmig-Adams & Adams, 2006).

In the resistant response of Ct (+Stb6) to IPO323 there was a clear diversion of carotenoids from α-carotene to β-carotene at 6hai. In contrast, β-carotene at 6hai was significantly lower in the *Stb6* line challenged with the virulent ZT22. This suggested that functional XC is essential for resistance as early as 6hai. Downregulation of qE in *Stb6* was also in line with reduced levels of β-carotene, zeaxanthin (Zea), violaxanthin (Vio) and DEP and a slight increase in neoxanthin (Neo). NCED expression was greater in Ct (+Stb6) in response to IPO323 compared to Zt22, suggesting possible increase in the synthesis of ABA, however the latter was not measured in this study. In contrast, inoculation with the virulent Zt22 resulted in no differences in PSII function for the susceptible interactions with Ct (+Stb6) or Courtot, although chlorophyll fluorescence and gas exchange parameters reduced over time.

Unaffected NPQ in Zt22-inoculated Ct (+Stb6), even when compared to IPO323 inoculation, did not correspond to the upregulated Zea and DEP and the downregulated PsbS expression, suggesting that Zt22 could be antagonising the XC. Taken that ZEP expression was significantly higher in *Stb6* at 24 hai, it is plausible to suggest that if Zt22 targeted ZEP this would result in blocking significant conversion to Vio and Neo. The regulation and function of the XC are affected by the affinity of Vio to bind to the antenna proteins of both photosystems and further by the conversion rate of violaxanthin (Vio) to zeaxanthin (Zea) (Jahns et al., 2009; Kress & Jahns, 2017). For example, in dark-adapted leaves conversion is rapid (10-20 min) when Vio is bound to peripheral V1 site in LHCII, Lhca3 or Lhcb5 (Jahns et al., 2009). A pre-requisite for Vio de-epoxidation and consequent conversion to Zea is the release of Vio from the binding site of the antenna proteins. Whilst the exact driving force in release of Vio remains unclear, lowering of the lumen pH or the absence of antenna proteins have been implicated in the rapid conversion of Vio and increase in Zea pool (Jahns et al., 2009). One of the observations in our studies was that in the compatible interaction between Ct (+Stb6) and Zt22, zeaxanthin increased significantly by 24hai in contrast to the incompatible interaction with IPO323. This was associated with downregulated antenna proteins in both photosystems (Lhcb1-4 and Lhca1-3).

Most studies on *Z. tritici* infections and ROS accumulation have focused on later time points when the pathogen switches to necrotrophy (for example Keon et al., 2007), or have focused only on H_2O_2, for example (Shetty et al., 2003, 2007). ROS production and signalling in plants has many layers, as it can be produced in the apoplast by NADPH oxidases upon perception of pathogen-associated molecular patterns (PAMPs) and initiate defence-related cascades, but it can also be produced in the chloroplast as a by-product of photosynthesis and can interfere with PSII repair and release manganese from the OEC (Murata et al., 2012; Sierla et al., 2013; Tyystjärvi, 2013; Trotta et al., 2014). Additionally, ROS can be manipulated directly by the pathogen and interfere with PSII proteins. For instance, the *Pseudomonas* effector molecule HopN1 directly targets the OEC protein PsbQ and annuls ROS production to inhibit callose deposition and cell death (Rodríguez-Herva et al., 2012).

Another study found a rapid increase in abundance of PsbO and PsbP upon infection by an avirulent *P. syringae* strain, highlighting the importance of an intact OEC that modulates ROS metabolism and cell death during ETI (Jones et al., 2006). Furthermore, ROS can be modulated and detoxified by redox-active compounds, such as carotenoids, xanthophylls, tocopherols and other antioxidant enzymes like ascorbate, catalase and peroxidases (Mittler et al., 2004; Sierla et al., 2013). Here, we observed a slight increase in superoxide at 6hai in Ct (+Stb6) infected with the virulent Zt22. This agrees with our KEGG enrichment and protein-protein interaction (PPI) analysis demonstrating several PTI components being upregulated at this time point in the interaction between Ct (+Stb6) and Zt22. Chitin-related proteins (CERK1 and CEBiP), *Arabidopsis* Somatic Embryogenesis Receptor-Like Kinases SERKs and the coreceptors brassinosteroid-related BAK1 and BIR2, and calcium-dependent protein kinases (CDPKs) all were upregulated in Ct (+Stb6) in response to Zt22. In contrast, there was no H_2O_2 at 6hai and there was a slight increase in superoxide in Ct (+Stb6) inoculated with IPO323, however this did not induce the same PTI response, as seen by the absence of the proteins mentioned above in the KEGG and PPI maps. Instead, this was accompanied by the transient photoinhibitory qI, zeaxanthin and VDE reductions, downregulation of VTE1 (tocopherol), H_2O_2 catabolism and ascorbate peroxidase (APX), and upregulation of catalases (CAT). This could suggest two different responses of *Stb6* against the two isolates, whereby in the compatible interaction we observed apoplastic PTI responses associated with basal plant defences, whereas in the incompatible resistant reaction the recognition and ETI initiation takes place much faster and the plant regulates chloroplastic processes to fine-tune and balance signalling, detoxification and defence. Further RT-PCR analysis also showed that the *Stb6* had increased capacity to detoxify superoxide via FeSOD, which was significantly upregulated at all time points compared to Courtot. Other enzymes can also target superoxide but these may act in different organelles compared to FeSOD which functions specifically in the chloroplast. In this study, we did not measure the activities of other enzyme detoxification systems and it is possible that Cu/ZnSOD and MnSOD may also be active in Courtot or both genotypes as we failed to

observe significant ROS staining in infected leaves at the early stages of disease development.

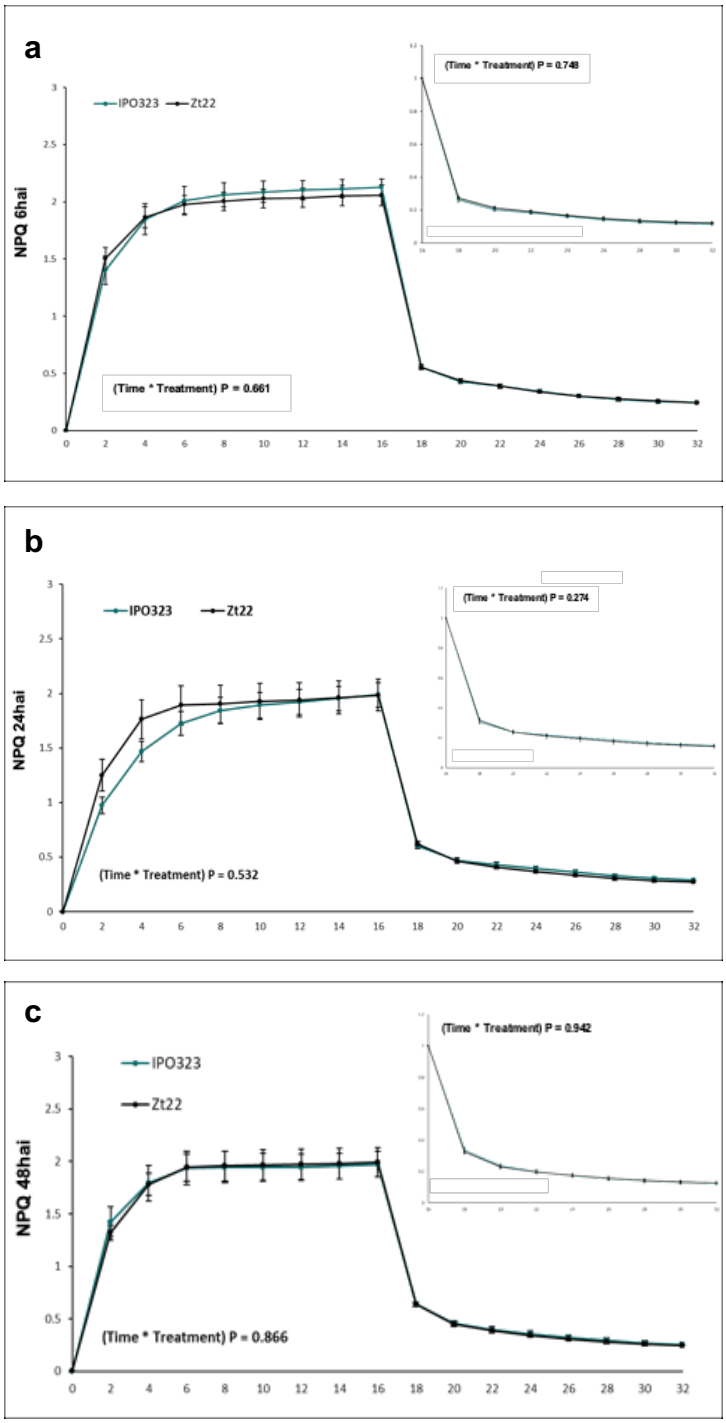
Despite of the different recognition and activation mechanisms between PTI and ETI, they both involve a similar set of downstream defence responses, including mitogen-activated protein kinases (MAPKs) upon chitin-triggered recognition, however the responses during ETI have a longer duration and higher magnitude (Sánchez-Vallet et al., 2015; Su et al., 2018). MPK3 and MPK6 have been shown to be critically involved in the recognition of *Z. tritici* in compatible interactions and initiation of PCD and symptom development (Rudd et al., 2008), but have also been shown to be targeted by bacterial effectors to suppress PAMP-triggered defences (Wang et al., 2010; le Roux et al., 2015). It has also been shown that the tobacco orthologs of MPK3/6 (SIPK and WIPK) were SA-induced and inhibited photosynthesis (Liu et al., 2007). A recent study also showed that MPK3/6 contributed to photosynthetic inhibition by downregulation of φPSII and PSII proteins while increasing ROS in chloroplasts as an effector-triggered resistance response (Su et al., 2018). In our results, we observed upregulation of MPK3/6 in Ct (+Stb6) in response to Zt22 at 6hai but also in response to IPO323 at 24hai. It is therefore possible that in the former, MPK3/6 activation was coupled with CERK1 and CEBiP for chitin-induced PTI signalling, however in the latter, MPK3/6 activation was associated with the photoinhibitory qI type of NPQ and overall reduction in photosynthetic processes. Another protein, Pto interaction 1 (Pti1), was only upregulated in response of *Stb6* to Zt22 inoculation. This protein has been reported to be involved with the phytohormones ABA, SA and MeJA, induced by H_2O_2, directly interacting with MPK3/6 and localise to the plasma membrane or epidermal cells (Sun et al., 2022). In tomato, Pti1 interacted directly with the *P. syringae* pv. t*omato* (Pst) avirulence protein AvrPto, which led to phosphorylation cascades and ultimately PCD for ETI. However in rice, Pti1 is a negative regulator of PTI and ETI, as *pti1* mutants infected with *Magnaporthe grisea* showed enhanced resistance to rice blast disease while *Pti1* overexpressing plants increased the sensitivity to compatible pathogens (Takahashi et al., 2007). As rice is similar to wheat and the KEGG enrichment analysis was mapped in rice, we suggest that Pti1 could be another potential

target for Zt22 virulence. Further investigation is needed to elucidate this hypothesis. Finally, the KEGG pathway for protein processing and export was significantly enriched in response of *Stb6* to Zt22 and involved genes on the Sec-dependent pathway (Sec61 translocon complex). Folded proteins in the endoplasmic reticulum (ER) can be relocated and imported into chloroplasts facilitated by the cytosolic chaperones HSP70 and HSP90, the latter found also upregulated in this study in the same interaction (Sun et al., 2021). Subsequently, chloroplast precursor proteins are transported into the stroma through translocon complexes in the outer (TOC) and inner chloroplast (TIC) envelope membranes (Thomson et al., 2020). During the cascade of further protein proteolysis and re-folding for the proteins to reach their final intra-organelle target (e.g. the thylakoids), some proteins can get damaged and are removed by proteases. Among the major proteases are the filamentation temperature-sensitive H (FtsH) and degradation of periplasmic (DEG) proteases (Sun et al., 2021). One FtsH, FtsH2 (VAR2) functions primarily on the degradation of photodamaged PSII reaction centre proteins such as D1 and D2, during the repair cycle (Theis & Schroda, 2016; Dogra et al., 2019). Moreover, *ftsh2* mutant in *Arabidopsis*, in which damaged PSII proteins accumulate, SA-responsive genes are upregulated (Duan et al., 2019). In our results, D2 protein was highly upregulated at 24hai in Ct (+Stb6) in response to Zt22 (data not shown), FtsH proteases appeared in the top downregulated PPI for *Stb6* and Zt22 and there was a consistent upregulation of ICS, the chloroplastic precursor of SA, in our gene expression studies. We propose that a virulence strategy of *Zymoseptoria tritici* may incorporate directly targeting the photoprotective mechanisms of the chloroplast to destabilise PSII function and repair leading to excessive ROS and irreversible damage to photosystems, as there was also a *Z. tritici* transcript appearing to localise into the chloroplast. On the other hand, the photoinhibited, resistant *Stb6* at 24hai reduced AOS and increased ICS. SA is typically antagonistic to JA and there is evidence to suggest that SA is essential for regulating redox homeostasis (Mateo et al., 2006) and is induced upon PSII re-organisation conditions (Duan et al., 2019). However, it is not yet clear why these observations were only apparent in the *Stb6* genotype and not in Courtot, which showed a

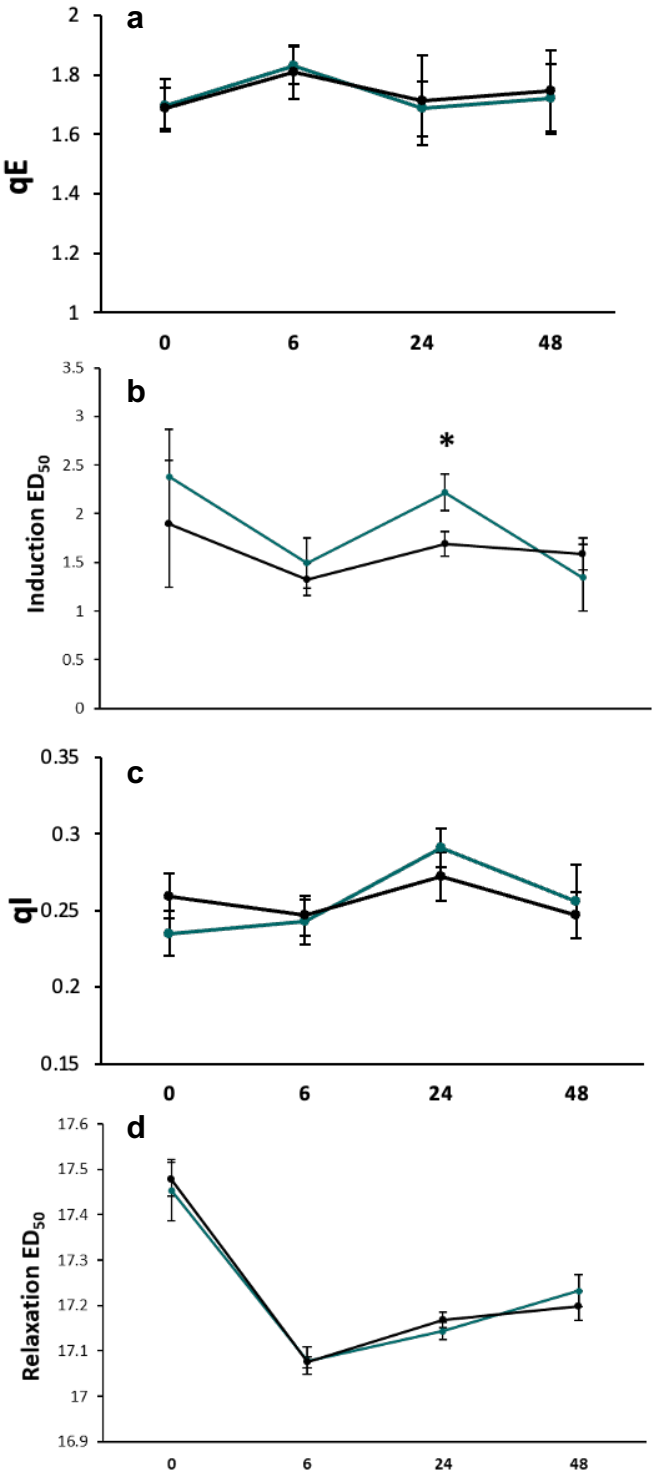
downregulation in both AOS and ICS over time, but an increase in PR1. *Stb6* is a WAK and early and recent studies have shown chloroplast migration (Kema et al., 1996; Savage et al., 2021). Also, Zt22 is an isoform of *AvrStb6* (Stephens et al., 2021), therefore *Stb6* may be required for virulence on all isolates possessing *AvrStb6* isoforms, whereas that might not be the virulence strategy exploited by *Z. tritici* in other genotypes. Finally, a closer search into our sequencing data, showed upregulation of *Snn1* in Ct (+Stb6) inoculated with Zt22, which is a wheat sensitivity WAK that binds and recognises the *Parastagonospora nodorum* necrotrophic effector Tox1 and results in susceptibility and cell death. This indicated another potential virulence strategy exploited by *Z. tritici*, which is discussed in the following chapter.

Overall, we propose that *Stb6* resistance functions through the chloroplast, via photoprotective responses, including re-organising the photosynthetic machinery components and balancing energy transfer to promote and mount defence whilst minimising oxidative stress. On the other hand, the virulent *Z. tritici* isolate could be deliberately hijacking chloroplastic processes to alter PSII dissipation and repair processes and ultimately initiate disease.

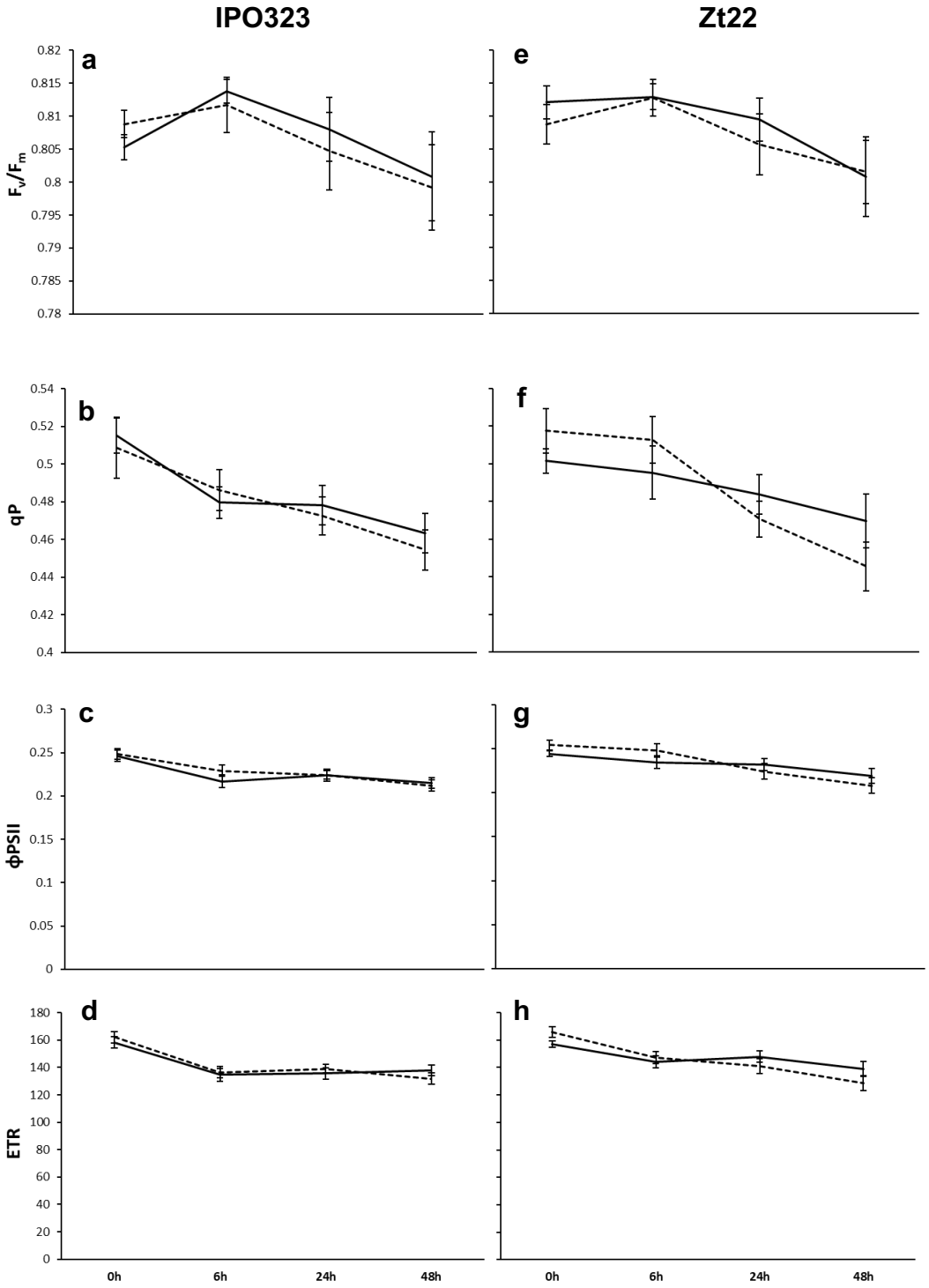
3.5 Supplementary data



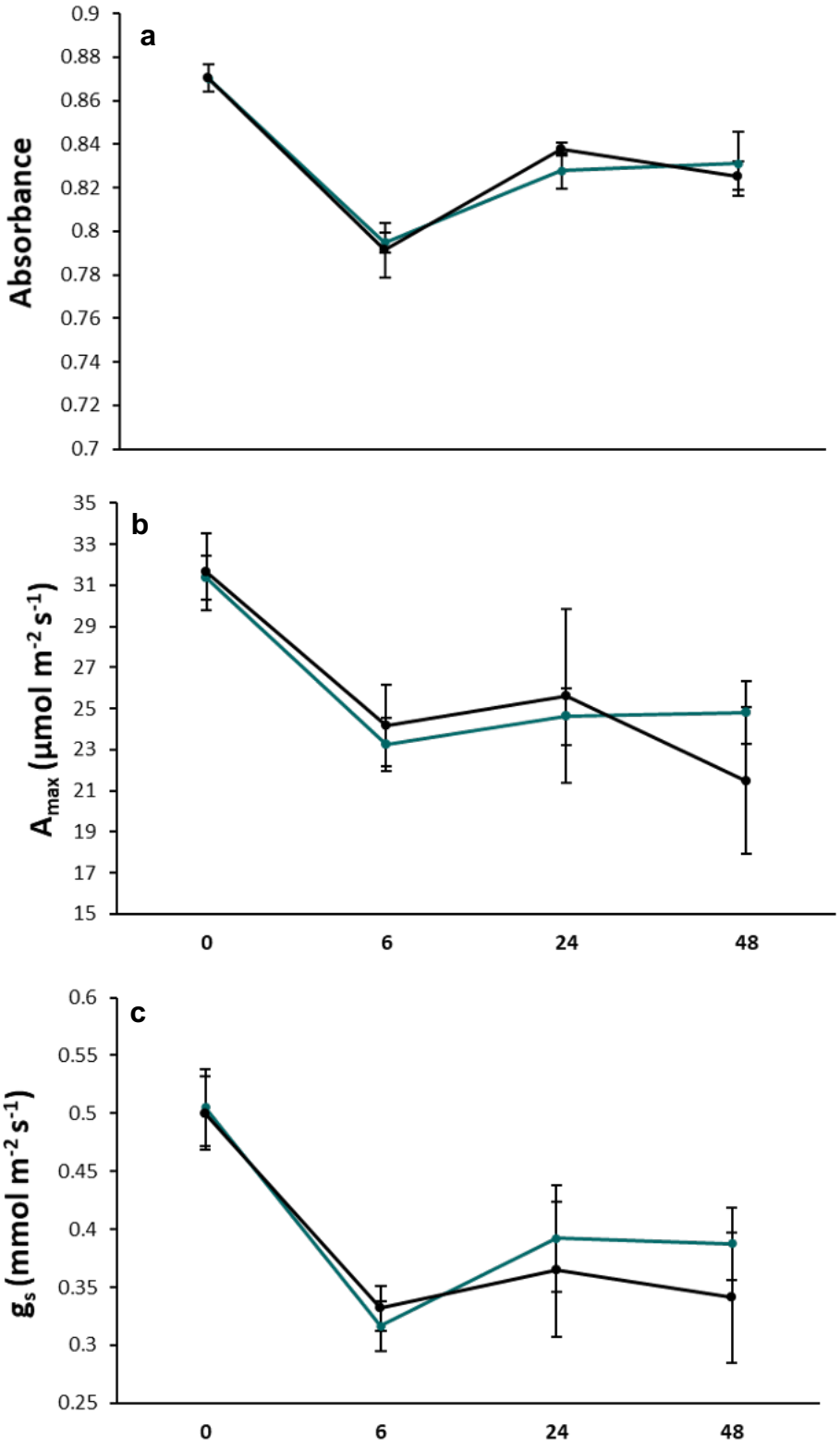
SF 3-1. NPQ Induction and Relaxation kinetics along with Normalised NPQ in the dark for Ct (+Stb6) between IPO323 and Zt22 at **(a)** 6hai, **(b)** 24hai and **(c)** 48hai. Teal and black lines represent IPO323 and Zt22, respectively. Data represent means ± SEM (n=8).



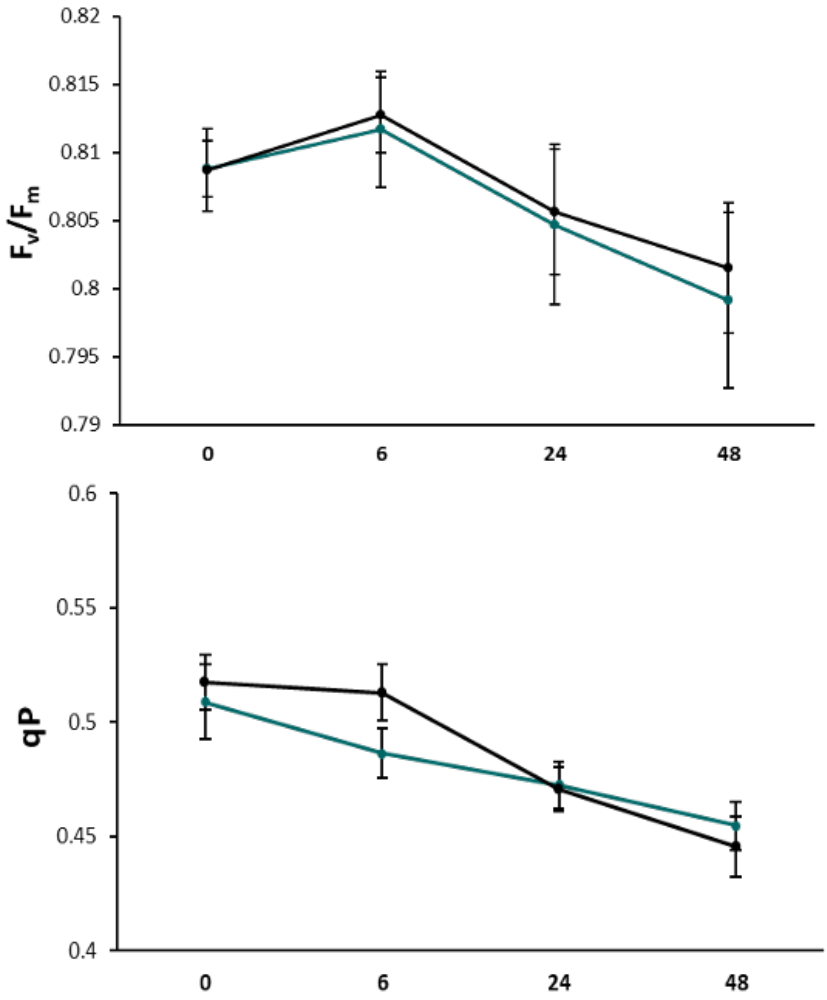
SF 3-2. NPQ-derived parameters for Ct (+Stb6) between the two isolates and across the measurement timings. **(a)** qE, **(b)** Induction ED_{50}, **(c)** qI and **(d)** Relaxation ED_{50}. Teal and black lines indicate IPO323 and Zt22, respectively. Data represent means ± SEM (n=8). Stars (*) denote significant differences ($P < 0.05$) of the genotypes at the equivalent time point.



SF 3-3. CF parameters for both isolates across the time measurements. **(a-d)** Maximum PSII efficiency (F_v/F_m), photochemical quenching (qP), operating PSII efficiency (φPSII) and electron transport rate (ETR) for IPO323-inoculated plants, **(e-h)** Maximum PSII efficiency (F_v/F_m), photochemical quenching (qP), operating PSII efficiency (φPSII) and electron transport rate (ETR) for Zt22-inoculated plants. Solid black line indicates Courtot and dashed black line indicates Ct (+Stb6). Data represent means ± SEM (n=8).



SF 3-4. (a) Chlorophyll absorbance, **(b)** CO_2 assimilation (A_{max}) and **(c)** stomatal conductance (g_s) for Ct (+Stb6) inoculated with IPO323 or Zt22, across the time measurements. Teal and black lines represent IPO323 and Zt22, respectively. Data represent means ± SEM (n=8).



SF 3-5. Maximum PSII efficiency (F_v/F_m) (top graph) and photochemical quenching (qP) (bottom graph) for Ct (+Stb6) inoculated with IPO323 or Zt22 across the time measurements. Teal and black lines represent IPO323 and Zt22, respectively. Data represent means ± SEM (n=8).

Supplementary Table 3-1. Table indicating the depth of coverage of the RNA sequencing experiment as well as the overall quality control, per sample (genotype, treatment, time and biological replicate).

Sample name	Raw reads	Clean reads	Raw bases	Clean bases	Error rate(%)	Q20(%)	Q30(%)	GC content(%)
Courtot 0h_1	38011985	37633849	11.4	11.3	0.02	98.07	94.59	56.06
Courtot 0h_2	37126484	36851403	11.1	11.1	0.02	97.94	94.26	56.18
Courtot 0h_3	33932495	33642542	10.2	10.1	0.02	98.07	94.56	55.68
Ct (+Stb6) 0h_1	36547633	36223877	11	10.9	0.03	97.89	94.17	56.47
Ct (+Stb6) 0h_2	39686342	39287244	11.9	11.8	0.02	98.14	94.73	55.32
Ct (+Stb6) 0h_3	30456547	30070665	9.1	9	0.02	97.95	94.33	56.54
Courtot 6h IPO323_1	34662685	34177469	10.4	10.3	0.02	98.05	94.49	55.37
Courtot 6h IPO323_2	36805414	36332232	11	10.9	0.03	97.81	94	55.48
Courtot 6h IPO323_3	28972278	28626190	8.7	8.6	0.02	97.97	94.38	56.55
Ct (+Stb6) 6h IPO323_1	35488456	35175323	10.6	10.6	0.02	98.04	94.53	55.81
Ct (+Stb6) 6h IPO323_2	36062586	35621316	10.8	10.7	0.02	97.97	94.36	56.44
Ct (+Stb6) 6h IPO323_3	41797124	41281139	12.5	12.4	0.02	97.95	94.32	56.09
Courtot 6h Zt22_1	33728402	33337668	10.1	10	0.02	97.98	94.36	55.92
Courtot 6h Zt22_2	37171835	36837348	11.2	11.1	0.02	98.01	94.43	56.22
Courtot 6h Zt22_3	37249375	36859799	11.2	11.1	0.02	98.06	94.56	56.28
Ct (+Stb6) 6h Zt22_1	43873354	43335510	13.2	13	0.02	98.12	94.66	55.68
Ct (+Stb6) 6h Zt22_2	31027955	30630086	9.3	9.2	0.02	98.1	94.66	56.27
Ct (+Stb6) 6h Zt22_3	41350622	40971044	12.4	12.3	0.02	98.07	94.52	55.54
Courtot 24h IPO323_1	33834381	33543214	10.2	10.1	0.03	97.9	94.26	56.51
Courtot 24h IPO323_2	27122544	26944318	8.1	8.1	0.03	97.63	93.68	56.21
Courtot 24h IPO323_3	33801509	33275617	10.1	10	0.02	98.09	94.57	56.13
Ct (+Stb6) 24h IPO323_1	38044407	37598360	11.4	11.3	0.03	97.83	93.97	56.46
Ct (+Stb6) 24h IPO323_2	34864404	34426353	10.5	10.3	0.02	98.1	94.59	56.56
Ct (+Stb6) 24h IPO323_3	32495507	32067764	9.7	9.6	0.03	97.93	94.23	56.35
Courtot 24h Zt22_1	37619545	37104374	11.3	11.1	0.02	98.1	94.65	56.74
Courtot 24h Zt22_2	31757043	31439812	9.5	9.4	0.02	98.28	95	56.46
Courtot 24h Zt22_3	35064356	34661359	10.5	10.4	0.02	98.11	94.63	56.28
Ct (+Stb6) 24h Zt22_1	37458955	37145187	11.2	11.1	0.02	98.14	94.73	56.22
Ct (+Stb6) 24h Zt22_2	32209828	31751585	9.7	9.5	0.02	98.05	94.51	56.41
Ct (+Stb6) 24h Zt22_3	36922537	36445726	11.1	10.9	0.02	98.16	94.76	56.22

Supplementary Table 3-2. A list of the top 10 up- and downregulated DEGs for each comparison. CP denotes the comparison number, as listed in Table 3-4. T_R denotes the direction of gene regulation (red arrow for upregulation, green arrow for downregulation). Transcript and Description refer to Transcript ID and molecular function or biological process, respectively. Average FPKM (Fragments Per Kilobase of transcript sequence per Millions base pairs sequenced) values denote the normalised read counts (considering sequencing depth and gene length) of all three biological replicates per comparison, reflecting gene expression levels. Log2 FC indicates the fold change of that transcript in the pairwise comparison. *P* value indicates the adjusted significant *P* value of that transcript. Table spans across four pages (1/4).

CP	T_R	Transcript	Description	Average FPKM Ct (+Stb6)	Average FPKM Courtot	Log2 FC	*P* value
1	↑	TraesCS3A02G039800	-	6.76	0	10.5	< 0.001
		TraesCS3A02G039900	-	1.11	0	8.9	< 0.001
		TraesCS3A02G038500	-	1.37	0	8.7	< 0.001
		TraesCS3A02G038600	-	0.54	0	7.7	< 0.001
		TraesCS3A02G038900	-	0.64	0	7.4	< 0.001
		TraesCS3A02G344700	Non-specific lipid transfer protein	1.30	0	7.4	< 0.001
		TraesCS2B02G550300	-	0.26	0	6.4	< 0.001
		TraesCS3A02G091900	-	0.89	0.02	5.8	< 0.001
		TraesCS3A02G040500	-	1.78	0.04	5.5	< 0.001
		TraesCS5A02G535400	-	1.16	0.04	5.1	0.026
	↓	TraesCS4B02G365300	-	0	4.82	-10.34	< 0.001
		TraesCS3A02G037900	-	0	1.70	-8.09	< 0.001
		TraesCS1A02G379200	-	0	2.09	-7.73	< 0.001
		TraesCS1A02G368100	-	0.19	36.68	-7.65	< 0.001
		TraesCS1A02G379100	-	0	0.56	-7.6	< 0.001
		TraesCS7A02G122500	-	0	0.48	-7.17	< 0.001
		TraesCS1A02G380400	-	0	1.05	-6.12	< 0.001
		TraesCS1A02G380300	-	0.05	2.98	-5.79	< 0.001
		TraesCS4B02G364900	-	2.15	42.41	-4.29	< 0.001
		TraesCS3A02G040800	-	0.92	12.44	-3.76	< 0.001

Supplementary Table 3-2. A list of the top 10 up- and downregulated DEGs for each comparison. CP denotes the comparison number, as listed in Table 3-4. T_R denotes the direction of gene regulation (red arrow for upregulation, green arrow for downregulation). Transcript and Description refer to Transcript ID and molecular function or biological process, respectively. Average FPKM (Fragments Per Kilobase of transcript sequence per Millions base pairs sequenced) values denote the normalised read counts (considering sequencing depth and gene length) of all three biological replicates per comparison, reflecting gene expression levels. Log2 FC indicates the fold change of that transcript in the pairwise comparison. *P* value indicates the adjusted significant *P* value of that transcript. Table spans across four pages (2/4).

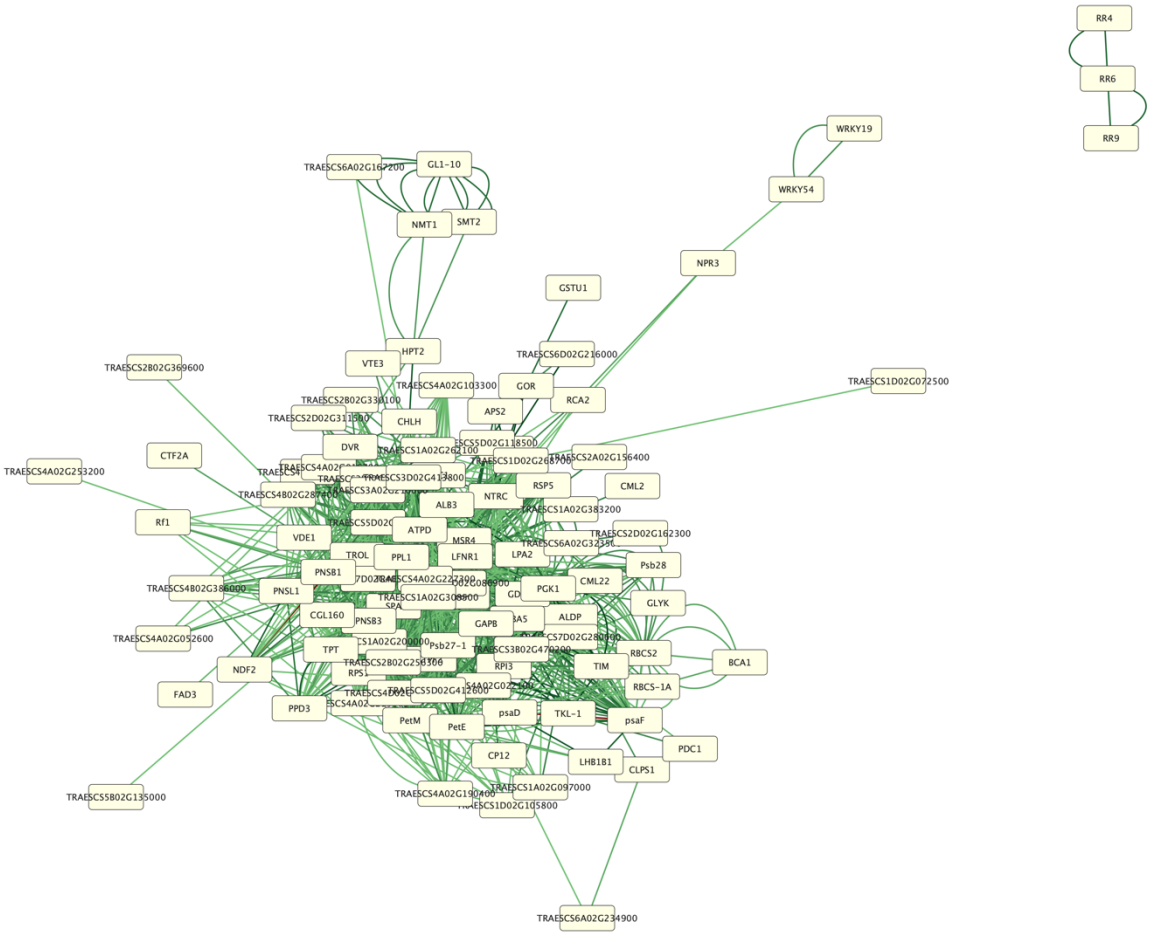
CP	T_R	Transcript	Description	Average FPKM Ct (+Stb6)	Average FPKM Courtot	Log2 FC	*P* value
2	↑	TraesCS7A02G219700	-	0.57	0.01	5.63	< 0.001
		TraesCS3A02G344700	Non-specific lipid transfer protein	1.12	0.04	5.03	0.01
		TraesCS7B02G467100	-	3.24	0.11	4.77	< 0.001
		TraesCS1A02G383900	-	0.42	0.02	4.62	< 0.001
		TraesCS1B02G398600	Dirigent protein	1.37	0.06	4.52	< 0.001
		TraesCS3A02G038900	-	0.53	0.03	4.41	< 0.001
		TraesCS3A02G110100	-	9.47	0.43	4.37	< 0.001
		TraesCS3A02G038600	-	0.56	0.03	4.32	< 0.001
		TraesCS7D02G530700	-	5.35	0.35	3.86	< 0.001
		TraesCS2B02G347200	-	5.60	0.40	3.74	< 0.001
	↓	TraesCS4B02G365300	-	0	6.97	-11.08	< 0.001
		TraesCS3A02G037900	-	0	2.45	-8.82	< 0.001
		TraesCS1A02G368100	-	0.10	35.79	-8.56	< 0.001
		TraesCS1A02G379200	-	0	2.07	-7.92	< 0.001
		TraesCS1A02G379100	-	0	0.55	-7.79	< 0.001
		TraesCS1A02G380300	-	0.01	1.64	-7.31	< 0.001
		TraesCS1A02G383600	-	0.02	1.36	-5.90	< 0.001
		TraesCS4B02G364900	-	2.56	55.97	-4.54	< 0.001
		TraesCS4B02G358500	-	0.22	1.52	-2.90	< 0.001
		TraesCS4D02G229600	-	1.26	7.79	-2.73	< 0.001

Supplementary Table 3-2. A list of the top 10 up- and downregulated DEGs for each comparison. CP denotes the comparison number, as listed in Table 3-4. T_R denotes the direction of gene regulation (red arrow for upregulation, green arrow for downregulation). Transcript and Description refer to Transcript ID and molecular function or biological process, respectively. Average FPKM (Fragments Per Kilobase of transcript sequence per Millions base pairs sequenced) values denote the normalised read counts (considering sequencing depth and gene length) of all three biological replicates per comparison, reflecting gene expression levels. Log2 FC indicates the fold change of that transcript in the pairwise comparison. *P* value indicates the adjusted significant *P* value of that transcript. Table spans across four pages (3/4).

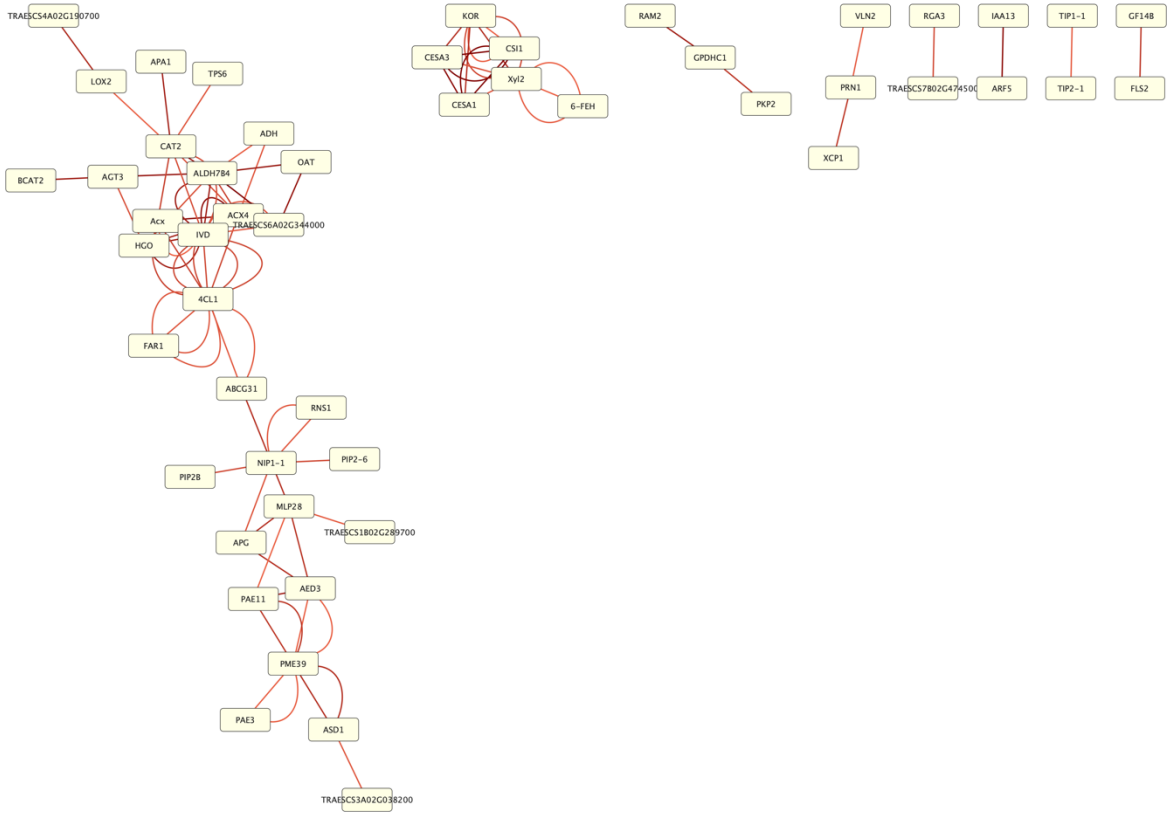
CP	T_R	Transcript	Description	Average FPKM Ct (+Stb6)	Average FPKM Courtot	Log2 FC	*P* value
3	↑	TraesCS3A02G039800	-	13.72	0	11.18	< 0.001
		TraesCS3A02G039900	-	1.55	0	9.04	< 0.001
		TraesCS3A02G038500	-	1.41	0	8.35	< 0.001
		TraesCS3A02G038600	-	0.58	0	7.49	< 0.001
		TraesCS3A02G040500	-	1.63	0.08	4.30	< 0.001
		TraesCS1B02G184100	-	2.18	0.11	4.29	< 0.001
		TraesCS3D02G500100	-	5.95	0.38	3.85	< 0.001
		TraesCS2B02G121600	-	3.43	0.29	3.51	0.02
		TraesCS2D02G104300	-	2.46	0.24	3.29	0.03
		TraesCS6B02G246800	Similar to chitinase	2.06	0.21	3.19	< 0.001
	↓	TraesCS4B02G365300	-	0	4.36	-10.27	< 0.001
		TraesCS3A02G037900	-	0	2.39	-8.65	< 0.001
		TraesCS1A02G368100	-	0.11	28.05	-8.08	< 0.001
		TraesCS1A02G379200	-	0.02	2.57	-7.15	< 0.001
		TraesCS4B02G383000	Xyloglucan endotransglucosylase/ hydrolase	0.03	1.36	-5.64	< 0.001
		TraesCS1A02G380300	-	0.05	1.53	-4.93	< 0.001
		TraesCS4B02G358500	-	0.06	1.61	-4.81	< 0.001
		TraesCSU02G196200	-	0.06	1.29	-4.35	< 0.001
		TraesCS4B02G364900	-	2.46	29.06	-3.64	< 0.001
		TraesCS3A02G040800	-	0.46	5.27	-3.62	< 0.001

Supplementary Table 3-2. A list of the top 10 up- and downregulated DEGs for each comparison. CP denotes the comparison number, as listed in Table 3-4. T_R denotes the direction of gene regulation (red arrow for upregulation, green arrow for downregulation). Transcript and Description refer to Transcript ID and molecular function or biological process, respectively. Average FPKM (Fragments Per Kilobase of transcript sequence per Millions base pairs sequenced) values denote the normalised read counts (considering sequencing depth and gene length) of all three biological replicates per comparison, reflecting gene expression levels. Log2 FC indicates the fold change of that transcript in the pairwise comparison. *P* value indicates the adjusted significant *P* value of that transcript. Table spans across four pages (4/4).

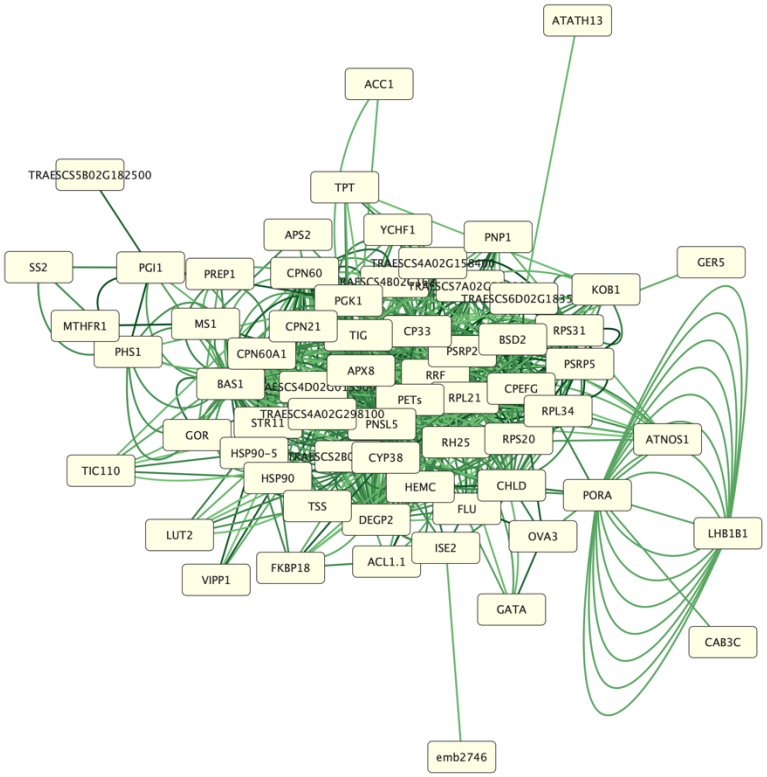
CP	T_R	Transcript	Description	Average FPKM Zt22	Average FPKM IPO323	Log2 FC	*P* value
4	↑	TraesCS1B02G074000	-	4.09	0	7.98	< 0.001
		TraesCS2A02G399500	CBFIa-A11	1.33	0	7.50	< 0.001
		TraesCS7B02G414900	-	0.53	0	7.40	< 0.001
		TraesCS2D02G203400	-	1.29	0	6.80	< 0.001
		TraesCS3B02G465200	-	0.49	0	6.65	< 0.001
		TraesCS2A02G490500	-	0.39	0	6.63	< 0.001
		TraesCS5B02G443000	-	1.39	0	6.62	< 0.001
		TraesCS6D02G074200	-	0.42	0	6.48	< 0.001
		TraesCS3B02G122800	-	0.34	0	6.41	< 0.001
		TraesCS6A02G256900	AP2 domain CBF protein	0.48	0	6.38	< 0.001
	↓	TraesCS6B02G427200	-	0	0.77	-7.74	0.001
		TraesCS2D02G132500	-	0	0.40	-6.87	< 0.001
		TraesCS4B02G207100	-	0	0.41	-6.56	< 0.001
		TraesCS1D02G266300	-	0	0.25	-6.16	< 0.001
		TraesCS4A02G382200	-	0	0.33	-6.10	< 0.001
		TraesCS6B02G277100	-	0.03	2.08	-6.07	< 0.001
		TraesCS3B02G157800	-	0	0.25	-6.00	0.001
		TraesCS3A02G092700	-	0	0.18	-6.00	0.001
		TraesCS4B02G383700	-	0	0.23	-5.89	0.001
		TraesCS3A02G318600	-	0.05	3.10	-5.84	< 0.001



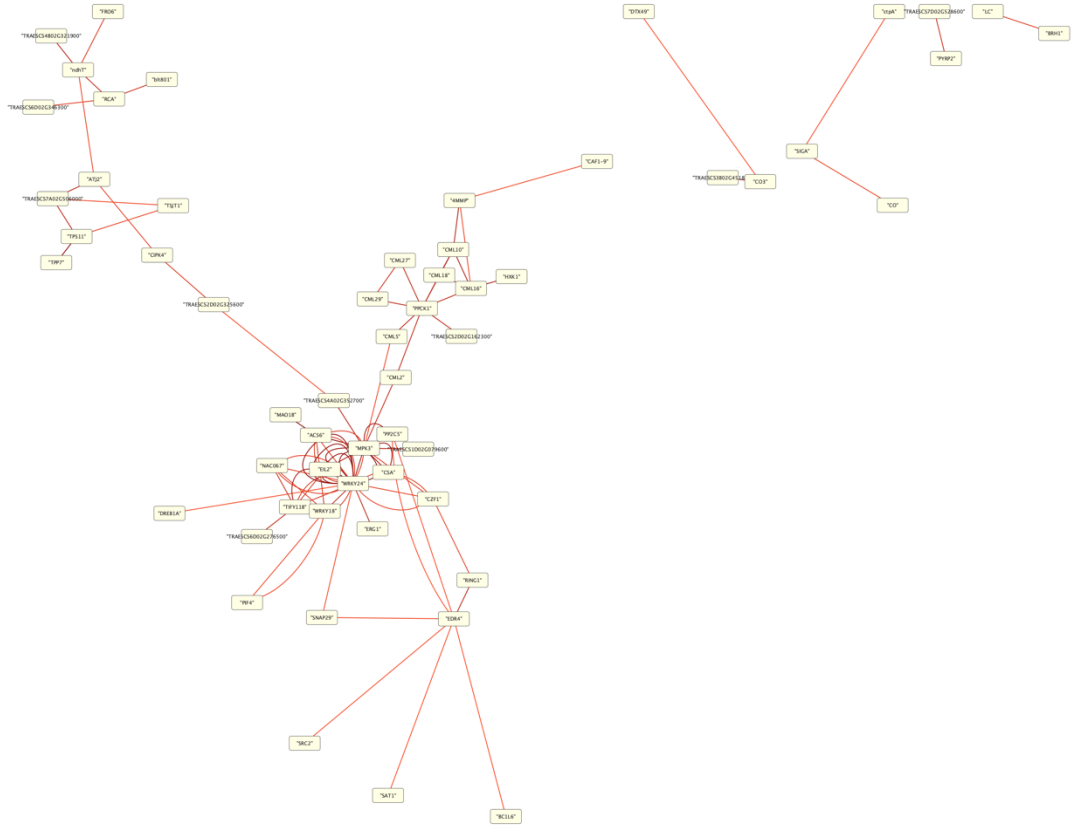
SF 3-6. Network of the top downregulated interacting proteins in the comparison between ± *Stb6* with IPO323 at 6hai. Green-coloured lines represent downregulation and their intensity denote the probability (=score) of the interaction to be true and accurate, according to String database.



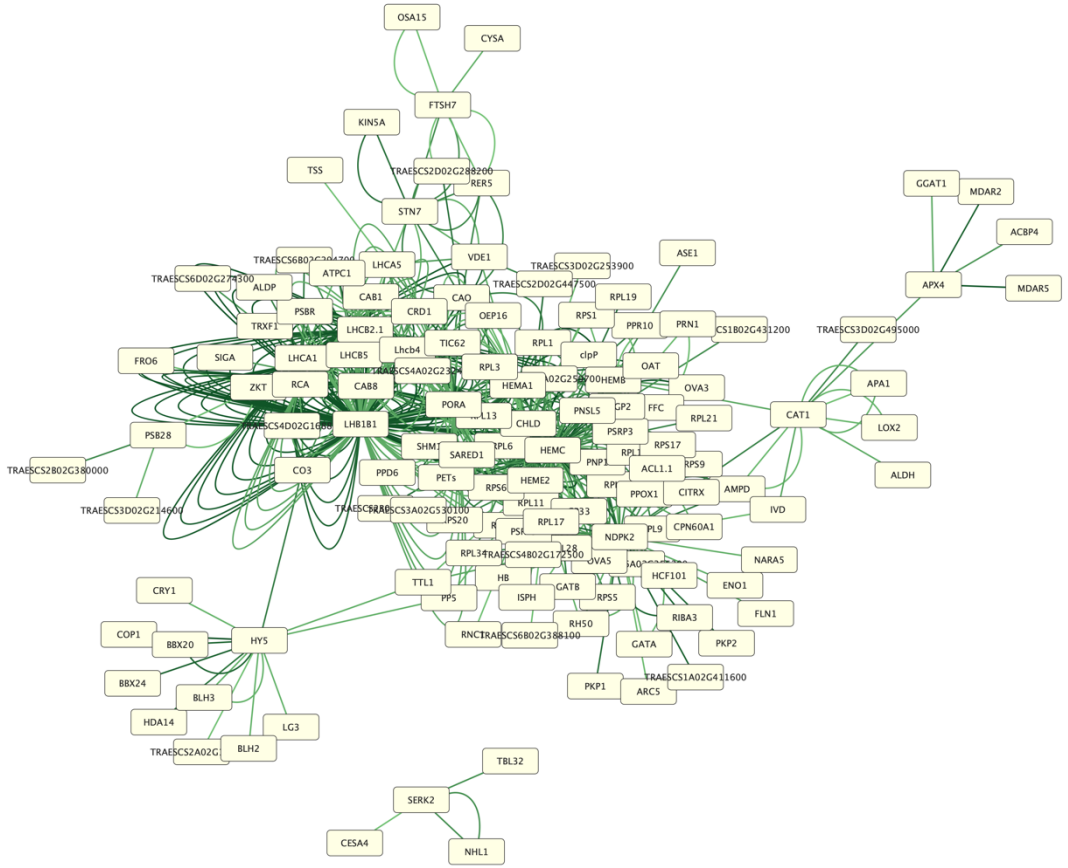
SF 3-7. Network of the top upregulated interacting proteins in the comparison between ± *Stb6* with IPO323 at 6hai. Red-coloured lines represent upregulation and their intensity denote the probability (=score) of the interaction to be true and accurate, according to String database.



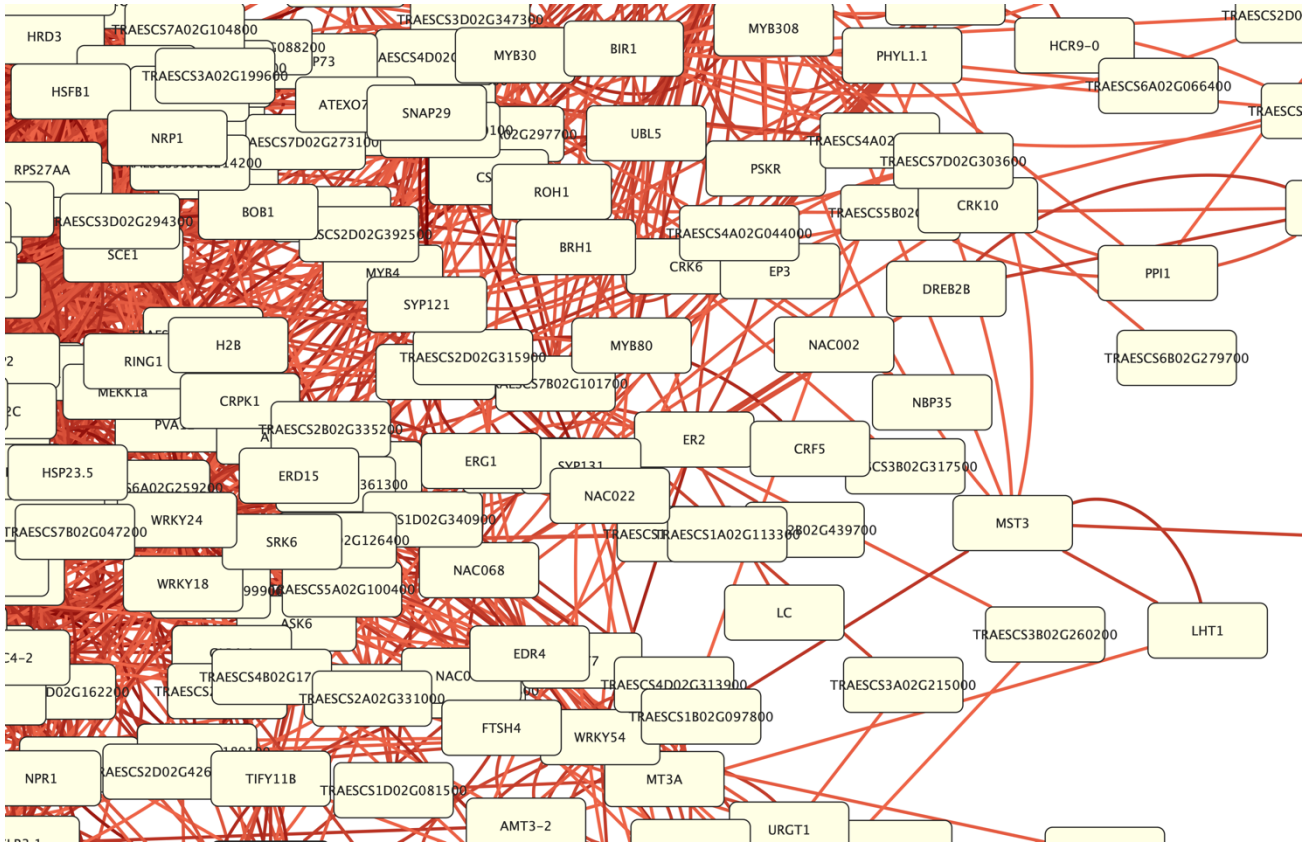
SF 3-8. Network of the top downregulated interacting proteins in the comparison between ±Stb6 with IPO323 at 24hai. Green-coloured lines represent downregulation and their intensity denote the probability (=score) of the interaction to be true and accurate, according to String database.



SF 3-9. Network of the top upregulated interacting proteins in the comparison between ± *Stb6* with IPO323 at 24hai. Red-coloured lines represent upregulation and their intensity denote the probability (=score) of the interaction to be true and accurate, according to String database.



SF 3-10. Network of the top downregulated interacting proteins in the comparison of *Stb6* inoculated with IPO323 or Zt22 at 6hai. Green-coloured lines represent downregulation and their intensity denote the probability (=score) of the interaction to be true and accurate, according to String database.



SF 3-11. Due to the complexity and high number of PPIs, a snapshot of the top upregulated interacting proteins in the comparison of *Stb6* inoculated with IPO323 or Zt22 at 6hai is shown. Red-coloured lines represent upregulation and their intensity denote the probability (=score) of the interaction to be true and accurate, according to String database.

Chapter 4 Effect of virulence of *Zymoseptoria tritici* on wheat sensitivity to necrotrophic effectors by *Parastagonospora nodorum*

Acknowledgment of contributions

We would like to thank Dr Huyen Phan and Dr Kar-Chun Tan from Curtin University (Perth, Australia) for providing the purified necrotrophic effectors ToxA and Tox1.

4.1 Introduction

Wheat (*Triticum aestivum*) is one of the world's most important staple grains and it has specialised foliar pathogens that cause severe yield losses annually worldwide (Figueroa, Hammond-Kosack & Solomon, 2018). These so called blotch diseases, include the Ascomycete fungi *Zymoseptoria tritici*, *Parastagonospora nodorum* and *Pyrenophora tritici-repentis* that are the causal agents of Septoria tritici blotch (STB), Septoria nodorum blotch (SNB) and Tan spot (TS), respectively (Figueroa, Hammond-Kosack & Solomon, 2018). STB is the primary leaf disease of wheat in temperate growing regions, such as Europe, whereas TS is found in most parts of the wheat-growing world and in contrast, SNB is prominent throughout Australia. *Z. tritici* infection is characterised by the long latent period (up to 14 days) before any symptom development, whereby the pathogen enters the plant through the stomata and colonises the apoplast without any significant increase in its biomass (Kema et al., 1996; Sánchez-Vallet et al., 2015). Then, the pathogen switches to its necrotrophic phase when necrotic lesions start spreading on the leaves while the characteristic asexual fruiting body of the fungus, the black pycnidia, appear on the necrotic areas. In contrast with *Z. tritici*, symptom development as a result of *P. nodorum* infection on susceptible cultivars develops rapidly with similar necrotic lesions on the leaves. However, pale brown, rather than black, pycnidia distinguish SNB from STB, which are also less visible (Downie et al., 2021). Finally, symptoms of TS are very similar to *Z. tritici* and *P. nodorum*, however *P. tritici-repentis* only forms dark, sexual fruiting structures,

called pseudothecia, that only develop and mature on wheat straw and not on the leaves (Wegulo, 2011).

Secreted effector molecules, avirulence genes (*Avr*) and host-selective toxins (HSTs) form part of the critical strategies of all three of the above necrotrophic pathogens, in order to suppress plant immunity, manipulate plant physiology and avoid recognition by the host surveillance mechanism (Faris & Friesen, 2020; Shao et al., 2021). Products of major plant disease resistance (*R*) genes recognise the products of specific *Avr* genes resulting in an incompatible interaction, in a gene-for-gene manner. However, in the case of *P. nodorum* and *P. tritici-repentis*, recognition of specific necrotrophic effectors (NEs) from the corresponding wheat sensitivity genes results in an interaction often described as 'inverse' gene-for-gene, as recognition results in increased disease and cell death (Shao et al., 2021). Two of the best characterised NEs from these pathogens, *PtrToxA* (or ToxA) and *SnTox1* (Tox1), along with their corresponding wheat sensitivity genes *Tsn1* and *Snn1*, respectively, thus work to hijack *R*-mediated resistance (Liu et al., 2004; Adhikari et al., 2009; Faris et al., 2010; Cockram et al., 2015; Liu et al., 2016).

ToxA was originally found in *P. nodorum* and was later identified also in *P. tritici-repentis*, probably through horizontal gene transfer (Friesen et al., 2007). Tsn1, encoding a nucleotide-binding leucine-rich repeat (NB-LRR) resistance protein, is required for plant sensitivity to ToxA, although Tsn1 does not directly interact with ToxA (Faris et al., 2010). ToxA translocates into plant cells possibly through the recognition of arginine-glycine-aspartic acid (RGD) motif in the protein by a plant surface receptor (Manning & Ciuffetti, 2005) and eventually localises to chloroplasts leading to light-dependent (Tsn1 is regulated by light) reactive oxygen species (ROS) accumulation and cell death (Ciuffetti et al., 2010; Faris et al., 2010). To date, the precise role of Tsn1 in ToxA sensitivity is unknown, though the evidence suggests Tsn1 is possibly acting as a sensor for ToxA (Faris et al., 2010). ToxA sensitivity in plants lacking Tsn1 has also been reported (Manning & Ciuffetti, 2005), suggesting the presence of other susceptibility factors linked to ToxA. Moreover, ToxA has been shown to manipulate the host defence system via interaction with the wheat pathogenicity-related PR-1 proteins (Lu et al., 2014; Breen et al., 2016),

but it has also been suggested to interact with a chloroplast-localised protein called ToxABP1 (Manning et al., 2007, 2010) and the photosynthetic electron transport protein plastocyanin (Tai et al., 2007), through Y2H assays.

ToxABP1, also known as Thylakoid Formation 1 (Thf1) in *Arabidopsis*, is a chloroplast membrane-localised protein, involved in photosystem-light harvesting complex II (PSII-LHCII) dynamics for the efficient disassembly/assembly of PSII megacomplexes during repair (Theis & Schroda, 2016). This protein is classified as a negative regulator of cell death and has been found to be targeted by other pathogens, such as *Pseudomonas syringae* DC3000 in tomato (tomato orthologue named *SlALC*) (Wangdi et al., 2010) and the virus *Tobamovirus* TBV in pepper (Hamel et al., 2016). The severity of tissue necrosis provoked by ToxA can be blocked by preventing the accumulation of ROS or by silencing ToxABP1 in wheat (Manning et al., 2010).

Tox1 was the first HST identified in *P. nodorum* requiring a single host sensitivity locus Snn1 to confer susceptibility (Liu et al., 2012). Snn1 gene, a member of the membrane-bound wall-associated kinases (WAKs), allows recognition of Tox1 also in a light-dependent manner, triggering hallmarks of PCD including upregulation of mitogen-activated protein kinase (MAPK) cascades, an oxidative burst, strong up-regulation of PR genes and DNA laddering (Liu et al., 2012; Shi et al., 2016). Tox1 has been also shown to bind to chitin, protecting the fungal cell wall from degrading chitinases (Liu et al., 2016).

Sequence and structure similarities of NEs have been found between pathogens. For example, ToxA has also been found in the pathogens *Cochliobolus heterostrophus* and *Bipolaris sorokiniana,* in which ToxA also causes cell death in a light-dependent manner in sensitive maize and wheat lines, respectively (Lu et al., 2015; Friesen et al., 2018; McDonald et al., 2018). *Z. tritici*, during the asymptomatic phase, secretes plant cell wall-degrading enzymes and/or effectors (ben M'Barek et al., 2015; Fantozzi et al., 2021). Genomic approaches have identified *Z. tritici* virulence strategies such as a chitin-binding effector protein *Mg3LysM* (Marshall et al., 2011), the *Avr* genes *AvrStb6* and *Avr3D1* which elicit a resistant phenotype in *Stb6* and *Stb7* wheat lines, respectively (Zhong et al., 2017; Meile et al., 2018) and one putative

necrotic factor involved in the formation of pycnidia *ZtNIP1* (Kettles & Kanyuka, 2016; Kettles et al., 2017). In another work, 14 *Z. tritici* secreted proteins demonstrated cell death-inducing activity in the non-host plant *Nicotiana benthamiana* and were shown to be light-dependent (Kettles et al., 2017). However, there is currently no known *Z. tritici* effector that can target the chloroplast directly nor that NEs produced by *Z. tritici* could be similar to those of *P. nodorum*/*P. tritici-repentis*.

All three aforementioned necrotrophic foliar pathogens, *Z. tritici*, *P. nodorum* and *P. tritici-repentis*, often co-occur in nature and they all gravely affect the photosynthetic capacity of the plant. Based on previous evidence **(Chapter 3)**, incompatible *Z. tritici* inoculation resulted in PSII downregulation, aimed at ROS shielding, whilst compatible interactions led to the activation of chitin-associated and MAPK genes related to HR. Surprisingly, in the compatible interaction with Zt22 we also observed downregulation of *Snn1* and upregulation of *Tsn1*, at 6 hours after inoculation (hai). Moreover, there seems to be a common light dependency on the action of NEs of the three foliar wheat pathogens, suggesting a potential involvement of the xanthophyll cycle in the regulation of the NE sensitivity. As we found that infection with a virulent *Z. tritici* isolate had an impact on *Snn1* and *Tsn1*, we hypothesised that in the potential interaction between *Z. tritici* and Tox1/ToxA (as so far there is no evidence to support this), sensitivity to the NEs will be reduced, possibly because *Z. tritici* effectors antagonise similar NE effectors targeting the function of the chloroplast. Here, we first infiltrated our parental plant material to establish their sensitivity to the toxins. Then, we inoculated our *Stb6* resistant and susceptible lines with *Z. tritici* isolates of differing virulence followed by toxin infiltrations, expecting that reduction of necrosis would be the result of reduced sensitivity. We also assessed the effect of toxin infiltrations on pycnidia production. Finally, we measured the expression of *Snn1*, *Tsn1*, *Thf1* as well as the xanthophyll cycle enzymes zeaxanthin epoxidase (ZEP) and violaxanthin de-epoxidase (VDE) upon each treatment.

4.2 Materials & Methods

4.2.1 Plant material and growth conditions

Two Near-Isogenic wheat lines (NILs) were used in this study, including the spring wheat Courtot with a highly susceptible phenotype (S) and its near-isogenic line Ct (+Stb6) with a resistant phenotype (R) for *Z. tritici* strains that contain the avirulent gene *AvrStb6* (Zhong et al., 2017). NILs were created by backcrossing Courtot with the resistant Chinese Spring that also contains *Stb6*. Seedlings were germinated and grown in FS2 soil compost in 4x3 modular trays. Plants were grown at 20 °C day and night temperature, 16h photoperiod, 55 ± 5% RH and ~500 µmols m^{-2} s^{-1} Photosynthetic Photon Flux Density (PPFD) light intensity. All experiments were performed on ~2-week-old seedlings. Each genotype/treatment combination was comprised by three biological replicates, whereas all experiments were performed twice (technical replication). However, only data from the first technical replication are shown in this Chapter, as data from the repetition were still being collected at the time of submission of this thesis.

4.2.2 Inoculations and infiltrations

Two *Z. tritici* (Zt) isolates with different level of virulence were used in this study, kindly provided by Dr Kostya Kanyuka (previously at Rothamsted Research, currently at NIAB, Cambridge, UK). The reference isolate IPO323 was used, which contains the avirulent gene *AvrStb6*, and results in an incompatible interaction with any wheat variety carrying *Stb6* (Zhong et al., 2017). The other isolate was an isoform of *AvrStb6*, named I-17 (Stephens et al., 2021), hereafter termed as Zt22, and was expected to result in compatible interactions with both genotypes, Courtot and Ct (+Stb6).

All isolates were kept in 70% sterile glycerol stock solutions in -80 °C and were grown on yeast peptone dextrose (YPD) agar (Sigma Aldrich) for 5 days at room temperature. Spores were then suspended in sterile, deionised 0.01% (v/v) Tween20 H_2O and concentration was calculated and adjusted to 10^6 spores/ml using a haemocytometer. Seedling were sprayed until runoff could be observed on the leaves and high humidity was maintained by placing

the seedlings in propagating trays with transparent covering lids for 4 days. Inoculations with sterile, de-ionised H_2O were used as controls.

For all infiltration treatments, 100 µl aliquots of each purified necrotrophic protein, kindly provided by Dr Huyen Phan (Curtin University, Australia), were infiltrated on the adaxial side of the youngest, fully-expanded leaf, using a 1 ml needless syringe. The infiltrated area was marked with a nontoxic permanent marker. Infiltrations with sterile, de-ionised H_2O were used as controls. In the experiment to test the effect of *Z. tritici* inoculation on toxin sensitivity, *Z. tritici* spray inoculations were performed first and infiltrations were made 6 hours later (6hai). The timing of infiltration was decided based on the transcriptomics data from Chapter 3, showing a change in transcript expression of *Snn1* and *Tsn1* at 6 hours upon inoculation with *Z. tritici*. Spray inoculation with sterile H_2O was used as the *Z. tritici* inoculation control, whereas sterile H_2O infiltration at 6hai was used as toxins infiltrations control. A list of all experimental treatments can be seen in Table 1.

Table 4-1. A list of all experimental treatments used in this study.

Treatments	First application (0h)	Second application (6h later)
	Spray	*Infiltration*
1	H_2O	H_2O
2	H_2O	Tox1
3	H_2O	ToxA
4	IPO323	H_2O
5	Zt22	H_2O
6	IPO323	Tox1
7	IPO323	ToxA
8	Zt22	Tox1
9	Zt22	ToxA

4.2.3 Sampling, RNA extractions and qPCRs

Inoculated and infiltrated leaves were sampled 24 hours after the infiltration treatment (24hai). Leaf material was ground using liquid nitrogen and total RNA was extracted with Trizol and chloroform, followed by the guidelines of the RNeasy Mini Kit (Qiagen), with the addition of a RNase-free DNase step (Qiagen) to remove any traces of DNA in the RNA extracts. Samples were eluted in 35 µl RNA-free water and their concentration and purity were determined with a NanoDrop ND-1000 Spectrophotometer. 1 µg per sample were used for cDNA synthesis using the iScript cDNA synthesis kit (Biorad). 12.5 ng of cDNA were used for qPCR reaction with SYBR reaction mix (Biorad) and primers were at 50 µM concentration. Ubiquitin was used as the housekeeping gene, as it didn't show any significant change in expression across the experimental conditions. All samples had three biological replicates and qPCRs were performed twice. The conditions were as following: 95 °C for 30 sec, 40 cycles of 95 °C for 15 sec and 58-60 °C for 30 sec, followed by a melt curve between 65 and 95 °C. Primers used are shown in Table 4-2. All primers were run at 60 °C, apart from ZEP and VDE (58 °C). Relative expression was calculated as $2^{-\Delta Ct}$, whereby ΔCt was calculated as (Ct target – Ct housekeeping gene).

Table 4-2. A list of all the primers used in this study.

Gene	Forward primer (5' – 3')	Reverse primer (5' – 3')
Snn1	TGCCTTGAAGTTGATGCCCCTAT	GTTGAGGGCCACCTTGTTATTACTG
Tsn1	GATCGTCACTGCCAAGTCCA	GTCCCTAGTGCTGGCTTCGT
Thf1	GTCGCTTCCTTTCGCTGCAC	GAACGTGATCCCCGCCGAG
ZEP	GGACTTCAACGACCCCTTGT	TACCCTATTGTACACCCTCGGT
VDE	CCCGAGCTAGAAAGGGCTAC	ACCACAGGTGTTGTCTGTCC
Ubi	GCACCTTGGCGGACTACAACATTC	GACACCGAAGACGAGACTTGTGAACC

4.2.4 Symptoms monitoring

Toxin sensitivity monitoring was performed at 1, 2, 3, 5, 7 and 9 days after inoculation (dai). Images were taken with a 26mm 12MP, f1.8 wide angle camera. Necrosis was assessed visually, however no image analysis was performed in order to extract quantifiable data on disease. For the inoculations/infiltrations combinational experiment, plants were also monitored for their pycnidia development. Due to low seed germination, H_2O only treatment and Zt22 + H_2O treatment only had two biological replicates for visual assessment.

4.2.5 Statistical analysis

Gene expression results from RNAseq (Chapter 3) were analysed with Tukey's t-tests ($P < 0.05$), whereas gene expression results in this experiment were analysed with ANOVA to find significant differences of the interaction of the main effects (Genotype x Treatment).

4.3 Results

4.3.1 Presence and expression of wheat sensitivity genes

We investigated our RNAseq analysis for the differential expression of the wheat sensitivity genes to the NEs, *Tsn1* (TraesCS5B02G519900), *Thf1* (TraesCS2B02G233300) and *Snn1* (TraesCS1B02G004100), through a simple search of the transcript IDs of the genes across all comparisons (Table 4-3). For Ct (+Stb6) and Courtot inoculated with IPO323, genes were not present at 6hai, whereas they were present but not significantly different at 24hai. However, when the *Stb6* line was inoculated with the virulent Zt22, there was a significant upregulation of *Snn1* and downregulation of *Tsn1* at 6hai (Table 4-3).

We validated the expression of these genes with qPCR (Figure 4-1). For *Tsn1*, gene expression validated the sequencing, with a significant downregulation in Ct (+Stb6) inoculated with Zt22 compared to IPO323 at 6hai (Figure 4-1a). Moreover, at 24hai, there was a significant upregulation for Courtot inoculated with Zt22 and in contrast, a significant reduction of *Tsn1* for Ct (+Stb6) inoculated with Zt22 (Figure 4-1a). *Thf1* expression was significantly upregulated for Courtot and IPO323 by 24hai, however inoculation with Zt22 upregulated *Thf1* faster at 6hai (Figure 4-1b). In contrast, Ct (+Stb6) upregulated *Thf1* at 6hai for both isolates and it was significantly downregulated at 24hai in Zt22 inoculation (Figure 4-1b). Finally, qPCR of *Snn1* also confirmed the differential expression observed in the transcriptomics, with a significant upregulation at 6hai for Ct (+Stb6) with Zt22 compared to IPO323 (Figure 4-1c). Courtot *Snn1* expression was also upregulated at 6hai with Zt22 but only increased over time for IPO323 inoculation (Figure 4-1c).

Table 4-3. Presence and expression of the wheat toxin sensitivity genes, *Tsn1*, *Thf1* and *Snn1*, in RNAseq experiment (Chapter 3). Log FC refers to the level of transcript change (up- or downregulation) and *P* refers to the adjusted *P*-value of each transcript. Significantly differentially expressed transcripts are highlighted in bold.

	Tsn1		***Thf1***		***Snn1***	
Comparison	Log FC	*P*	Log FC	*P*	Log FC	*P*
Ct (+Stb6) vs Courtot 0h	0.13	0.99	0.02	0.99	0.31	0.99
Ct (+*Stb6*) vs Courtot 6h IPO323	n/a		n/a		n/a	
Ct (+*Stb6*) vs Courtot 24h IPO323	0.20	0.95	-0.21	0.28	0.79	0.14
Ct (+*Stb6*) Zt22 vs Ct (+*Stb6*) IPO323 6h	**-0.59**	**0.01**	-0.17	0.30	**1.88**	**< 0.001**
Ct (+*Stb6*) Zt22 vs Ct (+*Stb6*) IPO323 24h	0.14	0.99	0.03	0.99	0.006	0.99

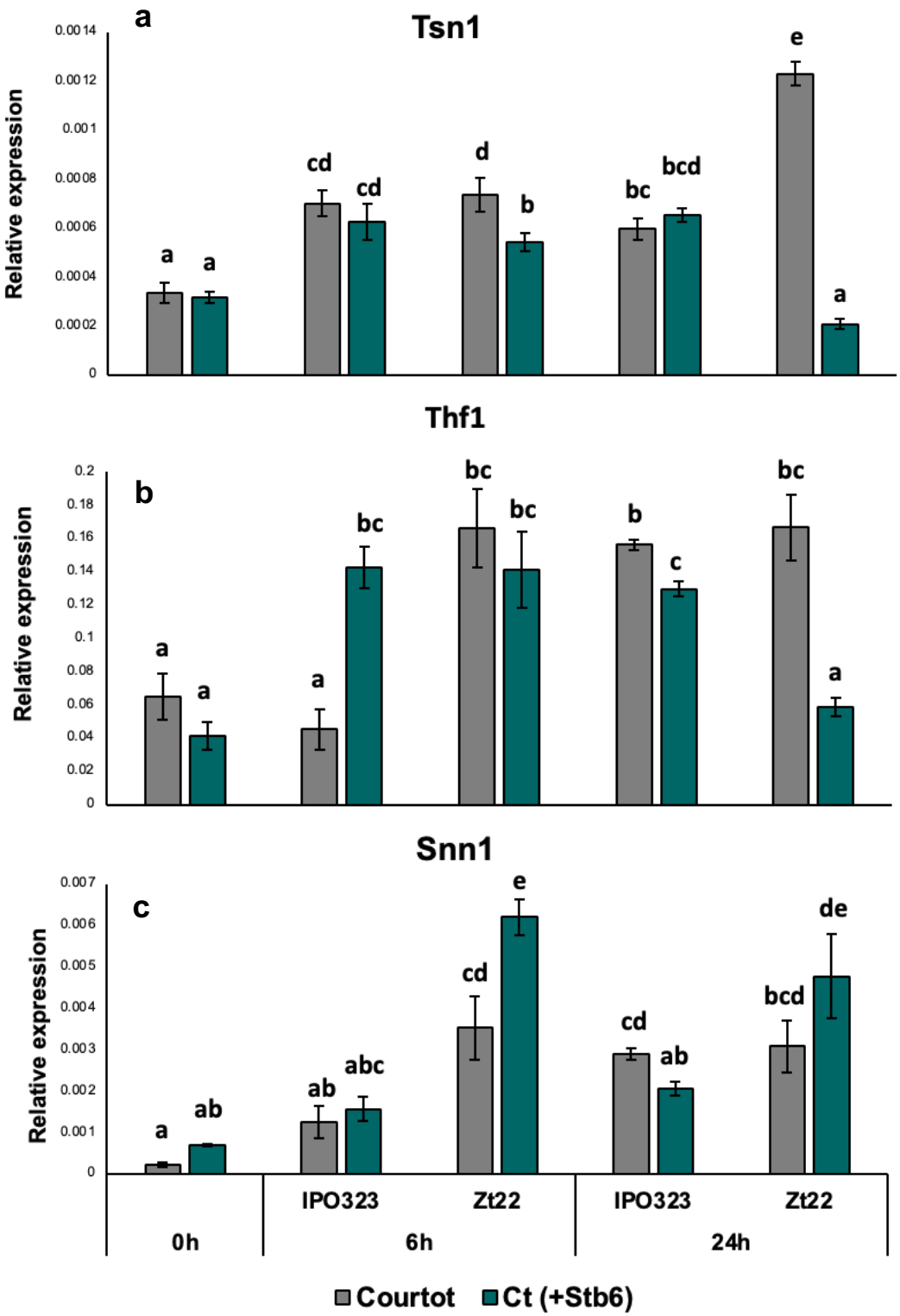


Figure 4-1. Gene expression validation of **(a)** *Tsn1*, **(b)** *Thf1* and **(c)** *Snn1* from RNAseq experiment (Chapter 3). Bars represent means ± SEM (n=3). Grey and teal bars represent Courtot and Ct (+Stb6), respectively. Letters above bars indicate statistical differences between the means (t-tests $P < 0.05$).

4.3.2 Sensitivity assessment of the parental lines

In order to proceed with our hypothesis, we first established whether the parental lines used in the creation of the NILs, as well as the NIL Ct (+Stb6), were sensitive to the NEs. Therefore, we infiltrated seedlings of Courtot and Chinese Spring, along with the near-isogenic Ct (+Stb6), with either Tox1 or ToxA and monitored the appearance of necrosis on the infiltrated area at 3 dai and again at 7 dai. Previously described databases (Downie et al., 2018) scored sensitivity as 0 for insensitive plants and as 4 for highly sensitive plants, based on the extend of necrosis on the leaf. The same authors classified Courtot as highly sensitive (score = 4) for ToxA and moderately sensitive (score = 3) for Tox1. Chinese Spring has been classified as insensitive to ToxA (Liu et al., 2006) but sensitive to Tox1 (Liu et al., 2012). Our results confirmed these previous observations, while demonstrated that Ct (+Stb6) must have obtained the sensitivity to Tox1 from Chinese Spring and the sensitivity to ToxA from Courtot, during the backcrossing events (Figures 4-2 and 4-3).

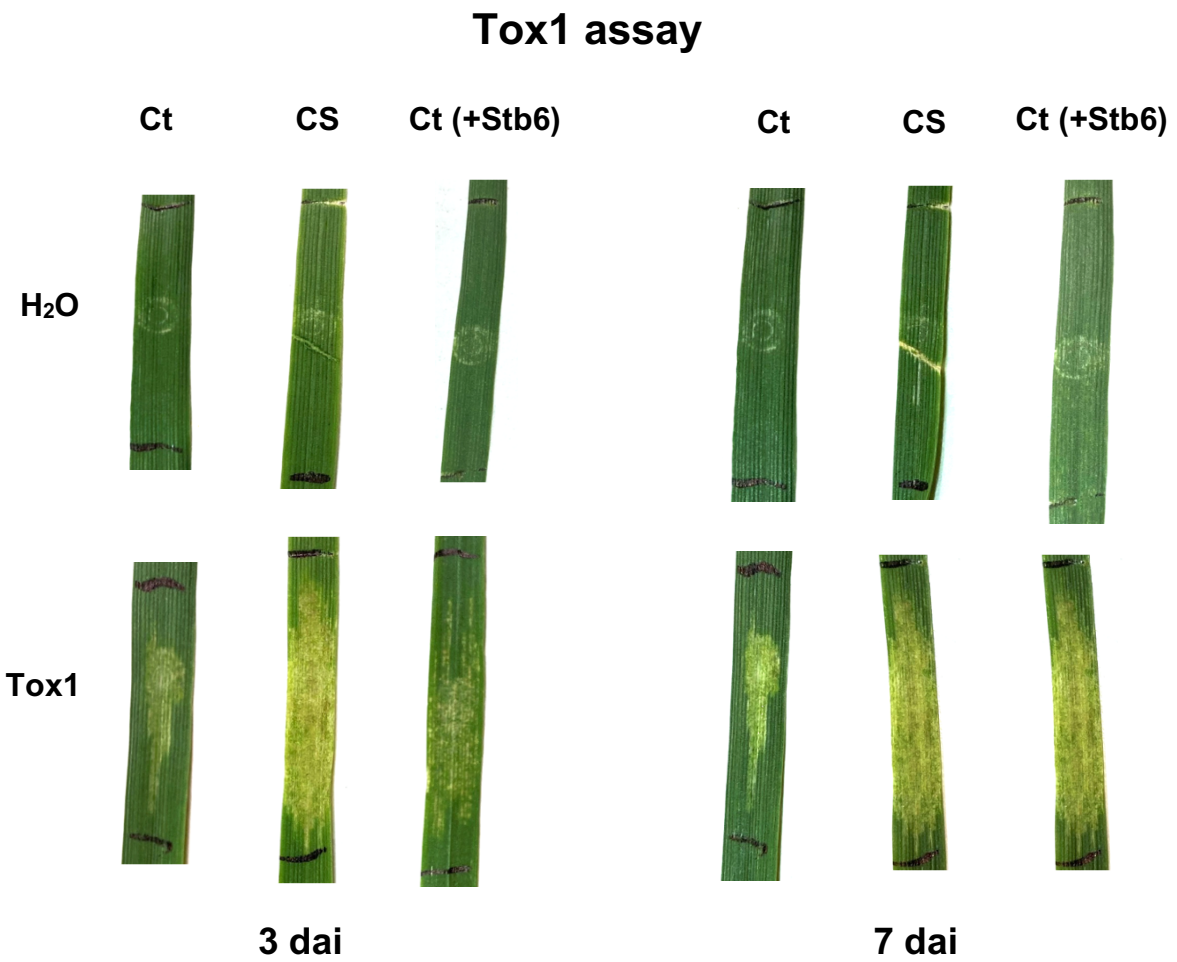


Figure 4-2. Tox1 infiltration assay for Courtot (Ct) and Chinese Spring (CS), along with the near-isogenic Ct (+Stb6), at 3 and 7 days after infiltration (dai). H_2O infiltration was used as a control.

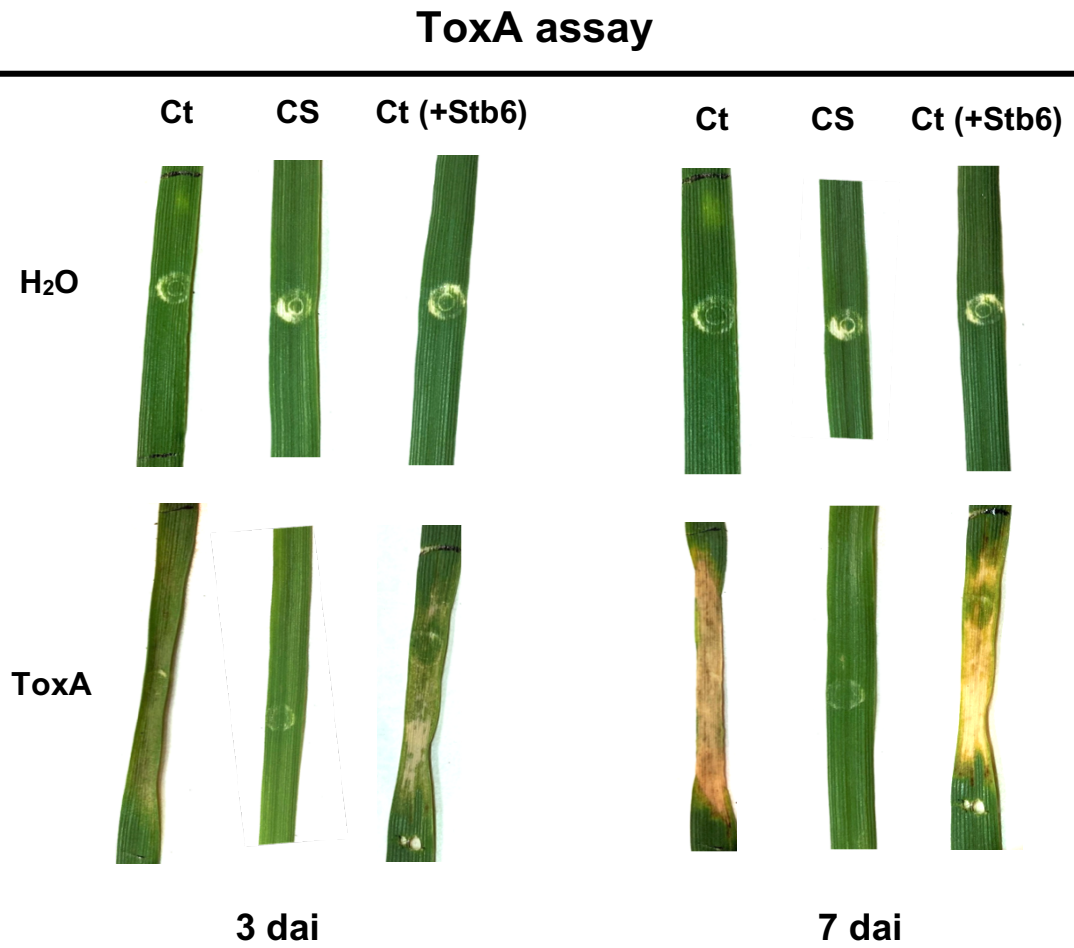


Figure 4-3. ToxA infiltration assay for Courtot (Ct) and Chinese Spring (CS), along with the near-isogenic Ct (+Stb6), at 3 and 7 days after infiltration (dai). H_2O infiltration was used as a control.

4.3.3 Sensitivity assessment of *Z. tritici*-inoculated and Toxin-infiltrated plants

Once we established that Courtot and Ct (+Stb6) were sensitive upon infiltration to ToxA and Tox1, we set to test our hypothesis with treatments described in Table 4-1. Seedlings were monitored at 1, 2, 3, 5, 7 and 9 dai for the appearance of necrosis on the infiltrated area. Symptom discrimination was based on personal experience and available publications and was only assessed visually, without performing any image analysis.

No necrosis was observed on the first day. However, by Day 2, necrosis appeared in ToxA-infiltrated plants and seemed greater in leaves that had been pre-inoculated with IPO323 (Figure 4-4). Only mild chlorosis appeared in Tox1-infiltrated plants (Figure 4-4). As expected, no necrosis appeared on spray-inoculated plants with *Z. tritici* isolates or with H_2O (Figure 4-4). The necrotic effect of ToxA was even more prevalent at 3 dai, compared to Tox1-infiltrated plants which had just started to exhibit some necrotic areas (Figure 4-5). Once more, plants pre-inoculated with IPO323 and Zt22 before being infiltrated with ToxA, appeared considerably more necrotic than the ones that had received only H_2O inoculation and ToxA infiltration (Figure 4-5). Moreover, the IPO323 + ToxA Ct (+Stb6) line appeared slightly more necrotic than its equivalent Courtot (Figure 4-5). This trend continued at Day 5, whereby ToxA infiltrations were more aggressive (more and faster necrosis) than Tox1, for both genotypes (Figure 4-6). Ct (+Stb6) with IPO323 and ToxA did not seem more necrotic compared to Courtot or the control inoculations (H_2O + ToxA), however there were no chlorotic areas around the necrosis, compared to the rest (Figure 4-6). Interestingly, IPO323 +Tox1 treatment appeared more necrotic than the control treatment (H_2O + Tox1) but also than the Zt22 +Tox1 treatment, for both genotypes (Figure 4-6). By 7 dai, no more differences in necrosis could be observed among the ToxA-infiltrated treatments (Figure 4-7). Similar to 5 dai, IPO323 + Tox1 was, once more, more necrotic than the control (H_2O + Tox1) and this time more necrotic than Ct (+Stb6) with Zt22 and Tox1. Courtot + Tox1 maintained to have very little chlorotic symptoms (Figure 4-7). Chlorotic spots associated with *Z. tritici* inoculations made their

appearance at 7dai. However, to our surprise, these appeared significantly worse in Ct (+Stb6) which should have exhibited a fully resistant phenotype with very few, if any, chlorotic spots (Figure 4-7). Finally, leaves infiltrated with ToxA were completely degraded by 9 dai (Figure 4-8). It was not until this point that more extensive necrosis surfaced on the leaves of Tox1 infiltrated plants, yet Courtot with Zt22 + Tox1 was still less affected (Figure 4-8). *Z. tritici* symptoms were also enhanced and some necrosis also appeared in IPO323-inoculated plants (Figure 4-8).

Pycnidia production at 15dai was not affected for the compatible interactions in terms of ability of the pathogen to sporulate, however they were (visibly) reduced or they would be more prominent in other inoculated leaves. For example, in Courtot inoculated with IPO323, there were more pycnidia on the infiltrated area for H_2O and Tox1 infiltrations, but very little pycnidia for ToxA infiltration (Figure 4-9). In contrast, both genotypes inoculated with Zt22 did not show any pycnidia on the infiltrated areas, however, pycnidia could be observed on the remaining inoculated leaves of the seedlings (Figure 4-9). No pycnidia were observed in any of the IPO323 treatments for the resistant Ct (+Stb6) (Figure 4-9).

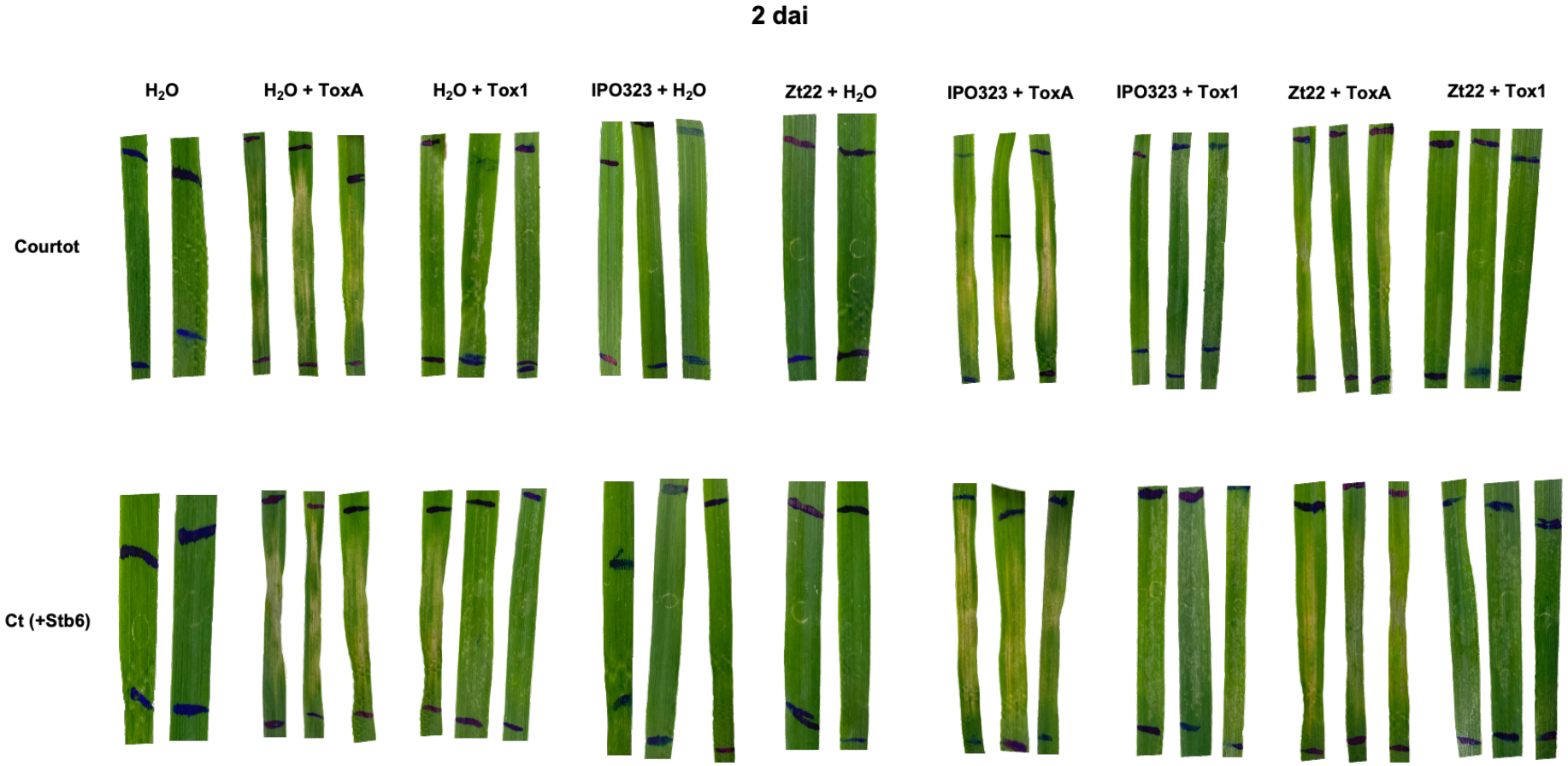


Figure 4-4. Symptoms of *Z. tritici* inoculations followed by Toxin infiltrations at 2 days after inoculations (dai).

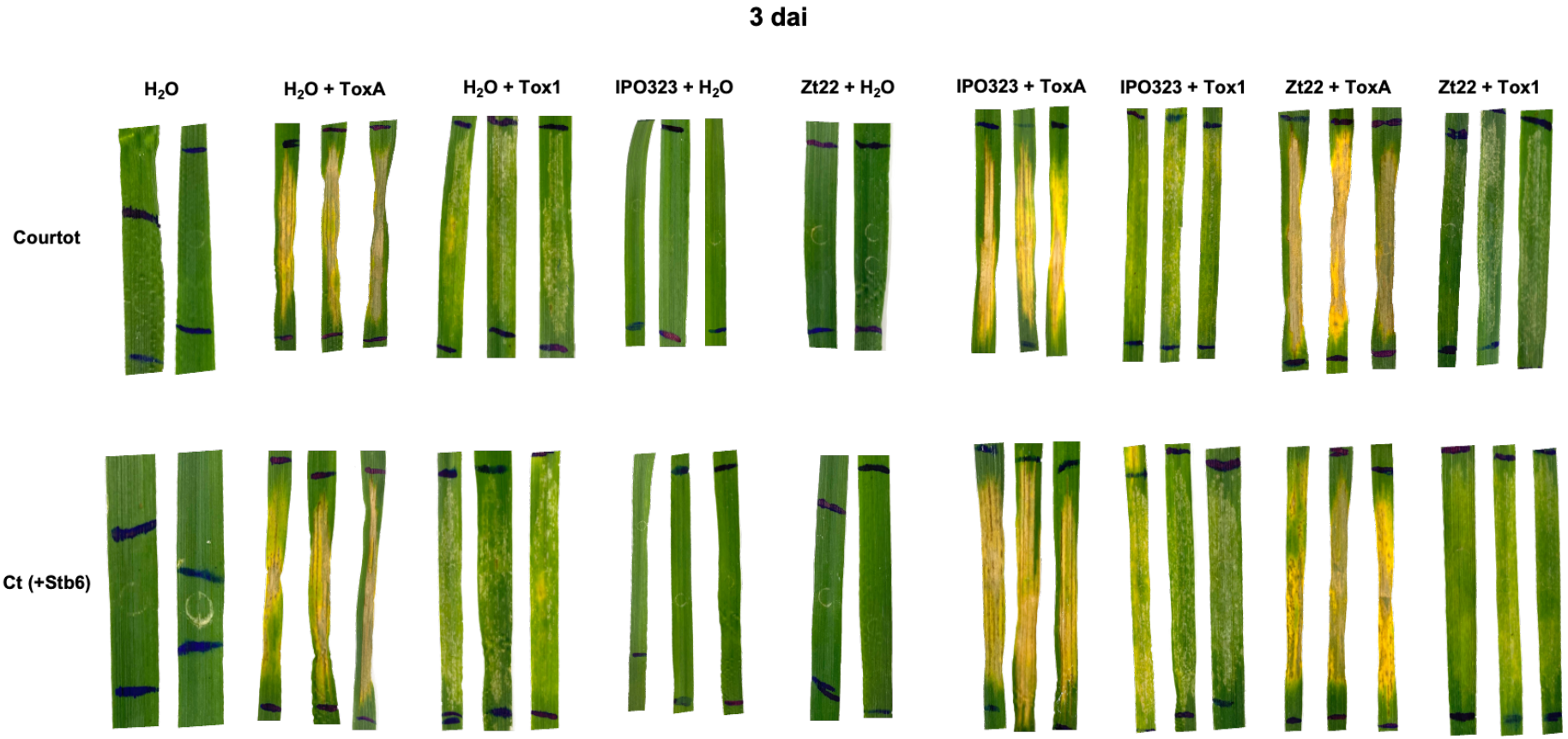


Figure 4-5. Symptoms of *Z. tritici* inoculations followed by Toxin infiltrations at 3 days after inoculations (dai).

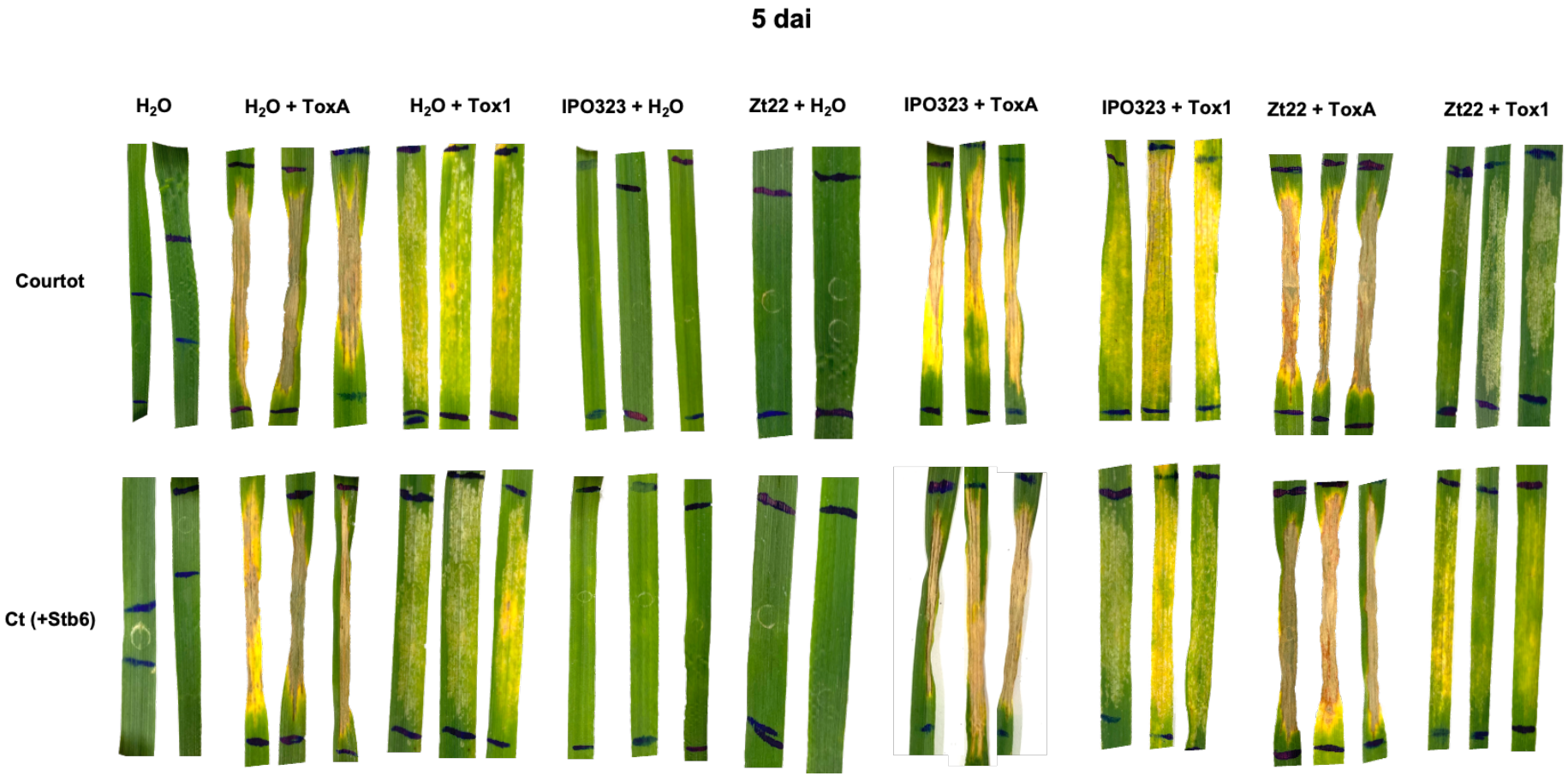


Figure 4-6. Symptoms of *Z. tritici* inoculations followed by Toxin infiltrations at 5 days after inoculations (dai).

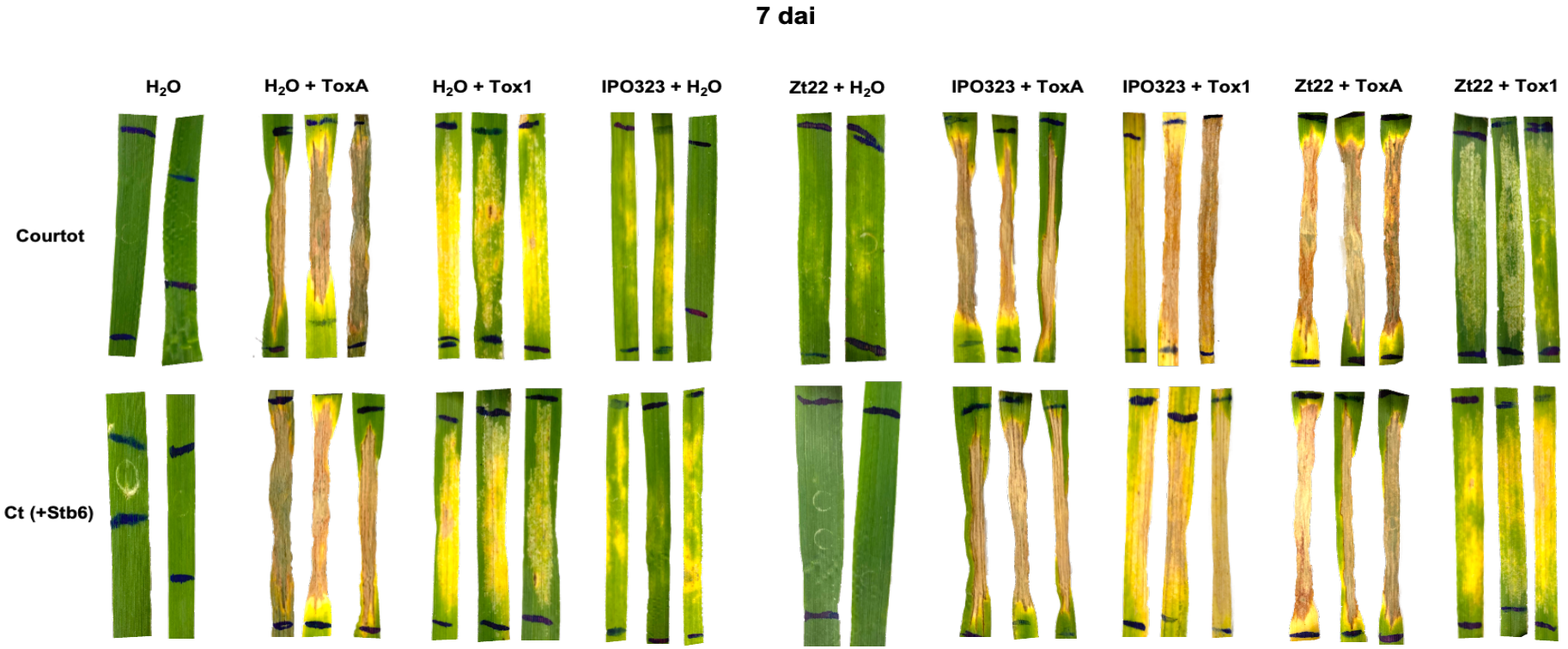


Figure 4-7. Symptoms of *Z. tritici* inoculations followed by Toxin infiltrations at 7 days after inoculations (dai).

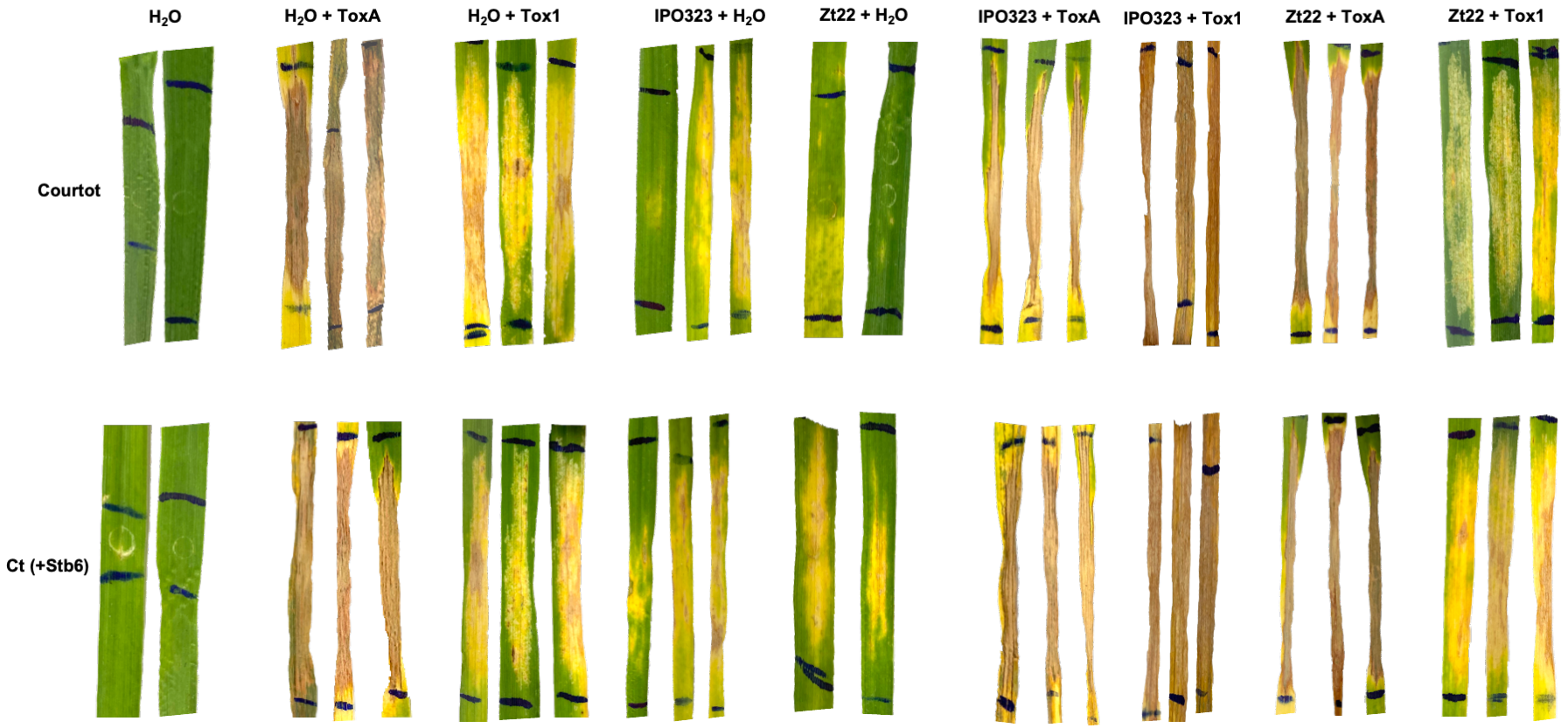


Figure 4-8. Symptoms of *Z. tritici* inoculations followed by Toxin infiltrations at 9 days after inoculations (dai).

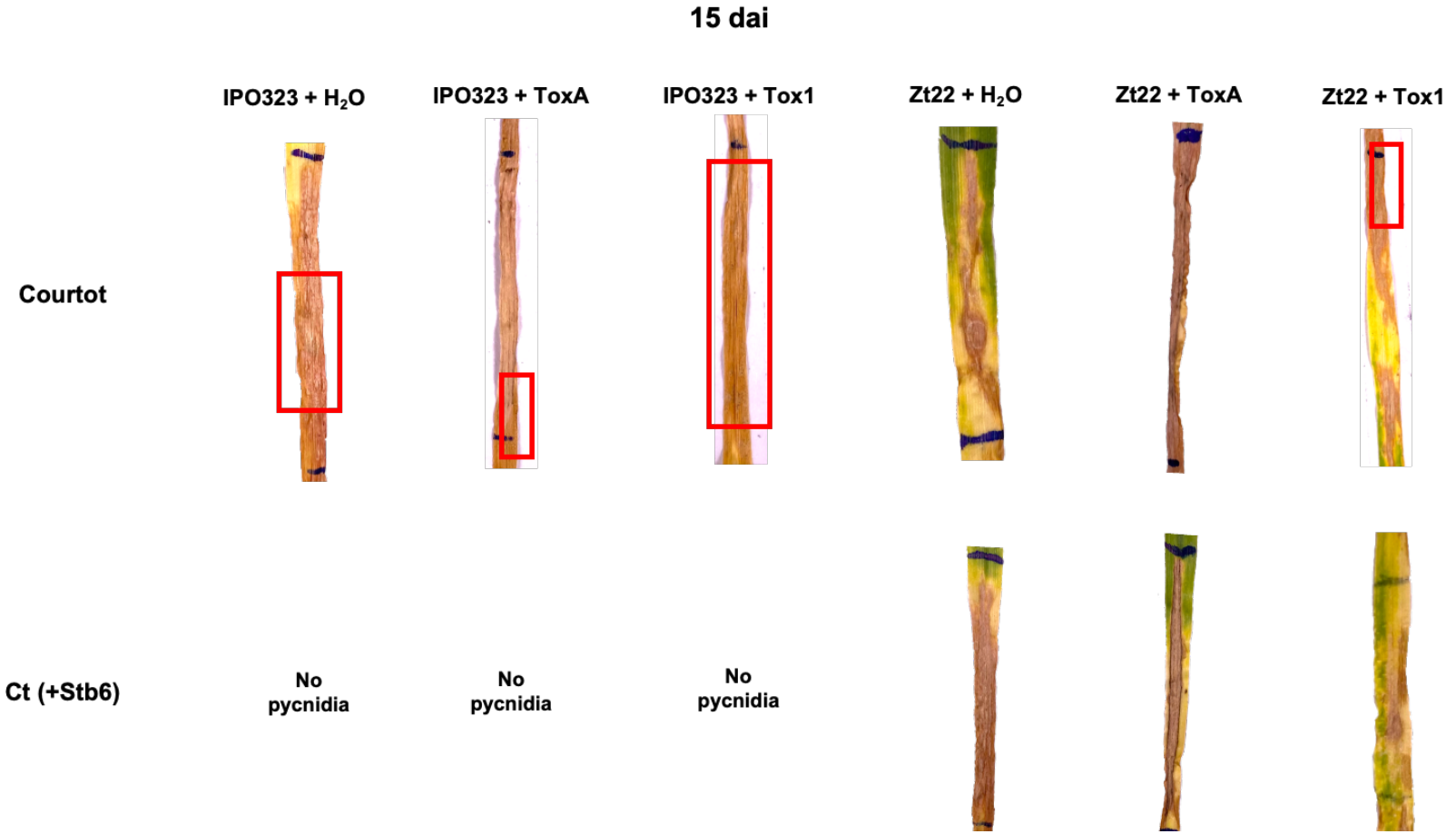


Figure 4-9. Symptoms of *Z. tritici* inoculations followed by Toxin infiltrations at 15 days after inoculations (dai). Red boxes indicate necrotic areas where pycnidia appeared.

4.3.4 Gene expression

To test the expression of wheat sensitivity genes *Tsn1* and *Snn1*, as well as *Thf1* and the xanthophyll cycle (XC) conversion enzymes zeaxanthin epoxidase (ZEP) and violaxanthin de-epoxidase (VDE), in response to the spray inoculations and toxin infiltrations, we sampled leaf material 24hai after infiltration treatment. Genes were selected for their involvement in response to the necrotrophic effectors and in photoprotection, respectively.

Statistical analysis revealed a significant interaction between the genotypes and treatments for *Tsn1* (P = 0.004) and *Thf1* (P = 0.005). Inoculation with Zt22 significantly increased the expression of *Tsn1* for both genotypes, compared to all remaining treatments, with Courtot also being significantly higher than Ct (+Stb6) (Figure 4-10a). In the treatment of IPO323 + ToxA, Ct (+Stb6) downregulated the expression of *Tsn1*, whereas it was Courtot that downregulated *Tsn1* in response to both Zt22 and ToxA (Figure 4-10a). Similarly, when Ct (+Stb6) was infected with both IPO322 and ToxA, *Thf1* expression was significantly reduced compared to IPO323 treatment alone and compared to H_2O control (Figure 4-10b). Following the expression of *Tsn1*, *Thf1* was also downregulated in Ct (+Stb6) inoculated with Zt22 compared to the control, while Courtot maintained high expression with Zt22 but significantly reduced *Thf1* with IPO323, compared to the control (Figure 4-10b). *Snn1* expression showed significant increases when plants were inoculated with IPO323 but also when Ct (+Stb6) was first inoculated with Zt22 and then infiltrated with Tox1 (Figure 4-10c). It remained low and not significantly different for the remaining treatments (Figure 4-10c).

ZEP was only maintained at higher expression levels for both genotypes inoculated with IPO323, along with the H_2O control, and was significantly reduced for the remaining treatments (Figure 4-11a). No differences however were observed between genotypes (Figure 4-11a). Lastly, VDE was also reduced across the majority of the treatments, compared to the control (Figure 4-11b). However, the +*Stb6* line inoculated with IPO323 as well as Zt22 + Tox1 maintained high expression of this enzyme at the time of sampling (Figure 4-11b).

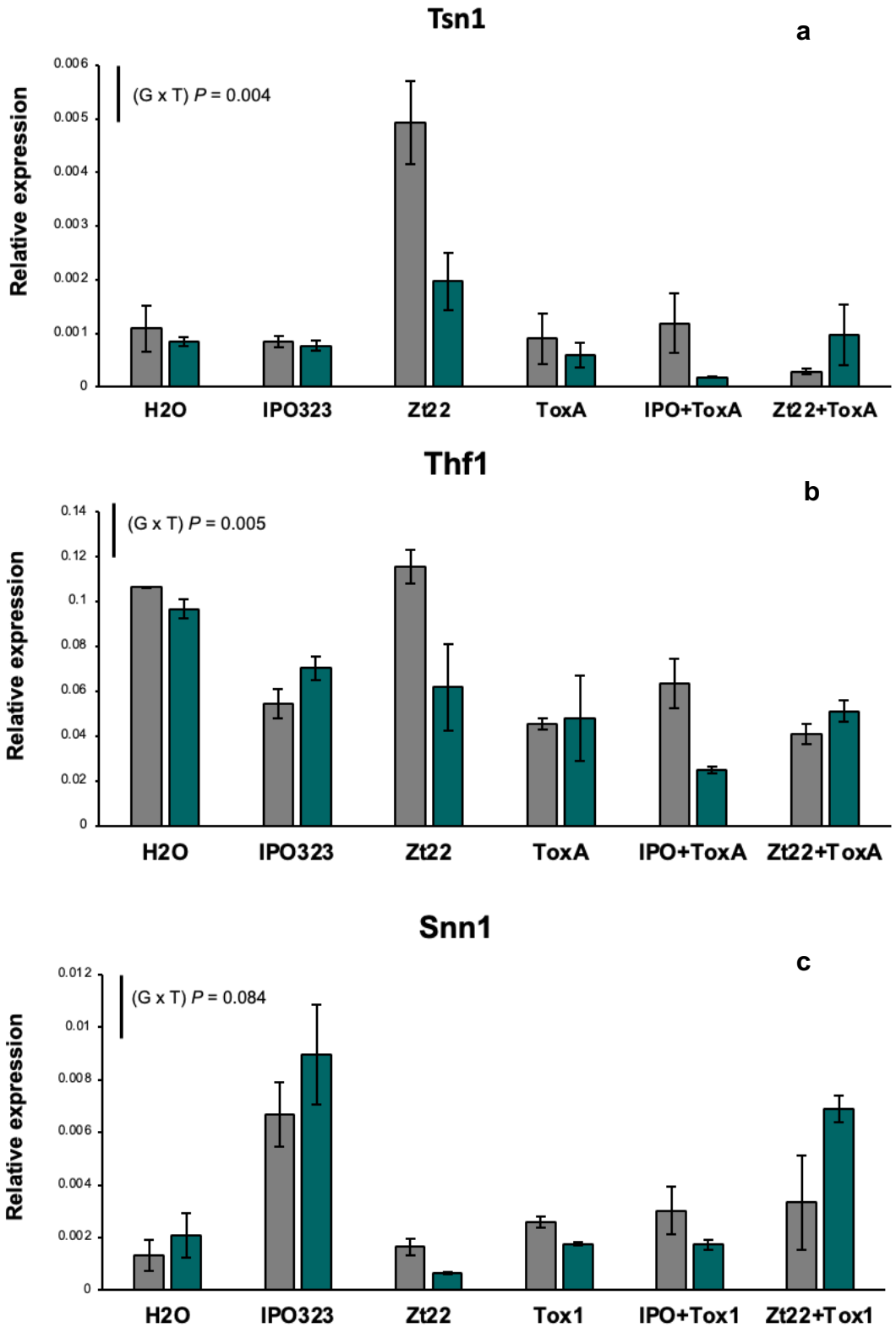


Figure 4-10. Gene expression analysis of **(a)** *Tsn1*, **(b)** *Thf1* and **(c)** *Snn1* across all treatments, 24h after infiltration. Grey and teal bars represent Courtot and Ct (+Sbt6), respectively. Bars represent means ± SEM (n=3). ANOVA of the interaction between the genotypes and treatments, along with the LSD, are shown on the top left of each graph. Abbreviation IPO stands for IPO323.

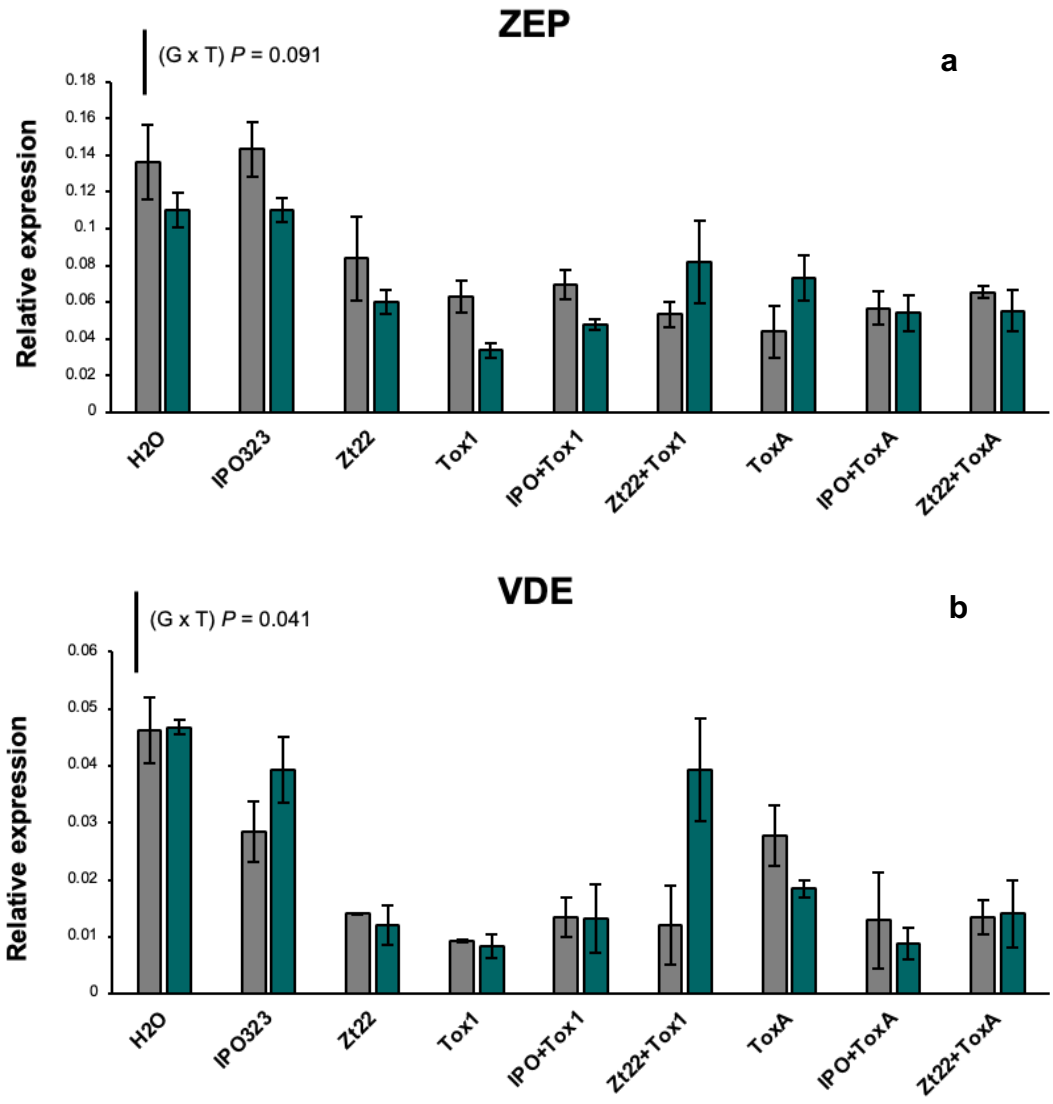


Figure 4-11. Gene expression analysis of **(a)** zeaxanthin epoxidase ZEP and **(b)** violaxanthin de-epoxidase VDE across all treatments. Grey and teal bars represent Courtot and Ct (+Sbt6), respectively. Bars represent means ± SEM (n=3). ANOVA of the interaction between the genotypes and treatments, along with the LSD, are shown on the top left of each graph. Abbreviation IPO stands for IPO323.

4.4 Discussion

To the best of our knowledge, no published work has investigated the effect of *Zymoseptoria tritici* virulence on wheat sensitivity response to necrotrophic effectors (NEs) from *Parastagonospora nodorum*.

Snn1, a WAK-like protein that binds to the necrotrophic effector Tox1 and results in cell death, was found to be upregulated in the +*Stb6* line in response to the virulent *Z. tritici* isolate Zt22 at 6hai. Research on *Snn1*-Tox1 pathosystem has shown that *Snn1* was downregulated at 6hai after exposure to Tox1 in a Tox1-sensitive genotype, but increased again at 24hai, based on its diurnal rhythm and tight light regulation (Shi et al., 2016). This was also observed here where *Snn1* expression in +*Stb6* Zt22-inoculated line was downregulated compared to the control, potentially suggesting recognition of Tox1-like structure from *Stb6*, a WAK similar to *Snn1*. However, our expression studies were performed at 24hai after infiltration, while our sequencing observations, which follow the 24hai upregulation observations from Liu et al. (2016), were at 6hai. This could suggest that *Z. tritici* pathogenicity also relies on light perception by the host's phytochrome receptors but further research is needed to elucidate this further. There is extensive research on the effect of red:far-red (R:FR) ratios on plant immunity, for example low R:FR ratio enhanced tomato susceptibility to the necrotrophic *Botrytis cinerea* due to delayed pathogen recognition (Courbier et al., 2021), however this has never been studied in wheat and *Zymoseptoria tritici* (Ballaré, 2014; Courbier & Pierik, 2019). Moreover, the hypothesis that Zt22 recognition lowered *Snn1* expression at 24hai, would not explain why +*Stb6* plants first inoculated with Zt22 and then infiltrated with Tox1 exhibited more necrosis and higher *Snn1* expression, compared to Courtot, and did not show dampened sensitivity as per our hypothesis. Perhaps the different effectors from Zt22 and Tox1 exploit several pathways that all culminate to effector-mediated disease or multiple effectors utilising the same pathway and the most efficient effector prevails and manifests disease (Phan et al., 2016). Furthermore, inoculation with Zt22 or infiltration with Tox1 had an impact on the XC for both genotypes, by lowering the expression of ZEP and VDE. However, +*Stb6* plants first inoculated with Zt22 and then infiltrated with Tox1, restored the expression of VDE, suggesting

a more effective XC and energy dissipation. This could imply that Zt22 and Tox1 have the same effect on *Stb6* and during antagonistic conditions, Zt22 is protecting the chloroplast from cell death due to Tox1 for its own benefit. However, this hypothesis does not explain the phenotype on these plants, which did not differ from infiltration with Tox1 alone. It was only Courtot plants inoculated with Zt22 and infiltrated with Tox1 that exhibited reduced necrosis, however they did not differ in their *Snn1*, ZEP and VDE expression. This could potentially indicate the *Z. tritici* could have an epistatic, dampening effect on necrosis induced by Tox1, irrespective of the chloroplast. This has been previously observed among *P. nodorum* pathosystems, where for instance Tox3 – *Snn3* interaction was suppressed by Tox1 – *Snn1* interaction (Phan et al., 2016). Interestingly, *Snn1*, ZEP and VDE expression for Zt22 inoculated or Tox1 infiltrated *Stb6* plants seemed to follow the same pattern. The XC and the associated carotenoids (for example zeaxanthin and violaxanthin) play important roles in regulating the excess energy but also serve as powerful antioxidants. As described in previous chapters, ZEP catalyses the conversion of zeaxanthin to violaxanthin under low light conditions, whereas VDE converts violaxanthin back to zeaxanthin under high light conditions (Jahns et al., 2009). Interestingly, this resembles the diurnal transcriptional patterns of *Snn1* which decreases throughout daylight (could be seen as “high light”) and increases throughout darkness (could be seen as “low light”) (Shi et al., 2016). One of the key differences between *Z. tritici* and *P. nodorum* is that the former has a latent period with no visible symptoms appearing, when the host remains alive. It is not yet clear whether Zt22 could also be exploiting the chloroplast and the xanthophyll cycle or the gene expression observed was just an artefact. Moreover, it has recently been shown that *Z. tritici* also benefited from light during the early infection process (Ajigboye et al., 2021). Finally, the total disintegration of +*Stb6* plants treated with IPO323 + Tox1, could be explained by our previous observations of photoinhibition-mediated resistance already taking place at 6hai. As plants were infiltrated 6h after spray inoculations to account for our previous results, it could suggest that an already dissembled photosystem due to IPO323 resistance response was unable to cope with

Tox1-triggered ROS and de-activation of the XC, leading to accelerated death and total tissue collapse.

It is also known that upon Tox1 recognition, *Snn1* triggers the activation of MAP kinase (MAPK) cascades, which regulate multiple biological processes such as growth, development and immune responses, and that Tox1 binds to chitin to protect *P. nodorum*, but can also protect other fungal species from multiple wheat chitinases upregulated during defence (Peters Haugrud et al., 2022). MPK3 and MPK6 are commonly associated with plant defence and it has been shown that the expression of the susceptibility factor *Snn1* is linked to the expression of MPK3 (Liu et al., 2012). This could further support the idea that the *Z. tritici* isolate Zt22 possess a Tox1-like NE or share virulence strategies with *P. nodorum*, as a strong upregulation of MPK3/6, CERK and CEBiP was found in Zt22-inoculated plants at 6 and 24hai in transcriptomic analysis (Chapter 3).

Tsn1, the wheat susceptibility factor, along with ToxABP/*Thf1*, are involved in the recognition and downstream cell death from ToxA. In this work, ToxA seemed significantly more aggressive than Tox1 when the +*Stb6* line was first inoculated with IPO323. IPO323 confers resistance to +*Stb6* genotypes through the interaction with its avirulent gene *AvrStb6* (Zhong et al., 2017). Although no direct interaction between those genes has been observed, a Y2H screen with AvrStb6 as a bait showed a putative interaction with ToxABP/Thf1 (Chris Stephens PhD Thesis and Kostya Kanyuka, personal communication). Moreover, overexpression of AvrStb6 in wheat leaves has been observed to result in a photobleaching phenotype (Bouton and Kanyuka, unpublished; Chris Stephens PhD thesis, personal communication). This could perhaps explain the reduced expression of *Tsn1* and *Thf1* in IPO323-inoculated plants and the even-further reduction of the combined IPO323 + ToxA treatment. *Thf1* is also involved in protecting the photosystems from irreversible damage, interacts with Lhcb antenna proteins and has also been shown to have a similar phenotype and properties to PsbP-like proteins and PsbS in *Arabidopsis* (Huang et al., 2013; Theis & Schroda, 2016; Hong et al., 2020). Our hypothesis and observations from the transcriptomics results suggest that *Stb6* resistance involves the re-organisation of PSII, starting at 6hai, which

protects the chloroplast from ROS. Therefore, when plants were first inoculated with IPO323 and 6h later infiltrated with ToxA, PSII could have already been disassembled and *Thf1* activity already impaired, thus unable to protect the chloroplast against photodamage and cell death as a result to ToxA infiltration. This was also previously observed in ToxABP-silenced wheat leaves (Manning et al., 2010). In contrast, ToxABP/Thf1 has been also identified as a target of other pathogens, for example the bacteria *Pseudomonas syringae* (Wangdi et al., 2010) and the *Tobamovirus* (Hamel et al., 2016). Therefore, it could be possible that the virulent isolate Zt22 targets this protein or, in line with the Tox1 discussion above, that it contains a ToxA-like necrotrophic effector, as seen by the over-reduction of *Tsn1* and *Thf1* transcripts from gene expression analysis. However, in this hypothesis, *Stb6* needs to be involved, as the expression of *Tsn1* and *Thf1* was not affected in the genotype Courtot. Moreover, ToxA has also been shown to be light-dependent (Manning et al., 2010) and therefore the XC could also be involved, as described above, however there were no differences observed for ZEP and VDE between the genotypes and treatments, apart from their downregulation compared to the H_2O control. Finally, compatible *Tsn1*-ToxA interaction was found to activate calmodulins (CaM) and phosphatases (PP2Cs) (Adhikari et al., 2009), which were also found to be upregulated in our studies (Chapter 3) in Ct (+Stb6) inoculated with the virulent isolate Zt22.

Pycnidia production was not affected and all compatible interactions resulted in pycnidia formation at approximately 14dai. Although they appeared to be reduced in numbers, it could not be deduced whether it was an effect of the toxin infiltrations or whether the plants were much older, lacking nutrients or being compromised by that point. However, if it was an effect of the toxins and the induced necrosis, it could indicate that *Z. tritici* requires the latent phase in the apoplast in order to then trigger the switch to necrotrophy. Repetition of this experiment is currently ongoing to confirm these results. It would be interesting to test the opposite, whether toxin infiltrations first (and thus necrosis), followed by *Z. tritici* inoculations, would accelerate the production of pycnidia, indicating that *Z. tritici* needs the necrotrophic switch to sporulate but not necessary the prolonged latent phase.

It was interesting to observe the appearance of symptoms on IPO323 +*Stb6* plants that were subsequently infiltrated with H_2O. *Stb6*-mediated resistance is characterised by the complete absence of necrosis and only slight amount of chlorosis. It is not yet clear why this could have happened but one hypothesis could be that the wounding event from the infiltration initiated a HR signal and PCD that overcame the incompatible interaction between *AvrStb6* and *Stb6*. Another hypothesis could suggest that water infiltration also allowed a faster, forced entrance of *Z. tritici* spores inside the mesophyll, thus suggesting that *Stb6* could be located on the guard cells of the stomata and *AvrStb6* recognition takes place there. Stomata could be particularly important in defence against *Z. tritici*. They are linked with the circadian rhythm and phytochrome perception of different wavelengths of light, as in the case of the light-dependent Tox1 and ToxA (Roden & Ingle, 2009; Courbier & Pierik, 2019), they have been linked with *Thf1* (Hong et al., 2020) and malate, which is produced either by pathogens such *P. nodorum* and *P. tritici-repentis* (Solomon et al., 2004; Pandelova et al., 2012) or in the plant and accumulate in the chloroplast causing cell death (Ding et al., 2018) and are overall considered as the first barrier of immunity against pathogen invasion (Melotto et al., 2008). Ajigboye et al. (2021) also found that a *Z. tritici* resistant genotype had lower stomatal density yet rapid aperture kinetics than the susceptible genotype and elevated levels of ABA, a hormone directly linked with stomatal function (Chater et al., 2014). Future work is required to further investigate the precise role of stomata in defence against *Z. tritici*.

Chapter 5 General Discussion

5.1 Main Findings

In this thesis, I have investigated the connection between the pathogen *Zymoseptoria tritici*, causing Septoria Tritici Blotch (STB) in wheat, and chloroplastic photoprotective processes. The chloroplast is a key player in defence response and regulation, however very little is known about photoprotection, *Stb6* and resistance to *Z. tritici*.

A novel investigation utilising PsbS over-expressing wheat lines, that also contained the resistance gene *Stb6*, and a range of *Z. tritici* isolates that differed in virulence were used to determine the effect of the photoprotective protein PsbS in resistance to *Zymoseptoria tritici*. Wheat plants with high, "primed" NPQ in the form of qE resulted in enhanced tolerance to the majority of virulent isolates, manifested as maintained green area on the leaf tissue, reduced necrosis and reduced pycnidia formation. Upon inoculation at 24hai, qE dropped but remained higher than the controls and no superoxide was observed. As most studies investigate PsbS based on NPQ response or have utilised knockout lines, it was difficult to draw firm conclusions on the mechanism of overexpressing PsbS in relation to disease resistance. However, results on *Stb6,* discussed in **Chapter 3,** also demonstrated a reduction in qE and PsbS in the interaction with the avirulent isolate (IPO323), and a similar decrease in PsbS and downregulation of light-harvesting antenna proteins in the interaction with the virulent isolate (Zt22), with no significant superoxide being detected in either case. It is well known that plants temporarily switch off their primary metabolism to initiate their defence responses against pathogens (Figueroa-Macías et al., 2021). In **Chapter 2**, the OX lines were also characterised by reduced stomatal conductance and φPSII. Also, PsbS acts synergistically with the carotenoid zeaxanthin to bind to several proposed LHC proteins and together they allow for changes in the membrane organisation and dynamics. It could therefore be possible that by over-expressing PsbS, there is no trade-off between production of assimilates and defence. PsbS over-expression could allow for the necessary re-organisation of PSII in response to *Z. tritici*, while also maintaining certain

features of the machinery intact to keep an active Calvin cycle, since there were no significant reductions in photosynthetic assimilation in this work. Over-expressing PsbS also has an impact on ROS production, as PsbS knockouts exhibit increased amounts of superoxide (Zulfugarov et al., 2014). As seen in **Chapter 3**, *Stb6* has increased detoxification capacity. Although the isolates used in **Chapter 2** are virulent in *Stb6*, it may also be possible that both the presence of *Stb6* and more PsbS allowed for energy re-distribution in the photosynthetic machinery, through reduced φPSII. Additionally, PsbS knockouts have been associated with elevated levels of jasmonic acid-related compounds, through increased ROS production and subsequent lipid peroxidation. Therefore, it could also be possible that by over-expressing PsbS, salicylic acid is more prevalent, as it is normally antagonistic to jasmonic acid. Salicylic acid also regulates light acclimatory processes and is interconnected with redox changes in the chloroplast (Karpinski et al., 2003). Finally, it is likely that PsbS assists in the repair cycle of PSII, similar to *Thf1* which was downregulated in response to the virulent isolate Zt22 in **Chapter 4**, therefore PsbS-overexpression could be compensating for the reduction of *Thf1* and allow for efficient repair and ultimately reduced disease due to virulent *Z. tritici* isolates.

Wheat resistance to *Z. tritici* in relation to the chloroplast has only been investigated in two other studies. Lee et al. (2015) showed how a mutation in two chloroplastic genes involved in carotenoid and chlorophyll biosynthesis rendered *Stb6*-containing genotypes susceptible to *Z. tritici*. Recently, Ajigboye et al. (2021) demonstrated the role of photoprotection in response to *Z. tritici* in two contrasting genotypes, resistant and susceptible, and explained the importance of the different components of NPQ and the xanthophyll cycle in disease resistance. In this study, I used Near-Isogenic Lines of *Stb6* to allow for precise description of my results due to the presence or absence of *Stb6* in the same genetic background. The *Stb6* resistance gene is one of only two *Z. tritici* resistance genes currently cloned and therefore presents a promising insight into the mechanism of STB resistance in wheat. Using detailed physiological measurements and RNA sequencing, I was able to demonstrate the importance of the photoprotective mechanism for *Stb6*-mediated

resistance. Downregulation of photoprotection in the form of qE (and PsbS) and enhanced transient photoinhibition in the form of qI very early in the disease progression (24hai) allows the chloroplast to re-organise and re-balance the energy distribution and initiate the defence mechanism. Through this energy balancing, *Stb6* is also able to fine-tune ROS production either via enhanced detoxification from chloroplastic enzymes, temporary downregulation of the oxygen-evolving complex and activation of a functional β-carotene-derived XC. It is also possible that *Stb6* is utilising the salicylic acid hormonal pathway at 24hai, based on gene expression analysis, which is interconnected with redox changes and repair processes in the chloroplast, potentially exploring a similar response as the PsbS over-expressers as hypothesised in **Chapter 2**.

Transcriptomic analysis in **Chapter 3** between two different *Z. tritici* isolates at the early disease stages highlighted the capability of *Stb6* to recognise the invasive pathogen and trigger the downstream events. Although *Stb6* was not found differentially expressed in this study, *AvrStb6* can be expressed throughout the latent period before peaking in the switch to necrotrophy (Zhong et al., 2017). *Stb6* physiological responses with gas exchange and chlorophyll fluorescence analysis exhibited several similarities between the virulent isolate Zt22 and the avirulent IPO323. However, it was only in the resistance response that protective photoinhibition played a significant role. In contrast, the response to the virulent Zt22 was associated with PAMP-triggered responses, suggesting that as early as 24hai, effector-triggered immunity (ETI) could have already been triggered in the incompatible interaction between *Stb6* and IPO323. Moreover, it was in response to the virulent isolate that susceptibility genes involved in other pathosystems appeared in the results. **Chapter 4** investigated the impact of *Z. tritici* inoculations in antagonising effectors from another foliar fungal pathogen, *Parastagonospora nodorum*, with the aim to understand *Z. tritici* infection strategies towards the chloroplast. Zt22 in the presence of *Stb6* could be targeting the same sensitivity gene as Tox1, *Snn1*, while involving the xanthophyll cycle for energy dissipation and ROS avoidance. Similarly, ZEP expression and Zea were upregulated in *Stb6* plants inoculated with Zt22 in

Chapter 3, with no significant conversion to Vio or Neo and no dissipation through qE, while the VDE was upregulated when *Stb6* plants were inoculated with Zt22 and infiltrated with Tox1 in **Chapter 4**. Therefore, there is a possibility that *Z. tritici* targets and/or antagonises the XC, whereas over-expressing PsbS (**Chapter 2**) compensates for the energy imbalance and results in *Z. tritici* tolerance. On the other hand, by the time of Tox1 or ToxA infiltrations in IPO323-inoculated *Stb6* plants, there is photoinhibition taking place in the chloroplast during the incompatible response, as discussed in **Chapter 3**, and therefore the Tox1/A-generated ROS led to total tissue collapse. The work in **Chapter 4** is being repeated for confirmation and no firm conclusions can yet be drawn, however evidence so far point to the hypothesis that Zt22 virulence exploits chloroplastic processes for its own benefit.

Overall, through this work I have demonstrated the importance of the chloroplast and specific photoprotective mechanisms in response to *Zymoseptoria tritici* infections. Resistance involved the disassembly and re-organisation of the photosynthetic machinery, while susceptibility requires impaired chloroplastic processes for the initiation of defence.

5.2 Recommendations for future studies

- This work resulted in some very interesting findings that generated several ideas for future studies. In **Chapter 2**, a few ideas for further work have been discussed there. However, the major further investigations could include Virus Induced Gene Silencing (VIGS), to transiently silence PsbS, and analysis of carotenoids, pathogenesis- and hormone-related genes. VIGS was planned, pre-pandemic, to be performed towards the end of my experimental work. However, this was no longer possible in the end due to limited time under strict laboratory Covid rules as well as relocation of my third supervisor to a new position in a different institute. In the future, silencing PsbS and performing similar phenotyping measurements in order to observe whether loss of resistance would occur, could further pinpoint the role of PsbS in disease response to *Z. tritici*. Moreover, as PsbS is tightly linked with the carotenoid zeaxanthin and there are indications of its involvement with hormones such as ABA and JA, carotenoid and hormone

analysis would allow an in-depth investigation of the mechanism of over-expressing PsbS in relation to *Z. tritici* infections.

- RNA sequencing in **Chapter 3** did not identify any candidate genes, partly due to delays occurring during the pandemic and partly due to not applying a cut-off in the fold change of differentially expressed genes. However, continued exploration into the transcriptomic data may result in the identification of candidate gene(s) suitable for VIGS and the subsequent characterisation of their function in relation to photoprotection and *Z. tritici* resistance. Moreover, another bioinformatics approach could be adopted that would enable us to observe transcriptional changes over-time, through clustering analysis across the different time points used in this study. Furthermore, there were strong indications from the transcriptomic data that photosystem I (PSI) could also play a role in *Stb6*-mediated resistance, such as downregulation of PSI light-harvesting complex antenna proteins and downregulation of ferredoxin and ferredoxin oxidoreductase. Ferredoxin is also used as a substrate for ZEP catalysis, therefore supporting the idea of PSI involvement in *Stb6* resistance. Measurements on functionality and activity of PSI of inoculated plants could provide indications of its involvement in *Z. tritici* resistance. Additionally, other physiological processes such as photorespiration, which appeared as a GO term in the transcriptomic data, and the role of stomata could be explored in the future. Specifically, the stomata have been described as the first barrier of resistance against a variety of pathogens and have a direct impact on NPQ responses and chloroplastic signalling. In this work, we also observed loss of resistance and induction of HR in response to H_2O infiltration upon IPO323 inoculation, suggesting the possibility that *Stb6* could be located in, or, in close proximity to the stomata guard cells, thus infiltration bypassing *Stb6*/stomata recognition. Microscopic studies on *Stb6* genotypes have indicated stomatal closure upon contact with the germinating hyphae of *AvrStb6*-containing *Z. tritici* (Andrea Sánchez-Vallet, Dublin ISCLB 2019 presentation and personal communication). With this work, stomatal responsiveness to light was measured, which was not impaired in the *Stb6* line, however there are several methods with which

stomata limitations could be explored, such as high CO_2 gas exchange or low light measurements on inoculated plants. Additionally, there are several established methods using chemical inhibitors that would allow the separation of different photoprotective components and therefore pinpoint the exact mechanism by which photoprotection through *Stb6* operates. For example, dithiothreitol (DTT) inhibits the xanthophyll cycle enzyme VDE and therefore contribution of qE and qI components of NPQ can be separated, or treatment with DCMU that blocks the electron transport chain, which would lead to superoxide production, and therefore help to identify as to whether *Stb6* maintains the detoxification capacity. Enzyme assays or antioxidant quantifications could replace tissue staining for a more accurate estimation of reactive oxygen species. Finally, this study was only able to measure gene expression of some hormone-related genes, however hormone quantification and metabolomics would complete the resistance profile of *Stb6* in relation to photoprotection and the chloroplast.

- The work in **Chapter 4** is still at the very early stages and repetition of my results is first needed to establish the correct phenotype. Microscopy studies with fluorescent strains of both *Z. tritici* and *P. nodorum* could help elucidate the interactions taking place in our experimental design. Finally, as the necrotrophic effectors are light-dependent, experiments with low and high light intensities could be performed, followed by gene expression analysis.

5.3 Final conclusions

Our understanding of plant immunity has progressed rapidly over the past 30 years, with the cloning of plant disease resistance (R) proteins, discovery of new PTI- and ETI-related molecules and an ever-growing list of signalling kinases and transcription factors. However, only recently a pivotal and previously underappreciated role for chloroplasts in elaborating a variety of plant immune responses has emerged. Apart from oxygenic photosynthesis and primary metabolism, chloroplasts, as the metabolic powerhouses of cells, are capable of integrating, decoding and responding to environmental signals

through complex reprogramming of primary and secondary metabolite synthesis, while also communicate via a diversity of retrograde signals to the nucleus. They contribute not only to *de novo* synthesis of defence phytohormones but also to the generation of ROS, which are indispensable for proper growth and development. Specifically Photosystem II is a highly dynamic and sophisticated complex of proteins, that plays a central role in integrating multiple environmental stimuli. Moreover, a growing list of publications now reports findings on pathogens deploying effector proteins that directly or indirectly target chloroplasts to weaken chloroplast immunity.

We are only just beginning to appreciate the critical role of chloroplasts in plant immune responses and the mechanism of contribution of the photosystems in defence. A better understanding of chloroplast biology or how pathogens have evolved to target chloroplast immunity, may help develop more resilient crops and provide new ideas for developing powerful strategies for achieving a more sustainable crop production in the future. This thesis aimed to contribute and broaden our knowledge on chloroplast-mediated plant defence.

Chapter 6 References

Adhikari, T. B., Bai, J., Meinhardt, S. W., Gurung, S., Myrfield, M., Patel, J., Ali, S., Gudmestad, N. C., & Rasmussen, J. B. (2009). Tsn1-Mediated Host Responses to ToxA from *Pyrenophora tritici-repentis*. *Molecular Plant-Microbe Interactions*, 22 (9), 1056–1068. DOI: 10.1094/MPMI-22-9-1056

Adhikari, T. B., Cavaletto, J. R., Dubcovsky, J., Gieco, J. O., Schlatter, A. R., & Goodwin, S. B. (2004a). Molecular Mapping of the *Stb4* Gene for Resistance to Septoria tritici Blotch in Wheat. *Phytopathology*, 94 (11), 1198–1206. https://doi.org/10.1094/PHYTO.2004.94.11.1198

Adhikari, T. B., Yang, X., Cavaletto, J. R., Hu, X., Buechley, G., Ohm, H. W., Shaner, G., & Goodwin, S. B. (2004b). Molecular mapping of *Stb1*, a potentially durable gene for resistance to septoria tritici blotch in wheat. *Theoretical and Applied Genetics*, 109 (5), 944–953. https://doi.org/10.1007/s00122-004-1709-6

Afzal, F., Khurshid, R., Ashraf, M., & Gul Kazi, A. (2014). Reactive Oxygen Species and Antioxidants in Response to Pathogens and Wounding. In *Oxidative Damage to Plants: Antioxidant Networks and Signaling*, 397–424. https://doi.org/10.1016/B978-0-12-799963-0.00013-7

Ahn, T. K., Avenson, T. J., Ballottari, M., Cheng, Y. C., Niyogi, K. K., Bassi, R., & Fleming, G. R. (2008). Architecture of a charge-transfer state regulating light harvesting in a plant antenna protein. *Science*, 320 (5877), 794–797. https://doi.org/10.1126/science.1154800

Ajigboye, O. O., Jayaweera, D. P., Angelopoulou, D., Ruban, A. V., Murchie, E. H., Pastor, V., Summers, R., & Ray, R. V. (2021). The role of photoprotection in defence of two wheat genotypes against *Zymoseptoria tritici*. *Plant Pathology*, 70 (6), 1421–1435. https://doi.org/10.1111/ppa.13392

Alscher, R. G., Erturk, N., & Heath, L. S. (2002). Role of superoxide dismutases (SODs) in controlling oxidative stress in plants. *Journal of Experimental Botany* 53 (372), 1331-1341. https://doi.org/10.1093/jexbot/53.372.1331

Apel, K., & Hirt, H. (2004). Reactive oxygen species: Metabolism, oxidative stress, and signal transduction. *Annual Review of Plant Biology*, 55, 373–399. https://doi.org/10.1146/annurev.arplant.55.031903.141701

Arraiano, L. S., Balaam, N., Fenwick, P. M., Chapman, C., Feuerhelm, D., Howell, P., Smith, S. J., Widdowson, J. P. & Brown, J. K. M. (2009). Contributions of disease resistance and escape to the control of septoria tritici blotch of wheat. *Plant Pathology* 58 (5), 910–922. https://doi.org/10.1111/j.1365-3059.2009.02118.x

Arraiano, L. S., & Brown, J. K. M. (2006). Identification of isolate-specific and partial resistance to septoria tritici blotch in 238 European wheat cultivars and breeding lines. *Plant Pathology*, 55 (6), 726–738. https://doi.org/10.1111/j.1365-3059.2006.01444.x

Asada, K. (1999). THE WATER-WATER CYCLE IN CHLOROPLASTS: Scavenging of Active Oxygens and Dissipation of Excess Photons. *Annual Review of Plant Physiology and Plant Molecular Biology*, 50, 601-639. https://doi.org/10.1146/annurev.arplant.50.1.601

Asada, K. (2006). Production and scavenging of reactive oxygen species in chloroplasts and their functions. *Plant Physiology*, 141 (2), 391–396. https://doi.org/10.1104/pp.106.082040

Baker, N. R. (2008). Chlorophyll fluorescence: A probe of photosynthesis in vivo. *Annual Review of Plant Biology*, 59, 89–113. https://doi.org/10.1146/annurev.arplant.59.032607.092759

Ballaré, C. L. (2014). Light regulation of plant defense. *Annual Review of Plant Biology*, 65, 335–363. https://doi.org/10.1146/annurev-arplant-050213-040145

Bebber, D. P., Ramotowski, M. A. T., & Gurr, S. J. (2013). Crop pests and pathogens move polewards in a warming world. *Nature Climate Change*, 3 (11), 985–988. https://doi.org/10.1038/nclimate1990

Bechtold, U., Karpinski, S., & Mullineaux, P. M. (2005). The influence of the light environment and photosynthesis on oxidative signalling responses in plant-biotrophic pathogen interactions. *Plant, Cell and Environment*, 28 (8), 1046-1055. https://doi.org/10.1111/j.1365-3040.2005.01340.x

Bechtold, U., Richard, O., Zamboni, A., Gapper, C., Geisler, M., Pogson, B., Karpinski, S., & Mullineaux, P. M. (2008). Impact of chloroplastic- and extracellular-sourced ROS on high light-responsive gene expression in Arabidopsis. *Journal of Experimental Botany*, 59 (2), 121–133. https://doi.org/10.1093/jxb/erm289

Belgio, E., Johnson, M. P., Jurić, S., & Ruban, A. V. (2012). Higher plant photosystem II light-harvesting antenna, not the reaction center, determines the excited-state lifetime - Both the maximum and the non-photochemically quenched. *Biophysical Journal*, 102 (12), 2761–2771. https://doi.org/10.1016/j.bpj.2012.05.004

ben M'Barek, S., Cordewener, J. H. G., van der Lee, T. A. J., America, A. H. P., Mirzadi Gohari, A., Mehrabi, R., Hamza, S., de Wit, P. J. G. M., & Kema, G. H. J. (2015). Proteome catalog of *Zymoseptoria tritici* captured during pathogenesis in wheat. *Fungal Genetics and Biology*, 79, 42–53. https://doi.org/10.1016/j.fgb.2015.04.018

Bouwmeester, K., & Govers, F. (2009). Arabidopsis L-type lectin receptor kinases: Phylogeny, classification, and expression profiles. *Journal of Experimental Botany*, 60 (15), 4383–4396. https://doi.org/10.1093/jxb/erp277

Boyd, L. A., Ridout, C., O'Sullivan, D. M., Leach, J. E., & Leung, H. (2013). Plant-pathogen interactions: Disease resistance in modern agriculture. *Trends in Genetics*, 29 (4), 233–240. https://doi.org/10.1016/j.tig.2012.10.011

Brading, P. A, Verstappen, E. C. P., Kema, G. H. J., & Brown, J. K. M. (2002). A Gene-for-Gene Relationship Between Wheat and *Mycosphaerella graminicola*, the Septoria Tritici Blotch Pathogen. *Phytopathology*, 92 (4), 439–445. https://doi.org/10.1094/PHYTO.2002.92.4.439

Breen, S., Williams, S. J., Winterberg, B., Kobe, B., & Solomon, P. S. (2016). Wheat PR-1 proteins are targeted by necrotrophic pathogen effector proteins. *Plant Journal*, 88 (1), 13–25. https://doi.org/10.1111/tpj.13228

Breseghello, F. & Siqueira Guedes Coelho, A. (2013). Traditional and Modern Plant Breeding Methods with Examples in Rice (*Oryza sativa* L.). *Journal*

of Agricultural and Food Chemistry, 61 (35), 8277-8286. DOI: 10.1021/jf305531j

Brooks, M. D., Sylak-Glassman, E. J., Fleming, G. R., & Niyogi, K. K. (2013). A thioredoxin-like/β-propeller protein maintains the efficiency of light harvesting in Arabidopsis. *PNAS*, 110 (29), e2733-e2740. https://doi.org/10.1073/pnas.1305443110

Brown, J. K. M., Chartrain, L., Lasserre-Zuber, P., & Saintenac, C. (2015). Genetics of resistance to *Zymoseptoria tritici* and applications to wheat breeding. *Fungal Genetics and Biology*, 79, 33–41. https://doi.org/10.1016/j.fgb.2015.04.017

Brown, J. K. M., & Rant, J. C. (2013). Fitness costs and trade-offs of disease resistance and their consequences for breeding arable crops. *Plant Pathology*, 62 (S1), 83–95. https://doi.org/10.1111/ppa.12163

Brunner, P. C., Torriani, S. F. F., Croll, D., Stukenbrock, E. H., & McDonald, B. A. (2013). Coevolution and life cycle specialization of plant cell wall degrading enzymes in a hemibiotrophic pathogen. *Molecular Biology and Evolution*, 30 (6), 1337–1347. https://doi.org/10.1093/molbev/mst041

Busch, F. A. (2014). Opinion: The red-light response of stomatal movement is sensed by the redox state of the photosynthetic electron transport chain. *Photosynthesis Research*, 119, 131–140. https://doi.org/10.1007/s11120-013-9805-6

Caffarri, S., Tibiletti, T., Jennings, R. C., & Santabarbara, S. (2014). A Comparison Between Plant Photosystem I and Photosystem II Architecture and Functioning. *Current Protein and Peptide Science*, 15 (4), 296-331. DOI: 10.2174/1389203715666140327102218

Camejo, D., Guzmán-Cedeño, Á., & Moreno, A. (2016). Reactive oxygen species, essential molecules, during plant-pathogen interactions. *Plant Physiology and Biochemistry*, 103, 10–23. https://doi.org/10.1016/j.plaphy.2016.02.035

Ceusters, J., & van de Poel, B. (2018). Ethylene exerts species-specific and age-dependent control of photosynthesis. *Plant Physiology*, 176 (4), 2601–2612. https://doi.org/10.1104/pp.17.01706

Chartrain, L., Brading, P. A., & Brown, J. K. M. (2005). Presence of the *Stb6* gene for resistance to septoria tritici blotch (*Mycosphaerella graminicola*) in cultivars used in wheat-breeding programmes worldwide. *Plant Pathology*, 54 (2), 134–143. https://doi.org/10.1111/j.1365-3059.2005.01164.x

Chartrain, L., Brading, P. A., Makepeace, J. C., & Brown, J. K. M. (2004). Sources of resistance to septoria tritici blotch and implications for wheat breeding. *Plant Pathology*, 53 (4), 454–460. https://doi.org/10.1111/j.1365-3059.2004.01052.x

Chater, C. C. C., Oliver, J., Casson, S., & Gray, J. E. (2014). Putting the brakes on: Abscisic acid as a central environmental regulator of stomatal development. *New Phytologist*, 202 (2), 76–391. https://doi.org/10.1111/nph.12713

Che, Y., Kusama, S., Matsui, S., Suorsa, M., Nakano, T., Aro, E. M., & Ifuku, K. (2020). Arabidopsis PsbP-Like Protein 1 Facilitates the Assembly of the Photosystem II Supercomplexes and Optimizes Plant Fitness under Fluctuating Light. *Plant and Cell Physiology*, 61 (6), 1168–1180. https://doi.org/10.1093/pcp/pcaa045

Choi, Y. E., Lee, C., & Goodwin, S. B. (2016). Generation of Reactive Oxygen Species via NOXa Is Important for Development and Pathogenicity of *Mycosphaerella graminicola*. *Mycobiology*, 44 (1), 38–47. https://doi.org/10.5941/MYCO.2016.44.1.38

Ciuffetti, L. M., Manning, V. A., Pandelova, I., Betts, M. F., & Martinez, J. P. (2010). Host-selective toxins, Ptr ToxA and Ptr ToxB, as necrotrophic effectors in the *Pyrenophora tritici-repentis*-wheat interaction. *New Phytologist*, 187 (4), 911–919. https://doi.org/10.1111/j.1469-8137.2010.03362.x

Cockram, J., Scuderi, A., Barber, T., Furuki, E., Gardner, K. A., Gosman, N., Kowalczyk, R., Phan, H. P., Rose, G. A., Tan, K. C., Oliver, R. P., & Mackay, I. J. (2015). Fine-mapping the wheat Snn1 locus conferring sensitivity to the *Parastagonospora nodorum* necrotrophic effector SnTox1 using an eight founder multiparent advanced generation inter-

cross population. *G3: Genes, Genomes, Genetics*, 5 (11), 2257–2266. https://doi.org/10.1534/g3.115.021584

Cook, R. J. & Yarham, D. J. (2006). Epidemiology in sustainable systems. In: The epidemiology of plant diseases 2nd eds. Springer, Dordrecht, The Netherlands. pp. 309.

Cools, H. J., & Fraaije, B. A. (2013). Update on mechanisms of azole resistance in *Mycosphaerella graminicola* and implications for future control. *Pest Management Science*, 69 (2), 150–155. https://doi.org/10.1002/ps.3348

Courbier, S., & Pierik, R. (2019). Canopy Light Quality Modulates Stress Responses in Plants. *Cell Press*, 22, 441-452. https://doi.org/10.1016/j.isci.2019.11.035

Courbier, S., Snoek, B. L., Kajala, K., Wees, S. C. M. van, & Pierik, R. (2021). Mechanisms of far-red light-mediated dampening of defense against *Botrytis cinerea* in tomato leaves. *Plant Physiology*, 187 (3), 1250-1266. https://doi.org/10.1093/plphys/kiab354

Crouchman, S., Ruban, A. V., & Horton, P. (2006). PsbS enhances nonphotochemical fluorescence quenching in the absence of zeaxanthin. *FEBS Letters*, 580 (8), 2053–2058. https://doi.org/10.1016/j.febslet.2006.03.005

Dagdas, Y. F., Yoshino, K., Dagdas, G., Ryder, L. S., Bielska, E., Steinberg, G., & Talbot, N. J. (2012). Septin-mediated plant cell invasion by the rice blast fungus, *Magnaporthe oryzae*. *Science*, 336 (6088), 1590–1595. https://doi.org/10.1126/science.1222934

Davletova, S., Rizhsky, L., Liang, H., Shengqiang, Z., Oliver, D. J., Coutu, J., Shulaev, V., Schlauch, K., & Mittler, R. (2005). Cytosolic ascorbate peroxidase 1 is a central component of the reactive oxygen gene network of Arabidopsis. *Plant Cell*, 17 (1), 268–281. https://doi.org/10.1105/tpc.104.026971

Dean, R., van Kan, J. A. L., Pretorius, Z. A., Hammond-Kosack, K. E., di Pietro, A., Spanu, P. D., Rudd, J. J., Dickman, M., Kahmann, R., Ellis, J., & Foster, G. D. (2012). The Top 10 fungal pathogens in molecular plant

pathology. *Molecular Plant Pathology*, 13 (4), 414–430. https://doi.org/10.1111/j.1364-3703.2011.00783.x

Demmig-Adams, B., & Adams, W. W. (2006). Photoprotection in an ecological context: The remarkable complexity of thermal energy dissipation. *New Phytologist*, 172 (1), 11–21. https://doi.org/10.1111/j.1469-8137.2006.01835.x

Demmig-Adams, B., & Adams, W. W. I. (1992). Photoprotection and Other Responses of Plants to High Light Stress. *Annual Review of Plant Physiology and Plant Molecular Biology*, 43 (1), 599–626. https://doi.org/10.1146/annurev.arplant.43.1.599

Demmig-Adams, B., Cohu, C. M., Amiard, V., van Zadelhoff, G., Veldink, G. A., Muller, O., & Adams, W. W. (2013). Emerging trade-offs - impact of photoprotectants (PsbS, xanthophylls, and vitamin E) on oxylipins as regulators of development and defense. *New Phytologist*, 197 (3), 720–729. https://doi.org/10.1111/nph.12100

Demmig-Adams, B., Cohu, C. M., Muller, O., & Adams, W. W. (2012). Modulation of photosynthetic energy conversion efficiency in nature: From seconds to seasons. *Photosynthesis Research*, 113, 75–88. https://doi.org/10.1007/s11120-012-9761-6

Denancé, N., Sánchez-Vallet, A., Goffner, D., & Molina, A. (2013). Disease resistance or growth: The role of plant hormones in balancing immune responses and fitness costs. *Frontiers in Plant Science*, 4. https://doi.org/10.3389/fpls.2013.00155

Dietz, K. J., Mittler, R., & Noctor, G. (2016). Recent progress in understanding the role of reactive oxygen species in plant cell signaling. *Plant Physiology*, 171 (3), 1535–1539. https://doi.org/10.1104/pp.16.00938

Ding, P., Guo, H., & Jones, J. D. G. (2018). Deadlier than the malate. *Cell Research*, 28 (6), 609–610. https://doi.org/10.1038/s41422-018-0042-6

do Amaral, A.M., Antoniw, J., Rudd, J.J. & Hammond-Kosack, K.E. (2012). Defining the predicted protein secretome of the fungal wheat leaf pathogen *Mycosphaerella graminicola*. PLOS One, 7 (12), e49904. https://doi.org/10.1371/journal.pone.0049904

Dodds, P. N., & Rathjen, J. P. (2010). Plant immunity: Towards an integrated view of plant-pathogen interactions. *Nature Reviews Genetics*, 11, 539–548. https://doi.org/10.1038/nrg2812

Dogra, V., Duan, J., Lee, K. P., & Kim, C. (2019). Impaired PSII proteostasis triggers a UPR-like response in the var2 mutant of Arabidopsis. *Journal of Experimental Botany*, 70 (12), 3075–3088. https://doi.org/10.1093/jxb/erz151

Downie, R. C., Bouvet, L., Furuki, E., Gosman, N., Gardner, K. A., Mackay, I. J., Mantello, C. C., Mellers, G., Phan, H. T. T., Rose, G. A., Tan, K. C., Oliver, R. P., & Cockram, J. (2018). Assessing European wheat sensitivities to *Parastagonospora nodorum* necrotrophic effectors and fine-mapping the Snn3-B1 locus conferring sensitivity to the effector SnTox3. *Frontiers in Plant Science*, 9. https://doi.org/10.3389/fpls.2018.00881

Downie, R. C., Lin, M., Corsi, B., Ficke, A., Lillemo, M., Oliver, R. P., Phan, H. T. T., Tan, K-C., & Cockram, J. (2021). Septoria nodorum blotch of wheat: Disease management and resistance breeding in the face of shifting disease dynamics and a changing environment. *Phytopathology*, 111, 906-920. https://doi.org/10.1094/PHYTO-07-20-0280-RVW

Duan, J., Lee, K. P., Dogra, V., Zhang, S., Liu, K., Caceres-Moreno, C., Lv, S., Xing, W., Kato, Y., Sakamoto, W., Liu, R., Macho, A. P., & Kim, C. (2019). Impaired PSII proteostasis promotes retrograde signaling via salicylic acid. *Plant Physiology*, 180 (4), 2182–2197. https://doi.org/10.1104/pp.19.00483

Dubiella, U., Seybold, H., Durian, G., Komander, E., Lassig, R., Witte, C. P., Schulze, W. X., & Romeis, T. (2013). Calcium-dependent protein kinase/NADPH oxidase activation circuit is required for rapid defense signal propagation. *PNAS*, 110 (21), 8744–8749. https://doi.org/10.1073/pnas.1221294110

Estep, L. K., Torriani, S. F. F., Zala, M., Anderson, N. P., Flowers, M. D., Mcdonald, B. A., Mundt, C. C., & Brunner, P. C. (2015). Emergence and early evolution of fungicide resistance in North American populations of

Zymoseptoria tritici. *Plant Pathology*, 64 (4), 961–971. https://doi.org/10.1111/ppa.12314

Fantozzi, E., Kilaru, S., Gurr, S. J., & Steinberg, G. (2021). Asynchronous development of *Zymoseptoria tritici* infection in wheat. *Fungal Genetics and Biology*, 146. https://doi.org/10.1016/j.fgb.2020.103504

Färber, A., Young, A. J., Ruban, A. V., Horton, P., & Jahns, P. (1997). Dynamics of Xanthophyll-Cycle Activity in Different Antenna Subcomplexes in the Photosynthetic Membranes of Higher Plants' The Relationship between Zeaxanthin Conversion and Nonphotochemical Fluorescence Quenching. *Plant Physiology*, 115 (4), 1609-1618. doi: 10.1104/pp.115.4.1609

Faris, J. D., & Friesen, T. L. (2020). Plant genes hijacked by necrotrophic fungal pathogens. *Current Opinion in Plant Biology,* 56, 74–80. https://doi.org/10.1016/j.pbi.2020.04.003

Faris, J. D., Zhang, Z., Lu, H., Lu, S., Reddy, L., Cloutier, S., Fellers, J. P., Meinhardt, S. W., Rasmussen, J. B., Xu, S. S., Oliver, R. P., Simons, K. J., & Friesen, T. L. (2010). A unique wheat disease resistance-like gene governs effector-triggered susceptibility to necrotrophic pathogens. *PNAS*, 107 (30), 13544–13549. https://doi.org/10.1073/pnas.1004090107

Figueroa, M., Hammond-Kosack, K. E., & Solomon, P.S. (2018). A review of wheat diseases – a field perspective. *Molecular Plant Pathology*, 19 (6), 1523-1536. https://doi.org/10.1111/mpp.12618

Figueroa-Macías, J. P., García, Y. C., Núñez, M., Díaz, K., Olea, A. F., & Espinoza, L. (2021). Plant growth-defense trade-offs: Molecular processes leading to physiological changes. *International Journal of Molecular Sciences*, 22 (2), 1–18. https://doi.org/10.3390/ijms22020693

Filipe, J. A. N., & Maule, M. M. (2004). Effects of dispersal mechanisms on spatio-temporal development of epidemics. *Journal of Theoretical Biology*, 226 (2), 125–141. https://doi.org/10.1016/S0022-5193(03)00278-9

Fisher, M. C., Henk, D. A., Briggs, C. J., Brownstein, J. S., Madoff, L. C., McCraw, S. L., & Gurr, S. J. (2012). Emerging fungal threats to animal,

plant and ecosystem health. *Nature*, 484, 186–194. https://doi.org/10.1038/nature10947

Fones, H., & Gurr, S. (2015). The impact of Septoria tritici Blotch disease on wheat: An EU perspective. *Fungal Genetics and Biology*, 79, 3–7. https://doi.org/10.1016/j.fgb.2015.04.004

Fones, H. N., Bebber, D. P., Chaloner, T. M., Kay, W. T., Steinberg, G., & Gurr, S. J. (2020). Threats to global food security from emerging fungal and oomycete crop pathogens. *Nature Food*, 1, 332–342. https://doi.org/10.1038/s43016-020-0075-0

Foyer, C. H. (2018). Reactive oxygen species, oxidative signaling and the regulation of photosynthesis. *Environmental and Experimental Botany*, 154, 134–142. https://doi.org/10.1016/j.envexpbot.2018.05.003

Foyer, C. H., & Noctor, G. (2011). Ascorbate and glutathione: The heart of the redox hub. *Plant Physiology*, 155 (1), 2–18. https://doi.org/10.1104/pp.110.167569

Fraaije, B. a, Cools, H. J., Fountaine, J., Lovell, D. J., Motteram, J., West, J. S., & Lucas, J. a. (2005). Role of Ascospores in Further Spread of QoI-Resistant Cytochrome b Alleles (G143A) in Field Populations of *Mycosphaerella graminicola*. *Phytopathology*, 95 (8), 933–941. https://doi.org/10.1094/PHYTO-95-0933

Fraaije, B. A., Cools, H. J., Kim, S. H., Motteram, J., Clark, W. S., & Lucas, J. A. (2007). A novel substitution I381V in the sterol 14α-demethylase (CYP51) of *Mycosphaerella graminicola* is differentially selected by azole fungicides. *Molecular Plant Pathology*, 8 (3), 245–254. https://doi.org/10.1111/j.1364-3703.2007.00388.x

Freeman, B.C. & Beattie, G.A. (2008). An Overview of Plant Defenses against Pathogens and Herbivores. The Plant Health Instructor. DOI: 10.1094/PHI-I-2008-0226-01

Frenkel, M., Külheim, C., Jänkänpää, H. J., Skogström, O., Dall'Osto, L., Ågren, J., Bassi, R., Moritz, T., Moen, J., & Jansson, S. (2009). Improper excess light energy dissipation in Arabidopsis results in a metabolic reprogramming. *BMC Plant Biology*, 9. https://doi.org/10.1186/1471-2229-9-12

Friesen, T. L., Holmes, D. J., Bowden, R. L., & Faris, J. D. (2018). ToxA Is Present in the U.S. *Bipolaris sorokiniana* Population and Is a Significant Virulence Factor on Wheat Harboring Tsn1. *Plant Disease*, 102 (12), 2446–2452. https://doi.org/10.1094/pdis-03-18-0521-re

Friesen, T. L., Meinhardt, S. W., & Faris, J. D. (2007). The Stagonospora nodorum-wheat pathosystem involves multiple proteinaceous host-selective toxins and corresponding host sensitivity genes that interact in an inverse gene-for-gene manner. *Plant Journal*, 51 (4), 681–692. https://doi.org/10.1111/j.1365-313X.2007.03166.x

Friesen, T. L., Stukenbrock, E. H., Liu, Z., Meinhardt, S., Ling, H., Faris, J. D., Rasmussen, J. B., Solomon, P. S., McDonald, B. A., & Oliver, R. P. (2006). Emergence of a new disease as a result of interspecific virulence gene transfer. *Nature Genetics*, 38 (8), 953–956. https://doi.org/10.1038/ng1839

García-Plazaola, J. I., Esteban, R., Fernández-Marín, B., Kranner, I., & Porcar-Castell, A. (2012). Thermal energy dissipation and xanthophyll cycles beyond the Arabidopsis model. *Photosynthesis Research*, 113 (1–3), 89–103. https://doi.org/10.1007/s11120-012-9760-7

Ghaffary, S. M. T., Faris, J. D., Friesen, T. L., Visser, R. G. F., van der Lee, T. A. J., Robert, O., & Kema, G. H. J. (2012). New broad-spectrum resistance to septoria tritici blotch derived from synthetic hexaploid wheat. *Theoretical and Applied Genetics*, 124 (1), 125–142. https://doi.org/10.1007/s00122-011-1692-7

Ghosh, S., Kanwar, P., & Jha, G. (2017). Alterations in rice chloroplast integrity, photosynthesis and metabolome associated with pathogenesis of *Rhizoctonia solani*. *Scientific Reports*, 7. https://doi.org/10.1038/srep41610

Gigot, C., Saint-Jean, S., Huber, L., Maumené, C., Leconte, M., Kerhornou, B., & de Vallavieille-Pope, C. (2013). Protective effects of a wheat cultivar mixture against splash-dispersed septoria tritici blotch epidemics. *Plant Pathology*, 62 (5), 1011–1019. https://doi.org/10.1111/ppa.12012

Gill, S. S., & Tuteja, N. (2010). Reactive oxygen species and antioxidant machinery in abiotic stress tolerance in crop plants. *Plant Physiology and*

Biochemistry, 48 (12), 909–930. https://doi.org/10.1016/j.plaphy.2010.08.016

Głowacka, K., Kromdijk, J., Kucera, K., Xie, J., Cavanagh, A. P., Leonelli, L., Leakey, A. D. B., Ort, D. R., Niyogi, K. K., & Long, S. P. (2018). Photosystem II Subunit S overexpression increases the efficiency of water use in a field-grown crop. *Nature Communications*, 9 (1). https://doi.org/10.1038/s41467-018-03231-x

Göhre, V. (2015). Immune responses: Photosynthetic defence. *Nature Plants*, 1. https://doi.org/10.1038/NPLANTS.2015.79

Göhre, V., Jones, A. M. E., Sklenář, J., Robatzek, S., & Weber, A. P. M. (2012). Molecular Crosstalk Between PAMP-Triggered Immunity and Photosynthesis. *Molecular Plant-Microbe Interactions*, 25 (8), 1083–1092. doi: 10.1094/MPMI-11-11-0301

Gómez-Gómez, L. & Boller, T. (2000). FLS2: An LRR Receptor-like Kinase Involved in the Perception of the Bacterial Elicitor Flagellin in Arabidopsis. *Molecular Cell*, 5 (6): 1003-1011. doi: 10.1016/s1097-2765(00)80265-8

Goodwin, S. B. (2007). Back to basics and beyond: Increasing the level of resistance to Septoria tritici blotch in wheat. *Australasian Plant Pathology*, 36 (6), 532–538. https://doi.org/10.1071/AP07068

Goodwin, S. B., M'Barek, S. ben, Dhillon, B., Wittenberg, A. H. J., Crane, C. F., Hane, J. K., Foster, A. J., van der Lee, T. A. J., Grimwood, J., Aerts, A., Antoniw, J., Bailey, A., Bluhm, B., Bowler, J., Bristow, J., van der Burgt, A., Canto-Canché, B., Churchill, A. C. L., Conde-Ferràez, L., … Kema, G. H. J. (2011). Finished genome of the fungal wheat pathogen *Mycosphaerella graminicola* reveals dispensome structure, chromosome plasticity, and stealth pathogenesis. *PLOS Genetics*, 7 (6). https://doi.org/10.1371/journal.pgen.1002070

Goral, T. K., Johnson, M. P., Duffy, C. D. P., Brain, A. P. R., Ruban, A. V., & Mullineaux, C. W. (2012). Light-harvesting antenna composition controls the macrostructure and dynamics of thylakoid membranes in Arabidopsis. *Plant Journal*, 69 (2), 289–301. https://doi.org/10.1111/j.1365-313X.2011.04790.x

Hajiboland, R. (2014). Reactive Oxygen Species and Photosynthesis. In *Oxidative Damage to Plants: Antioxidant Networks and Signaling*, pp. 1–63. Elsevier Inc. https://doi.org/10.1016/B978-0-12-799963-0.00001-0

Hamel, L. P., Sekine, K. T., Wallon, T., Sugiwaka, Y., Kobayashi, K., & Moffett, P. (2016). The chloroplastic protein THF1 interacts with the Coiled-Coil domain of the disease resistance protein N´ and regulates light-dependent cell death. *Plant Physiology*, 171 (1), 658–674. https://doi.org/10.1104/pp.16.00234

Hammond-Kosack, K. E., & Rudd, J. J. (2008). Plant resistance signalling hijacked by a necrotrophic fungal pathogen. *Plant Signaling and Behavior*, 3 (11), 993–995. https://doi.org/10.4161/psb.6292

Hassani-Pak, K., Singh, A., Brandizi, M., Hearnshaw, J., Parsons, J. D., Amberkar, S., Phillips, A. L., Doonan, J. H., & Rawlings, C. (2021). KnetMiner: a comprehensive approach for supporting evidence-based gene discovery and complex trait analysis across species. *Plant Biotechnology Journal*, 19 (8), 1670–1678. https://doi.org/10.1111/pbi.13583

Haueisen, J., Möller, M., Eschenbrenner, C. J., Grandaubert, J., Seybold, H., Adamiak, H., & Stukenbrock, E. H. (2019). Highly flexible infection programs in a specialized wheat pathogen. *Ecology and Evolution*, 9 (1), 275–294. https://doi.org/10.1002/ece3.4724

Havaux, M. (2014). Carotenoid oxidation products as stress signals in plants. *Plant Journal*, 79 (4), 597–606. https://doi.org/10.1111/tpj.12386

Hong, Y., Wang, Z., Liu, X., Yao, J., Kong, X., Shi, H., & Zhu, J. K. (2020). Two chloroplast proteins negatively regulate plant drought resistance through separate pathways. *Plant Physiology*, 182 (2), 1007–1021. https://doi.org/10.1104/pp.19.01106

Horton, P. (2000). Prospects for crop improvement through the genetic manipulation of photosynthesis: morphological and biochemical aspects of light capture. *Journal of Experimental Botany*, 51, 475–485. https://doi.org/10.1093/jexbot/51.suppl_1.475

Horton, P., Wentworth, M., & Ruban, A.V. (2005). Control of the light harvesting function of chloroplast membranes: The LHCII-aggregation

model for non-photochemical quenching. *FEBS Letters*, 579 (20), 4201–4206. https://doi.org/10.1016/j.febslet.2005.07.003

Hou, X., Fu, A., Garcia, V. J., Buchanan, B. B., & Luan, S. (2015). Psb27: A thylakoid protein enabling Arabidopsis to adapt to changing light intensity. *PNAS*, 112 (5), 1613–1618. https://doi.org/10.1073/pnas.1424040112

Hua, D., Wang, C., He, J., Liao, H., Duan, Y., Zhu, Z., Guo, Y., Chen, Z., & Gong, Z. (2012). A plasma membrane receptor kinase, GHR1, mediates abscisic acid- and hydrogen peroxide-regulated stomatal movement in Arabidopsis. *Plant Cell*, 24 (6), 2546–2561. https://doi.org/10.1105/tpc.112.100107

Huang, W., Chen, Q., Zhu, Y., Hu, F., Zhang, L., Ma, Z., He, Z., & Huang, J. (2013). Arabidopsis thylakoid formation 1 is a critical regulator for dynamics of PSII-LHCII complexes in leaf senescence and excess light. *Molecular Plant*, 6 (5), 1673–1691. https://doi.org/10.1093/mp/sst069

Hubbart, S., Ajigboye, O. O., Horton, P., & Murchie, E. H. (2012). The photoprotective protein PsbS exerts control over CO2 assimilation rate in fluctuating light in rice. *Plant Journal*, 71 (3), 402–412. https://doi.org/10.1111/j.1365-313X.2012.04995.x

Hubbart, S., Smillie, I. R. A., Heatley, M., Swarup, R., Foo, C. C., Zhao, L., & Murchie, E. H. (2018). Enhanced thylakoid photoprotection can increase yield and canopy radiation use efficiency in rice. *Communications Biology*, 1 (1). https://doi.org/10.1038/s42003-018-0026-6

Idnurm, A., & Howlett, B. J. (2002). Isocitrate Lyase Is Essential for Pathogenicity of the Fungus *Leptosphaeria maculans* to Canola (*Brassica napus*). *EUKARYOTIC CELL*, 1 (5), 719–724. doi: 10.1128/EC.1.5.719-724.2002

Ifuku, K., Yamamoto, Y., Ono, T. A., Ishihara, S., & Sato, F. (2005). PsbP protein, but not PsbQ protein, is essential for the regulation and stabilization of photosystem II in higher plants. *Plant Physiology*, 139 (3), 1175–1184. https://doi.org/10.1104/pp.105.068643

Ikeuchi, M., Uebayashi, N., Sato, F., & Endo, T. (2014). Physiological functions of PsbS-dependent and PsbS-independent NPQ under naturally

fluctuating light conditions. *Plant and Cell Physiology*, 55 (7), 1286–1295. https://doi.org/10.1093/pcp/pcu069

Ishida, S., Morita, K. I., Kishine, M., Takabayashi, A., Murakami, R., Takeda, S., Shimamoto, K., Sato, F., & Endo, T. (2011). Allocation of absorbed light energy in PSII to thermal dissipations in the presence or absence of PsbS subunits of rice. *Plant and Cell Physiology*, 52 (10), 1822–1831. https://doi.org/10.1093/pcp/pcr119

Ishiga, Y., Ishiga, T., Wangdi, T., Mysore, K. S., & Uppalapati, S. R. (2012). NTRC and Chloroplast-Generated Reactive Oxygen Species Regulate *Pseudomonas syringae* pv. *tomato* Disease Development in Tomato and Arabidopsis. *Molecular Plant-Microbe Interactions*, 25 (3), 294–306. doi: 10.1094/MPMI-05-11-0130

Ishihara, S., Takabayashi, A., Ido, K., Endo, T., Ifuku, K., & Sato, F. (2007). Distinct functions for the two PsbP-like proteins PPL1 and PPL2 in the chloroplast thylakoid lumen of Arabidopsis. *Plant Physiology*, 145 (3), 668–679. https://doi.org/10.1104/pp.107.105866

Jahns, P., & Holzwarth, A. R. (2012). The role of the xanthophyll cycle and of lutein in photoprotection of photosystem II. *Biochimica et Biophysica Acta – Bioenergetics*. 1817 (1), 182–193. https://doi.org/10.1016/j.bbabio.2011.04.012

Jahns, P., Latowski, D., & Strzalka, K. (2009). Mechanism and regulation of the violaxanthin cycle: The role of antenna proteins and membrane lipids. *Biochimica et Biophysica Acta – Bioenergetics*, 1787 (1), 3–14. https://doi.org/10.1016/j.bbabio.2008.09.013

Jang, C., Seo, E. Y., Nam, J., Bae, H., Gim, Y. G., Kim, H. G., Cho, I. S., Lee, Z. W., Bauchan, G. R., Hammond, J., & Lim, H. S. (2013). Insights into Alternanthera mosaic virus TGB3 functions: Interactions with *Nicotiana benthamiana* PsbO correlate with chloroplast vesiculation and veinal necrosis caused by TGB3 over-expression. *Frontiers in Plant Science*, 4. https://doi.org/10.3389/fpls.2013.00005

Jeger, M. J., & Viljanen, S. L. H. (2001). The use of the area under the disease-progress curve (AUDPC) to assess quantitative disease resistance in crop

cultivars. *Theoretical and Applied Genetics*, 102 (1), 32-40. DOI: 10.1007/s001220051615

Jelenska, J., Yao, N., Vinatzer, B. A., Wright, C. M., Brodsky, J. L., & Greenberg, J. T. (2007). A J Domain Virulence Effector of *Pseudomonas syringae* Remodels Host Chloroplasts and Suppresses Defenses. *Current Biology*, 17 (6), 499–508. https://doi.org/10.1016/j.cub.2007.02.028

Jensen, P. E., Bassi, R., Boekema, E. J., Dekker, J. P., Jansson, S., Leister, D., Robinson, C., & Scheller, H. V. (2007). Structure, function and regulation of plant photosystem I. *Biochimica et Biophysica Acta – Bioenergetics*, 1767 (5), 335–352. https://doi.org/10.1016/j.bbabio.2007.03.004

Jänkänpää, J. H., Frenkel, M., Zulfugarov, I., Reichelt, M., Krieger-Liszkay, A., Mishra, Y., Gershenzon, J., Moen, J., Lee, C. H., & Jansson, S. (2013). Non-Photochemical Quenching Capacity in *Arabidopsis thaliana* Affects Herbivore Behaviour. *PLOS ONE*, 8 (1). https://doi.org/10.1371/journal.pone.0053232

Johnson, G. N. (2011). Physiology of PSI cyclic electron transport in higher plants. *Biochimica et Biophysica Acta – Bioenergetics*, 1807 (3), 384–389. https://doi.org/10.1016/j.bbabio.2010.11.009

Johnson, M. P. (2016). Photosynthesis. *Essays in Biochemistry*, 60 (3), 255–273. https://doi.org/10.1042/EBC20160016

Johnson, M. P., Goral, T. K., Duffy, C. D. P., Brain, A. P. R., Mullineaux, C. W., & Ruban, A. V. (2011). Photoprotective energy dissipation involves the reorganization of photosystem II light-harvesting complexes in the grana membranes of spinach chloroplasts. *Plant Cell*, 23 (4), 1468–1479. https://doi.org/10.1105/tpc.110.081646

Johnson, M. P., & Ruban, A. V. (2010). Arabidopsis plants lacking PsbS protein possess photoprotective energy dissipation. *Plant Journal*, 61 (2), 283–289. https://doi.org/10.1111/j.1365-313X.2009.04051.x

Jones, A. M. E., Thomas, V., Bennett, M. H., Mansfield, J., & Grant, M. (2006). Modifications to the Arabidopsis defense proteome occur prior to significant transcriptional change in response to inoculation with

Pseudomonas syringae. *Plant Physiology*, 142 (4), 1603–1620. https://doi.org/10.1104/pp.106.086231

Jones, J. D. G., & Dangl, J. L. (2006). The plant immune system. *Nature*, 444, 323–329. https://doi.org/10.1038/nature05286

Jung, H. S., & Niyogi, K. K. (2009). Quantitative Genetic Analysis of Thermal Dissipation in Arabidopsis. *Plant Physiology*, 150 (2), 977–986. https://doi.org/10.1104/pp.109.137828

Kadota, Y., Shirasu, K., & Zipfel, C. (2015). Regulation of the NADPH Oxidase RBOHD during Plant Immunity. *Plant and Cell Physiology*, 56 (8), 1472–1480. https://doi.org/10.1093/pcp/pcv063

Kadota, Y., Sklenar, J., Derbyshire, P., Stransfeld, L., Asai, S., Ntoukakis, V., Jones, J. D., Shirasu, K., Menke, F., Jones, A., & Zipfel, C. (2014). Direct Regulation of the NADPH Oxidase RBOHD by the PRR-Associated Kinase BIK1 during Plant Immunity. *Molecular Cell*, 54 (1), 43–55. https://doi.org/10.1016/j.molcel.2014.02.021

Kaku, H., Nishizawa, Y., Ishii-Minami, N., Akimoto-Tomiyama, C., Dohmae, N., Takio, K., Minami, E., Shibuya, N., & Clarence Ryan, by A. (2006). Plant cells recognize chitin fragments for defense signaling through a plasma membrane receptor. *PNAS*, 103 (29), 11086-11091. https://doi.org/10.1073/pnas.0508882103

Kangasjärvi, S., Neukermans, J., Li, S., Aro, E. M., & Noctor, G. (2012). Photosynthesis, photorespiration, and light signalling in defence responses. *Journal of Experimental Botany* 63 (4), 1619–1636. https://doi.org/10.1093/jxb/err402

Kanyuka, K., & Rudd, J. J. (2019). Cell surface immune receptors: the guardians of the plant's extracellular spaces. *Current Opinion in Plant Biology*, 50, 1–8. https://doi.org/10.1016/j.pbi.2019.02.005

Karpinski, S., Gabrys, H., Mateo, A., Karpinska, B., & Mullineaux, P. M. (2003). Light perception in plant disease defence signalling. *Current Opinion in Plant Biology*, 6 (4), 390–396. https://doi.org/10.1016/S1369-5266(03)00061-X

Kasajima, I., Ebana, K., Yamamoto, T., Takahara, K., Yano, M., Kawai-Yamada, M., & Uchimiya, H. (2011). Molecular distinction in genetic

regulation of nonphotochemical quenching in rice. *PNAS*, 108 (33), 13835–13840. https://doi.org/10.1073/pnas.1104809108

Kawahara, Y., de la Bastide, M., Hamilton, J. P., Kanamori, H., Mccombie, W. R., Ouyang, S., Schwartz, D. C., Tanaka, T., Wu, J., Zhou, S., Childs, K. L., Davidson, R. M., Lin, H., Quesada-Ocampo, L., Vaillancourt, B., Sakai, H., Lee, S. S., Kim, J., Numa, H., … Matsumoto, T. (2013). Improvement of the *Oryza sativa* nipponbare reference genome using next generation sequence and optical map data. *Rice*, 6 (1), 3–10. https://doi.org/10.1186/1939-8433-6-4

Kellner, R., Bhattacharyya, A., Poppe, S., Hsu, T. Y., Brem, R. B., & Stukenbrock, E. H. (2014). Expression profiling of the wheat pathogen *Zymoseptoria tritici* reveals genomic patterns of transcription and host-specific regulatory programs. *Genome Biology and Evolution*, 6 (6), 1353–1365. https://doi.org/10.1093/gbe/evu101

Kema, G. H. J., Yu, D., Rijkenberg, F. H. J., Shaw, M. W., & Baayen R. P. (1996). Histology of pathogenesis of *Mycosphaerella graminicola* in wheat. *Phytopathology* 7: 777–786.

Kema, G. H. J., Mirzadi Gohari, A., Aouini, L., Gibriel, H. A. Y., Ware, S. B., van den Bosch, F., Manning-Smith, R., Alonso-Chavez, V., Helps, J., ben M'Barek, S., Mehrabi, R., Diaz-Trujillo, C., Zamani, E., Schouten, H. J., van der Lee, T. A. J., Waalwijk, C., de Waard, M. A., de Wit, P. J. G. M., Verstappen, E. C. P., … Seidl, M. F. (2018). Stress and sexual reproduction affect the dynamics of the wheat pathogen effector AvrStb6 and strobilurin resistance. *Nature Genetics*, 50 (3), 375–380. https://doi.org/10.1038/s41588-018-0052-9

Keon, J., Antoniw, J., Carzaniga, R., Deller, S., Ward, J. L., Baker, J. M., Beale, M. H., Hammond-Kosack, K., & Rudd, J. J. (2007). Transcriptional Adaptation of *Mycosphaerella graminicola* to Programmed Cell Death (PCD) of Its Susceptible Wheat Host. *Molecular Plant-Microbe Interactions*, 20 (2), 178–193. doi: 10.1094/MPMI-20-2-0178

Kereïche, S., Kiss, A. Z., Kouřil, R., Boekema, E. J., & Horton, P. (2010). The PsbS protein controls the macro-organisation of photosystem II

complexes in the grana membranes of higher plant chloroplasts. *FEBS Letters*, 584 (4), 759–764. https://doi.org/10.1016/j.febslet.2009.12.031

Kettles, G. J., Bayon, C., Canning, G., Rudd, J. J., & Kanyuka, K. (2017). Apoplastic recognition of multiple candidate effectors from the wheat pathogen *Zymoseptoria tritici* in the nonhost plant *Nicotiana benthamiana*. *New Phytologist*, 213 (1), 338–350. https://doi.org/10.1111/nph.14215

Kettles, G. J., & Kanyuka, K. (2016). Dissecting the molecular interactions between wheat and the fungal pathogen *Zymoseptoria tritici*. *Frontiers in Plant Science*, 7 (4). https://doi.org/10.3389/fpls.2016.00508

Kildea, S., Byrne, J. J., Cucak, M., & Hutton, F. (2020). First report of virulence to the septoria tritici blotch resistance gene Stb16q in the Irish *Zymoseptoria tritici* population. *New Disease Reports*, 41 (1), 13–13. https://doi.org/10.5197/j.2044-0588.2020.041.013

Kim, T. H., Böhmer, M., Hu, H., Nishimura, N., & Schroeder, J. I. (2010). Guard cell signal transduction network: Advances in understanding abscisic acid, CO2, and Ca2+ signaling. *Annual Review of Plant Biology*, 61, 561–591. https://doi.org/10.1146/annurev-arplant-042809-112226

Kimura, S., Waszczak, C., Hunter, K., & Wrzaczek, M. (2017). Bound by fate: The role of reactive oxygen species in receptor-like kinase signaling. *Plant Cell*, 29 (4), 638–654. https://doi.org/10.1105/tpc.16.00947

Kiss, A. Z., Ruban, A. V., & Horton, P. (2008). The PsbS protein controls the organization of the photosystem II antenna in higher plant thylakoid membranes. *Journal of Biological Chemistry*, 283 (7), 3972–3978. https://doi.org/10.1074/jbc.M707410200

Kobayashi, M., Yoshioka, M., Asai, S., Nomura, H., Kuchimura, K., Mori, H., Doke, N., & Yoshioka, H. (2012). StCDPK5 confers resistance to late blight pathogen but increases susceptibility to early blight pathogen in potato via reactive oxygen species burst. *New Phytologist*, 196 (1), 223–237. https://doi.org/10.1111/j.1469-8137.2012.04226.x

Kono, M., & Terashima, I. (2016). Elucidation of photoprotective mechanisms of PSI against fluctuating light photoinhibition. *Plant and Cell Physiology*, 57 (7), 1405–1414. https://doi.org/10.1093/pcp/pcw103

Kress, E., & Jahns, P. (2017). The dynamics of energy dissipation and xanthophyll conversion in Arabidopsis indicate an indirect photoprotective role of zeaxanthin in slowly inducible and relaxing components of non-photochemical quenching of excitation energy. *Frontiers in Plant Science*, 8. https://doi.org/10.3389/fpls.2017.02094

Krieger-Liszkay, A., Fufezan, C., & Trebst, A. (2008). Singlet oxygen production in photosystem II and related protection mechanism. *Photosynthesis Research*, 98, 551–564. https://doi.org/10.1007/s11120-008-9349-3

Kwak, J. M., Mori, I. C., Pei, Z-M., Leonhardt, N., Torres, M. A., Dangl, J. L., Bloom, R. E., Bodde, S., Jones, J. D. G., & Schroeder, J. I. (2003) NADPH oxidase AtrbohD and AtrbohF genes function in ROS-dependent ABA signaling in Arabidopsis. *The EMBO Journal*, 22 (11), 2623-2633. doi: 10.1093/emboj/cdg277

Latgé, J. P. (2010). Tasting the fungal cell wall. *Cellular Microbiology*, 12 (7), 863–872). https://doi.org/10.1111/j.1462-5822.2010.01474.x

Le, M. H., Cao, Y., Zhang, X. C., & Stacey, G. (2014). LIK1, a CERK1-interacting kinase, regulates plant immune responses in Arabidopsis. *PLOS ONE*, 9 (7). https://doi.org/10.1371/journal.pone.0102245

le Marquer, M., San Clemente, H., Roux, C., Savelli, B., & Frei Dit Frey, N. (2019). Identification of new signalling peptides through a genome-wide survey of 250 fungal secretomes. *BMC Genomics*, 20. https://doi.org/10.1186/s12864-018-5414-2

le Roux, C., Huet, G., Jauneau, A., Camborde, L., Trémousaygue, D., Kraut, A., Zhou, B., Levaillant, M., Adachi, H., Yoshioka, H., Raffaele, S., Berthomé, R., Couté, Y., Parker, J. E., & Deslandes, L. (2015). A receptor pair with an integrated decoy converts pathogen disabling of transcription factors to immunity. *Cell*, 161 (5), 1074–1088. https://doi.org/10.1016/j.cell.2015.04.025

Lee, W. S., Devonshire, B. J., Hammond-Kosack, K. E., Rudd, J. J., & Kanyuka, K. (2015). Deregulation of plant cell death through disruption of chloroplast functionality affects asexual sporulation of *Zymoseptoria tritici*

on wheat. *Molecular Plant-Microbe Interactions*, 28 (5), 590–604. https://doi.org/10.1094/MPMI-10-14-0346-R

Lee, W. S., Rudd, J. J., Hammond-Kosack, K. E., & Kanyuka, K. (2014). *Mycosphaerella graminicola* Lysm effector-mediated stealth pathogenesis subverts recognition through both cerk1 and cebip homologues in wheat. *Molecular Plant-Microbe Interactions*, 27 (3), 236–243. https://doi.org/10.1094/MPMI-07-13-0201-R

Lee, W. S., Rudd, J. J., & Kanyuka, K. (2015). Virus induced gene silencing (VIGS) for functional analysis of wheat genes involved in *Zymoseptoria tritici* susceptibility and resistance. *Fungal Genetics and Biology*, 79, 84-88. https://doi.org/10.1016/j.fgb.2015.04.006

Lehto, K., Tikkanen, M., Hiriart, J.-B., Paakkarinen, V., & Aro, E.-M. (2003). Depletion of the Photosystem II Core Complex in Mature Tobacco Leaves Infected by the Flavum Strain of Tobacco mosaic virus. *Molecular Plant-Microbe Interactions*, 16 (12), 1135-1144. DOI: 10.1094/MPMI.2003.16.12.1135

Li, X. P., Gilmore, A. M., & Niyogi, K. K. (2002a). Molecular and global time-resolved analysis of a PsbS gene dosage effect on pH- and xanthophyll cycle-dependent nonphotochemical quenching in photosystem II. *Journal of Biological Chemistry*, 277 (37), 33590–33597. https://doi.org/10.1074/jbc.M204797200

Li, X.-P., Bjo, O., Rkman, È., Shih, C., Grossman, A. R., Rosenquist, M., Jansson, S., & Niyogi, K. K. (2000). A pigment-binding protein essential for regulation of photosynthetic light harvesting. *Nature*, 403, 391-395.

Li, X.-P., Müller-Moulé, P., Gilmore, A. M., & Niyogi, K. K. (2002b). PsbS-dependent enhancement of feedback de-excitation protects photosystem II from photoinhibition. *PNAS*, 99 (23), 15222-15227. https://doi.org/10.1073/pnas.232447699

Lima Neto, M. C., Lobo, A. K. M., Martins, M. O., Fontenele, A. V., & Silveira, J. A. G. (2014). Dissipation of excess photosynthetic energy contributes to salinity tolerance: A comparative study of salt-tolerant *Ricinus communis* and salt-sensitive *Jatropha curcas*. *Journal of Plant Physiology*, 171 (1), 23–30. https://doi.org/10.1016/j.jplph.2013.09.002

Lima-Melo, Y., Kiliç, M., Aro, E. M., & Gollan, P. J. (2021). Photosystem I Inhibition, Protection and Signalling: Knowns and Unknowns. *Frontiers in Plant Science*, 12. https://doi.org/10.3389/fpls.2021.791124

Littlejohn, G. R., Breen, S., Smirnoff, N., & Grant, M. (2021). Chloroplast immunity illuminated. *New Phytologist*, 229 (6), 3088–3107. https://doi.org/10.1111/nph.17076

Liu, M., Zhang, S., Hu, J., Sun, W., Padilla, J., He, Y., Li, Y., Yin, Z., Liu, X., Wang, W., Shen, D., Li, D., Zhang, H., Zheng, X., Cui, Z., Wang, G. L., Wang, P., Zhou, B., & Zhang, Z. (2019). Phosphorylation-guarded light-harvesting complex II contributes to broad-spectrum blast resistance in rice. *PNAS*, 116 (35), 17572–17577. https://doi.org/10.1073/pnas.1905123116

Liu, Y., Ren, D., Pike, S., Pallardy, S., Gassmann, W., & Zhang, S. (2007). Chloroplast-generated reactive oxygen species are involved in hypersensitive response-like cell death mediated by a mitogen-activated protein kinase cascade. *Plant Journal*, 51 (6), 941–954. https://doi.org/10.1111/j.1365-313X.2007.03191.x

Liu, Z., Friesen, T. L., Ling, H., Meinhardt, S. W., Oliver, R. P., Rasmussen, J. B., & Faris, J. D. (2006). The Tsn1-ToxA interaction in the wheat-*Stagonospora nodorum* pathosystem parallels that of the wheat-tan spot system. *Genome*, 49 (10), 1265–1273. https://doi.org/10.1139/G06-088

Liu, Z., Gao, Y., Kim, Y. M., Faris, J. D., Shelver, W. L., de Wit, P. J. G. M., Xu, S. S., & Friesen, T. L. (2016). SnTox1, a *Parastagonospora nodorum* necrotrophic effector, is a dual-function protein that facilitates infection while protecting from wheat-produced chitinases. *New Phytologist*, 211 (3), 1052–1064. https://doi.org/10.1111/nph.13959

Liu, Z. H., Faris, J. D., Meinhardt, S. W., Ali, S., Rasmussen, J. B., & Friesen, T. L. (2004). Genetic and Physical Mapping of a Gene Conditioning Sensitivity in Wheat to a Partially Purified Host-Selective Toxin Produced by *Stagonospora nodorum*. *Phytopathology*, 94 (10), 1056-1060. DOI: 10.1094/PHYTO.2004.94.10.1056

Liu, Z., Zhang, Z., Faris, J. D., Oliver, R. P., Syme, R., McDonald, M. C., McDonald, B. A., Solomon, P. S., Lu, S., Shelver, W. L., Xu, S., & Friesen,

T. L. (2012). The cysteine rich necrotrophic effector SnTox1 produced by *Stagonospora nodorum* triggers susceptibility of wheat lines harboring Snn1. *PLOS Pathogens*, 8 (1). https://doi.org/10.1371/journal.ppat.1002467

Livak, K. J., & Schmittgen, T. D. (2001). Analysis of relative gene expression data using real-time quantitative PCR and the $2^{-\Delta\Delta CT}$ method. *Methods*, 25 (4), 402–408. https://doi.org/10.1006/meth.2001.1262

Lo Presti, L., Lanver, D., Schweizer, G., Tanaka S., Liang, L., Tollot, M., Zuccaro, A., Reissmann, S. & Kahmann, R. (2015). Fungal effectors and plant susceptibility. *Annual Review of Plant Biology*, 65, 513-545. https://doi.org/10.1146/annurev-arplant-043014-114623

Lovell, D. J., Hunter, T., Powers, S. J., Parker, S. R., & van den Bosch, F. (2004). Effect of temperature on latent period of septoria leaf blotch on winter wheat under outdoor conditions. *Plant Pathology*, 53, 170–181. Doi: 10.1111/j.1365-3059.2004.00983.x

Lovell, D. J., Parker, S. R., Hunter, T., Welham, S. J., & Nichols, A. R. (2004b). Position of inoculum in the canopy affects the risk of septoria tritici blotch epidemics in winter wheat. *Plant Pathology*, 53 (1), 11–21. https://doi.org/10.1046/j.1365-3059.2003.00939.x

Lu, S., Faris, J. D., Sherwood, R., Friesen, T. L., & Edwards, M. C. (2014). A dimeric PR-1-type pathogenesis-related protein interacts with ToxA and potentially mediates ToxA-induced necrosis in sensitive wheat. *Molecular Plant Pathology*, 15 (7), 650–663. https://doi.org/10.1111/mpp.12122

Lu, S., Gillian Turgeon, B., & Edwards, M. C. (2015). A ToxA-like protein from *Cochliobolus heterostrophus* induces light-dependent leaf necrosis and acts as a virulence factor with host selectivity on maize. *Fungal Genetics and Biology*, 81, 12–24. https://doi.org/10.1016/j.fgb.2015.05.013

Lu, Y. (2016). Identification and roles of photosystem II assembly, stability, and repair factors in Arabidopsis. *Frontiers in Plant Science*, 7 (2). https://doi.org/10.3389/fpls.2016.00168

Lu, Y., & Yao, J. (2018). Chloroplasts at the crossroad of photosynthesis, pathogen infection and plant defense. *International Journal of Molecular Sciences*, 19 (12). https://doi.org/10.3390/ijms19123900

Ma, Z., & Michailides, T. J. (2005). Advances in understanding molecular mechanisms of fungicide resistance and molecular detection of resistant genotypes in phytopathogenic fungi. *Crop Protection*, 24 (10), 853–863. https://doi.org/10.1016/j.cropro.2005.01.011

Macho, A. P., Boutrot, F., Rathjen, J. P., & Zipfel, C. (2012). ASPARTATE OXIDASE plays an important role in Arabidopsis stomatal immunity. *Plant Physiology*, 159 (4), 1845–1856. https://doi.org/10.1104/pp.112.199810

Malnoë, A. (2018). Photoinhibition or photoprotection of photosynthesis? Update on the (newly termed) sustained quenching component qH. *Environmental and Experimental Botany* 154, 123–133. https://doi.org/10.1016/j.envexpbot.2018.05.005

Manning, V. A., Chu, A. L., Scofield, S. R., & Ciuffetti, L. M. (2010). Intracellular expression of a host-selective toxin, ToxA, in diverse plants phenocopies silencing of a ToxA-interacting protein, ToxABP1. *New Phytologist*, 187 (4), 1034–1047. https://doi.org/10.1111/j.1469-8137.2010.03363.x

Manning, V. A., & Ciuffetti, L. M. (2005). Localization of Ptr ToxA produced by *Pyrenophora tritici-repentis* reveals protein import into wheat mesophyll cells. *Plant Cell*, 17 (11), 3203–3212. https://doi.org/10.1105/tpc.105.035063

Manning, V. A., Hardison, L. K., & Ciuffetti, L. M. (2007). Ptr ToxA Interacts with a Chloroplast-Localized Protein. *Molecular Plant-Microbe Interactions*, 20 (2), 168–177. https://doi.org/10.1094/MPMI-20-2-0168

Marshall, R., Kombrink, A., Motteram, J., Loza-Reyes, E., Lucas, J., Hammond-Kosack, K. E., Thomma, B. P. H. J., & Rudd, J. J. (2011). Analysis of two in planta expressed LysM effector homologs from the fungus *Mycosphaerella graminicola* reveals novel functional properties and varying contributions to virulence on wheat. *Plant Physiology*, 156 (2), 756–769. https://doi.org/10.1104/pp.111.176347

Maruta, T., Noshi, M., Tanouchi, A., Tamoi, M., Yabuta, Y., Yoshimura, K., Ishikawa, T., & Shigeoka, S. (2012). H_2O_2-triggered retrograde signaling from chloroplasts to nucleus plays specific role in response to stress. *Journal of Biological Chemistry*, 287 (15), 11717–11729. https://doi.org/10.1074/jbc.M111.292847

Mateo, A., Funck, D., Mühlenbock, P., Kular, B., Mullineaux, P. M., & Karpinski, S. (2006). Controlled levels of salicylic acid are required for optimal photosynthesis and redox homeostasis. *Journal of Experimental Botany*, 57 (8), 1795–1807. https://doi.org/10.1093/jxb/erj196

Mateo, A., Mühlenbock, P., Rustérucci, C., Chang, C. C. C., Miszalski, Z., Karpinska, B., Parker, J. E., Mullineaux, P. M., & Karpinski, S. (2004). LESION SIMULATING DISEASE 1 is required for acclimation to conditions that promote excess excitation energy. *Plant Physiology*, 136 (1), 2818–2830. https://doi.org/10.1104/pp.104.043646

Matloobi, M. (2012). Light harvesting and photosynthesis by the canopy. In *Advances in Photosynthesis - Fundamental Aspects*, pp. 235–256.

Maxwell, K., & Johnson, G. N. (2000). Chlorophyll fluorescence - a practical guide. *Journal of Experimental Botany*, 51 (345), 659–668. https://doi.org/10.1093/jexbot/51.345.659

McDonald, B. A., & Mundt, C. C. (2016). How knowledge of pathogen population biology informs management of Septoria tritici blotch. *Phytopathology*, 106 (9), 948–955. https://doi.org/10.1094/PHYTO-03-16-0131-RVW

McDonald, M. C., Ahren, D., Simpfendorfer, S., Milgate, A., & Solomon, P. S. (2018). The discovery of the virulence gene ToxA in the wheat and barley pathogen *Bipolaris sorokiniana*. *Molecular Plant Pathology*, 19 (2), 432–439. https://doi.org/10.1111/mpp.12535

Meile, L., Croll, D., Brunner, P. C., Plissonneau, C., Hartmann, F. E., McDonald, B. A., & Sánchez-Vallet, A. (2018). A fungal avirulence factor encoded in a highly plastic genomic region triggers partial resistance to septoria tritici blotch. *New Phytologist*, 219 (3), 1048–1061. https://doi.org/10.1111/nph.15180

Melotto, M., Underwood, W., Koczan, J., Nomura, K., & He, S. Y. (2006). Plant Stomata Function in Innate Immunity against Bacterial Invasion. *Cell*, 126 (5), 969–980. https://doi.org/10.1016/j.cell.2006.06.054

Melotto, M., Underwood, W., & Sheng, Y. H. (2008). Role of stomata in plant innate immunity and foliar bacterial diseases. *Annual Review of*

Phytopathology, 46, 101–122. https://doi.org/10.1146/annurev.phyto.121107.104959

Mentlak, T. A., Kombrink, A., Shinya, T., Ryder, L. S., Otomo, I., Saitoh, H., Terauchi, R., Nishizawa, Y., Shibuya, N., Thomma, B. P. H. J., & Talbot, N. J. (2012). Effector-mediated suppression of chitin-triggered immunity by *Magnaporthe oryzae* is necessary for rice blast disease. *Plant Cell*, 24 (1), 322–335. https://doi.org/10.1105/tpc.111.092957

Mersmann, S., Bourdais, G., Rietz, S., & Robatzek, S. (2010). Ethylene signalling regulates accumulation of the FLS2 receptor and is required for the oxidative burst contributing to plant immunity. *Plant Physiology*, 154 (1), 391–400. https://doi.org/10.1104/pp.110.154567

Miller, G., Suzuki, N., Rizhsky, L., Hegie, A., Koussevitzky, S., & Mittler, R. (2007). Double mutants deficient in cytosolic and thylakoid ascorbate peroxidase reveal a complex mode of interaction between reactive oxygen species, plant development, and response to abiotic stresses. *Plant Physiology*, 144 (4), 1777–1785. https://doi.org/10.1104/pp.107.101436

Mirzadi Gohari, A., Ware, S. B., Wittenberg, A. H. J., Mehrabi, R., ben M'Barek, S., Verstappen, E. C. P., van der Lee, T. A. J., Robert, O., Schouten, H. J., de Wit, P. P. J. G. M., & Kema, G. H. J. (2015). Effector discovery in the fungal wheat pathogen *Zymoseptoria tritici*. *Molecular Plant Pathology*, 16 (9), 931–945. https://doi.org/10.1111/mpp.12251

Mishra, Y., Jänkänpää, J. H., Kiss, A. Z., Funk, C., Schröder, W. P., & Jansson, S. (2012). Arabidopsis plants grown in the field and climate chambers significantly differ in leaf morphology and photosystem components. *BMC Plant Biology*, 12. https://doi.org/10.1186/1471-2229-12-6

Mittler, R., Vanderauwera, S., Gollery, M., & van Breusegem, F. (2004). Reactive oxygen gene network of plants. *Trends in Plant Science*, 9 (10), 490–498. https://doi.org/10.1016/j.tplants.2004.08.009

Miya, A., Albert, P., Shinya, T., Desaki, Y., Ichimura, K., Shirasu, K., Narusaka, Y., Kawakami, N., Kaku, H., & Shibuya, N. (2007). CERK1, a LysM receptor kinase, is essential for chitin elicitor signaling in Arabidopsis. *PNAS*, 104 (49), 19613-19618. https://doi.org/10.1073/pnas.0705147104

Morais, D., Sache, I., Suffert, F., & Laval, V. (2016). Is the onset of septoria tritici blotch epidemics related to the local pool of ascospores? *Plant Pathology*, 65 (2), 250–260. https://doi.org/10.1111/ppa.12408

Mühlenbock, P., Szechyńska-Hebda, M., Płaszczyca, M., Baudo, M., Mullineaux, P. M., Parker, J. E., Karpińska, B., & Karpińskie, S. (2008). Chloroplast signaling and lesion simulating disease1 regulate crosstalk between light acclimation and immunity in Arabidopsis. *Plant Cell*, 20 (9), 2339–2356. https://doi.org/10.1105/tpc.108.059618

Müller, P., Li, X., & Niyogi, K. K. (2001). Non-Photochemical Quenching. A Response to Excess Light Energy, *Plant Physiology*, 125 (4), 1558–1566. https://doi.org/10.1104/pp.125.4.1558

Murata, N., Allakhverdiev, S. I., & Nishiyama, Y. (2012). The mechanism of photoinhibition in vivo: Re-evaluation of the roles of catalase, α-tocopherol, non-photochemical quenching, and electron transport. *Biochimica et Biophysica Acta - Bioenergetics*, 1817 (8), 1127–1133. https://doi.org/10.1016/j.bbabio.2012.02.020

Murata, Y., Mori, I. C., & Munemasa, S. (2015). Diverse stomatal signaling and the signal integration mechanism. *Annual Review of Plant Biology*, 66, 369–392. https://doi.org/10.1146/annurev-arplant-043014-114707

Murchie, E. H. (2017). Safety conscious or living dangerously: what is the 'right' level of plant photoprotection for fitness and productivity? *Plant Cell and Environment*, 40 (8), 1239–1242. https://doi.org/10.1111/pce.12965

Murchie, E. H., Ali, A., & Herman, T. (2015). Photoprotection as a Trait for Rice Yield Improvement: Status and Prospects. *Rice*, 8 (1). https://doi.org/10.1186/s12284-015-0065-2

Murchie, E. H., & Lawson, T. (2013). Chlorophyll fluorescence analysis: A guide to good practice and understanding some new applications. *Journal of Experimental Botany*, 64 (13), 3983–3998. https://doi.org/10.1093/jxb/ert208

Murchie, E. H., & Niyogi, K. K. (2011). Manipulation of photoprotection to improve plant photosynthesis. *Plant Physiology*, 155 (1), 86–92. https://doi.org/10.1104/pp.110.168831

Murchie, E. H., & Ruban, A. V. (2020). Dynamic non-photochemical quenching in plants: from molecular mechanism to productivity. *Plant Journal*, 101 (4), 885–896. https://doi.org/10.1111/tpj.14601

Nelson, N., & Yocum, C. F. (2006). Structure and function of photosystems I and II. *Annual Review of Plant Biology*, 57, 521–565. https://doi.org/10.1146/annurev.arplant.57.032905.105350

Nguyen, Q. M., Iswanto, A. B. B., Son, G. H., & Kim, S. H. (2021). Recent advances in effector-triggered immunity in plants: New pieces in the puzzle create a different paradigm. *International Journal of Molecular Sciences*, 22 (9). MDPI. https://doi.org/10.3390/ijms22094709

Nickelsen, J., & Rengstl, B. (2013). Photosystem II assembly: From cyanobacteria to plants. *Annual Review of Plant Biology*, 64, 609–635. https://doi.org/10.1146/annurev-arplant-050312-120124

Nilkens, M., Kress, E., Lambrev, P., Miloslavina, Y., Müller, M., Holzwarth, A. R., & Jahns, P. (2010). Identification of a slowly inducible zeaxanthin-dependent component of non-photochemical quenching of chlorophyll fluorescence generated under steady-state conditions in Arabidopsis. *Biochimica et Biophysica Acta - Bioenergetics*, 1797 (4), 466–475. https://doi.org/10.1016/j.bbabio.2010.01.001

Niyogi, K. K., & Truong, T. B. (2013). Evolution of flexible non-photochemical quenching mechanisms that regulate light harvesting in oxygenic photosynthesis. *Current Opinion in Plant Biology*, 16 (3), 307–314. https://doi.org/10.1016/j.pbi.2013.03.011

Nomura, H., Komori, T., Uemura, S., Kanda, Y., Shimotani, K., Nakai, K., Furuichi, T., Takebayashi, K., Sugimoto, T., Sano, S., Suwastika, I. N., Fukusaki, E., Yoshioka, H., Nakahira, Y., & Shiina, T. (2012). Chloroplast-mediated activation of plant immune signalling in Arabidopsis. *Nature Communications*, 3. https://doi.org/10.1038/ncomms1926

O'Driscoll, A., Kildea, S., Doohan, F., Spink, J., & Mullins, E. (2014). The wheat-Septoria conflict: A new front opening up? *Trends in Plant Science*, 19 (9), 602–610. https://doi.org/10.1016/j.tplants.2014.04.011

Oerke, E. C. (2006). Crop losses to pests. *Journal of Agricultural Science*, 144 (1), 31–43. https://doi.org/10.1017/S0021859605005708

Orellana-Torrejon, C., Vidal, T., Boixel, A. L., Gélisse, S., Saint-Jean, S., & Suffert, F. (2022). Annual dynamics of *Zymoseptoria tritici* populations in wheat cultivar mixtures: A compromise between the efficacy and durability of a recently broken-down resistance gene? *Plant Pathology*, 71 (2), 289–303. https://doi.org/10.1111/ppa.13458

Orton, E. S., Deller, S., & Brown, J. K. M. (2011). *Mycosphaerella graminicola*: From genomics to disease control. *Molecular Plant Pathology*, 12 (5), 413–424. https://doi.org/10.1111/j.1364-3703.2010.00688.x

Pagán, I. & García-Arenal, F. (2018). Tolerance to Plant Pathogens: Theory and Experimental Evidence. *International Journal of Molecular Sciences*. 19 (3). https://doi.org/10.3390/ijms19030810

Pal, N., Saini, D. K., & Kumar, S. (2022). Breaking Yield Ceiling in Wheat: Progress and Future Prospects, in M. Ansari (ed.), Wheat, IntechOpen, London. 10.5772/intechopen.102919.

Palma-Guerrero, J., Torriani, S. F. F., Zala, M., Carter, D., Courbot, M., Rudd, J. J., McDonald, B. A., & Croll, D. (2016). Comparative transcriptomic analyses of *Zymoseptoria tritici* strains show complex lifestyle transitions and intraspecific variability in transcription profiles. *Molecular Plant Pathology*, 17 (6), 845–859. https://doi.org/10.1111/mpp.12333

Pandelova, I., Figueroa, M., Wilhelm, L. J., Manning, V. A., Mankaney, A. N., Mockler, T. C., & Ciuffetti, L. M. (2012). Host-selective toxins of *Pyrenophora tritici-repentis* induce common responses associated with host susceptibility. *PLOS ONE*, 7 (7). https://doi.org/10.1371/journal.pone.0040240

Papageorgiou, G. C., & Govindjee, R. (2014). The Non-Photochemical Quenching of the Electronically Excited State of Chlorophyll a in Plants: Definitions, Timelines, Viewpoints, Open Questions. In *Non-Photochemical quenching and energy dissipation in plants, algae and cyanobacteria,* pp. 1–44. https://doi.org/10.1007/978-94-017-9032-1_1

Pastori, G. M., Kiddle, G., Antoniw, J., Bernard, S., Veljovic-Jovanovic, S., Verrier, P. J., Noctor, G., & Foyer, C. H. (2003). Leaf vitamin C contents modulate plant defense transcripts and regulate genes that control

development through hormone signaling. *Plant Cell*, 15 (4), 939–951. https://doi.org/10.1105/tpc.010538

Paulus, J. K., & van der Hoorn, R. A. L. (2018). Tricked or trapped—Two decoy mechanisms in host–pathogen interactions. *PLOS Pathogens*, 14 (2). https://doi.org/10.1371/journal.ppat.1006761

Perez-Nadales, E., Almeida Nogueira, M. F., Baldin, C., Castanheira, S., el Ghalid, M., Grund, E., Lengeler, K., Marchegiani, E., Mehrotra, P. V., Moretti, M., Naik, V., Oses-Ruiz, M., Oskarsson, T., Schäfer, K., Wasserstrom, L., Brakhage, A. A., Gow, N. A. R., Kahmann, R., Lebrun, M. H., … Wendland, J. (2014). Fungal model systems and the elucidation of pathogenicity determinants. *Fungal Genetics and Biology*, 70, 42–67. https://doi.org/10.1016/j.fgb.2014.06.011

Peters Haugrud, A. R., Zhang, Z., Friesen, T. L., & Faris, J. D. (2022). Genetics of resistance to septoria nodorum blotch in wheat. *Theoretical and Applied Genetics*. https://doi.org/10.1007/s00122-022-04036-9

Petit-Houdenot, Y., Lebrun, M.-H., & Scalliet, G. (2021). Understanding plant-pathogen interactions in Septoria tritici blotch infection of cereals. In *Achieving durable disease resistance in cereals*, Burleigh Dodds Science Publishing, pp. 263–302. https://doi.org/10.19103/as.2021.0092.10

Phan, H. T. T., Rybak, K., Furuki, E., Breen, S., Solomon, P. S., Oliver, R. P., & Tan, K. C. (2016). Differential effector gene expression underpins epistasis in a plant fungal disease. *The Plant Journal: For Cell and Molecular Biology*, 87 (4), 343–354. https://doi.org/10.1111/tpj.13203

Ponomarenko, A., Goodwin, S. B., & Kema, G. H. J. (2011). Septoria tritici blotch (STB) of wheat. *Plant Health Instructor.*

Poppe, S., Dorsheimer, L., Happel, P., & Stukenbrock, E. H. (2015). Rapidly Evolving Genes Are Key Players in Host Specialization and Virulence of the Fungal Wheat Pathogen *Zymoseptoria tritici* (*Mycosphaerella graminicola*). *PLOS Pathogens*, 11 (7). https://doi.org/10.1371/journal.ppat.1005055

Porra, R. J., Thompson, W. A., & Kriedemann, P. E. (1989). Determination of accurate extinction coefficients and simultaneous equations for assaying chlorophylls a and b extracted with four different solvents: verification of

the concentration of chlorophyll standards by atomic absorption spectroscopy. *Biochimica et Biophysica Acta – Bioenergetics*, 975 (3), 384-394. https://doi.org/10.1016/S0005-2728(89)80347-0

Qi, J., Song, C. P., Wang, B., Zhou, J., Kangasjärvi, J., Zhu, J. K., & Gong, Z. (2018). Reactive oxygen species signaling and stomatal movement in plant responses to drought stress and pathogen attack. *Journal of Integrative Plant Biology*, 60 (9), 805–826. https://doi.org/10.1111/jipb.12654

Ravanel, S., Block, M. A., Rippert, P., Jabrin, S., Curien, G., Rébeillé, F., & Douce, R. (2004) Methionine Metabolism in Plants: chloroplasts are autonomous for *de novo* methionine synthesis and can import s-adenosylmethionine from the cytosol, *Journal of Biological Chemistry*, 279 (21), 22548-22557. https://doi.org/10.1074/jbc.M313250200

Ray, D. K., Mueller, N. D., West, P. C., & Foley, J. A. (2013). Yield Trends Are Insufficient to Double Global Crop Production by 2050. *PLOS ONE*, 8 (6). https://doi.org/10.1371/journal.pone.0066428

Ray, S., Anderson, J. M., Urmeev, F. I., & Goodwin, S. B. (2003). Rapid induction of a protein disulfide isomerase and defense-related genes in wheat in response to the hemibiotrophic fungal pathogen *Mycosphaerella graminicola*. *Plant Molecular Biology*, 53 (5), 701-714. DOI: 10.1023/B:PLAN.0000019120.74610.52

Rekhter, D., Lüdke, D., Ding, Y., Feussner, K., Zienkiewicz, K., Lipka, V., Wiermer, M., Zhang, Y., & Feussner, I. (2019). Isochorismate-derived biosynthesis of the plant stress hormone salicylic acid. *Science*, 365 (6452), 498-502. DOI: 10.1126/science.aaw1720

Roach, T., & Krieger-Liszkay, A. (2012). The role of the PsbS protein in the protection of photosystems I and II against high light in *Arabidopsis thaliana*. *Biochimica et Biophysica Acta - Bioenergetics*, 1817 (12), 2158–2165. https://doi.org/10.1016/j.bbabio.2012.09.011

Robert, C., Bancal, M. O., Lannou, C., & Ney, B. (2006). Quantification of the effects of Septoria tritici blotch on wheat leaf gas exchange with respect to lesion age, leaf number, and leaf nitrogen status. *Journal of Experimental Botany*, 57 (1), 225–234. https://doi.org/10.1093/jxb/eri153

Robert-Seilaniantz, A., Grant, M., & Jones, J. D. G. (2011). Hormone crosstalk in plant disease and defense: More than just JASMONATE-SALICYLATE antagonism. *Annual Review of Phytopathology*, 49, 317–343. https://doi.org/10.1146/annurev-phyto-073009-114447

Roden, L. C., & Ingle, R. A. (2009). Lights, rhythms, infection: The role of light and the circadian clock in determining the outcome of plant-pathogen interactions. *Plant Cell*, 21 (9), 2546–2552. https://doi.org/10.1105/tpc.109.069922

Rodríguez-Herva, J. J., González-Melendi, P., Cuartas-Lanza, R., Antúnez-Lamas, M., Río-Alvarez, I., Li, Z., López-Torrejón, G., Díaz, I., del Pozo, J. C., Chakravarthy, S., Collmer, A., Rodríguez-Palenzuela, P., & López-Solanilla, E. (2012). A bacterial cysteine protease effector protein interferes with photosynthesis to suppress plant innate immune responses. *Cellular Microbiology*, 14 (5), 669–681. https://doi.org/10.1111/j.1462-5822.2012.01749.x

Ruban, A. V. (2016). Nonphotochemical chlorophyll fluorescence quenching: Mechanism and effectiveness in protecting plants from photodamage. *Plant Physiology*, 170 (4), 1903–1916. https://doi.org/10.1104/pp.15.01935

Rudd, J. J. (2015). Previous bottlenecks and future solutions to dissecting the *Zymoseptoria tritici*-wheat host-pathogen interaction. *Fungal Genetics and Biology*, 79, 24–28. https://doi.org/10.1016/j.fgb.2015.04.005

Rudd, J. J., Kanyuka, K., Hassani-Pak, K., Derbyshire, M., Andongabo, A., Devonshire, J., Lysenko, A., Saqi, M., Desai, N. M., Powers, S. J., Hooper, J., Ambroso, L., Bharti, A., Farmer, A., Hammond-Kosack, K. E., Dietrich, R. A., & Courbot, M. (2015). Transcriptome and metabolite profiling of the infection cycle of *Zymoseptoria tritici* on wheat reveals a biphasic interaction with plant immunity involving differential pathogen chromosomal contributions and a variation on the hemibiotrophic lifestyle definition. *Plant Physiology*, 167 (3), 1158–1185. https://doi.org/10.1104/pp.114.255927

Rudd, J. J., Keon, J., & Hammond-Kosack, K. E. (2008). The wheat mitogen-activated protein kinases TaMPK3 and TaMPK6 are differentially

regulated at multiple levels during compatible disease interactions with *Mycosphaerella graminicola*. *Plant Physiology*, 147 (2), 802–815. https://doi.org/10.1104/pp.108.119511

Saccon, F., Giovagnetti, V., Shukla, M. K., & Ruban, A. V. (2020). Rapid regulation of photosynthetic light harvesting in the absence of minor antenna and reaction centre complexes. *Journal of Experimental Botany*, 71 (12), 3626–3637. https://doi.org/10.1093/jxb/eraa126

Sacharz, J., Giovagnetti, V., Ungerer, P., Mastroianni, G., & Ruban, A. V. (2017). The xanthophyll cycle affects reversible interactions between PsbS and light-harvesting complex II to control non-photochemical quenching. *Nature Plants*, 3. https://doi.org/10.1038/nplants.2016.225

Saintenac, C., Lee, W. S., Cambon, F., Rudd, J. J., King, R. C., Marande, W., Powers, S. J., Bergès, H., Phillips, A. L., Uauy, C., Hammond-Kosack, K. E., Langin, T., & Kanyuka, K. (2018). Wheat receptor-kinase-like protein Stb6 controls gene-for-gene resistance to fungal pathogen *Zymoseptoria tritici. Nature Genetics*, 50 (3), 368–374. https://doi.org/10.1038/s41588-018-0051-x

Sánchez-Vallet, A., Fouché, S., Fudal, I., Hartmann, F. E., Soyer, J. L., Tellier, A., & Croll, D. (2018). The Genome Biology of Effector Gene Evolution in Filamentous Plant Pathogens. *Annual Review of Phytopathology*, 56, 21-40. https://doi.org/10.1146/annurev-phyto-080516-035303

Sánchez-Vallet, A., López, G., Ramos, B., Delgado-Cerezo, M., Riviere, M. P., Llorente, F., Fernández, P. V., Miedes, E., Estevez, J. M., Grant, M., & Molina, A. (2012). Disruption of abscisic acid signaling constitutively activates *Arabidopsis* resistance to the necrotrophic fungus *Plectosphaerella cucumerina*. *Plant Physiology*, 160 (4), 2109–2124. https://doi.org/10.1104/pp.112.200154

Sánchez-Vallet, A., McDonald, M. C., Solomon, P. S., & McDonald, B. A. (2015). Is *Zymoseptoria tritici* a hemibiotroph? *Fungal Genetics and Biology*, 79, 29–32. https://doi.org/10.1016/j.fgb.2015.04.001

Sánchez-Vallet, A., Mesters, J. R., & Thomma, B. P. H. J. (2015). The battle for chitin recognition in plant-microbe interactions. *FEMS Microbiology Reviews*, 39 (2), 171–183. https://doi.org/10.1093/femsre/fuu003

Sasi, S., Venkatesh, J., Daneshi, R. F., & Gururani, M. A. (2018). Photosystem II extrinsic proteins and their putative role in abiotic stress tolerance in higher plants. *Plants*, 7 (4). https://doi.org/10.3390/plants7040100

Savage, Z., Duggan, C., Toufexi, A., Pandey, P., Liang, Y., Segretin, M. E., Yuen, L. H., Gaboriau, D. C. A., Leary, A. Y., Tumtas, Y., Khandare, V., Ward, A. D., Botchway, S. W., Bateman, B. C., Pan, I., Schattat, M., Sparkes, I., & Bozkurt, T. O. (2021). Chloroplasts alter their morphology and accumulate at the pathogen interface during infection by *Phytophthora infestans*. *Plant Journal*, 107 (6), 1771–1787. https://doi.org/10.1111/tpj.15416

Serrano, I., Audran, C., & Rivas, S. (2016). Chloroplasts at work during plant innate immunity. *Journal of Experimental Botany*, 67 (13), 3845–3854. https://doi.org/10.1093/jxb/erw088

Shao, D., Smith, D. L., Kabbage, M., & Roth, M. G. (2021). Effectors of Plant Necrotrophic Fungi. *Frontiers in Plant Science*, 12. https://doi.org/10.3389/fpls.2021.687713

Shapiguzov, A., Vainonen, J. P., Wrzaczek, M., & Kangasjärvi, J. (2012). ROS-talk - how the apoplast, the chloroplast, and the nucleus get the message through. *Frontiers in Plant Science*, 3. https://doi.org/10.3389/fpls.2012.00292

Sharma, P., Jha, A. B., Dubey, R. S., & Pessarakli, M. (2012). Reactive Oxygen Species, Oxidative Damage, and Antioxidative Defense Mechanism in Plants under Stressful Conditions. *Journal of Botany*, 1–26. https://doi.org/10.1155/2012/217037

Shetty, N. P., Jensen, J. D., Knudsen, A., Finnie, C., Geshi, N., Blennow, A., Collinge, D. B., & Jørgensen, H. J. L. (2009). Effects of β-1,3-glucan from *Septoria tritici* on structural defence responses in wheat. *Journal of Experimental Botany*, 60 (15), 4287–4300. https://doi.org/10.1093/jxb/erp269

Shetty, N. P., Kristensen, B. K., Newmana, M. A., Møller, K., Gregersen, P. L., & Jørgensen, H. J. L. (2003). Association of hydrogen peroxide with restriction of *Septoria tritici* in resistant wheat. *Physiological and Molecular*

Plant Pathology, 62 (6), 333–346. https://doi.org/10.1016/S0885-5765(03)00079-1

Shetty, N. P., Mehrabi, R., Lütken, H., Haldrup, A., Kema, G. H. J., Collinge, D. B., & Jørgensen, H. J. L. (2007). Role of hydrogen peroxide during the interaction between the hemibiotrophic fungal pathogen *Septoria tritici* and wheat. *New Phytologist*, 174 (3), 637–647. https://doi.org/10.1111/j.1469-8137.2007.02026.x

Shewry, P. R. (2009). Wheat. *Journal of Experimental Botany*, 60 (60, 1537–1553. https://doi.org/10.1093/jxb/erp058

Shi, G., Zhang, Z., Friesen, T. L., Raats, D., Fahima, T., Brueggeman, R. S., Lu, S., Trick, H. N., Liu, Z., Chao, W., Frenkel, Z., Xu, S. S., Rasmussen, J. B., & Faris, J. D. (2016). The hijacking of a receptor kinase-driven pathway by a wheat fungal pathogen leads to disease. *Science Advances*, 2 (10). DOI: 10.1126/sciadv.1600822

Sierla, M., Hõrak, H., Overmyer, K., Waszczak, C., Yarmolinsky, D., Maierhofer, T., Vainonen, J. P., Salojärvi, J., Denessiouk, K., Laanemets, K., Tõldsepp, K., Vahisalu, T., Gauthier, A., Puukko, T., Paulin, L., Auvinen, P., Geiger, D., Hedrich, R., Kollist, H., & Kangasjärvi, J. (2018). The receptor-like pseudokinase GHR1 is required for stomatal closure. *Plant Cell*, 30 (11), 2813–2837. https://doi.org/10.1105/tpc.18.00441

Sierla, M., Rahikainen, M., Salojärvi, J., Kangasjärvi, J., & Kangasjärvi, S. (2013). Apoplastic and chloroplastic redox signaling networks in plant stress responses. *Antioxidants and Redox Signaling*, 18 (16), 2220–2239. https://doi.org/10.1089/ars.2012.5016

Sierla, M., Waszczak, C., Vahisalu, T., & Kangasjärvi, J. (2016). Reactive oxygen species in the regulation of stomatal movements. *Plant Physiology*, 171 (3), 1569–1580. https://doi.org/10.1104/pp.16.00328

Singh, R., Singh, S., Parihar, P., Singh, V. P., & Prasad, S. M. (2015). Retrograde signaling between plastid and nucleus: A review. *Journal of Plant Physiology*, 181, 55–66. https://doi.org/10.1016/j.jplph.2015.04.001

Smirnoff, N., & Arnaud, D. (2019). Hydrogen peroxide metabolism and functions in plants. *New Phytologist*, 221 (3), 1197–1214. https://doi.org/10.1111/nph.15488

Solomon, P. S., Lee, R. C., Wilson, T. J. G., & Oliver, R. P. (2004). Pathogenicity of *Stagonospora nodorum* requires malate synthase. *Molecular Microbiology*, 53 (4), 1065–1073. https://doi.org/10.1111/j.1365-2958.2004.04178.x

Sperschneider, J., Catanzariti, A. M., Deboer, K., Petre, B., Gardiner, D. M., Singh, K. B., Dodds, P. N., & Taylor, J. M. (2017). LOCALIZER: Subcellular localization prediction of both plant and effector proteins in the plant cell. *Scientific Reports*, 7. https://doi.org/10.1038/srep44598

Sperschneider, J., Gardiner, D. M., Dodds, P. N., Tini, F., Covarelli, L., Singh, K. B., Manners, J. M., & Taylor, J. M. (2016). EffectorP: Predicting fungal effector proteins from secretomes using machine learning. *New Phytologist*, 210 (2), 743–761. https://doi.org/10.1111/nph.13794

Stael, S., Kmiecik, P., Willems, P., van der Kelen, K., Coll, N. S., Teige, M., & van Breusegem, F. (2015). Plant innate immunity - sunny side up? *Trends in Plant Science*, 20 (1), 3–11. https://doi.org/10.1016/j.tplants.2014.10.002

Steinberg, G. (2015). Cell biology of *Zymoseptoria tritici*: Pathogen cell organization and wheat infection. *Fungal Genetics and Biology*, 79, 17–23. https://doi.org/10.1016/j.fgb.2015.04.002

Stephens, C., Ölmez, F., Blyth, H., McDonald, M., Bansal, A., Turgay, E. B., Hahn, F., Saintenac, C., Nekrasov, V., Solomon, P., Milgate, A., Fraaije, B., Rudd, J., & Kanyuka, K. (2021). Remarkable recent changes in the genetic diversity of the avirulence gene *AvrStb6* in global populations of the wheat pathogen *Zymoseptoria tritici*. *Molecular Plant Pathology*, 22 (9), 1121–1133. https://doi.org/10.1111/mpp.13101

Stewart, E. L., Croll, D., Lendenmann, M. H., Sanchez-Vallet, A., Hartmann, F. E., Palma-Guerrero, J., Ma, X., & Mcdonald, B. A. (2017). Quantitative trait locus mapping reveals complex genetic architecture of quantitative virulence in the wheat pathogen *Zymoseptoria tritici*. *Molecular Plant Pathology*, 19 (1), 201-216. https://doi.org/10.1111/mpp.12515

Stewart, E. L., & McDonald, B. A. (2014). Measuring quantitative virulence in the wheat pathogen *Zymoseptoria tritici* using high-throughput automated

image analysis. *Phytopathology*, 104 (9), 985–992. https://doi.org/10.1094/PHYTO-11-13-0328-R

Stotz, H. U., Mitrousia, G. K., de Wit, P. J. G. M., & Fitt, B. D. L. (2014). Effector-triggered defence against apoplastic fungal pathogens. *Trends in Plant Science*, 19 (8), 491–500. https://doi.org/10.1016/j.tplants.2014.04.009

Su, J., Yang, L., Zhu, Q., Wu, H., He, Y., Liu, Y., Xu, J., Jiang, D., & Zhang, S. (2018). Active photosynthetic inhibition mediated by MPK3/MPK6 is critical to effector-triggered immunity. *PLOS Biology*, 16 (5). https://doi.org/10.1371/journal.pbio.2004122

Suffert, F., Sache, I., & Lannou, C. (2011). Early stages of septoria tritici blotch epidemics of winter wheat: Build-up, overseasoning, and release of primary inoculum. *Plant Pathology*, 60 (2), 166–177. https://doi.org/10.1111/j.1365-3059.2010.02369.x

Sun, J. L., Li, J. Y., Wang, M. J., Song, Z. T., & Liu, J. X. (2021). Protein Quality Control in Plant Organelles: Current Progress and Future Perspectives. *Molecular Plant*, 14 (1), 95–114. https://doi.org/10.1016/j.molp.2020.10.011

Sun, M., Qiu, L., Liu, Y., Zhang, H., Zhang, Y., Qin, Y., Mao, Y., Zhou, M., Du, X., Qin, Z., & Dai, S. (2022). Pto Interaction Proteins: Critical Regulators in Plant Development and Stress Response. *Frontiers in Plant Science*, 13. https://doi.org/10.3389/fpls.2022.774229

Tai, Y. S., Bragg, J., & Meinhardt, S. W. (2007). Functional Characterization of ToxA and Molecular Identification of its Intracellular Targeting Protein in Wheat. *American Journal of Plant Physiology.* 2 (2), 76-89. DOI: 10.3923/ajpp.2007.76.89

Takahashi, A., Agrawal, G. K., Yamazaki, M., Onosato, K., Miyao, A., Kawasaki, T., Shimamoto, K., & Hirochika, H. (2007). Rice Pti1a negatively regulates RAR1-dependent defense responses. *Plant Cell*, 19 (9), 2940–2951. https://doi.org/10.1105/tpc.106.047142

Takahashi, S., & Badger, M. R. (2011). Photoprotection in plants: A new light on photosystem II damage. *Trends in Plant Science*, 16 (1), 53–60. https://doi.org/10.1016/j.tplants.2010.10.001

Talbot, N. J. (2015). Taming a wild beast: Developing molecular tools and new methods to understand the biology of *Zymoseptoria tritici*. *Fungal Genetics and Biology*, *79*, 193–195. https://doi.org/10.1016/j.fgb.2015.05.004

Tang, D., Wang, G., & Zhou, J. M. (2017). Receptor kinases in plant-pathogen interactions: More than pattern recognition. *Plant Cell*, 29 (4), 618–637. https://doi.org/10.1105/tpc.16.00891

Tang, L., Yang, G., Ma, M., Liu, X., Li, B., Xie, J., Fu, Y., Chen, T., Yu, Y., Chen, W., Jiang, D., & Cheng, J. (2020). An effector of a necrotrophic fungal pathogen targets the calcium-sensing receptor in chloroplasts to inhibit host resistance. *Molecular Plant Pathology*, 21 (5), 686–701. https://doi.org/10.1111/mpp.12922

Tang, Y., Wen, X., Lu, Q., Yang, Z., Cheng, Z., & Lu, C. (2007). Heat stress induces an aggregation of the light-harvesting complex of photosystem II in spinach plants. *Plant Physiology*, 143 (2), 629–638. https://doi.org/10.1104/pp.106.090712

Theis, J., & Schroda, M. (2016). Revisiting the photosystem II repair cycle. *Plant Signaling and Behavior*, 11 (9). https://doi.org/10.1080/15592324.2016.1218587

Thomma, B. P. H. J., Nürnberger, T., & Joosten, M. H. A. J. (2011). Of PAMPs and effectors: The blurred PTI-ETI dichotomy. *Plant Cell*, 23 (1), 4–15. https://doi.org/10.1105/tpc.110.082602

Thomson, S. M., Pulido, P., & Jarvis, R. P. (2020). Protein import into chloroplasts and its regulation by the ubiquitin-proteasome system. *Biochemical Society Transactions*, 48 (1), 71–82. https://doi.org/10.1042/BST20190274

Tikkanen, M., & Aro, E. M. (2012). Thylakoid protein phosphorylation in dynamic regulation of photosystem II in higher plants. *Biochimica et Biophysica Acta – Bioenergetics*, 1817 (1), 232–238. https://doi.org/10.1016/j.bbabio.2011.05.005

Tikkanen, M., Mekala, N. R., & Aro, E. M. (2014). Photosystem II photoinhibition-repair cycle protects Photosystem I from irreversible

damage. *Biochimica et Biophysica Acta - Bioenergetics*, 1837 (1), 210–215. https://doi.org/10.1016/j.bbabio.2013.10.001

Ton, J., Flors, V., & Mauch-Mani, B. (2009). The multifaceted role of ABA in disease resistance. *Trends in Plant Science*, 14 (6), 310-317. https://doi.org/10.1016/j.tplants.2009.03.006

Torriani, S. F. F., Brunner, P. C., McDonald, B. A., & Sierotzki, H. (2009). QoI resistance emerged independently at least 4 times in European populations of *Mycosphaerella graminicola*. *Pest Management Science*, 65 (2), 155–162. https://doi.org/10.1002/ps.1662

Torriani, S. F. F., Melichar, J. P. E., Mills, C., Pain, N., Sierotzki, H., & Courbot, M. (2015). *Zymoseptoria tritici*: A major threat to wheat production, integrated approaches to control. *Fungal Genetics and Biology*, 79, 8–12. https://doi.org/10.1016/j.fgb.2015.04.010

Triantaphylidès, C., & Havaux, M. (2009). Singlet oxygen in plants: production, detoxification and signaling. *Trends in Plant Science*, 14 (4), 219–228. https://doi.org/10.1016/j.tplants.2009.01.008

Trotta, A., Rahikainen, M., Konert, G., Finazzi, G., & Kangasjärvi, S. (2014). Signalling crosstalk in light stress and immune reactions in plants. *Philosophical Transactions of the Royal Society B: Biological Sciences*, 369 (1640). https://doi.org/10.1098/rstb.2013.0235

Tyystjärvi, E. (2013). Photoinhibition of Photosystem II. *International Review of Cell and Molecular Biology*, 300, 243–303. https://doi.org/10.1016/B978-0-12-405210-9.00007-2

Vahisalu, T., Puzõrjova, I., Brosché, M., Valk, E., Lepiku, M., Moldau, H., Pechter, P., Wang, Y. S., Lindgren, O., Salojärvi, J., Loog, M., Kangasjärvi, J., & Kollist, H. (2010). Ozone-triggered rapid stomatal response involves the production of reactive oxygen species, and is controlled by SLAC1 and OST1. *Plant Journal*, 62 (3), 442–453. https://doi.org/10.1111/j.1365-313X.2010.04159.x

Vleeshouwers, V. G. A. A., & Oliver, R. P. (2014). Effectors as tools in disease resistance breeding against biotrophic, hemibiotrophic, and necrotrophic plant pathogens. *Molecular Plant-Microbe Interactions*, 27 (3), 196–206. https://doi.org/10.1094/MPMI-10-13-0313-IA

Walter, H. (2011). New Fungicides and New Modes of Action. In: *Modern Fungicides and Antifungal Compounds, Vol. VI*, Eds: Dehne HW, Deising HB, Gisi U, Kuck KH, Russell PE, Lyr H, DPG, Braunschweig, Germany.

Wang, X., Zhai, T., Zhang, X., Tang, C., Zhuang, R., Zhao, H., Xu, Q., Cheng, Y., Wang, J., Duplessis, S., Kang, Z., & Wang, X. (2021). Two stripe rust effectors impair wheat resistance by suppressing import of host Fe-S protein into chloroplasts. *Plant Physiology*, 187 (4), 2530–2543. https://doi.org/10.1093/plphys/kiab434

Wang, Y., Li, J., Hou, S., Wang, X., Li, Y., Ren, D., Chen, S., Tang, X., & Zhou, J. M. (2010). A *Pseudomonas syringae* ADP-ribosyltransferase inhibits Arabidopsis mitogen-activated protein kinase kinases. *Plant Cell*, 22 (6), 2033–2044. https://doi.org/10.1105/tpc.110.075697

Wangdi, T., Uppalapati, S. R., Nagaraj, S., Ryu, C. M., Bender, C. L., & Mysore, K. S. (2010). A role for chloroplast-localized thylakoid formation 1 (THF1) in bacterial speck disease development. *Plant Signaling and Behavior*, 5 (4), 425–427. https://doi.org/10.4161/psb.5.4.11284

Wasternack, C., & Feussner, I. (2017). The Oxylipin Pathways: Biochemistry and Function. *Annual Review of Plant Biology*, 69, 363-386. https://doi.org/10.1146/annurev-arplant-042817-040440

Wegulo, S. N. (2011). Tan spot of cereals. *The Plant Health Instructor*. DOI: 10.1094/PHI-I-2011-0426-01

Xu, Q., Tang, C., Wang, X., Sun, S., Zhao, J., Kang, Z., & Wang, X. (2019). An effector protein of the wheat stripe rust fungus targets chloroplasts and suppresses chloroplast function. *Nature Communications*, 10 (1). https://doi.org/10.1038/s41467-019-13487-6

Yamori, W., & Shikanai, T. (2016). Physiological Functions of Cyclic Electron Transport Around Photosystem I in Sustaining Photosynthesis and Plant Growth. *Annual Review of Plant Biology*, 67, 81–106. https://doi.org/10.1146/annurev-arplant-043015-112002

Yang, F., Li, W., & Jørgensen, H. J. L. (2013). Transcriptional reprogramming of wheat and the hemibiotrophic pathogen *Septoria tritici* during two phases of the compatible interaction. *PLOS ONE*, 8 (11). https://doi.org/10.1371/journal.pone.0081606

Yao, N., & Greenberg, J. T. (2006). Arabidopsis ACCELERATED CELL DEATH2 modulates programmed cell death. *Plant Cell*, 18 (2), 397–411. https://doi.org/10.1105/tpc.105.036251

Zabala, M. de T., Littlejohn, G., Jayaraman, S., Studholme, D., Bailey, T., Lawson, T., Tillich, M., Licht, D., Bölter, B., Delfino, L., Truman, W., Mansfield, J., Smirnoff, N., & Grant, M. (2015). Chloroplasts play a central role in plant defence and are targeted by pathogen effectors. *Nature Plants*, 1 (6). https://doi.org/10.1038/NPLANTS.2015.74

Zhang, J., Chen, L., Fu, C., Wang, L., Liu, H., Cheng, Y., Li, S., Deng, Q., Wang, S., Zhu, J., Liang, Y., Li, P., & Zheng, A. (2017). Comparative transcriptome analyses of gene expression changes triggered by *Rhizoctonia solani* AG1 IA infection in resistant and susceptible rice varieties. *Frontiers in Plant Science*, 8. https://doi.org/10.3389/fpls.2017.01422

Zhao, X., Chen, T., Feng, B., Zhang, C., Peng, S., Zhang, X., Fu, G., & Tao, L. (2017). Non-photochemical quenching plays a key role in light acclimation of rice plants differing in leaf color. *Frontiers in Plant Science*, 7. https://doi.org/10.3389/fpls.2016.01968

Zhong, Z., Marcel, T. C., Hartmann, F. E., Ma, X., Plissonneau, C., Zala, M., Ducasse, A., Confais, J., Compain, J., Lapalu, N., Amselem, J., McDonald, B. A., Croll, D., & Palma-Guerrero, J. (2017). A small secreted protein in *Zymoseptoria tritici* is responsible for avirulence on wheat cultivars carrying the *Stb6* resistance gene. *New Phytologist*, 214 (2), 619–631. https://doi.org/10.1111/nph.14434

Zhou, J., Zeng, L., Liu, J., & Xing, D. (2015). Manipulation of the Xanthophyll Cycle Increases Plant Susceptibility to *Sclerotinia sclerotiorum*. *PLOS Pathogens*, 11 (5). https://doi.org/10.1371/journal.ppat.1004878

Zipfel, C. (2009). Early molecular events in PAMP-triggered immunity. *Current Opinion in Plant Biology*, 12 (4), 414–420. https://doi.org/10.1016/j.pbi.2009.06.003

Zipfel, C., Kunze, G., Chinchilla, D., Caniard, A., Jones, J. D. G., Boller, T., & Felix, G. (2006). Perception of the Bacterial PAMP EF-Tu by the Receptor

EFR Restricts Agrobacterium-Mediated Transformation. *Cell*, 125 (4), 749–760. https://doi.org/10.1016/j.cell.2006.03.037

Zulfugarov, I. S., Tovuu, A., Eu, Y. J., Dogsom, B., Poudyal, R. S., Nath, K., Hall, M., Banerjee, M., Yoon, U. C., Moon, Y. H., An, G., Jansson, S., & Lee, C. H. (2014). Production of superoxide from Photosystem II in a rice (*Oryza sativa* L.) mutant lacking PsbS. *BMC Plant Biology*, 14 (1). https://doi.org/10.1186/s12870-014-0242-2

Zulfugarov, I. S., Tovuu, A., Kim, C. Y., Xuan Vo, K. T., Ko, S. Y., Hall, M., Seok, H. Y., Kim, Y. K., Skogstrom, O., Moon, Y. H., Jansson, S., Jeon, J. S., & Lee, C. H. (2016). Enhanced resistance of PsbS-deficient rice (*Oryza sativa* L.) to fungal and bacterial pathogens. *Journal of Plant Biology*, 59 (6), 616–626. https://doi.org/10.1007/s12374-016-0068-6

Zurbriggen, M. D., Carrillo, N., Tognetti, V. B., Melzer, M., Peisker, M., Hause, B., & Hajirezaei, M. R. (2009). Chloroplast-generated reactive oxygen species play a major role in localized cell death during the non-host interaction between tobacco and *Xanthomonas campestris* pv. *vesicatoria*. *Plant Journal*, 60 (6), 962–973. https://doi.org/10.1111/j.1365-313X.2009.04010.x